

SEISMIC RESPONSE OF THE GEORGE MASSEY TUNNEL

by

SURINDER S. PUAR

B.A.Sc., The University of British Columbia, 1992

A THESIS SUBMITTED IN PARTIAL FULFILLMENT OF
THE REQUIREMENTS FOR THE DEGREE OF:

MASTER OF APPLIED SCIENCE in
THE FACULTY OF GRADUATE STUDIES
(Department of Civil Engineering -- Geotechnical Engineering Programme)

We accept this thesis as conforming to
~~the~~ required standard

THE UNIVERSITY OF BRITISH COLUMBIA

April 1996

© Surinder Singh Puar, 1996

In presenting this thesis in partial fulfilment of the requirements for an advanced degree at the University of British Columbia, I agree that the Library shall make it freely available for reference and study. I further agree that permission for extensive copying of this thesis for scholarly purposes may be granted by the head of my department or by his or her representatives. It is understood that copying or publication of this thesis for financial gain shall not be allowed without my written permission.

Department of Civil Engineering

The University of British Columbia
Vancouver, Canada

Date APRIL 24, 1996

ABSTRACT

The George Massey Tunnel, in Richmond, British Columbia, is a 630-meter long submerged concrete tunnel, with 550-meter and 335-meter long approaches on the north and south ends, respectively. The tunnel crosses the Fraser River and is founded on a deep deposit of unconsolidated sediments consisting mainly of sands and silts that are susceptible to liquefaction during earthquake loading.

This thesis represents a comprehensive analytical investigation to evaluate the liquefaction potential of the foundation soils and the performance of the tunnel during a major earthquake. The evaluation procedures and post-liquefaction stability and deformation results are presented.

Liquefaction potential analyses based on the total stress approach were conducted. Liquefaction was predicted by comparing the earthquake-induced stresses to soil resistance. Dynamic ground response analyses were performed to assess the magnitude of the cyclic stresses; the cyclic resistance of the soil was computed using various methods, depending on the soil type.

Estimated acceleration levels could potentially trigger liquefaction in substantial zones of the tunnel's foundation. The residual (peak post-liquefaction) shear strength of liquefied soils was estimated to be adequate to maintain post-earthquake stability of the tunnel at all of the locations analyzed. The main problem to be addressed, therefore, was

the displacements due to triggering of liquefaction in directions transverse to- and parallel to the tunnel alignment, as a result of the 475-year seismic event.

Post-liquefaction deformations of the tunnel were computed using both empirical and numerical methods. The numerical methods incorporate post-liquefaction stress-strain relationships and account for the effects of both gravity and inertia forces.

Analyses suggested that liquefaction would occur at four of the five locations. Liquefaction was not predicted at the south shore. The liquefaction resistance at the south shore location was on the borderline in terms of the triggering criteria. The south shore location stratum is very similar to that of the north shore (where significant liquefaction is predicted). The displacement analyses at the two locations were compared and contrasted, revealing what movements could be expected at either end if liquefaction were to occur or not (i.e., depending on assessment of different earthquake magnitudes).

Since the computed liquefaction-induced displacements were, often, beyond tolerances, potential remedial options were analyzed at the offshore location determined to be the most susceptible to liquefaction. Those analyses showed that the use of certain remedial schemes will decrease the displacements significantly. Because it is very difficult to access the stratum directly beneath the tunnel, densification of zones adjacent to the tunnel is the most effective and economically feasible solution to limit displacements.

Table of Contents

Abstract.....	ii
Table of Contents.....	iv
List of Tables.....	x
List of Figures.....	xv
Acknowledgements.....	xx
1 Introduction.....	1
1.1 Purpose.....	1
1.2 Scope & Organization of Thesis.....	2
2 SITE DETAILS.....	4
2.1 Site Location.....	4
2.2 Tunnel Layout, Construction, and Cross-section View.....	4
2.3 Locations of Analyses.....	9
2.4 Available Information & Literature Review.....	9
3 SEISMICITY & SEISMIC LOADING.....	13
3.1 Local Seismicity.....	13
3.2 Seismic Loading for Ground Response Analyses.....	14
3.2.1 Modification of Acceleration Time-Histories.....	15
4 ANALYSIS PROCEDURES & ENGINEERING PARAMETERS.....	18
4.1 Introduction.....	18
4.2 Liquefaction Assessment.....	21
4.2.1 Triggering Resistance (CRR) of Sands.....	22
4.2.1.1 Overburden Pressure Correction (K_o).....	25
4.2.1.2 Magnitude Correction (K_M).....	27
4.2.1.3 Static Shear Correction (K_α).....	27
4.2.1.4 Estimation of Fines Content.....	28

Table of Contents

4.2.2	Triggering Resistance (CRR) of Fine-grained Soils.....	30
4.2.2.1	Non-Plastic Silts.....	30
4.2.2.2	Plastic Silts.....	32
4.2.3	Cyclic Loading (CSR) -- SHAKE Analyses.....	34
4.2.3.1	Maximum Shear Modulus (G_{\max}).....	35
4.2.3.2	Spectral Response.....	37
4.3	Post-liquefaction Stability.....	38
4.3.1	Flow Slide.....	38
4.3.2	Estimation of Residual Strengths (S_r).....	39
4.3.3	Estimation of Limiting Strains (γ_{Lim}).....	43
4.4	Liquefaction-induced Displacements.....	46
4.4.1	Introduction.....	46
4.4.2	Empirical Case-History Based Methods.....	47
4.4.2.1	Introduction.....	47
4.4.2.2	Bartlett & Youd.....	47
4.4.2.3	Hamada	49
4.4.2.4	Tokimatsu & Seed -- Liquefaction-Induced Settlements.....	50
4.4.3	Numerical Methods.....	52
4.4.3.1	Introduction.....	52
4.4.3.2	SOILSTRESS: Finite Element Analyses.....	53
4.4.3.2.1	Estimation of Pre-Liquefaction Shear Modulus Constant.....	53
4.4.3.2.2	Estimation of Post-Liquefaction Shear Modulus Constant.....	53
4.4.3.3	LIQDISP: Single-Degree-of-Freedom Analyses.....	58
5	LOCAL GEOLOGY & REVIEW OF SOIL DATA.....	60
5.1	Introduction.....	60
5.2	General Surficial Geology.....	60
5.3	Available Soil Data -- Site Specific Surficial Geology.....	62
5.4	Interpretation of Available Soil Data.....	66
5.4.1	Introduction.....	66
5.4.2	Location #2.....	68
5.4.3	Location #3.....	69

Table of Contents

5.4.4	Location #4.....	70
5.4.5	Location #7.....	71
5.4.6	Location #8.....	72
5.4.7	Development of Longitudinal-Direction Soil Profile.....	73
6	RESULTS: Liquefaction Triggering and Post-Earthquake Stability.....	74
6.1	Introduction.....	74
6.2	Liquefaction Assessment and Associated Parameters.....	74
6.2.1	Zones of Liquefaction.....	74
6.2.1.1	Location #2.....	78
6.2.1.2	Location #3.....	81
6.2.1.3	Location #4.....	83
6.2.1.4	Location #7.....	85
6.2.1.5	Location #8.....	88
6.3	Post-Liquefaction Stability & Strength and Stiffness Parameters.....	91
6.3.1	Flowslide Potential.....	91
6.3.2	Residual Strength (S_r) & Limit Strain (γ_{Lim}) Summaries.....	95
7	DISCUSSION of Chapter 6 Results.....	100
7.1	Introduction.....	100
7.2	Liquefaction Assessment.....	100
7.2.1	Zones of Liquefaction.....	100
7.2.2	SHAKE: Cyclic Loading and Spectral Response	102
7.3	Post-Liquefaction Stability.....	106
7.4	Future Work.....	108
8	RESULTS: Post-Earthquake Displacements & Associated Parameters.....	109
8.1	Introduction.....	109
8.2	Empirical Methods -- Displacement Predictions.....	109

8.3	Numerical Methods -- Displacement Predictions & Engineering Parameter Summaries.....	112
8.3.1	Introduction.....	112
8.3.2	Finite Element (SOILSTRESS) Displacements.....	112
8.3.2.1	Transverse-direction	113
8.3.2.1.1	Displacements at North and South Shores.....	115
8.3.2.1.2	Displacements at Offshore Locations.....	125
8.3.2.2	Longitudinal-Direction Displacements.....	139
8.3.3	LIQDISP -- Single-degree-of-freedom Displacements.....	148
9	DISCUSSION of Chapter 8 Results.....	150
9.1	Introduction.....	150
9.2	Comparison of Displacement Predictions.....	150
9.2.1	Comparison of Empirical and Numerical Method Predictions.....	150
9.2.2	Underground Structure Case-Histories.....	154
9.3	Empirical Method Displacements.....	155
9.4	Numerical Method Displacements.....	159
9.4.1	Finite Element (SOILSTRESS) Displacements.....	159
9.4.1.1	Transverse-direction Analyses.....	163
9.4.1.2	Longitudinal-direction Analyses.....	166
9.4.2	LIQDISP -- Single-degree-of-freedom Analyses.....	168
10	REMEDIAL MEASURES.....	171
10.1	Introduction.....	171
10.2	Presentation and Discussion of Results.....	172
10.3	Preliminary Remediation Recommendation.....	189
11	CONCLUSIONS.....	192

REFERENCES	194
APPENDICES	201
Appendix A Numerical Method Displacement Predictions.....	201
A.1 Additional SOILSTRESS Analyses.....	201
A.1.1 Displacements at Offshore Locations -- Case 2: No Sediment Loading.....	201
A.1.2 Case 3: Displacements With Increased Sediment Loads.....	205
A.1.3 Case 4: Displacements With Increased Ground Velocity.....	208
A.1.4 Full-Section Longitudinal Analyses.....	210
A.2 Extended Newmark Model.....	215
A.3 Extended Newmark Model -- Integration with SOILSTRESS Code.....	221
Appendix B SHAKE Analyses.....	225
B.1 SHAKE Analysis Method.....	225
B.2 Comparison of CSR's Using Various Bedrock Velocities.....	226
B.3 Surface Spectral Response Results.....	227
B.4 Ground Motion Amplification Summary.....	232
B.5 Liquefaction Analysis Summaries.....	233
B.5.1 Location #2.....	233
B.5.2 Location #3.....	234
B.5.3 Location #4.....	235
B.5.4 Location #7.....	236
B.5.5 Location #8.....	237
B.6 Idriss (1990) Ground Motion Attenuation.....	238
Appendix C Post-Earthquake Stability	239
C.1 Flowslide Analyses: Limit Equilibrium Stability at Offshore Locations...	240
C.2 Flowslide Analyses with Higher Residual Strengths	243

C.3	Residual Strength (S_r) in Sands -- Stark & Mesri (1992).....	246
C.4	Residual Strength -- Seed & Harder (1990).....	247
Appendix D	Empirical Method Displacement Predictions.....	249
D.1	Bartlett/Youd: Analysis Details.....	249
D.1.1	Displacement Predictions with Epicentral Distance of 30km and Varying Slopes	249
D.1.2	Displacement Predictions with Epicentral Distance of 60km and Varying Slopes.....	250
D.2	Hamada: Analysis Details.....	252
D.2.1	Model Details.....	252
D.2.2	Analysis Parameters and Predictions.....	253
D.3	Tokimatsu/Seed: Analysis Details.....	255
Appendix E	Additional Figures and Charts Used in Analyses.....	256
Appendix F	Remediation Calculations for Each Location.....	259
Appendix G	Available Soil Data.....	260
G.1	CPT and Borehole Soil Profiles and Summaries.....	261
G.2	Fine-grained Soils Data.....	275

List of Tables

Table 3.1 - Seismic Design Parameters for George Massey Tunnel Site.....	13
Table 3.2 - Ground motion parameters of chosen earthquake motions.....	15
Table 4.1 - Corrections to Measured $(N_1)_{60}$ for Fines Content.....	28
Table 6.1 - Depth of Liquefaction at Each Location.....	76
Table 6.2 - Estimated Soil Parameters for Liquefaction Assessment at #2 Location.....	79
Table 6.3 - Estimated Soil Parameters for Liquefaction Assessment at #3 Location.....	81
Table 6.4 - Estimated Soil Parameters for Liquefaction Assessment at #4 Location.....	84
Table 6.5 - Estimated Soil Parameters for Liquefaction Assessment at #7 Location.....	86
Table 6.6 - Estimated Soil Parameters for Liquefaction Assessment at #8 Location.....	89
Table 6.7 - Residual Strength (S_r) and Limiting Strain (γ_{Lim}) Magnitudes for Transverse Analyses.....	95
Table 6.8 - Residual Strength (S_r) and Limiting Strain (γ_{Lim}) Magnitudes for Longitudinal Analyses.....	96
Table 8.1 - Empirical Method Displacement Estimates.....	110
Table 8.2 - Tokimatsu/Seed Method Post-liquefaction Settlement Estimates.....	111
Table 8.3 - SOILSTRESS Pre- and Post-earthquake Inputs for Transverse Analyses at All Locations.....	114
Table 8.5 - SOILSTRESS Pre- and Post-earthquake Inputs -- Location #7.....	117

List of Tables

Table 8.6 - SOILSTRESS Pre- and Post-earthquake Inputs -- Location #8.....	117
Table 8.4 - SOILSTRESS Inputs for Liquefied Materials at North Shore.....	115
Table 8.7 - Displacements at North and South Shore Locations.....	119
Table 8.8 - SOILSTRESS Pre- and Post-earthquake Inputs -- Location #2.....	125
Table 8.9 - SOILSTRESS Pre- and Post-earthquake Inputs -- Location #3.....	128
Table 8.10 - SOILSTRESS Pre- and Post-earthquake Inputs -- Location #4.....	128
Table 8.11 - SOILSTRESS Soil Input Parameters for Liquefied Materials at Offshore Locations.....	130
Table 8.12 - Displacements at Offshore Locations.....	131
Table 8.13 - SOILSTRESS Pre- and Post-Earthquake Inputs for Materials Common to Both Halves.....	139
Table 8.14 - SOILSTRESS Pre- and Post-Earthquake Inputs for North End -- Longitudinal Analysis.....	140
Table 8.15 - SOILSTRESS Pre- and Post-Earthquake Inputs for South End -- Longitudinal Analysis.....	141
Table 8.16 - Northern Half -- Longitudinal-direction Displacement Predictions.....	142
Table 8.17 - Southern Half -- Longitudinal-direction Displacement Predictions.....	143
Table 8.18 - LIQDISP Input Parameters and Displacement Predictions at Offshore Locations.....	148
Table 8.19 - LIQDISP Input Parameters and Displacement Predictions at Onshore Locations.....	149
Table 9.1 - Results from Empirical and Numerical Displacement Methods.....	151
Table 9.2 - Comparison of SOILSTRESS Results -- Varying Sediment Loads.....	164

Table 10.1 - Descriptions of Densification Schemes.....	172
Table 10.2 - Modelling of Remediation Schemes -- Displacements at Location #2.....	173
Table 10.3 - Required Densification to Prevent Liquefaction at Location #2.....	189
Table 10.4 - Required Densification to Prevent Liquefaction at Location #3.....	190
Table 10.5 - Required Densification to Prevent Liquefaction at Location #4.....	190
Table 10.6 - Required Densification to Prevent Liquefaction at Location #7.....	190
Table 10.7 - Required Densification to Prevent Liquefaction at Location #8.....	191
Table A.1.1 - Displacements at Offshore Locations -- No Sediment Loading.....	201
Table A.1.2 - Displacements at Location #2 -- Increased Sediment Loading.....	205
Table A.1.3 - Displacements at Location #2 -- Increased Ground Velocity.....	208
Table A.1.4 - SOILSTRESS Pre- and Post-liquefaction Inputs For Longitudinal Section Analyses.....	210
Table A.1.5 - Longitudinal-direction Analysis Displacement Predictions.....	211
Table B.4.1 - Ground Motion Amplification at Each Location.....	232
Table B.5.1 - Triggering Summary for Location #2.....	233
Table B.5.2 - Triggering Summary for Location #2 -- Continued.....	233
Table B.5.3 - Triggering Summary for Location #3.....	234
Table B.5.4 - Triggering Summary for Location #3 -- Continued.....	234
Table B.5.5 - Triggering Summary for Location #4.....	235
Table B.5.6 - Triggering Summary for Location #4 -- Continued.....	235
Table B.5.7 - Triggering Summary for Location #7.....	236

Table B.5.8 - Triggering Summary for Location #7 -- Continued.....	236
Table B.5.9 - Triggering Summary for Location #8.....	237
Table B.5.10 - Triggering Summary for Location #8 -- Continued.....	237
Table B.6.1 - Estimation of Target Spectrum for Modification of Time-Histories.....	238
Table C.4.1 - Residual Strength Estimates -- Seed & Harder (1990).....	248
Table D.1.1 - Bartlett/Youd Parameters and Displacement Predictions at Location #2 -- R=30km.....	249
Table D.1.2 - Bartlett/Youd Parameters and Displacement Predictions at Location #3 -- R=30km.....	249
Table D.1.3 - Bartlett/Youd Parameters and Displacement Predictions at Location #4 -- R=30km.....	249
Table D.1.4 - Bartlett/Youd Parameters and Displacement Predictions at Location #8 -- R=30km.....	250
Table D.1.5 - Bartlett/Youd Parameters and Displacement Predictions at Location #2 -- R=60km.....	250
Table D.1.6 - Bartlett/Youd Parameters and Displacement Predictions at Location #3 -- R=60km.....	250
Table D.1.7 - Bartlett/Youd Parameters and Displacement Predictions at Location #4 -- R=60km.....	251
Table D.1.8 - Bartlett/Youd Parameters and Displacement Predictions at Location #8 -- R=60km.....	251
Table D.2.1 -- Hamada Parameters and Predictions at Location #2.....	253
Table D.2.2 -- Hamada Parameters and Predictions at Location #3.....	253
Table D.2.3 -- Hamada Parameters and Predictions at Location #4.....	253

Table D.2.4 -- Hamada Parameters and Predictions at Location #8.....	254
Table D.3.1 - Tokimatsu/Seed Parameters and Predictions at Location #2.....	255
Table D.3.2 - Tokimatsu/Seed Parameters and Predictions at Location #3.....	255
Table D.3.3 - Tokimatsu/Seed Parameters and Predictions at Location #4.....	255
Table D.3.4 - Tokimatsu/Seed Parameters and Predictions at Location #8.....	255
Table E.1 - Correction Factors for Earthquake Magnitude.....	258
Table F.1 - Blowcounts Required to Prevent Liquefaction at Location #2.....	259
Table F.2 - Blowcounts Required to Prevent Liquefaction at Location #3.....	259
Table F.3 - Blowcounts Required to Prevent Liquefaction at Location #4.....	259
Table F.4 - Blowcounts Required to Prevent Liquefaction at Location #7.....	260
Table F.5 - Blowcounts Required to Prevent Liquefaction at Location #8.....	260
Table G.2.1 - Test Information and Summary of Silt Test Results (BC Hydro, 1991).....	291

List of Figures

Figure 2.1 - Map of Fraser Delta.....	5
Figure 2.2 - Layout of Construction Site.....	6
Figure 2.3 - George Massey Tunnel Cross-section.....	8
Figure 2.4 - Overhead (plan) View of Cone Penetration Test and Preconstruction Borehole Locations.....	10
Figure 2.5 - Locations of Test Holes -- Profile View.....	11
Figure 3.1 - Target Spectrum Corresponding to the Mean+1 σ Level of Attenuation.....	16
Figure 4.1 - Seismic Assessment Procedure Flowchart.....	20
Figure 4.2 - Relationship Between Stress Ratios Causing Liquefaction and $(N_1)_{60}$ for M=7.5 Earthquakes.....	24
Figure 4.3 - K_o vs. Effective Overburden Pressure -- Comparison of Duncan Dam Estimations with Other K_o Curves.....	25
Figure 4.4 - Correlation Between Normalized Shear Wave Velocity and Cyclic Stress Ratio (CSR) to Cause Liquefaction.....	31
Figure 4.5 - Idealized Post-cyclic Stress-strain Response.....	40
Figure 4.6 - Shear Strains as a Function of Factor of Safety to Liquefaction and $(N_1)_{60}$	43
Figure 4.7 - Shear Strains and Likely Damage as a Function of $(N_1)_{60}$ if Liquefaction is Triggered.....	44
Figure 4.8 - Determination of Volumetric Strains in Saturated Sands.....	51
Figure 5.1 - Comparison of Soil Data at Location #2.....	68
Figure 5.2 - Comparison of Soil Data at Location #3.....	69
Figure 5.3 - Comparison of Soil Data at Location #4.....	70
Figure 5.4 - Comparison of Soil Data at Location #7.....	71
Figure 5.5 - Comparison of Soil Data at Location #8.....	72

List of Figures

Figure 6.1 - Zones of Liquefaction in Profile View.....	75
Figure 6.2 - Comparison of Cyclic Stress and Cyclic Resistance Ratios at Location #2.....	78
Figure 6.3 - Factor of Safety Against Liquefaction (FS_L) at Location #2.....	80
Figure 6.4 - Factor of Safety Against Liquefaction (FS_L) at Location #3.....	82
Figure 6.5 - Factor of Safety Against Liquefaction (FS_L) at Location #4.....	83
Figure 6.6 - Comparison of Cyclic Stress and Cyclic Resistance Ratios at Location #7.....	85
Figure 6.7 - Factor of Safety Against Liquefaction (FS_L) at Location #7.....	87
Figure 6.8 - Comparison of Cyclic Stress and Cyclic Resistance Ratios at Location #8	88
Figure 6.9 - Factor of Safety Against Liquefaction (FS_L) at Location #8	90
Figure 6.10 - Post-liquefaction Limit Equilibrium Stability Analysis at Location #7 (South Shore Dyke).....	93
Figure 6.11 - Post-liquefaction Limit Equilibrium Stability Analysis at Location #8 (South Shore Dyke).....	94
Figure 6.12 - Material Numbering Scheme for Transverse Sections at Onshore Locations.....	97
Figure 6.13 - Material Numbering Scheme for Transverse Sections at Offshore Locations.....	98
Figure 6.14 - Material Numbering Scheme for Longitudinal Section.....	99
Figure 8.1 - Final Stratigraphy at Location #7.....	116
Figure 8.2 - Final Stratigraphy at Location #8.....	118
Figure 8.3 - Displacement Pattern -- Location #7.....	120
Figure 8.4 - Displacement Vectors -- Location #7.....	121
Figure 8.5 - Displacement Pattern -- Location #8	123
Figure 8.6 - Displacement Vectors -- Location #8	124

List of Figures

Figure 8.7 - Final Stratigraphy at Location #2.....	126
Figure 8.8 - Final Stratigraphy at Location #3.....	127
Figure 8.9 - Final Stratigraphy at Location #4.....	129
Figure 8.10 - Displacement Pattern for Case #1 -- Location #2.....	132
Figure 8.11 - Displacement Vectors for Case #1 -- Location #2.....	133
Figure 8.12 - Displacement Pattern for Case #1 -- Location #3.....	134
Figure 8.13 - Displacement Vectors for Case #1 -- Location #3.....	135
Figure 8.14 - Displacement Pattern for Case #1 -- Location #4.....	136
Figure 8.15 - Displacement Vectors for Case #1 -- Location #4.....	137
Figure 8.16 - Displacement Pattern for Northern Half of Tunnel.....	144
Figure 8.17 - Displacement Vectors for Northern Half of Tunnel.....	145
Figure 8.18 - Displacement Pattern for Southern Half of Tunnel.....	146
Figure 8.19 - Displacement Vectors for Southern Half of Tunnel.....	147
Figure 10.1 - Displacement Pattern -- Remediation Case #D1.....	175
Figure 10.2 - Displacement Pattern -- Remediation Case #D2.....	176
Figure 10.3 - Displacement Pattern -- Remediation Case #D3.....	178
Figure 10.4 - Displacement Vectors -- Remediation Case #D3.....	179
Figure 10.5 - Displacement Pattern -- Remediation Case #D4.....	181
Figure 10.6 - Displacement Vectors -- Remediation Case #D4.....	182
Figure 10.7 - Displacement Pattern -- Remediation Case #D5.....	184

Figure 10.8 - Displacement Vectors -- Remediation Case #D5.....	185
Figure 10.9 - Displacement Pattern -- Remediation Case #D6.....	187
Figure 10.10 - Displacement Vectors -- Remediation Case #D6.....	188
Figure A.1.1 - Displacement Pattern for Case #2 -- Location #2.....	202
Figure A.1.2 - Displacement Pattern for Case #2 -- Location #3.....	203
Figure A.1.3 - Displacement Pattern for Case #2 -- Location #4.....	204
Figure A.1.4 - Displacement Pattern for Case #3a (4 meters of Sediment Loading).....	206
Figure A.1.5 - Displacement Pattern for Case #3b (6 meters of Sediment Loading).....	207
Figure A.1.6 - Displacement Pattern for Case #4 (Increased Ground Velocity).....	209
Figure A.1.7 - Displacement Pattern -- Parallel to the Axis of the Tunnel.....	213
Figure A.1.8 - Displacement Vectors -- Parallel to the Axis of the Tunnel.....	214
Figure A.2.1 - Block on an Inclined Plane Subjected to a Velocity Pulse -- Newmark Model.....	215
Figure A.2.2 - Work-Energy Principle -- Extended Newmark.....	217
Figure A.2.3 - Work-Energy (Rigid-Plastic Behaviour) -- Newmark Model.....	219
Figure A.2.4 - SOILSTRESS -- Idealized Nonlinear Shear Modulus Estimation.....	223
Figure A.2.5 - SOILSTRESS -- Idealized Nonlinear Bulk Modulus Estimation.....	224
Figure B.1.1 - Estimation of Shear Modulus and Damping -- SHAKE.....	225
Figure B.2.1 - Comparison of C.S.R.'s Using Varying Bedrock Velocities at Location #2.....	226
Figure B.3.1 - Ground Surface Spectral Response at Location #2.....	227
Figure B.3.2 - Ground Surface Spectral Response at Location #3.....	228

List of Figures

Figure B.3.3 - Ground Surface Spectral Response at Location #4.....	229
Figure B.3.4 - Ground Surface Spectral Response at Location #7.....	230
Figure B.3.5 - Ground Surface Spectral Response at Location #8.....	231
Figure C.1.1 - Post-liquefaction Limit Equilibrium Stability Analysis at Location #2.....	240
Figure C.1.2 - Post-liquefaction Limit Equilibrium Stability Analysis at Location #3.....	241
Figure C.1.3 - Post-liquefaction Limit Equilibrium Stability Analysis at Location #4.....	242
Figure C.2.1 - Post-liquefaction Stability Analysis at Location #7 with Higher Residual Strength.....	244
Figure C.2.2 - Post-liquefaction Stability Analysis at Location #8 with Higher Residual Strength.....	245
Figure C.3.1 - Comparison of Undrained Critical and Yield Strength Ratios Back- -calculated from Field Case-histories.....	246
Figure C.4.1 - Relationship Between Residual Strength and $(N_1)_{60}$	247
Figure D.2.1 - Displacement Vectors and SPT Boreholes for Part of Niigata, Japan Analysis by Hamada.....	252
Figure E.1 - Ranges in K_α Factors.....	256
Figure E.2 - Relationship Between Volumetric Strain Ratio and Number of Cycles.....	257
Figure G.2.1 - Post-Cyclic Loading of Silt -- Test #HSS1 (BC Hydro, 1991).....	292
Figure G.2.2 - Post-Cyclic Loading of Silt -- Test #HSS2 (BC Hydro, 1991).....	293

ACKNOWLEDGEMENTS

This research project was carried out under the supervision of Dr. P.M. Byrne, whose expert advice, guidance, and confidence are gratefully acknowledged.

The project was done under contract with the British Columbia Ministry of Transportation & Highways (M.O.T.H). I am thankful for the financial support that facilitated the study.

I would like to very sincerely thank Dr. Turgut Ersoy for his support and advice throughout the course of this study. Special thanks are also extended to Dr. Hendra Jitno and Dr. Don Gillespie for providing their insight in the early stages of this project; it was a pleasure working with all of you.

And finally, thanks are offered to the support staffs at the ministry's Headquarters (Victoria), and Operations (Burnaby) branches; thank you for all of the little favours you provided.

Surinder Puar

April, 1996

Vancouver, British Columbia

CHAPTER 1

INTRODUCTION

1.1 Purpose

This report presents the results and recommendations of a geotechnical seismic response assessment of the George Massey Tunnel. The tunnel is in British Columbia's Fraser Delta region -- an area where liquefaction is a major concern. The purpose of this report is to assess the seismic response of the submerged portion of the tunnel, and the connecting sections at the north and south banks of the Fraser River.

The tunnel is owned and operated by the British Columbia Ministry of Transportation & Highways (M.o.T.H.). It represents a vital link across the lower Fraser River, between the municipalities of Richmond and Delta. The site is underlain by loose saturated soils that could liquefy during the analyzed 1:475 year earthquake event. Seismic performance of the tunnel depends on the extent of liquefaction, post-earthquake limit equilibrium stability, and the total deformations -- the main concern being liquefaction-induced displacements.

The study is developed in four stages. First, available data describing the extent of the soil deposits and their engineering properties were collected and analyzed to produce soil profiles describing the dynamic soil properties of the site. The second stage involved dynamic analysis to predict the ground response to design earthquake motions. The third stage consisted of limit equilibrium analyses using post-liquefaction strength and strain

parameters to determine post-liquefaction stability of the tunnel. The final stage entailed using empirical and numerical solution methods to estimate earthquake-induced displacements. These displacements are the result of inertia forces, and gravity forces acting on the softened liquefied zones. Displacements were computed using a finite element method, a closed form solution, and two empirical methods. The settlements that occur with time (due to dissipation of excess pore pressure) were also computed.

1.2 Scope and Organization of Thesis

General information about the site and structure are provided in Chapter 2. Input seismic motions and the design earthquake ground motions are described in chapter 3. The main purpose of this study is to assess post-liquefaction deformations. Both numerical and empirical methods were applied to assess the potential displacements. Finite element (numerical) deformation analyses are the focal point of this study. Descriptions of the liquefaction assessment procedures and the different methods used to assess liquefaction-induced displacements are found in chapter 4.

Information about the general and local geology of the area is presented in chapter 5. The methods used to interpret available soil data and the procedures used to estimate soil input parameters for the various analyses are also found in chapter 5. Summaries of the soil stratigraphy input parameters used in the analyses are found in chapter 6 and 8. Chapter 6 contains summaries of the results of the liquefaction and post-earthquake

stability analyses, and chapter 7 contains discussions about those results. Chapter 8 summarizes the results of the displacement analyses, and chapter 9 discusses those results.

The analyses are focussed on foundation response and do not deal with the structural integrity of the tunnel. In the finite element analyses there is some recognition of soil-structure interaction, but the tunnel structure is not analyzed. Although investigation of structural tolerances is beyond the scope of this investigation, remediation options to reduce earthquake-induced displacements have been analyzed. Chapter 10 is concerned with the effect that remediation schemes would have on the tunnel's response to earthquake loading, and also contains a preliminary retrofit recommendation. Chapter 11 contains the report's conclusions.

CHAPTER 2

SITE DETAILS

2.1 Site Location

The George Massey Tunnel crosses the south arm of the Fraser River between Lulu Island and Deas Island, connecting the municipalities of Richmond and Delta via Highway#99 (refer to figure 2.1). The boundary separating the two municipalities is approximately at the midpoint of the tunnel.

2.2 Tunnel Layout, Construction, and Cross-section Geometry

Because this study focusses on the geotechnical aspects of the tunnel's seismic response, the description of the tunnel's structural details has been kept to a minimum. (Refer to Hall et al. (1957) for a comprehensive review of the structural features of the tunnel).

The British Columbia Toll Highways and Bridge Authority commissioned the development of the tunnel in 1955. It was designed by the Danish firm of Christiani & Nielsen, and constructed by the Foundation of Canada Engineering Corporation from Montreal, Quebec. The project was completed in 1958.

As shown in figure 2.2, the tunnel consists of three general sections: the 550-meter Lulu Island (northern) approach, the subaqueous section consisting of six precast concrete elements spanning 630 meters, and the 335-meter Deas Island (southern) approach. The

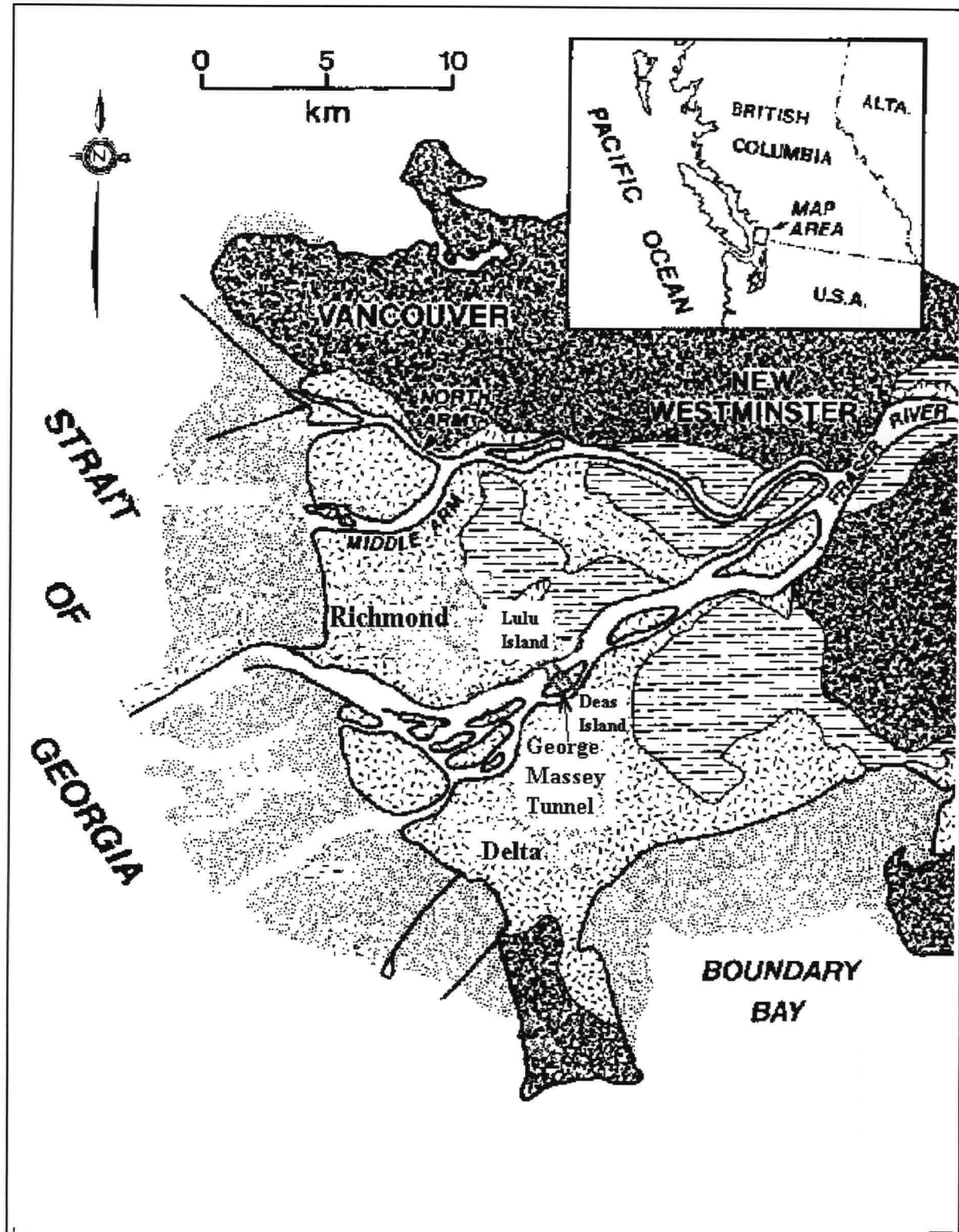


Figure 2.1: Map of Fraser Delta

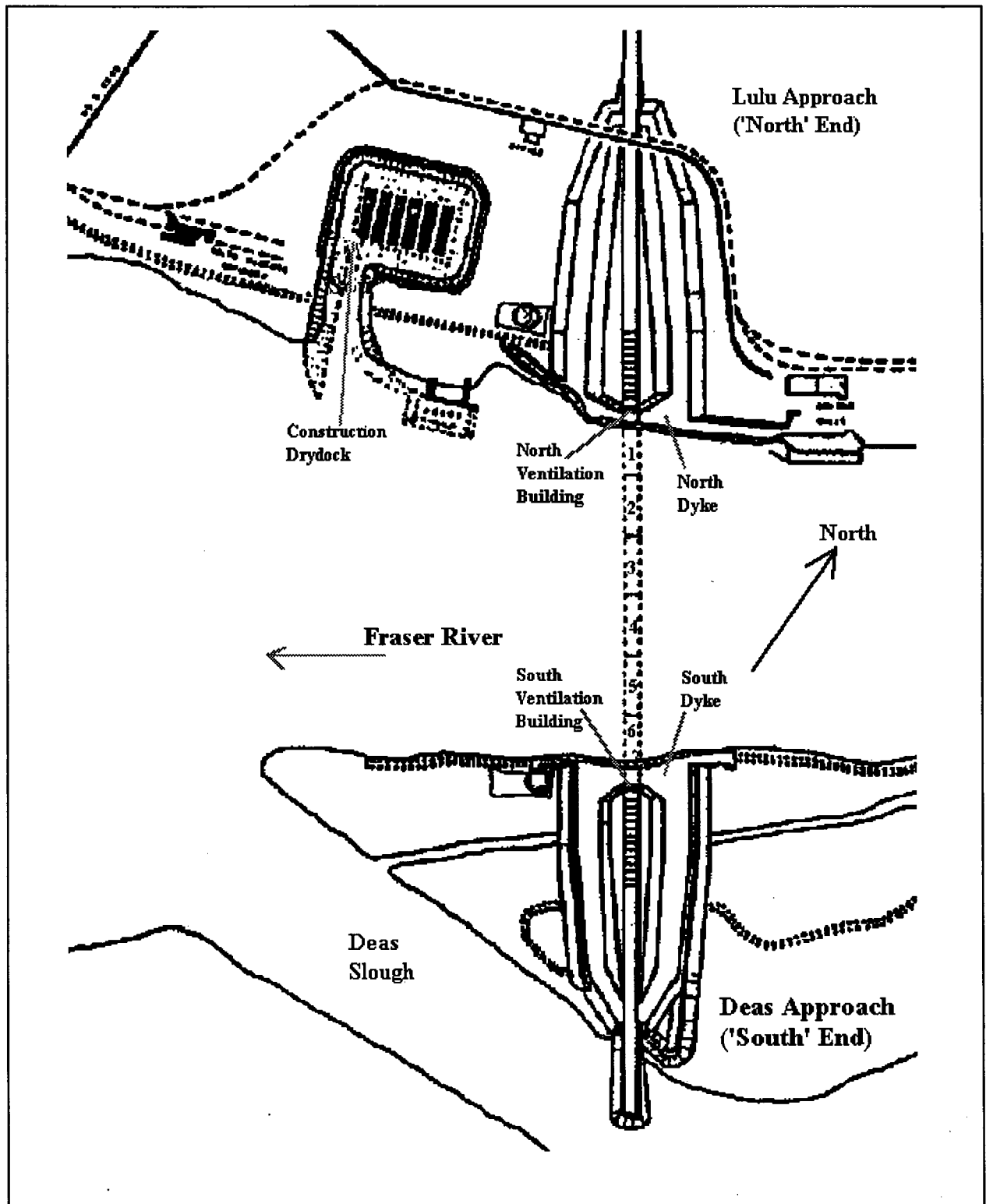


Figure 2.2: Layout of Construction Site

subaqueous portion of the tunnel consists of six precast concrete elements of rectangular cross-section. Each element is approximately 105 meters long, 24 meters wide, and 7.2 meters high. The six sections were constructed in a drydock, and were then floated out and sunk into position in a pre-dredged trench. Each element was placed on a series of foundation blocks, and hydraulic jacks were then used to position it vertically. Sand was jetted into the space between the bottom of the element and the excavation. Upon completion of the sand jetting, the remainder of the excavation was filled with gravel and rockfill materials (refer to figure 2.3). These materials prevent erosion and buoyant uplift of the tunnel. The trench side slopes were constructed to be shallow (1:3) to prevent refilling of the trench during excavation. Primary differential settlements were accounted for by applying a 3-month delay before constructing the structural joints that connect the subaqueous tunnel section to the ventilation buildings. The tunnel (in the cross-sectional plane) consists of two 2-lane roadways separated by a partition wall (refer to figure 2.3). Ventilation ducts run along the outer sides of the full length of the roadway. M.o.T.H provided copies of preconstruction and construction (as-built) drawings of the tunnel. These drawings were the main source for summarizing the tunnel geometry and layout. Tunnel dimensions were obtained from drawings #14-E-1615 and #14-E-1613, and the details of the protection plan (rip rap) from #14-J-1710. Based on drawing #14-E-1618, the 1500lb rock varies in thickness from 2.5 feet to 6.9 feet, so an average thickness of

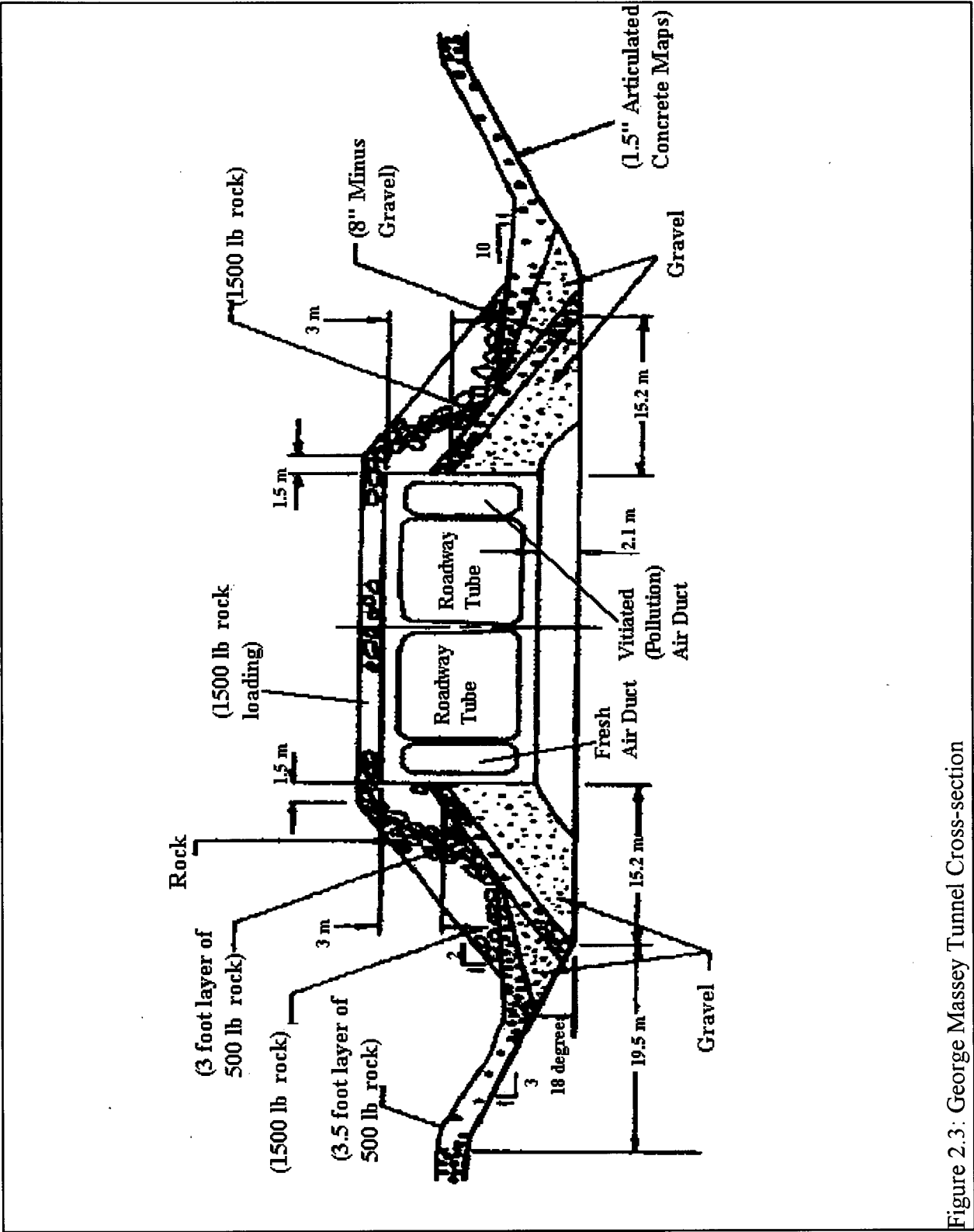


Figure 2.3: George Massey Tunnel Cross-section

4.7 feet was applied to construct the finite element meshes for the displacement analyses.

2.3 Locations of Analyses

The analyses correspond to the locations where five of six M.o.T.H Cone Penetration tests (CPT) were done. (The M.o.T.H CPT's are discussed in section 2.4). The five locations were chosen because both CPT and SCPT data were available there. Shown in figure 2.4 is an overhead (plan) view of the locations of the 1991 CPT's and the 1956 boreholes. The figure shows the offsets of the CPT's relative to the tunnel centerline. Figure 2.5 shows a profile view of the tunnel and the locations of the test holes. The locations have been numbered according to the original M.o.T.H 1991 CPT's (i.e., location #2 corresponds to CPT #91-2, etc.).

2.4 Available Information & Literature Review

In 1991, M.o.T.H undertook a geotechnical site investigation using current state-of-the-practice in-situ testing methods. Cone Penetration Tests (CPT), Seismic Cone Penetration tests (SCPT), and Standard Penetration Tests (SPT) were performed at the Lulu Island (north shore) and Deas Island (south shore) on-ramps, and at offshore locations. The offshore tests were performed at off-center locations that were outside the riprap boundaries on either side of the tunnel. The data was summarized and analyzed

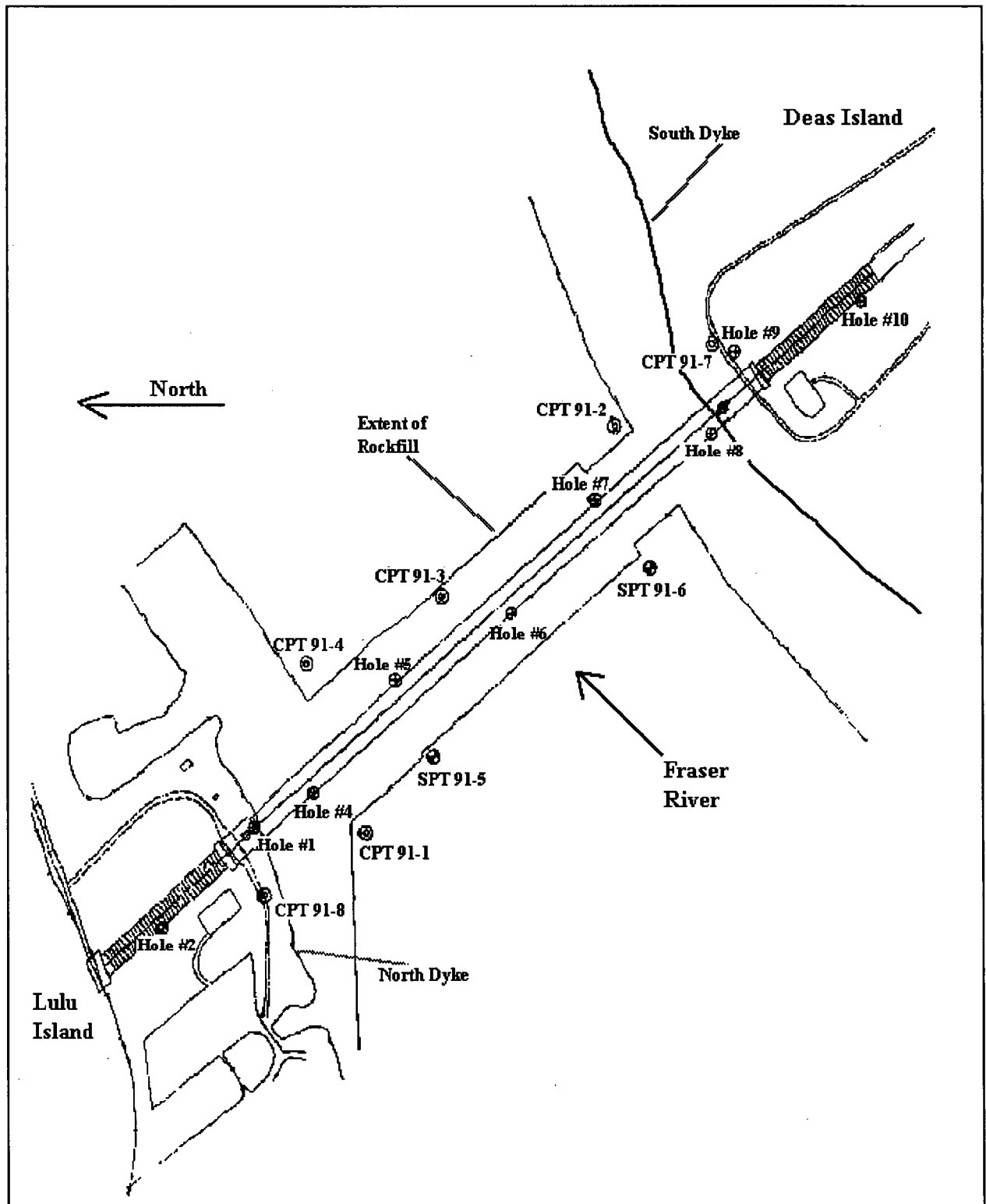


Figure 2.4: Plan View of Cone Penetration Test and Preconstruction Borehole Locations

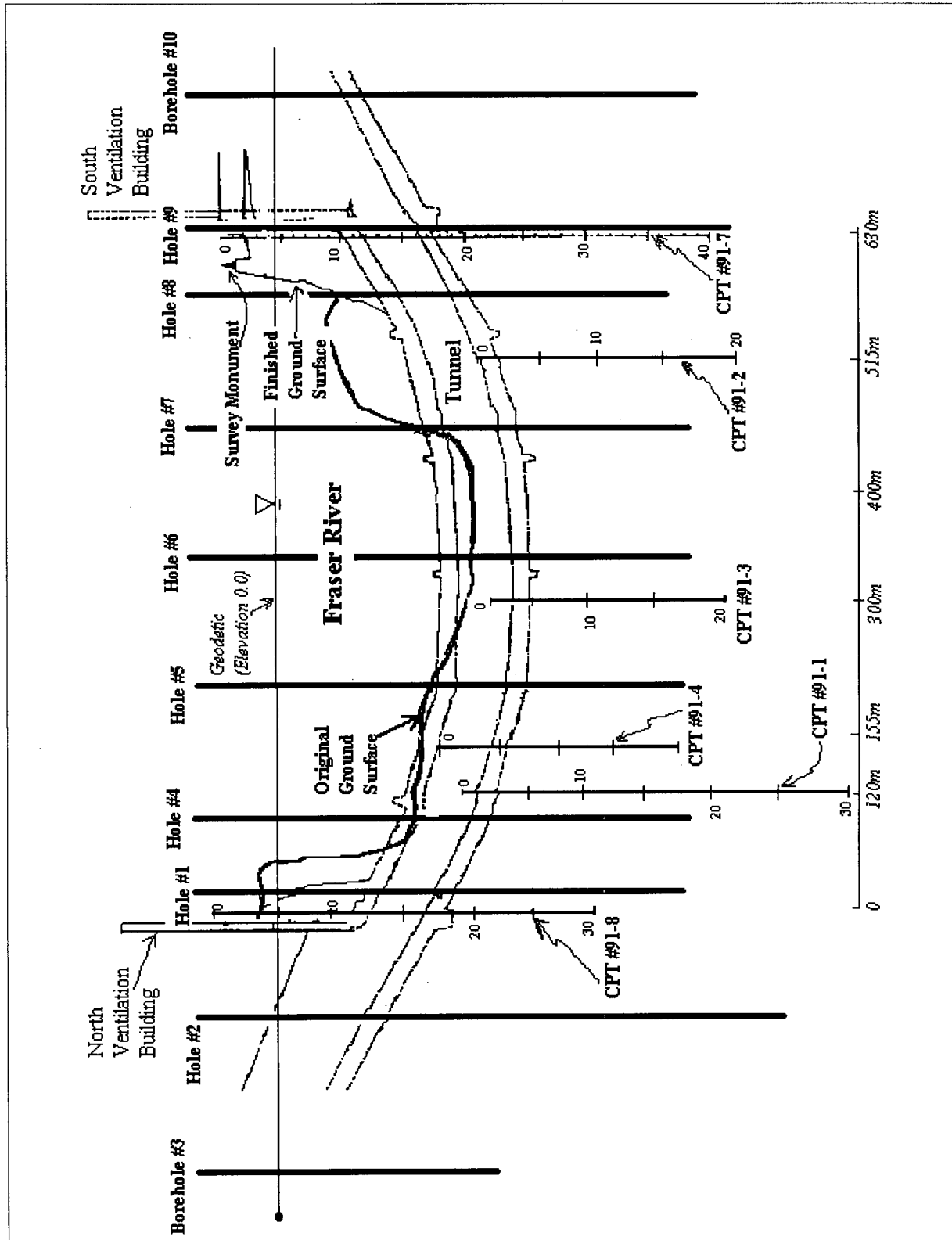


Figure 2.5 - Locations of Test Holes -- Profile View

for liquefaction potential in a report by Dr. Don Gillespie of M.o.T.H. Dr. Gillespie indicated that the foundation soils comprised mainly deltaic sands and silts that may be susceptible to liquefaction. Soil test data is limited. Before M.o.T.H.'s 1991 CPT's, soil data at the tunnel site was limited to the original Shelby tube and Dynamic Cone Penetration test (DCPT) data acquired during the preconstruction geotechnical site investigation in 1956. The firm of Ripley & Associates were responsible for acquiring and summarizing the data. Because no correlation exists between the DCPT and SPT, the penetration test data was of little value; however, the Shelby tube sample data played a significant role in this study.

Hall et al. (1957) described the site conditions, design requirements, and construction procedures that were to be applied in the development of the yet incomplete tunnel project. Traffic considerations and historical background are also discussed in the report.

In 1989, M.o.T.H. commissioned a preliminary seismic analysis of the tunnel. Ker Priestman & Associates (KPA) carried out a structural evaluation of the seismic response of the tunnel. Hardy BBT Ltd. (now known as Agra Earth & Environmental Ltd.) assessed available geotechnical data to provide parameters necessary for KPA's dynamic analysis of the tunnel's earthquake response. The geotechnical analysis was constrained by the lack of data relevant to current seismic analysis procedures.

CHAPTER 3

SEISMICITY & SEISMIC LOADING

3.1 Local Seismicity

In accordance with M.O.T.H Seismic Design and Rehabilitation Policy (1994) and the Fraser Delta Task Force Report (Anderson & Byrne, 1991) recommendations, a Richter magnitude $M7$ Maximum Design Earthquake (MDE) was selected in this study. The Task Force report predicts firm ground horizontal accelerations ranging between 0.16g and 0.27g, depending upon a site's location within the Fraser Delta. Results of a 1989 Pacific Geoscience Centre (PGC) seismic risk assessment at the north end of the tunnel are summarized in table 3.1. The table shows the peak ground accelerations and velocities with their respective return periods and probabilities of exceedance. The design earthquake corresponds to a return period of 475 years or, in other terms, a 10% probability of exceedance in a 50-year period (refer to table 3.1). A design peak horizontal ground acceleration of 0.24g was applied in this study.

Probability of exceedance in 50 years	40 %	22 %	10 %	5 %
Return Period (years)	100	200	475	1000
Peak Horizontal Ground Acceleration (g)	0.097	0.147	0.238	0.344
Peak Horizontal Ground Velocity (m/s)	0.078	0.124	0.219	0.334

Table 3.1 - Seismic Design Parameters for George Massey Tunnel Site

3.2 Seismic Loading for Ground Response Analyses

Seismic loading depends on the seismicity of the region and the level of risk the designer wishes to take. When choosing earthquake records (acceleration time-histories), ideally they should represent both local tectonic and soil conditions. Important factors to consider when assessing which input acceleration time-histories should be used are: earthquake magnitude, type (eg. strike-slip), duration, surface on which motions were recorded (i.e., rock or soil), frequency content, distance from epicenter to recording station, and focal depth. Acceleration time-histories recorded on bedrock are preferred because the frequency content, signal amplitude, and signal duration become altered after leaving the base bedrock and propagating up through the soil (Telford, W. et al., 1976).

The chosen design earthquake input motion is applied by the total stress dynamic ground response program SHAKE (described in section 4.2.3) as a base motion at an identified firm base within the soil profile. The SHAKE program scales the input accelerations to a site-specific firm ground maximum magnitude defined by the user (i.e., $a_{\max} = 0.24g$ at the tunnel site).

In this study, the recorded motions from the magnitude $M=6.4$ 1971 San Fernando, California earthquake were applied to the soil columns. Acceleration time-histories were modified to match a target response spectrum before being applied to the soil columns. (The next section describes the modification procedure). The chosen motions were those

recorded at three sites located less than 70 kilometers from the epicenter: Cal Tech Seismological Laboratory, Lake Hughes, and Griffith Park Observatory. Ground motion parameters recorded at the three sites are summarized in table 3.2.

Location	BASE Type	A (g)	V (m/s)	A/V (ratio)
Cal Tech	Granite	0.19	0.12	1.58
Griffith Park	Granite	0.18	0.21	0.86
Lake Hughes #4	Weathered Granite	0.17	0.06	2.83

Table 3.2 - Ground Motion Parameters From Chosen Earthquake Records

The PGC predictions of peak ground acceleration and velocity at the tunnel site for the 1:475 year earthquake are approximately 0.24g and 0.22m/s. Consequently, acceleration time-histories with A/V (acceleration/velocity) ratios approximately equal to 1 were preferred; although the Lake Hughes #4 record was an exception.

3.2.1 Modification of Acceleration Time-Histories

The 3 acceleration time-histories used in the ground response analyses were modified to match a target response spectrum before being applied in the SHAKE analyses. The target response spectrum (shown in figure 3.1) corresponds to the mean-plus-one standard-deviation level of attenuation.

To determine the target spectrum, Idriss' attenuation relation (1990) was applied.

(An attenuation relationship describes the decrease in a given earthquake ground motion parameter (Eg. peak acceleration) as a function, primarily, of both earthquake magnitude

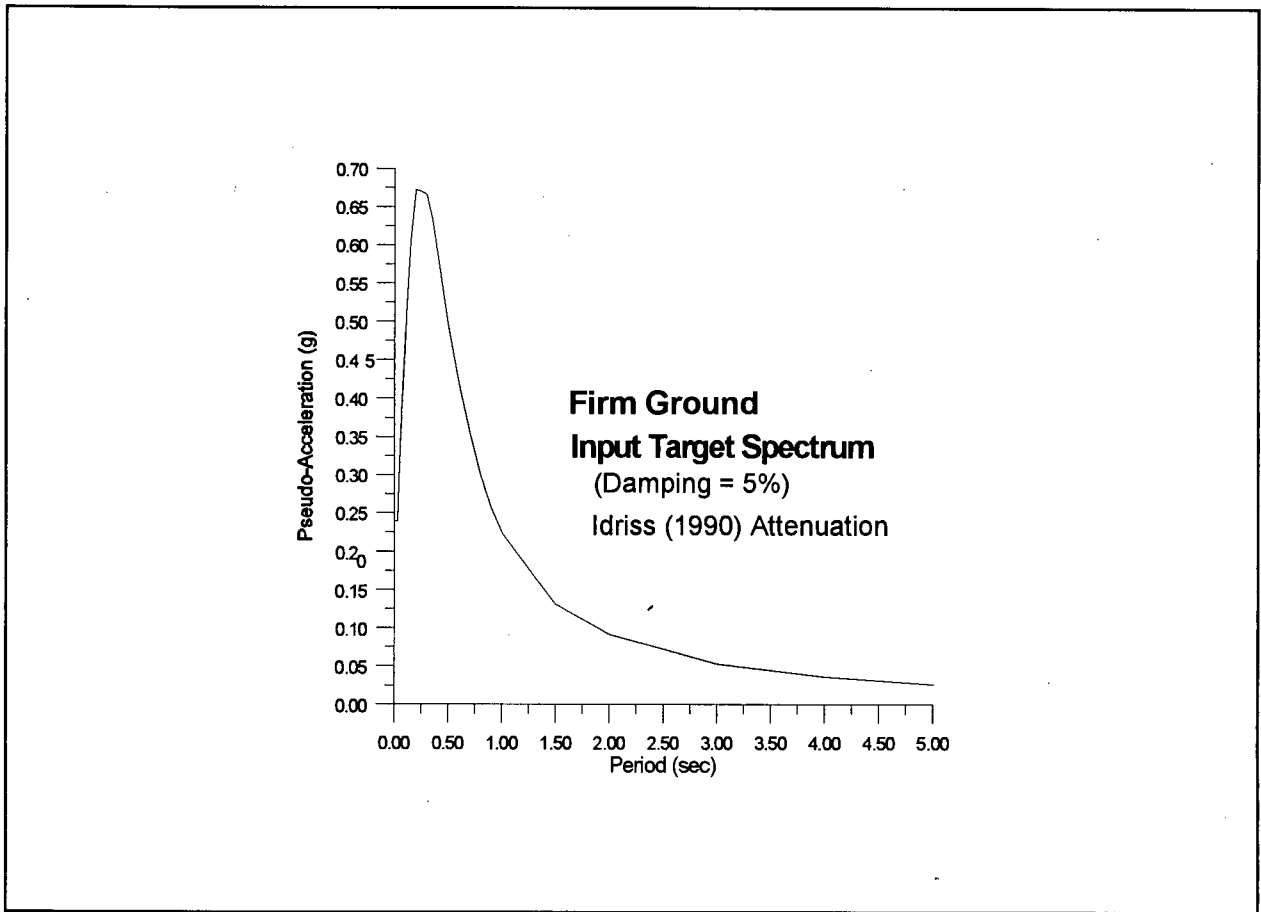


Figure 3.1 - Target Spectrum Corresponding to the Mean+1 σ Level of Attenuation

and the distance to the epicenter). All current attenuation relationships use a log-normal distribution to represent the ground motion parameters. The following equation estimates the attenuation in ground motion:

$$\ln(Y) = [\alpha_0 + \exp(\alpha_1 + \alpha_2 M)] + [\beta_0 - \exp(\beta_1 + \beta_2 M)] \ln(R + 20) + 0.2F + \varepsilon \quad (\text{Equation 3.1})$$

where: Y = the ground motion parameter, M = earthquake magnitude, R = closest distance to the source (in km), F = factor representing type of fault, ϵ = the standard error term, and values of α_n and β_n (summarized in appendix B.6) are for peak horizontal accelerations corresponding to a series of periods at a spectral damping ratio of 5%. As mentioned before, a suitable design earthquake for dynamic analysis in the Fraser Delta is one of magnitude 7.0, producing a bedrock acceleration of about 0.24g. An epicentral distance of 31 kilometers was applied in the attenuation estimate to anchor the target spectrum to a firm ground (i.e., period, $T=0$) acceleration of 0.24g.

The program SYNTH (Naumoski, 1985) was used to generate synthetic acceleration time-histories for each of the 3 records. The program generates an acceleration time-history whose response spectrum is a reasonable fit to a selected target spectrum. To match the computed artificial history's spectrum with the target spectrum, the computed spectrum is raised (or suppressed) iteratively as the Fourier coefficients are modified.

CHAPTER 4

ANALYSIS PROCEDURES & ENGINEERING PARAMETERS

4.1 Introduction

To analyze seismic response, two general approaches can be used:

- dynamic effective stress analysis, or
- total stress analyses.

A total stress equivalent-elastic dynamic analysis procedure was used in this study to evaluate the small strain onset of triggering. Unlike the total stress approach, the effective stress method attempts to capture the complete stress-strain--pore-pressure response of a soil element under cyclic loading. This approach accounts for both the small strain response and pore-pressure rise prior to triggering, as well as the large strain response after triggering. These results are then incorporated in a finite element analysis to predict the development of zones of liquefaction and the ensuing deformations. Refer to Finn et al. (1986) for an example of a proposed dynamic effective stress procedure. Although the effective stress approach is the most realistic, due to the nature of the data at this site, the determination of the dynamic soil properties would have been limited; consequently, the total stress analysis procedure was used in this study.

The main concerns when assessing liquefaction are:

- 1.) What level of cyclic stresses will trigger liquefaction(?), and if triggered
- 2.) What is the residual strength, and is it sufficient to prevent a flow slide(?), and

3.) What deformations will occur?

To evaluate these concerns, the procedure was uncoupled as follows:

- 1.) Assess which zones will be triggered to liquefy using a conventional total stress dynamic analysis procedure (explained in section 4.2),
- 2.) Use limit equilibrium stability analyses -- applying post-liquefaction residual strengths in the liquefied zones -- to assess flow failure (explained in section 4.3),
- 3.) Estimate liquefaction-induced displacements (section 4.4) using:
 - a.) empirical methods, and
 - b.) numerical methods,
- 4.) Estimate the further settlements that occur with time due to dissipation of excess pore-pressures.

A flow chart outlining the general framework used to do the seismic response analysis is shown in figure 4.1. Sections 4.2 to 4.4 present the procedures used to perform steps 1 to 4, as well as the methods used to estimate the engineering parameters required for each analysis.

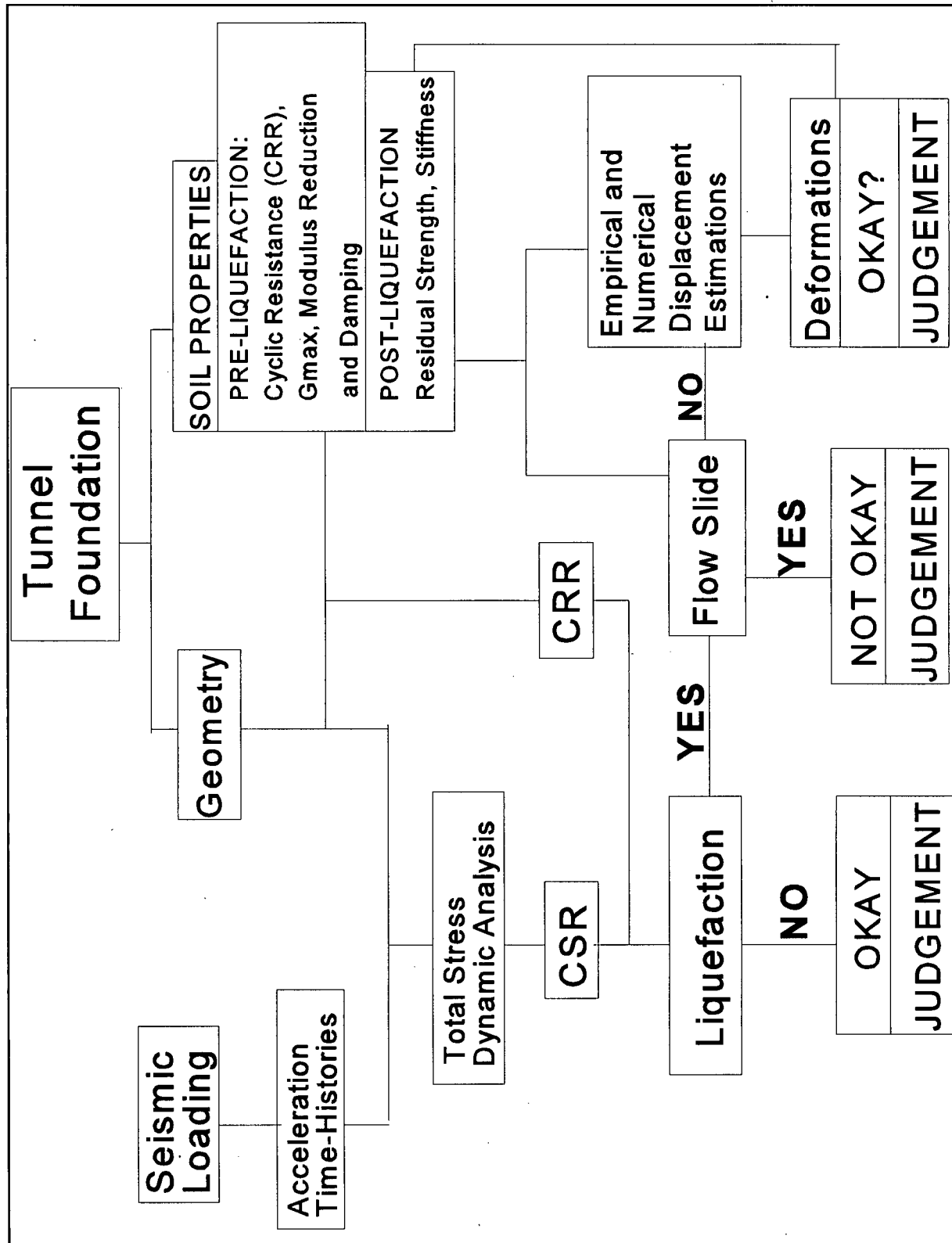


Figure 4.1 - Seismic Assessment Procedures Flowchart

4.2 Liquefaction Assessment

The characteristic behaviour of saturated granular soils under cycling loading is complex. Loose to medium dense sands and silts may be triggered to liquefy by the oscillating shear stresses induced by an earthquake. The shear strains required to trigger liquefaction are small -- generally between 0.1% and 1% (Byrne, 1991). Upon earthquake loading, granular soils undergo a pore-pressure rise during the sudden undrained loading condition; if the pore-pressures increase until they are equal to the overburden (total) stress, the effective stress in the soil will be nullified and, therefore, resistance to shear forces will be negated. Soil in this state is considered liquefied, and its behaviour resembles that of a dense fluid. Structures on (or in) the fluid soil will change elevation until their buoyant force is equal to the weight of the displaced fluid.

The liquefaction assessment procedure involves the analysis of each soil layer, and is segregated into 3 parts:

- i.) quantification of soil resistance (assessment of the cyclic resistance ratio, CRR) (sections 4.2.1 and 4.2.2), and
- ii.) quantification of dynamic earthquake effects (assessment of the cyclic stress ratio, CSR) (section 4.2.3),
- iii.) application of the liquefaction criterion.

The liquefaction criteria consists of a factor of safety against liquefaction (FS_L). The FS_L is simply the ratio of the CRR to the CSR ($FS_L = CRR/CSR$). If this ratio is

less than the prescribed value (for the site in question), then liquefaction is predicted to occur for that particular point within the soil. Depending on the type of structure, generally, a factor of safety between 1.1 and 1.4 is considered acceptable (Anderson, Byrne et al., Richmond Task Force -- 1991). In this study, when a FS_L less than 1.1 was estimated, that layer was predicted to liquefy.

It should be noted that the actual factor of safety is generally higher than that given by the FS_L ratio because the CRR is generally based on a lower bound of the observed data rather than an average value (Anderson, Byrne et al., 1991).

Results of the liquefaction assessments for each location are summarized in section 6.2.

4.2.1 Triggering Resistance (CRR) of Sands

Soil has an ability to resist cyclic loading defined in terms of its cyclic resistance ratio, $CRR = \tau/\sigma_o'$, where τ is the cyclic shear stress required to trigger liquefaction, and σ_o' is the initial effective normal stress. Factors that can affect the cyclic resistance of saturated sandy soils are: density, effective number of cycles (of loading), fines content, and existing static shear. The CRR is primarily dependent on soil density.

Triggering resistance of sands was determined using a procedure developed by Seed et al. (1984). The Seed correlation is an indirect method based on field penetration data obtained at sites where liquefaction has occurred. It should be noted that

liquefaction resistance can also be estimated from direct testing (of undisturbed soil samples). Refer to Pillai & Stewart (1994) for an example of the application and comparison of the two different approaches. Seed's liquefaction assessment chart (figure 4.2) correlates the CSR_{crit} (critical cyclic stress ratio to cause liquefaction) with normalized penetration resistance. The penetration resistance (denoted as $(N_1)_{60}$) is based on standard penetration values normalized to a confining stress of 1 T/Ft² and corrected to an energy level of 60%.

The applicable cyclic resistance is calculated by correction of the CSR_{crit} as follows:

$$CRR = (CSR)_{CRIT} \cdot K_\sigma \cdot K_M \cdot K_\alpha \quad (\text{equation 4.1})$$

where K_σ is an overburden pressure correction, K_M is an earthquake magnitude correction, and K_α accounts for existing static shear. The following sections describe the correction factors.

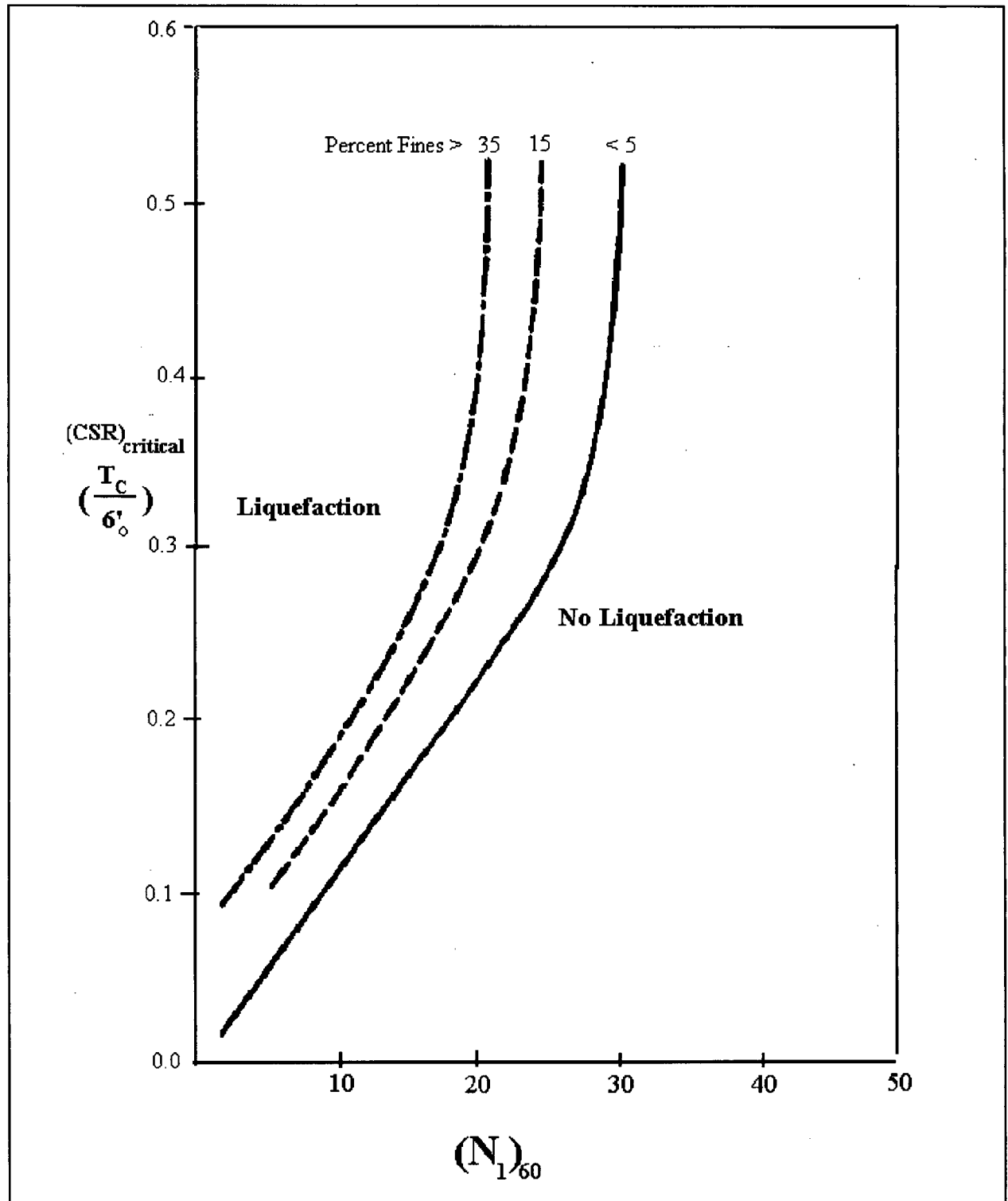


Figure 4.2 - Relationship Between Stress Ratios Causing Liquefaction and $(N_1)_{60}$ for $M=7.5$ Earthquakes (after Seed et al., 1984)

4.2.1.1 Overburden Pressure Correction (K_o)

Liquefaction is dependent upon the effective overburden stress -- the greater the effective stress, the greater the potential for liquefaction. This relationship is depicted in figure 4.3 by the decrease in K_o with increasing effective confining pressure. K_o values

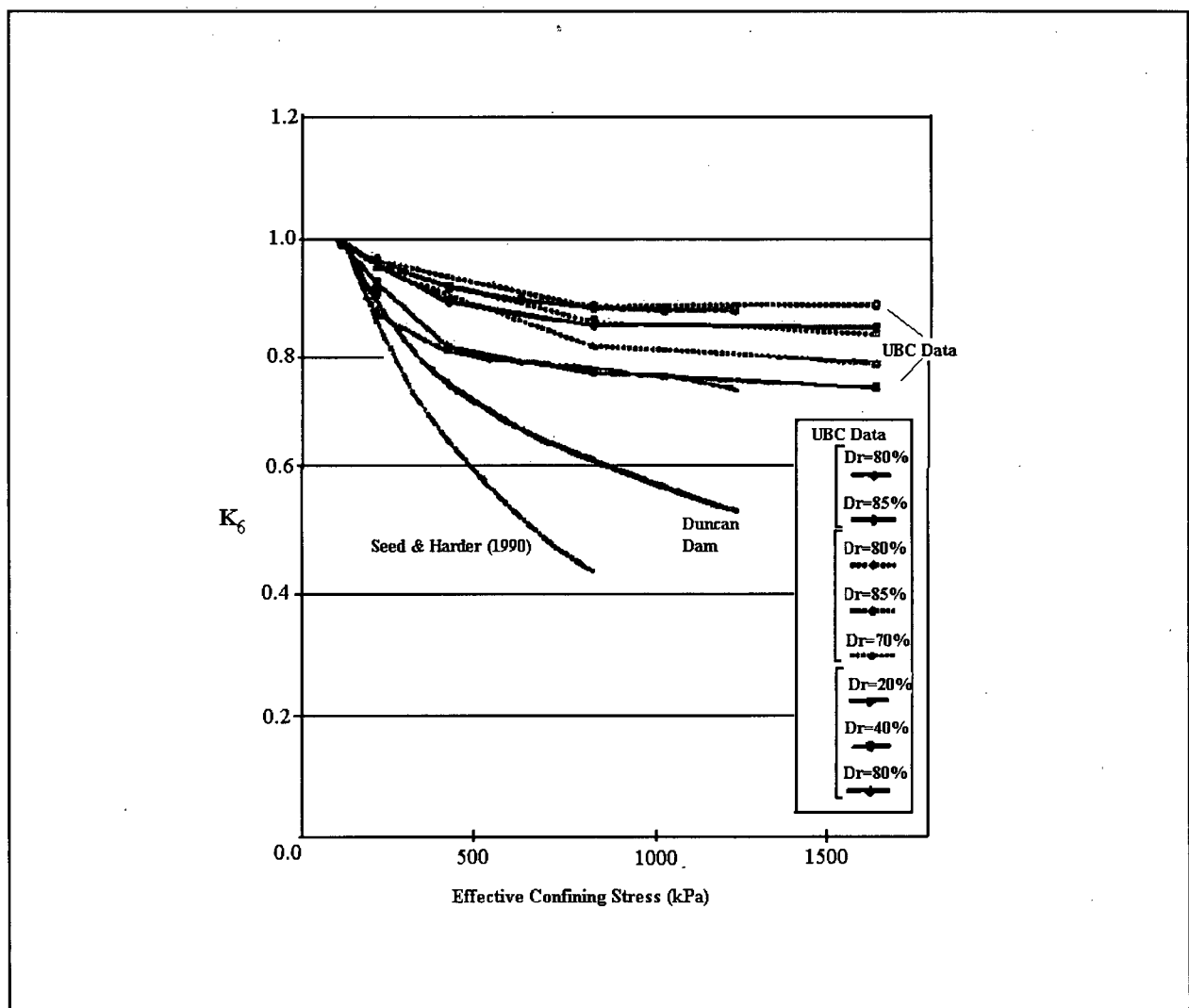


Figure 4.3 - K_o vs. Effective Overburden Pressure -- Comparison of Duncan Dam Estimations with Other K_o Curves (after Pillai & Byrne, 1994)

were estimated using a correlation (figure 4.3) published by Pillai & Byrne (1994). The 'Duncan Dam' curve was developed by comparing test results of CRR with estimations based on Seed's method. Tests were conducted on frozen samples taken during the extensive field tests for the Duncan Dam study. Figure 4.3 shows the Duncan Dam curve and the commonly used one developed by Seed and Harder (1990). The Seed & Harder curve is based on penetration resistance, and was developed from laboratory tests. The Seed & Harder field experience data base is limited to confining stresses of approximately 100 kPa. Additionally, figure 4.3 shows the results of laboratory test data carried out at the University of British Columbia (UBC) on both natural and tailings sands (Vaid & Thomas, 1994).

As the figure shows, the UBC tests reveal that sand type has little effect, whereas the sand's density (i.e., relative density -- D_r) does have a noticeable effect on K_o . The UBC estimates of K_o are much larger than those of Seed & Harder (1990). The choice of which curve to use is critical in estimating the cyclic shear resistance of the soil. For instance, use of the Seed & Harder curve may lead to lower CRR's, whereas use of the UBC results may lead to an overestimation of the CRR.

As figure 4.3 shows, the Duncan Dam curve lies between the UBC and Seed & Harder curves. Since the liquefaction testing of the Duncan Dam foundation soils was very comprehensive, the use of those results is more appropriate than the use of the Seed & Harder results. Furthermore, since the UBC test results indicate that sand type does

not have a significant effect on K_σ , the Duncan Dam curve should be applicable to the sands of the Fraser Delta.

4.2.1.2 Magnitude Correction (K_M)

Seed's chart (figure 4.2) is for an earthquake magnitude of 7.5 corresponding to 15 cycles; therefore an earthquake magnitude correction $K_M = 1.1$ was applied, as suggested by Seed (refer to table E.1 in appendix E), to account for the design magnitude 7, which is expected to produce approximately 12 effective cycles of dynamic loading.

4.2.1.3 Static Shear Correction (K_α)

A static bias (static driving shear stresses) can significantly decrease the liquefaction resistance of loose soils. ' α ' is defined as the ratio of shear stress on the horizontal plane to the effective normal stress. The factor ' α ' is used to estimate K_α ; K_α is the correction factor (in equation 4.1) that takes into account the effects of initial static bias on the horizontal plane.

Rigorous finite element programs can be used to estimate α (i.e., the existing stress state in non-level ground conditions). A correlation developed by Seed & Harder (1990) is commonly used to estimate K_α . (The Seed & Harder correlation is shown in figure E.1 (in appendix E)). K_α is the ratio of the CRR at the initial static shear stress to the CRR at zero static shear stress.

Because the Massey tunnel is founded on a level excavation, static shear is anticipated to be minimal; therefore, a value of $K_\alpha=1$ was assumed for this study. Refer to Pillai & Stewart (1994) for a correlation between K_α and α that was determined by direct testing of undisturbed sand samples.

4.2.1.4 Estimation of Fines Contents

The greater the fines content, the greater the resistance to liquefaction. Seed (1987) recommended that $(N_1)_{60}$ -values be corrected for fines content by adding to the blow count as shown in table 4.1.

Fines Content (%)	$(N_1)_{60}$
10	1
25	2
50	4
75	5

Table 4.1 - Corrections to Measured $(N_1)_{60}$ for Fines Content

In this study, fines content estimates for sands were derived from two sources. The off-center CPT data was compared with the original Shelby tube samples that were obtained along the tunnel centerline. First, a CPT-based estimate was derived: friction (F_r) ratio and pore pressure (B_q) ratio soil classification zone values were used to estimate the fines content of the sands. This procedure is explained in detail in the Robertson & Campanella publication, "Guidelines for use, interpretation and application of the CPT

and CPTU” (1986). Soil classification types 8 and 9 were presumed to contain approximately 5% fines, type 7 was taken to contain 15%, and type 6 was assumed to contain 35% fines. The estimates derived from that procedure were compared with the preconstruction borehole data obtained along the centerline of the tunnel. The comparison of the data at each location is discussed in more detail in section 5.3.

4.2.2 Triggering Resistance (CRR) of Fine-Grained Soils

4.2.2.1 Non-plastic Silts

To assess the liquefaction resistance of non-plastic silts, both the Seed (1984) approach (refer to section 4.2.1) and a shear wave velocity-based criteria were applied. The Seed (1984) data base represents an upper bound fines content of 35%. Fines content corrections were applied as discussed in section 4.2.1.4.

A shear wave velocity criteria published by Robertson (1990) was also applied to assess the liquefaction resistance of non-plastic silts. Accurate shear wave velocity profiles can be determined using current seismic downhole methods. Shear wave velocity is influenced by many variables that affect liquefaction resistance, such as soil density, confinement, stress history, and geologic age; therefore, V_s is a promising field index for evaluating liquefaction susceptibility. The advantage of using shear wave velocity as an index of liquefaction resistance is that it can be measured in soils that are hard to sample, such as cohesionless silts and sands.

Shown in figure 4.4 is the proposed correlation between normalized shear wave velocity (V_{s1}) and the cyclic stress ratio necessary to cause liquefaction. Since shear wave velocity varies with void ratio and effective confining stress, the V_s of a sand of constant density will increase with increasing depth; consequently, the measured V_s magnitudes were normalized to the effective overburden stress:

$$V_{s1} = V_s \left(\frac{P_a}{\sigma'_{vo}} \right)^{0.25} \quad (\text{equation 4.2})$$

where V_{s1} is the normalized shear wave velocity, and P_a is atmospheric pressure expressed in the same units as the effective overburden pressure (σ'_{vo}).

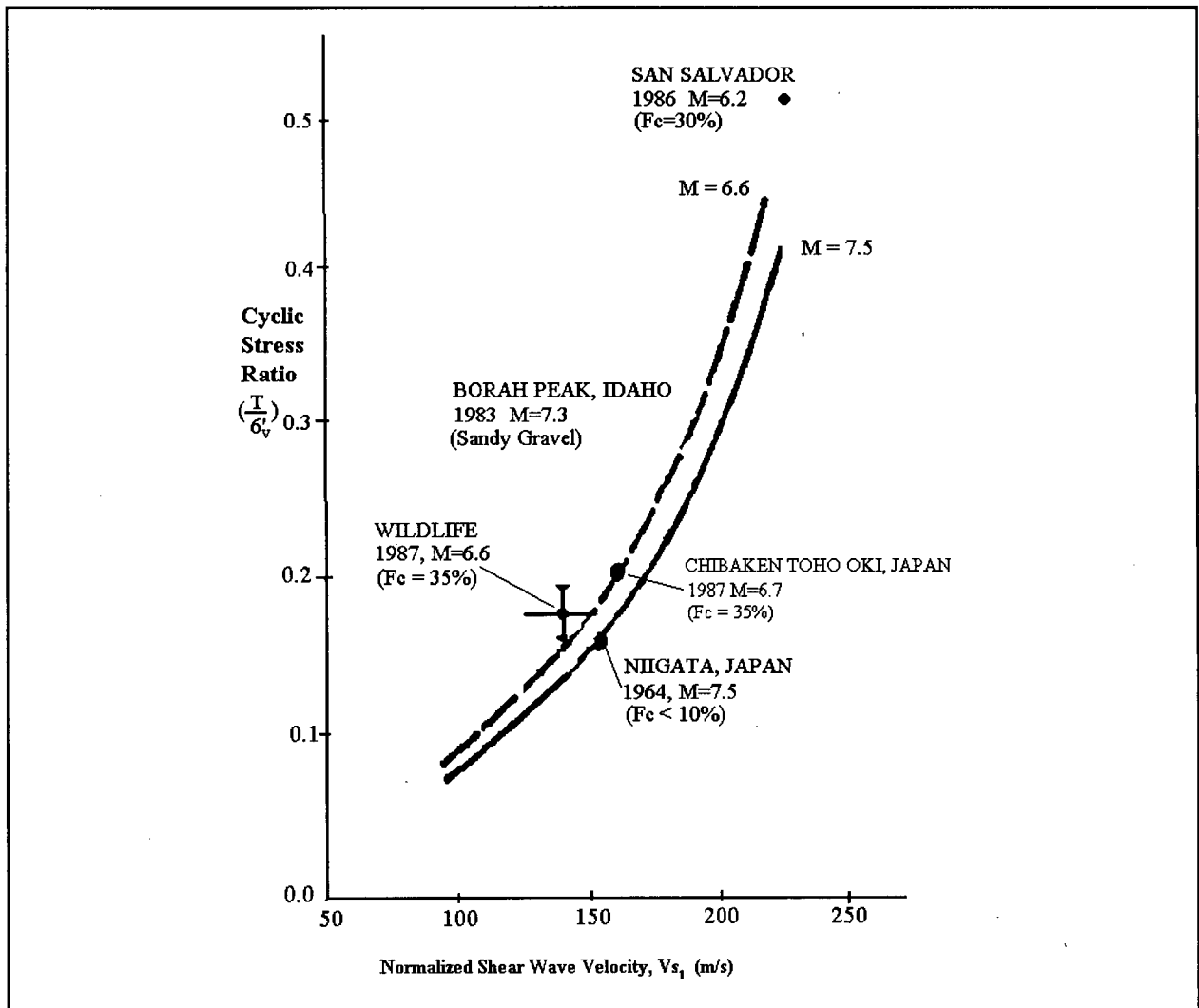


Figure 4.4 - Correlation Between Normalized Shear Wave Velocity and Cyclic Stress Ratio (CSR) to Cause Liquefaction (after Robertson, et al., 1990)

4.2.2.2 Liquefaction Assessment Procedure for Plastic Silts

In this study, when dealing with the liquefaction assessment of plastic silts, a different approach was used -- the Chinese criteria (Wang, 1979). The upper and lower limits of the range of water content over which a soil exhibits plastic behaviour are known as the liquid limit (L.L) and the plastic limit (P.L), respectively. The water content range itself is defined as the plasticity index (P.I) (i.e., $P.I. = L.L - P.L$).

The major variables that influence the liquefaction resistance of soils containing significant fines are the plasticity of the fines and the amount of clay size particles. If uncertainties in the measured soil variables can be accounted for, then the following criteria should be applied:

- | | |
|---|-----------------------|
| - percent finer than 0.005mm (#200 sieve) | $\leq 20\%$ |
| - liquid limit (L.L.) | $\leq 35\%$ |
| - natural water content (w_n) | $\geq 0.9 \cdot L.L.$ |
| - liquidity index (I_w) | ≥ 0.75 |
| AND/OR | |
| - SPT blows per foot ($(N1)_{60}$) | ≤ 4 |

Soils that satisfy the five criteria are considered vulnerable to liquefaction or significant strength loss.

If uncertainties in the measured variables cannot be accounted for, then the liquidity index should be ignored and the following criteria should be applied:

- | | |
|---|------------------------|
| - percent finer than 0.005mm (#200 sieve) | $\leq 15\%$ |
| - liquid limit (L.L.) | $\leq 36\%$ |
| - natural water content (w_n) | $\geq 0.92 \cdot L.L.$ |

The Chinese criteria are only a preliminary means of assessment, and should not be relied upon solely if the liquefaction resistance of a soil is questionable. If a soil fails the Chinese criteria, then its likelihood for liquefaction should be assessed by cyclic shear tests.

4.2.3 Estimation of Cyclic Loading (CSR)

To estimate the cyclic stress ratio (CSR), the maximum shear stress ($(\tau_c)_{\max}$) at the midpoint of each soil layer is normalized by dividing by the effective overburden stress (σ'_{vo}). Equation 4.3 estimates this uniform cyclic shear stress ratio (CSR):

$$CSR = 0.65 \cdot \frac{\tau_{c_{\max}}}{\sigma'_{vo}} \quad (\text{equation 4.3})$$

The factor 0.65 is applied to convert from a random loading to an equivalent uniform cyclic loading. The one-dimensional wave propagation analysis program SHAKE was used to estimate CSR's.

The computer code SHAKE -- a current state-of-the-practice total stress procedure -- was applied to estimate the small strain onset of triggering. The program conducts a total stress equivalent-elastic dynamic analysis; so, the effects of pore pressure development and dissipation, and soil hardening are not accounted for. A modified version of the SHAKE program (SHAKE [4]) was used; it allows nine different modulus reduction and damping curves to be used.

SHAKE uses the wave-equation method of solution, which is based on the theory of one-dimensional wave propagation in a continuous medium. The method assumes that the earthquake can be represented by a shear wave propagating vertically through soil layers that extend infinitely in the horizontal direction. Shear waves are input as

accelerations at equally spaced intervals. The wave equation methodology is discussed in the SHAKE instruction manual (Schnabel, Lysmer, and Seed, 1972). The SHAKE solution method is discussed in more detail in appendix B.1. The selection and modification of input ground motions (acceleration time-histories) for the SHAKE analyses is discussed in section 3.1.

The dynamic soil properties required for the analysis are: the maximum shear modulus (G_{\max}) at low strains; the reduction of G_{\max} with increasing shear strain; equivalent visco-elastic damping reduction curves, fraction of critical damping, total unit weights (γ_{sat}), and shear modulus coefficient ($K_{2\max}$). The methods used to estimate these parameters are discussed in upcoming sections (4.2.3.1 and 4.2.3.2).

To account for soil damping and modulus reduction, the data published by Sy et al. (1991) for the Fraser Delta were applied in the SHAKE analyses. The data is based on resonant column tests supplemented by other published data (Sy et al., 1991).

At all locations the estimated soil columns were taken to firm ground (Pleistocene) at a depth of 200 meters. (The firm ground estimate is discussed in detail in section 5.3). Input motions were applied at the top of the Pleistocene.

4.2.3.1 Maximum Shear Modulus (G_{\max})

The shear modulus at low strain amplitude (G_{\max}) was estimated from seismic downhole test shear wave velocity estimates. Estimates of G_{\max} were required for both

the ground response and deformation analyses.

The assessment of shear modulus was based on shear wave velocity (V_s) measurements:

$$G_{\max} = \rho \cdot V_s^2 \quad (\text{Equation 4.4})$$

where ρ is the soil density, and V_s is the shear wave velocity normalized with respect to effective overburden pressure (as described in section 4.2.2.1).

For comparison, low-strain shear moduli (G_{\max}) were also estimated using a relation based on penetration resistance proposed by Seed & Idriss (1970):

$$G_{\max} = 21.7 \cdot (K_2)_{\max} \cdot P_{\text{atm}} \cdot \left(\frac{\sigma'_m}{P_{\text{atm}}} \right)^{0.5} \quad (\text{Equation 4.5})$$

where,

$$(K_2)_{\max} = 10 \cdot ((N_1)_{60})^{0.6} \cdot F \quad (\text{Equation 4.6})$$

The relation for estimating the maximum shear modulus coefficient ($K_{2\max}$) was proposed by Harder & Byrne (1992). Generally, $K_{2\max}$ in sands ranges from 30 (loose) to 90 (dense). 'F' is a correction for material type: $F = 0.6$ in Silt, and $F = 1.0$ in Sand (Byrne, 1993). P_{atm} is atmospheric pressure, and σ'_m is the mean normal effective stress.

4.2.3.2 Surface Spectral Response

SHAKE was used to estimate the surface mean-plus-one standard deviation pseudo-acceleration response spectra for a damping ratio of 5%. The spectral response represents the response of a single-degree-of-freedom system to the estimated surface accelerations. Effectively, the single-degree-of-freedom system is subject to the acceleration time-history of the ground surface. Response spectra output at each of the five locations are summarized in appendix B.3.

4.3 Post-liquefaction Stability

Post-liquefaction performance of the tunnel was determined in terms of limit equilibrium stability. Stability (and the extent of deformation) depends on the shear stiffness and undrained residual shear strength.

In this section, the procedure for assessing the potential for a flow slide is initially discussed (section 4.3.1). A description of the methods used to estimate post-liquefaction strength and stiffness parameters follows (sections 4.3.2 and 4.3.3).

4.3.1 Flow Slide

Liquefaction of soil layers can lead to the development of a flow slide (unlimited strain). A flow slide occurs when driving stresses exceed the peak post-liquefaction ('residual') strength of the soil. (Residual strength (S_r) is discussed in the next section). Even if a flow slide does not result, lateral spreading may occur due to soil softening upon liquefaction.

To assess flow slide potential, limit equilibrium analyses were performed using Bishop's (Bishop, 1955) method of irregular surfaces. The analyses required defining the tunnel structure and foundation geometry. Reduced post-liquefaction strengths were applied to liquefied layers. A factor of safety against flow slide ($(F.S.)_{FL}$) was set at 1.3, since this value is commonly used to represent the post-earthquake short-term undrained

failure condition (Pillai & Salgado, 1994).

Analyses at the three offshore locations (described in section 2.3) were performed for tunnel cross-sections (i.e., in the plane transverse to the tunnel roadway). The north and south river banks (locations #8 and #7, respectively) were analyzed in the longitudinal plane. Results of the analyses are summarized in section 6.3.

4.3.2 Residual Strengths (S_r)

As discussed earlier, a soil is considered liquefied when pore-pressure rises to equal the total stress. After liquefying, sand shows a strain-hardening response due to dilation and the consequent pore-pressure decrease, which leads to increased effective stress (as strains increase). The soil will recover some strength at large deformations; the maximum strength it regains is termed the residual strength (S_r).

The relative density (D_r) of the soil will dictate how much dilation will occur after liquefaction; therefore, the D_r of the soil will control how much residual strength the soil can develop. Figure 4.5 graphically shows the applicable shear stress-strain relations as an idealized bilinear curve with initial slope equal to the shear modulus (G_L) of the liquefied soil, leading to the horizontal line at which the residual strength (S_r) is then in effect.

The proposed bilinear post-liquefaction stress-strain curve models have been

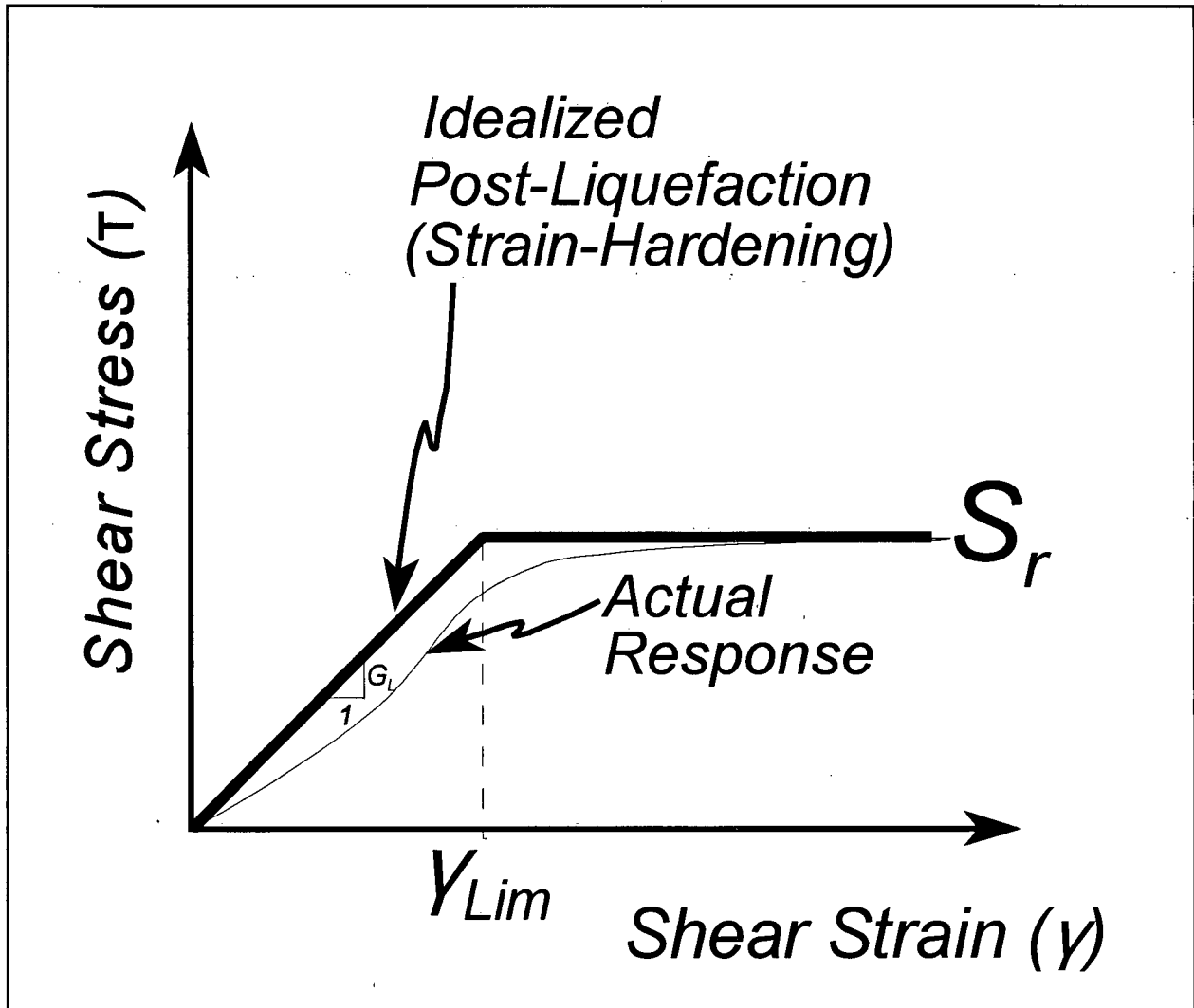


Figure 4.5 - Idealized Post-liquefaction Stress-strain Response

validated on samples from BC Hydro's Duncan Dam (Byrne et al., 1994). The preliminary results from testing carried out on undisturbed frozen core samples show that the post-liquefaction stress-strain relations can be adequately modelled as a bilinear curve. The test results confirm that, lacking site-specific laboratory tests, a reasonable

estimate of the bilinear post-liquefaction stress-strain curve can be obtained by using the methods described below to estimate the residual strength (S_r) and the limiting strain (γ_{Lim}). The Extended Newmark (Byrne, 1990) displacement estimation method recognizes this stress-strain relation. (Liquefaction-induced displacements are discussed in upcoming sections).

Within this study, the post-liquefaction stress-strain parameter estimates for sands are based on penetration resistance ($(N_1)_{60}$) magnitudes. Parameter estimates for silt are based on laboratory monotonic and cyclic load test results on samples from another site.

Stark & Mesri (1992) showed that the post-liquefaction (residual) shear strength of sands varies with effective vertical stress (σ'_{vo}), as opposed to common assumptions which disregard the link between residual strength and effective stress. Additionally, analyses of undisturbed soil samples from the Duncan Dam suggested that undrained shear strength is proportional to the initial consolidation effective vertical stress (Pillai & Salgado, 1994). The Stark & Mesri relation was developed through comparison with the $(N_1)_{60}$ -based correlation by Seed & Harder (1990). For reference and comparison, the Seed & Harder (1990) correlation is discussed in more detail in appendix C.4.

Stark & Mesri (1992) applied a sampling and laboratory testing program in which a relationship between the critical strength ratio (α) and the equivalent clean sand SPT blow count was determined. Values of yield strength, at 15 equivalent cycles (earthquake magnitude, $M=7.5$), and critical strength ratio were measured using cyclic

triaxial, cyclic simple shear, and cyclic torsional shear tests.

In this study, a general relation based on the findings of Stark & Mesri (1992) was used for estimating the undrained residual shear strength of the sands and silts:

$$\frac{S_u}{\sigma'} = \alpha \quad (\text{equation 4.7})$$

where,

i.) in sands $\alpha = 0.07, 0.2-0.6, 0.6$ for $(N_1)_{60} = 0-4, 10-14$, and $(N_1)_{60} \geq 15$, respectively

(Byrne, 1994a), and

ii.) in silts $\alpha = 0.4$ was applied. This value was derived from test data from BC

Hydro's Priority Transmission Tower Study (1990).

(The BC Hydro test results are summarized in appendix G.2). Sample #HSS1 showed the most similarity (i.e., in terms of Atterberg limits) to the non-plastic silts at the tunnel site, so that data was considered most suitable for this study.

Furthermore, to confirm the residual strength estimates in the silts, a relation suggested by Senneset (1981) was applied: $S_u = q_c' / N_c'$ where $q_c' = q_c - U_t$ and U_t is the total measured dynamic pressure, and N_c' varies between 9 and 20. This relation has been developed to assess the undrained shear strength of clays, but because the clay content of the silts is moderately high in some cases, the relation was assumed to be crudely applicable for comparison purposes.

Residual strength estimations are summarized in section 6.3.

4.3.3 Limiting Strains (γ_{Lim})

The limiting shear strain (γ_{lim}) is that strain at which dilation of the soil skeleton ceases, and the effective stress (and therefore, stiffness and strength) ceases to increase. The residual strength (S_r) of the soil is then considered in effect. (Refer to figure 4.5).

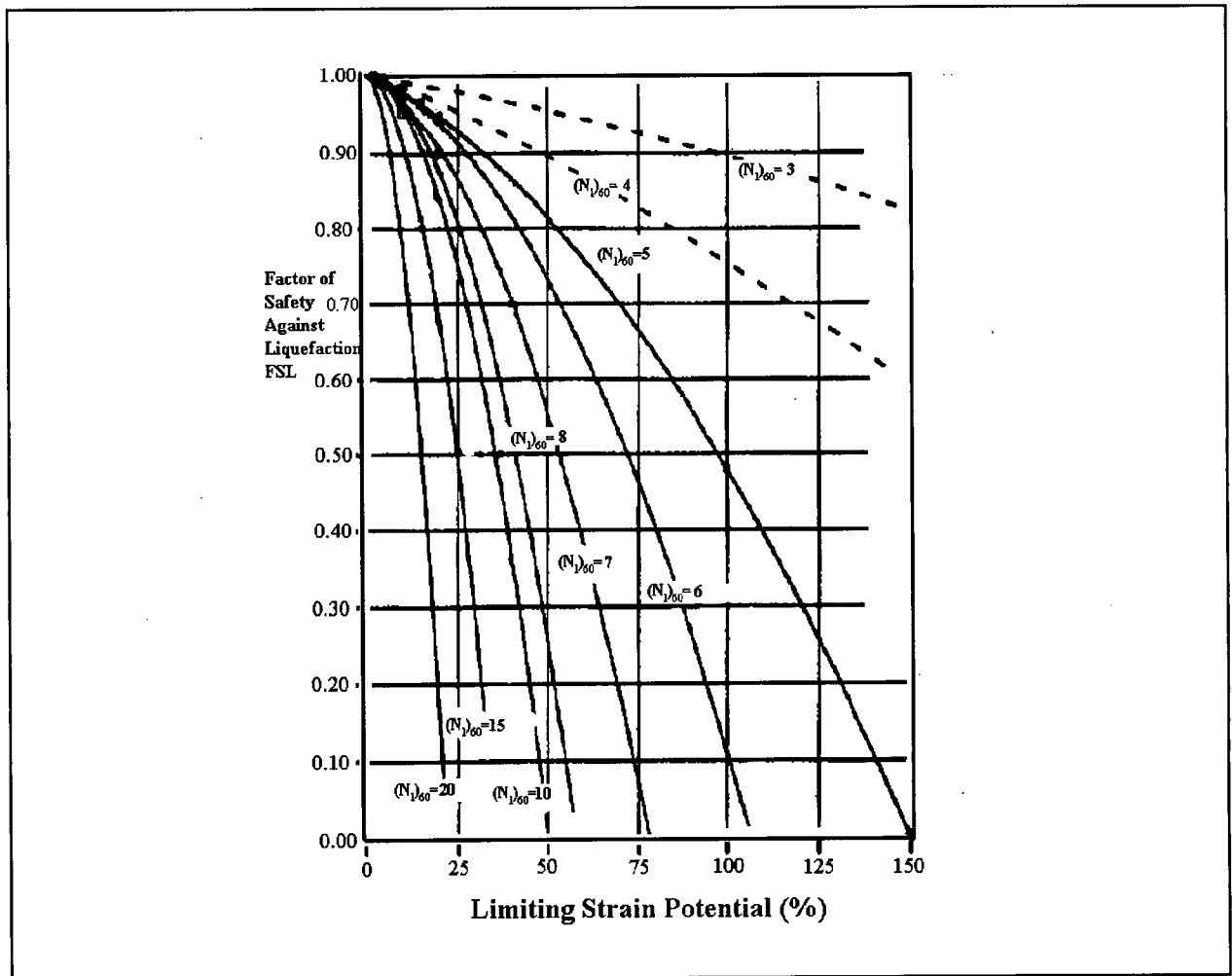


Figure 4.6 - Shear Strains as a Function of Factor of Safety to Liquefaction and $(N_1)_{60}$ (After Seed et al., 1986)

To estimate limit strains in sands, one of two methods was employed. First, if it

was possible to estimate the factor of safety against liquefaction $((FS)_L)$, then the Seed et al. (1986) graphic correlation (figure 4.6) was applied. The correlation requires blow counts $((N_1)_{60})$ and the $(FS)_L$ of the sand. (The procedures used to estimate the $(FS)_L$ are

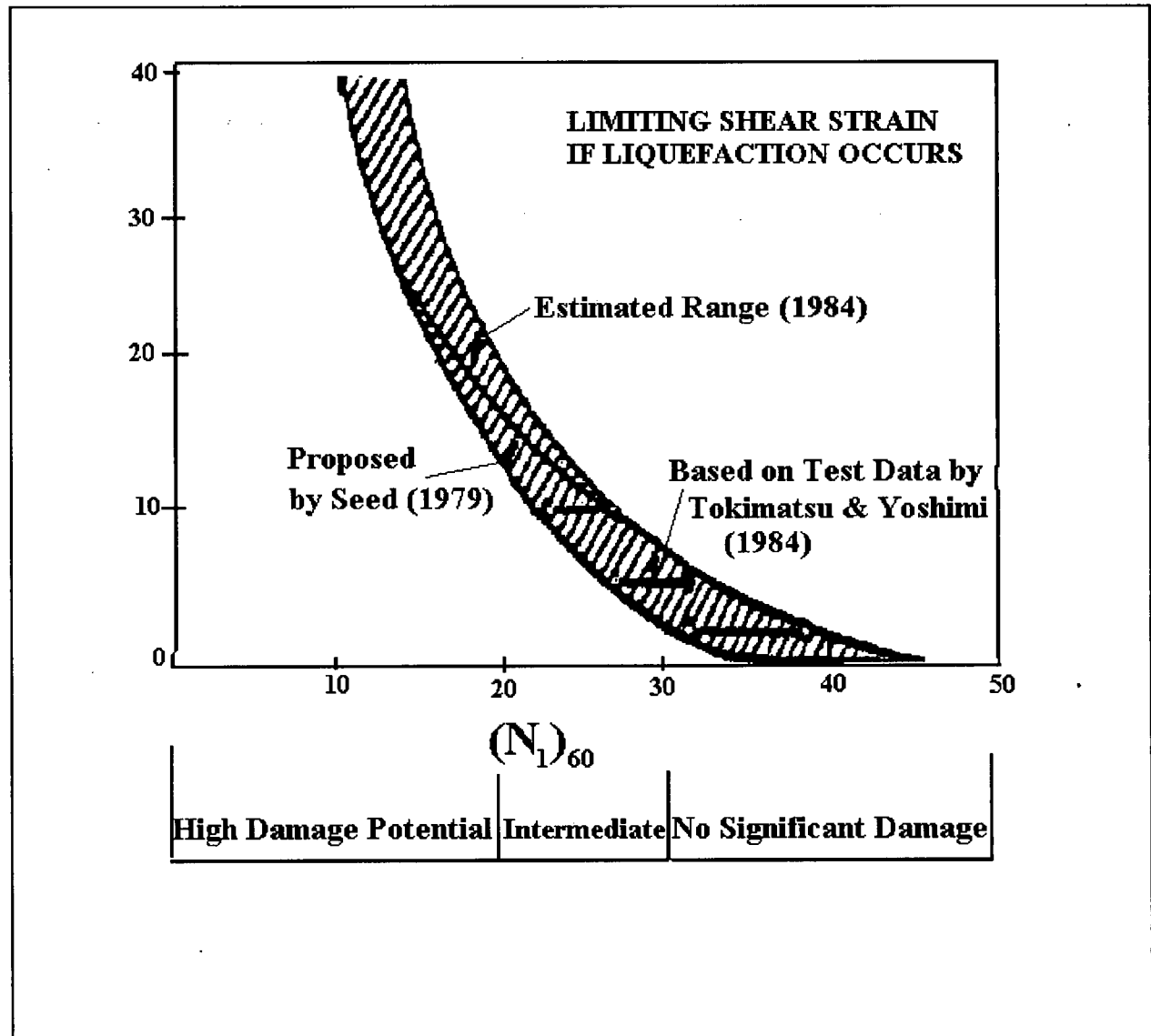


Figure 4.7 - Shear Strain and Likely Damage as a Function of $(N_1)_{60}$ if Liquefaction is Triggered (After Seed et al., 1984)

described in section 4.2). When the $(FS)_L$ of the sand could not be estimated, then the correlation developed by Seed et al.(1984) was used:

$$\gamma_{lim} = 10^{[2.2 - 0.05 \cdot (NI)_{60}]} \quad \text{(equation 4.8)}$$

Equation.4.8 represents an average approximation based on the correlation shown in figure 4.7 (Seed et al., 1984). The Seed et al. (1984) data is based on laboratory tests including tests on undisturbed samples of frozen cored samples. Limit strain estimates for liquefied silts were based on the BC Hydro Transmission Tower (1990) laboratory monotonic and cyclic load test data.

When the $(FS)_L$ of a sand was low (i.e., less than about 0.7), the predicted limit strains were high. The effect of high limit strain predictions was discussed in a review of of the seismic retrofit of the Second Narrows Bridge (Byrne, 1994c). In accordance with the recommendations of that review, an upper bound of $(\gamma_{lim})_{max} = 30\%$ was applied to the predictions for the sands in this study. Limit strain estimates are summarized in section 6.3.

4.4 Liquefaction-Induced Displacements

4.4.1 Introduction

Liquefaction-induced permanent ground displacements corresponding to the 475-year seismic event have been evaluated using two general types of methods:

- empirical, and
- numerical

Empirical methods are based on data from field observations, and numerical methods are physics-based approaches. Two numerical procedures based on the Extended Newmark method (Byrne, 1991) were applied in this study, and two empirical methods were applied for verification and comparison purposes. Liquefaction-induced settlements are discussed, also.

Initially, the procedures used in the empirical method analyses are outlined (in section 4.4.2). The empirical (Hamada, Bartlett & Youd, and Tokimatsu & Seed) methodologies are followed by descriptions of the numerical methods (SOILSTRESS and LIQDISP).

4.4.2 Empirical Case History-based Methods

4.4.2.1 Introduction

For comparison purposes, the Hamada (Hamada et al., 1987) and Bartlett-Youd (Bartlett & Youd, 1992) methods were applied to each transverse section profile to assess lateral displacements. Both methods use simplified equations to model observed trends of liquefaction induced displacements at liquefied sites. The data presented by Hamada et al. (1987) and by Bartlett & Youd (1992) are for slopes that retained sufficient residual strength to prevent a flow slide from occurring. Since these methods are based on observations of actual liquefaction induced displacements, they can serve the purpose of providing a range of displacements within which the numerical estimations should fall.

4.4.2.2 Bartlett & Youd

The Bartlett-Youd (1992) data base consists of lateral displacements compiled from 8 major earthquakes. It is an empirical model developed using multiple linear regression to determine which parameters most affect the horizontal ground displacement. The data base consists of displacements that occurred during the following earthquakes: 1971 San Fernando, California; 1964 Niigata, Japan; 1906 San Francisco, California; 1964 Alaska; 1979 Imperial Valley, California; 1983 Borah Peak, Idaho; 1983 Nihonkai-Chubu, Japan; and 1986 Superstition Hills, California.

The regression analyses delineated two different types of lateral spreads:

i.) lateral spread down gentle ground slopes (“Ground slope failure model”), and
 ii.) lateral spread toward a free face (“Free face failure model”). The ground slope model is applied to sloping terrain. The free face model is applied in cases where there is a lack of lateral resistance, such as those that would occur near the shore of a water body. For example, free-field displacements at the north and south banks of the Fraser River would be computed using the free face model (equation 4.9):

$$\begin{aligned} \text{LOG}(D_H+0.01) = & - 16.366 + 1.178 \cdot M - 0.927 \cdot \text{LOG } R - 0.013 \cdot R + \\ & + 0.657 \cdot \text{LOG } W + 0.348 \cdot \text{LOG } T_{15} + \\ & + 4.527 \cdot \text{LOG}(100 - F_{15}) - 0.922 \cdot (D_{50})_{15} \end{aligned} \quad (\text{eq'n. 4.9})$$

Displacements at the offshore locations would be computed using the ground slope model

$$\begin{aligned} \text{LOG}(D_H+0.01) = & - 15.787 + 1.178 \cdot M - 0.927 \cdot \text{LOG } R - 0.013 \cdot R + \\ & + 0.429 \cdot \text{LOG } S + 0.348 \cdot \text{LOG } T_{15} + \\ & + 4.527 \cdot \text{LOG}(100 - F_{15}) - 0.922 \cdot (D_{50})_{15} \end{aligned} \quad (\text{eq'n. 4.10})$$

where M = earthquake moment magnitude, R = horizontal distance (in kilometers) from the seismic energy source, S = ground slope (in percent), W (in percent) = $100 \cdot (\text{Height of free face/distance from free face})$, T_{15} = cumulative thickness (in meters) of saturated granular layers with $(N1)_{60} \leq 15$, F_{15} = average fines content (in percent) of saturated granular layers included in T_{15} , and $(D_{50})_{15}$ = the average mean grain size (in millimeters) in layers included in T_{15} .

The following parameter limits apply to the use of these equations:

$$\begin{aligned} 6.0 < M < 8.0 \\ 0.1 < S < 6.0 \\ 5 \% < W < 20 \% \\ 0.3 < T_{15} < 15 \\ 0.0 < F_{15} < 50 \\ 0.1 < (D_{50})_{15} < 1.0 \end{aligned}$$

In cases where 'W' is between 1 and 5 percent, it is suggested that both equations be applied, and the larger estimate be acknowledged (Bartlett & Youd, 1992).

4.4.2.3 Hamada

The Hamada empirical model (Hamada et al., 1987) was developed through analysis of liquefaction induced lateral spreads in Japan. The case histories consist of the liquefaction induced displacements caused by the 1964 Niigata (magnitude = 7.5) and 1983 Noshiro (M = 7.7) earthquakes. The Hamada model was developed using pre- and post-earthquake aerial photographs. From these, vector maps of liquefaction induced ground displacements were developed based on ground deformation patterns within areas of similar surface topography. (A displacement vector map for part of the Niigata site is shown in appendix D.2). Upon doing regression analyses, the following simplified equation was developed to model the observed displacements:

$$D = 0.75 \cdot H^{0.50} \cdot \theta^{0.33} \quad \text{(equation 4.11)}$$

where 'H' is the liquefied layer thickness (in meters) and 'θ' is the maximum ground

slope or slope at the base of the liquefied layer (in percent).

4.4.2.4 Tokimatsu & Seed -- Liquefaction-Induced Settlements

Post-liquefaction settlements occur due to dissipation of excess pore water pressures. From a structural standpoint, vertical differential movements are the main focus when assessing post-earthquake consolidation.

The post-liquefaction volumetric stiffness upon dissipation of excess pore pressures can be determined from laboratory tests, but in their absence, a correlation based on field and laboratory test data (Tokimatsu & Seed, 1987) can be applied.

$(N_1)_{60}$ values of each liquefied layer were correlated with the cyclic stress ratio at the midpoint of each of those layers using the volumetric strain chart (figure 4.8). The volumetric strain was used to estimate vertical displacements (Δ_v) due to liquefaction:

$$\Delta_v = \int_0^H \epsilon_v \cdot dz \quad (\text{equation 4.12})$$

where 'z' is the thickness of each liquefied layer, 'H' is the total layer thickness, and ' ϵ_v ' is the volumetric (i.e., vertical) strain induced by liquefaction.

It should be noted that figure 4.8 is applicable to Richter magnitude $M=7.5$ earthquakes, therefore figure E.2 (in appendix E) was used to adjust the volumetric strain according to the design event ($M=7.0$) applied in this study.

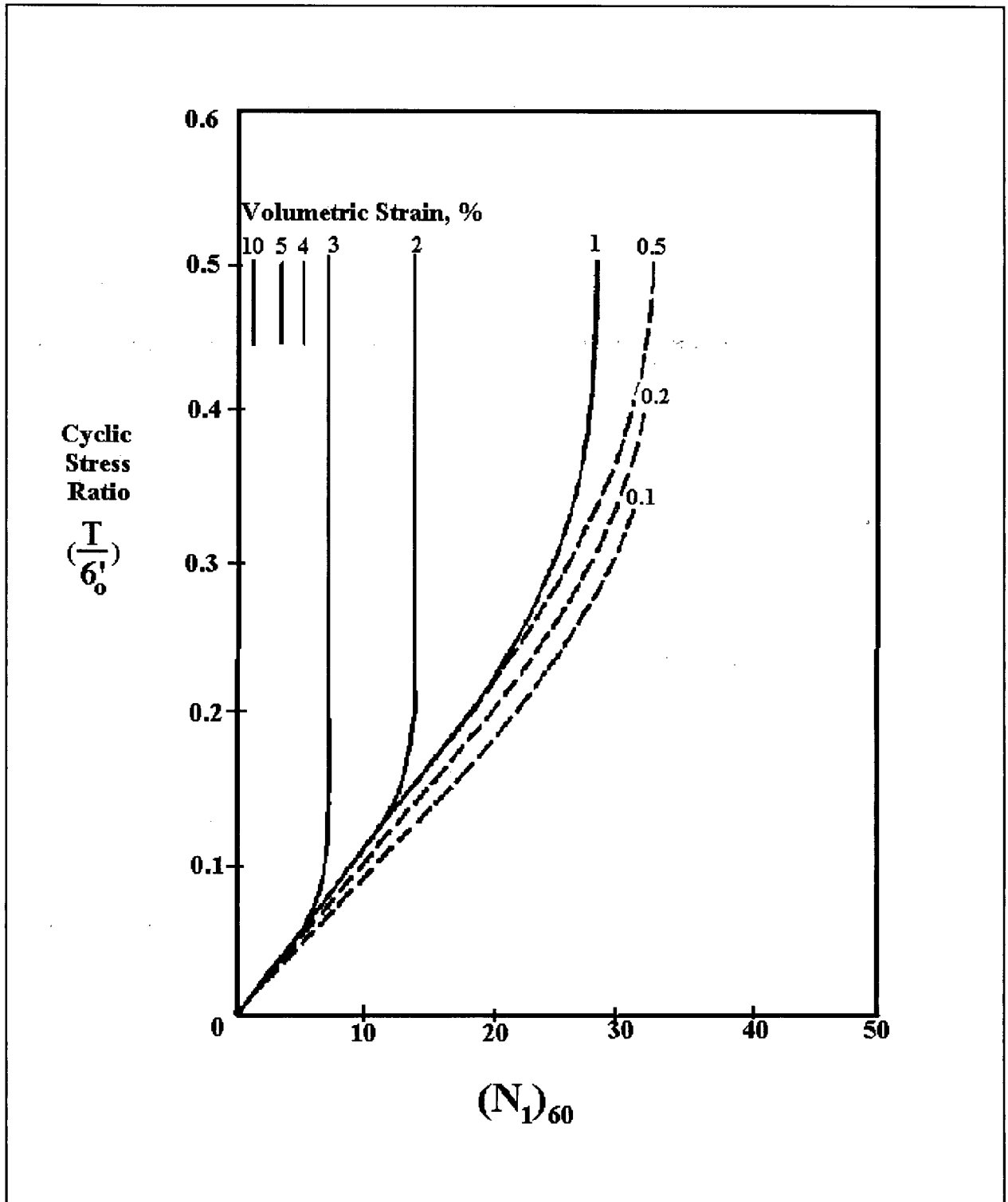


Figure 4.8 - Determination of Volumetric Strains in Saturated Sands (After Tokimatsu & Seed, 1987)

4.4.3 Numerical Models

4.4.3.1 Introduction

As mentioned earlier, numerical models are physics-based methodologies. Current procedures for estimating liquefaction-induced displacements range from simple to complex. Newmark (1965) developed a renowned simple procedure, whereas dynamic effective stress analyses represent the complex end of the spectrum of methods. (Refer to section 4.1 for a brief discussion of the dynamic effective stress method).

Most current procedures are hindered by too many simplifying assumptions. A relatively simple and realistic method of predicting seismic deformations was developed by Byrne (1990). Byrne's procedure is an extension of the simple Newmark method from a single-degree-of-freedom rigid-plastic to a multi-degree-of-freedom flexible system using post-liquefaction stress-strain relations and energy concepts. The method is commonly called the 'Extended Newmark' method. The Extended Newmark methodology is described in detail in appendix A.2

Both multi-degree-of-freedom finite element (SOILSTRESS) and single-degree-of-freedom (LIQDISP) computerized approaches were applied to estimate earthquake-induced displacements within this study. Both computer program codes are based on the Extended Newmark method. The application of the Extended Newmark method within a multi-degree-of-freedom framework is discussed in the next section, and a description of

the single-degree-of-freedom closed form (LIQDISP) analyses follows (in section 4.4.3.3).

4.4.3.2 SOILSTRESS: Pseudo-Dynamic Finite Element Analyses

Many simple procedures are currently available for estimating permanent liquefaction induced displacements, but most do not allow two-dimensional and rotational effects to be modelled. Often, the pattern of displacements, and effects of variations in geometry and stratigraphy cannot be accounted for.

In this study, the two-dimensional finite element program SOILSTRESS was used to assess in detail seismically-induced displacements of the tunnel. The analyses have been carried out using a modified version of the code developed by Byrne and Janzen (1989). Details of the computer code and the methods applied are given in Byrne and Janzen (1989).

The program models the behaviour of soil using a finite element formulation and equivalent-linear strain dependent moduli to model changes in soil properties. Liquefaction effects are modelled using the Extended Newmark method (Byrne, 1990). The SOILSTRESS multi-degree-of-freedom approach sums the displacements due to gravity loads (acting on the liquefied soil) and the earthquake-induced inertia forces to arrive at an estimate of the displacement at each node within the discretized domain. The incorporation of the Extended Newmark model within the SOILSTRESS finite element

procedure is described in detail in appendix A.3.

The SOILSTRESS code discriminates post-earthquake displacements by applying the following procedure:

- 1.) analyze using pre-cyclic stress-strain properties,
- 2.) re-analyze acknowledging post-cyclic stress-strain properties and gravity loads acting on the softened soil; apply a pseudo seismic coefficient (k) to represent the additional force needed to achieve the energy balance,
- 3.) determine earthquake induced displacements by subtracting the displacements obtained in step #1 from those in step #2,
- 4.) estimate post-liquefaction settlements due to excess pore-pressure dissipation, and add those to the displacements from step #3.

Hyperbolic stress-strain models are used to represent the shear modulus (G_s) and bulk modulus (B_s) in the SOILSTRESS program code. Excess pore-pressure dissipation is simulated by applying an accordingly reduced bulk modulus in the liquefied zones. The program requires a volumetric strain estimate which is used to estimate the reduction in the bulk modulus. Volumetric strains were estimated using the Tokimatsu & Seed empirical method. (The Tokimatsu & Seed method is described in section 4.4.2.4).

The key parameters that control the post-liquefaction stress-strain response are the residual shear strength (S_r) and the limiting shear strain (γ_{lim}). These parameters are described in section 4.3. All SOILSTRESS inputs for pre- and post-earthquake

conditions are summarized in section 8.3. The seismic coefficient (k) is described in detail in appendix A.3.

Displacements were analyzed in both the longitudinal plane and in the transverse (cross-sectional) plane. The longitudinal section was analyzed in two separate analyses -- northern and southern halves. The pre-consolidation vertical displacements from the longitudinal section analyses were added to the final vertical displacements (i.e., after settlement) from the corresponding cross-section analyses to arrive at the estimates of the total vertical displacements. The reverse procedure was applied to estimate the total vertical displacements in the longitudinal plane. These vertical displacements are referred to as '3-dimensional' in the result summaries (section 8.3.2).

In both the longitudinal and cross-section analyses, boundary pressures were acknowledged. Because a fixed condition would not be representative of actual conditions in the field, horizontal soil pressures corresponding to a liquefied soil (i.e., $K_0 = 1$) were applied to each element at the left and right boundaries of the finite element mesh in the transverse analyses, and at the outer boundary in each of the two longitudinal analyses. The central boundary in each of the longitudinal meshes was fixed because of the presumed horizontally counter-acting effect of the opposing northern and southern slopes. This, effectively, implies that there would be no lateral displacement at the midpoint of the length of the tunnel.

Additionally, at the offshore locations, vertical pressures corresponding to the

aqueous load were applied on each surface element of the mesh.

Key parameters in the SOILSTRESS method are described in the following sections.

4.4.3.2.1 Pre-earthquake Shear Modulus Constant (k_{gi})

One of the key input parameters in the SOILSTRESS analysis is the shear modulus constant (k_g). Experimental data suggest that G_{max} can be approximated by:

$$G_{max} = k_g \cdot P_{atm} \cdot \left(\frac{\sigma'_m}{P_{atm}} \right)^n \quad \text{(Equation 4.13)}$$

where σ'_m is the mean normal effective stress, 'n' is the shear modulus exponent that lies in the range 0 to 0.5 and is determined from experimental data (Duncan et al., 1980), and P_{atm} is atmospheric pressure, which is applied to make k_g and 'n' dimensionless. As mentioned earlier, the maximum shear modulus (G_{max}) was estimated from shear wave velocity data; that estimate was subsequently applied in equation 4.13 to solve for k_{gi} .

Since an initial shear modulus estimate for the tunnel excavation's coarse gravel/rockfill protection was not available, the gravel k_g -estimates of Duncan, et al. (1980) were referenced. SOILSTRESS inputs for each particular analysis are found in section 8.3.2 in tabular summaries preceding each displacement summary.

4.4.3.2.2 Post-liquefaction Shear Modulus Constant $[(k_g)_{liq}]$

The post-liquefaction shear modulus constant $(k_g)_{liq}$ represents the large degradation of stiffness of liquefied soils after pore-pressure rise. As described in the preceding section, k_g can be solved for using equation 4.13. Since the shear modulus is the ratio of shear strength to shear strain, the post-liquefaction shear modulus (G_{liq}) can be estimated as:

$$G_{liq} = \frac{S_r}{\gamma_{lim}} \quad (\text{Equation 4.14})$$

where S_r is the residual shear strength, and γ_{lim} is the limiting shear strain. The procedures used to estimate S_r and γ_{lim} are described in section 4.3. For a liquefied material, the shear modulus exponent (n) is approximately zero, so equation [4.14] reduces to:

$$G_{liq} = (k_g)_{liq} \cdot P_{atm} \quad (\text{Equation 4.15})$$

Combining equations [4.14] and [4.15], $(k_g)_{liq}$ can be solved for:

$$(k_g)_{liq} = \frac{S_r}{\gamma_{lim} \cdot P_{atm}} \quad (\text{Equation 4.16})$$

4.4.3.2.2 LIQDISP: Single-Degree-of-Freedom Analyses

The Extended Newmark method (Byrne, 1990) was incorporated in a single-degree-of-freedom analysis by Byrne (1990). The efficacy of the computer code LIQDISP has been confirmed through comparison with observed field and laboratory shaking table values.

The LIQDISP procedure requires the following inputs: non-liquefied ('crust') and liquefied layer thicknesses, residual strengths (S_r) and limit strains (γ_{lim}) within liquefied layers, and maximum ground velocity. The method considers the crust (i.e., non-liquefied layer) and liquefied soil to be a single-degree-of-freedom elastic-plastic system.

The concept is extended to a two-dimensional analysis in a manner similar to that outlined by Newmark (1965). To estimate the static driving stress (τ_{st}) that could be expected in a two-dimensional analysis, a factor of safety obtained from limit equilibrium analysis is used to simulate the effect:

$$\tau_{st} = \frac{S_r}{F} \quad (\text{equation 4.17})$$

where S_r is the residual strength of the liquefied layer. As in the post-earthquake static stability analyses (section 4.3), limit equilibrium analyses were performed using Bishop's method of irregular surfaces (Bishop, 1955). The factor of safety estimation is based on a circular failure surface that intersects the crust and liquefied zones.

When applying the LIQDISP method, linear (elastic-plastic) stress-strain relations can be assumed for simplification; alternatively, nonlinear stress-strain response

can be applied. Displacements based on the nonlinear stress-strain response tend to be larger and more accurate than those using the linear approximation; however, the linear approximation method has been corroborated by cyclic shear tests that have shown that linear stress-strain response can be used adequately to model (simulate) those results (Byrne, 1990).

The LIQDISP analysis results at each of the analyzed locations are summarized in section 8.3.3).

CHAPTER 5

LOCAL GEOLOGY & REVIEW OF SOIL DATA

5.1 Introduction

This chapter provides an overall description of the soil conditions at the site. Section 5.2 contains a broad description of the local geology. Section 5.3 provides information about the available soil data, and section 5.4 describes the interpretation procedure used to compare the data at each location.

5.2 General Surficial Geology

The geological history of the Western Fraser Lowlands was reviewed and information concerning the nature of the thick soil deposits that form the Fraser Delta was examined. (A map of the Fraser Delta is shown in Figure 2.1). The Fraser Delta has formed from the heavy load of sand, silt, and clay transported by the Fraser River. Most of the sediment is deposited in the Strait of Georgia, adding to the growing delta. Eighty percent of the sediment load is transported during May, June, and July. During these months, the bed of the river channel is heavily altered by rapid deposition and scour.

The Fraser River sediments are of Holocene age, and they overly glacial deposits of the Late Wisconsin age. The methods of transportation and the environments of deposition were the major factors that determined the physical makeup (i.e., variations in sand, silt, and clay content) of the Quaternary deposits (i.e., sedimentary units). These

units consist mainly of unconsolidated fine-grained glacio-marine sediments (silts and clays). The sediments are overlain by a thick unit of sandy foreset beds gently dipping to the south-southwest into Boundary Bay. The sandy unit is overlain by a thin (approximately 2-meter thick) sequence of fine silt and sand deposited in overbank environments (Clague et al., 1991).

Throughout the Fraser Delta, the sediment deposits vary in thickness from 10 to 300 meters. Bedrock outcrops are found on the southern slopes of the Coast Mountains and western slopes of the Cascade Mountains. Outcrops are also found on the south shore of Burrard Inlet, on isolated hills in the Fraser Lowland, and along several Lowland creeks. Bedrock is within 10 meters of the surface in less than 5% of the Fraser Lowland. During the Quaternary the lowland was subjected to repeated glaciations separated by nonglacial intervals. The ice, of thickness up to 1800 meters or more, overrode all the Fraser Lowland and much of the adjoining mountainous areas. Deposits of widely diversified origin were laid down and molded as a series of erosion (during deglaciation phases) and sedimentation sequences formed the present landscape. The Quaternary deposits (i.e., overlying bedrock) of the Lowland are underlain by plant-bearing, freshwater, sedimentary rocks (interbedded sandstones, siltstones, mudstones, shales, and conglomerates) of Upper Cretaceous (comprising 10% or less) and Tertiary (90% or more) ages. In downtown Vancouver, the Tertiary sedimentary rocks are at or within a few meters of the surface. Site-specific data is discussed in the next section.

5.3 Available Soil Data -- Site Specific Surficial Geology

Soil properties can be obtained using direct or indirect methods. Direct methods such as testing of undisturbed soil samples are often inappropriate due to the high cost of obtaining the samples. Indirect methods such as the cone penetration test (CPT), seismic cone penetration test (SCPT), Standard penetration test (SPT), Becker penetration test (BPT), and the pressuremeter are relatively inexpensive methods that are commonly used to obtain data required to estimate pre- and post-liquefaction soil properties.

The surficial geology at the tunnel site was assessed using Cone Penetration Test (CPT) data, preconstruction borehole logs, and Geological Survey of Canada (GSC) shear wave velocity survey data.

M.o.T.H carried out six Cone Penetration tests (CPT), five Seismic Cone Penetration tests (SCPT), and two Standard Penetration tests (SPT) in 1991 to identify the basic engineering properties of the foundation soil units, and to estimate the general stratigraphy along the length of the tunnel. The locations of the Geocon boreholes and the M.o.T.H. CPT's are shown on the plan and profile views of the tunnel site in figures 2.4 and 2.5. CPT and borehole data and interpretations are summarized in appendix G.

In addition to the M.o.T.H data, soil test data was available from the original preconstruction foundation investigation along the centerline of the proposed tunnel excavation. The testing was done by Geocon Ltd., and the data was summarized by Ripley & Associates (in 1956). The original soil data is based on dynamic cone

penetration tests (DCPT) and Shelby tube samples. A 3-inch (outside) diameter thin-walled Shelby tube and a 2-inch, 60-degree cone were advanced adjacent to each other. A rope and cathead system that dropped a 140-lb hammer a distance of 1 foot was used to advance both the Shelby tube and the 2-inch cone. The number of blows required to advance the tube and the cone a distance of 1 foot were recorded.

The DCPT results cannot be correlated with current methods (i.e., SPT, CPT) used to estimate liquefaction potential, therefore, the penetration data was of no use in this investigation. The Shelby tube soil samples, on the other hand, were used to estimate the stratigraphy (soil types and layer thicknesses) directly beneath the tunnel. The following soil classification tests were done: minimum and maximum void ratio tests, moisture content estimations, and grain size analyses. Additionally, triaxial and consolidation tests of fine grained samples were performed.

The basic engineering properties and strata were also estimated using the 1991 CPT data, but those data correspond to off-center test locations; therefore, the CPT-derived soil engineering properties were transferred to the corresponding centerline Shelby tube sample-based strata estimates. The comparisons of the CPT data with the borehole sample data at each location are discussed in section 5.4.

The more recent data used in this study was obtained using the CPT and SCPT. The four offshore CPT's were done using a drill rig and spud barge. For this study, the CPT data (cone resistance, friction ratio, pore-pressures) was interpreted using the

program CPTINT, which interprets data according to the methods outlined by Robertson & Campanella (1986). In figure 2.5, each CPT is plotted at an elevation relative to the geodetic survey control. The 1956 boreholes were done along the tunnel centerline at elevations corresponding to the 'original ground surface' shown in figure 2.5.

Offshore SPT's were also done, but due to equipment difficulties, the SPT data was considered unreliable; therefore, it was not used in this study. The CPT's, on the other hand, provided reliable continuous stratigraphy data.

The seismic cone penetration test (SCPT) is simply an extension of the CPT apparatus. The technique applies the downhole test procedure. A velocity seismometer is horizontally incorporated in the cone to measure the horizontal component of shear wave arrivals. For M.o.T.H's offshore investigation (locations #2, #3, #4), explosives were used to generate shear waves, and at the onshore locations (#7, #8), the conventional hammer-plank shear beam source was used. Refer to Robertson & Campanella (1986) for detailed descriptions of the CPT and SCPT equipment. The testing conditions and techniques in the M.o.T.H investigation are described in a report prepared by M.o.T.H engineer Dr. Don Gillespie.

At all locations, the CPT logs end approximately 40 meters below the geodetic datum survey control point (shown in figure 2.5). Where the CPT information ends, a silt layer is applied over the remainder of the stratigraphy to a depth of 200 meters. Although no shear wave data was available at location #1 (between locations #8 and #4), the soil

type (silt) was discernable from the CPT bearing resistance, friction ratio, and pore pressure ratio data. The silt encountered at the end of the CPT #91-1 log was extrapolated to a firm ground depth of 200 meters (for completing the SHAKE soil columns). The Geological Survey of Canada (GSC) performed shear wave refraction surveys at 70 sites within the Fraser Delta -- site #16 being near the tunnel. Because of the smooth travel-time-distance plot throughout the surveyed depth, it was presumed acceptable to extrapolate the silt layer to the firm ground depth. Recent seismic reflection surveys taken along the Fraser River show that firm ground is encountered at an approximate depth of 200 meters (Hamilton, 1994). The survey shows that it is the first firm surface encountered, and it has been assumed that this firm ground is the Pleistocene. Blunden (1975) estimated the bedrock surface to occur at depths of 250 meters or deeper under most of the delta. A recent estimate by the GSC suggests that the depth to bedrock in the vicinity southeast of the tunnel may be 700 meters (Hunter, 1994). The GSC's estimates are based on application of a velocity-depth function derived specifically for the Fraser Delta. The function was derived from unpublished 2-way travel time data obtained by the Dynamic Oil Company of Vancouver.

The following section provides comparisons of the CPT and borehole data at each location.

5.4 Interpretation of Available Soil Data

5.4.1 Introduction

This section compares the data from the 1956 boreholes with the 1991 CPT's. Soil layer types and their approximate thicknesses are identified for each location.

Because the 1956 boreholes were done before excavation of the trench took place, and the original preconstruction ground surface elevation along the tunnel centerline was known, it was possible to determine how much was eventually excavated in the vicinity of each borehole. From this, it was possible to summarize the borehole-based estimates of the post-construction stratigraphies. The engineering soil properties of those underlying soil layers were then derived from the off-center CPT data. The offshore CPT's were taken downstream of the tunnel centerline, at off-center distances of between 45 and 79 meters. (Figure 2.4 shows the off-center CPT locations). Since the CPT cannot measure some soil properties very precisely, properties such as fines content and D_{50} (mean grain size) were estimated by analyzing the corresponding layer in the 1956 borehole sample data. When comparing the borehole samples with the CPT data, patterns emerged at each location, such that soil layer types identified by the CPT were readily corroborated by an adjacent borehole log. It was determined which soil layers corresponded with each other in the CPT-based strata estimates and the borehole-based strata estimates. Consequently, transposing the CPT data to the centerline was possible,

thereby taking advantage of both the detailed CPT data and the informative Shelby tube samples.

The SOILSTRESS displacement analyses consisted of detailed discretization of the foundation and tunnel structure; therefore, it was deemed important to estimate as accurately as possible the characteristics of the soils that actually underlay the tunnel at each of the analyzed locations.

The full CPT profile was used in the ground response (SHAKE) analyses. Since structural effects of the tunnel could not be accounted for in the SHAKE soil column estimate, it was appropriate simply to do the analyses using the full CPT profiles to represent the free-field conditions within which the tunnel is constructed.

5.4.2 Location #2

At location #2, the data from CPT #91-2 was compared with the sampling data from boreholes #7 and #8. As shown in figure 2.4, CPT #91-2 is 52 meters downstream of the tunnel centerline. Borehole #7 is 53 meters north of CPT #91-2, and borehole #8 is 68 meters south of the CPT. Figure 5.1 shows the point where the excavation ends ('tunnel invert') relative to the beginning of each data source.

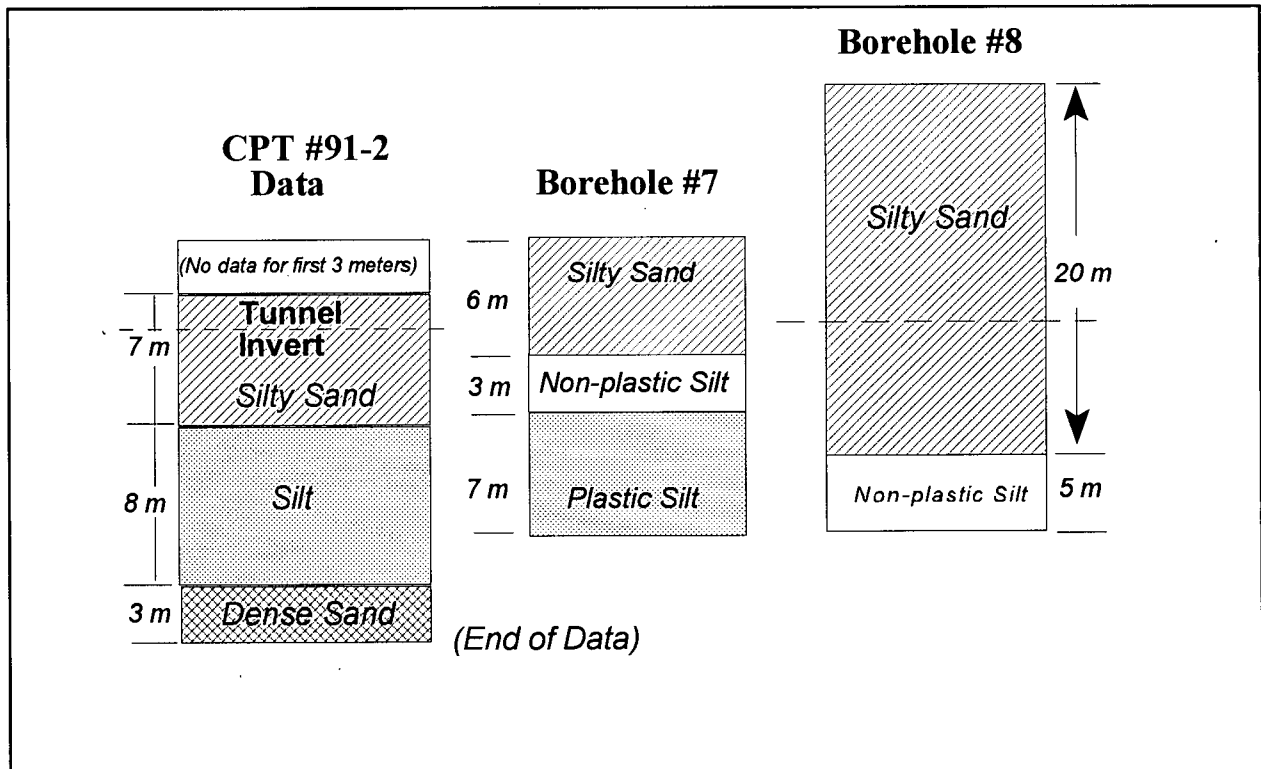


Figure 5.1 - Comparison of Soil Data at Location #2

The top 10 meters consist of interbedded layers of clean sand and silty sand; these layers are underlain by an 8-meter thick clayey silt unit. The clayey silt is underlain by a

3-meter thick dense sand lens.

5.4.3 Location #3

For location #3, the data from CPT #91-3 was compared to the sampling data from boreholes #5 and #6 (refer to figure 5.2). Borehole #5 is 75 meters north of CPT #91-3, and borehole #6 is 44 meters south of the CPT location. CPT #91-3 is 43 meters downstream of the tunnel centerline.

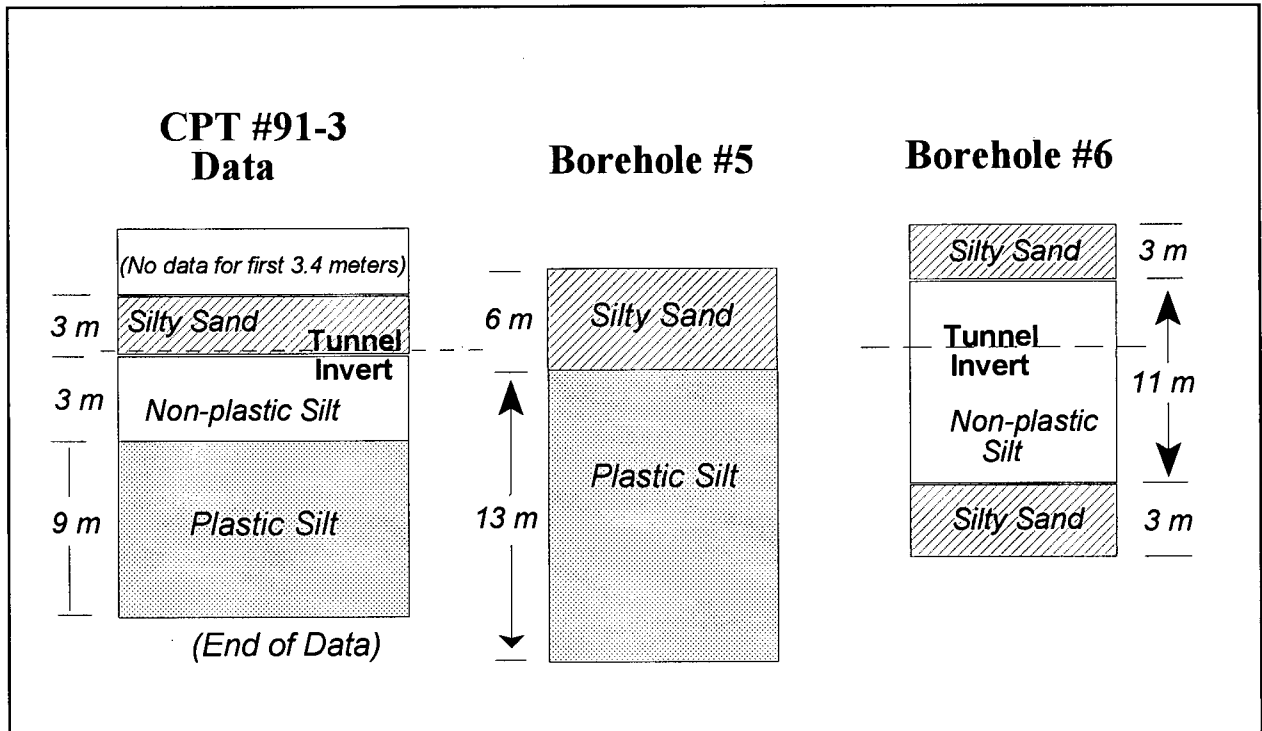


Figure 5.2 - Comparison of Soil Data at Location #3

Figure 5.2 shows the point where the excavation ends relative to the beginning of each test hole. Clean loose sands are interbedded with loose silty sands to a depth of approximately 6 meters; these interbedded layers are underlain by 3 meter thick

nonplastic sandy silt and 9 meter thick plastic clayey silt units. Borehole #6 confirms that the material encountered at the end of CPT #91-3 is a sand seam, and is approximately 4 meters thick.

5.4.4 Location #4

At location #4, the data from CPT #91-4 was compared with the Shelby tube samples from boreholes #4 and #5 (figure 5.3). Borehole #4 is 50 meters north of CPT #91-4, and borehole #5 is 60 meters south of the CPT location. Though CPT #91-4 is 79 meters downstream of the tunnel centerline, the soil profile corresponds well with the two boreholes.

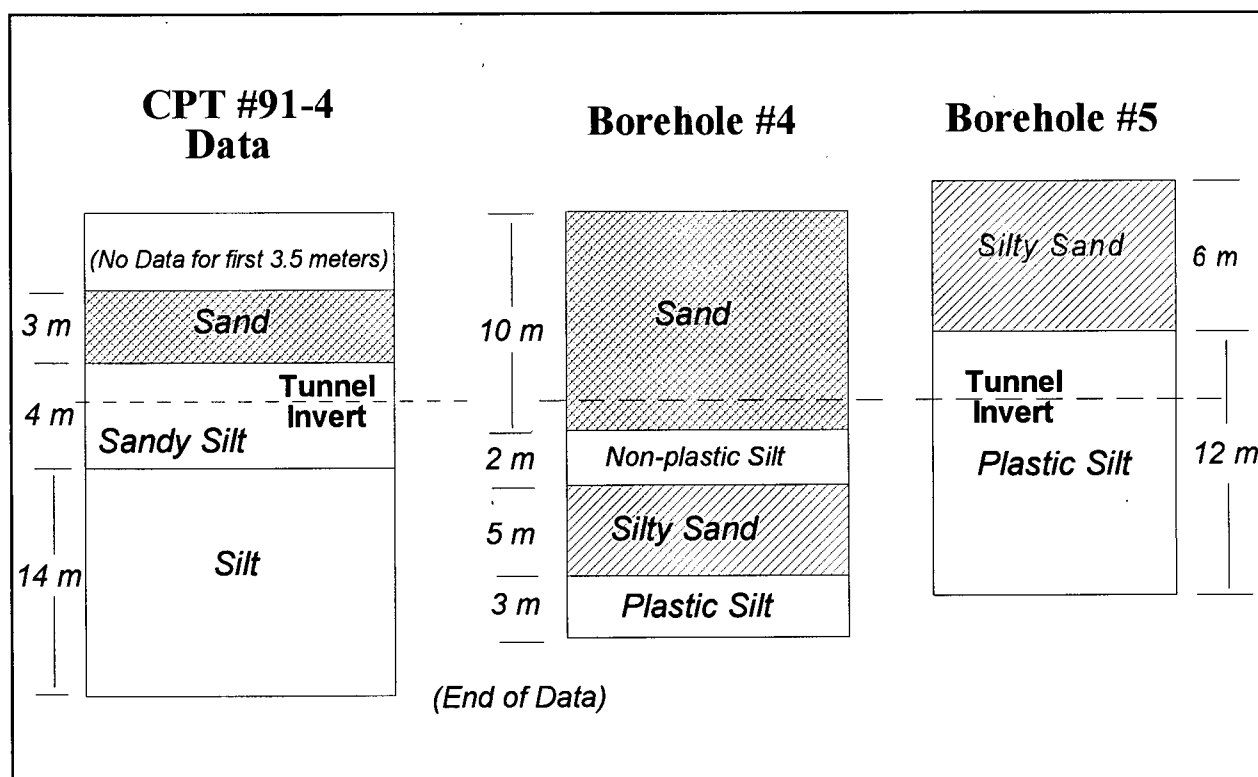


Figure 5.3 - Comparison of Soil Data at Location #4

At location #4, six meters of loose to dense clean sand is underlain by medium-dense sandy silts to a depth of 24 meters.

5.4.5 Location #7

For location #7, the data from CPT #91-7 was compared to the sampling data from borehole #9 (refer to figure 5.4). Borehole #9 is 15 meters south of the CPT #91-7 log, which is found 47 meters downstream of the tunnel centerline.

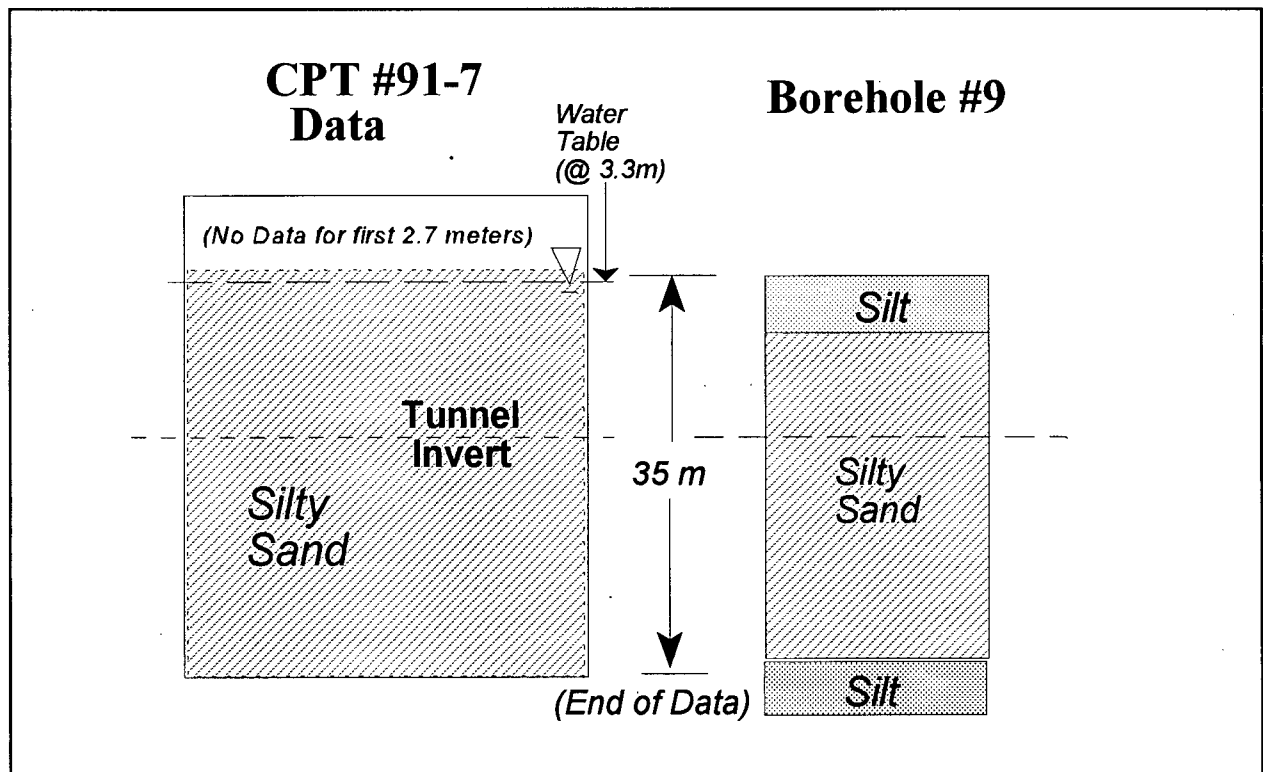


Figure 5.4 - Comparison of Soil Data at Location #7

Location #7 is comprised mainly loose to medium-dense silty sands. The

relatively clean sands (i.e., fines content = 5 % to 15 %) extend throughout the CPT data log to an approximate depth of 38 meters. Borehole #9 compares well with CPT #91-7.

5.4.6 Location #8

For location #8, CPT #91-8 was compared with the data from borehole #1. As shown in figure 2.4, borehole #1 is 30 meters south of the CPT #91-8 location, and CPT #91-8 is 48 meters upstream of the tunnel centerline.

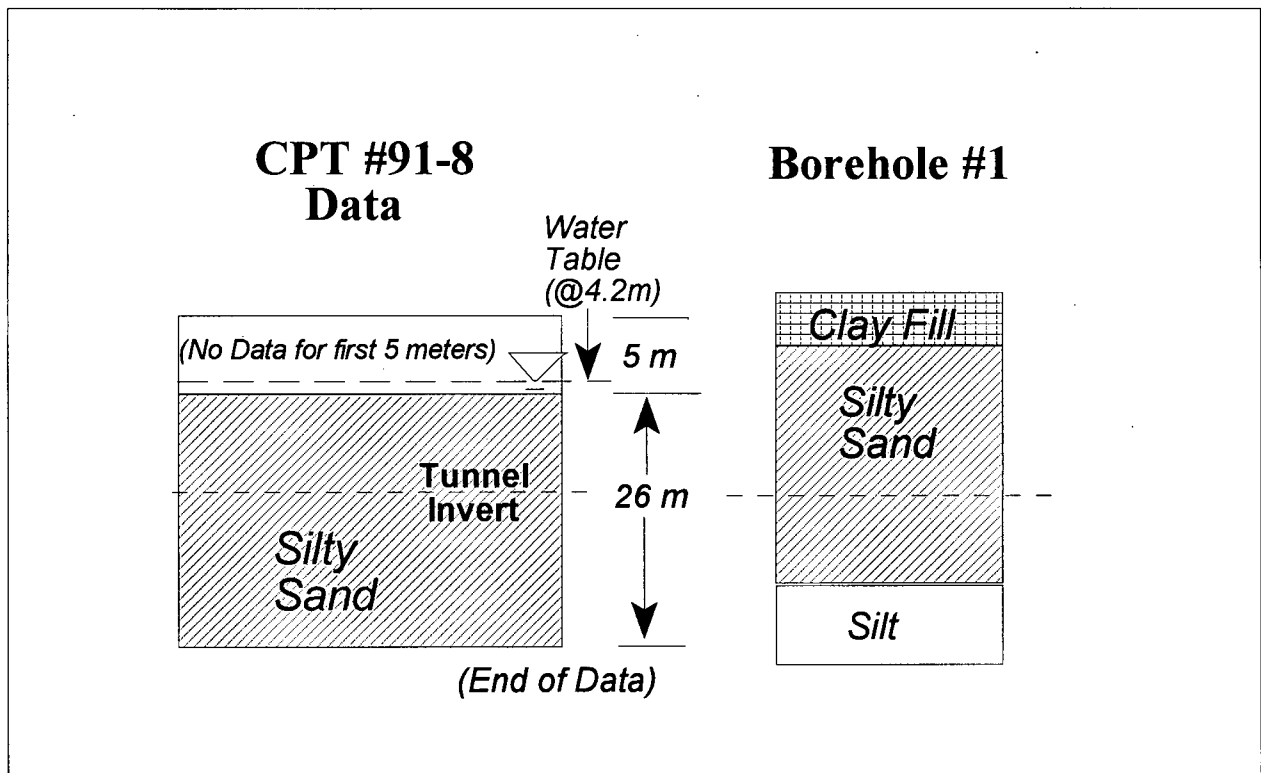


Figure 5.5 - Comparison of Soil Data at Location #8

Figure 5.5 shows the point where the excavation ends relative to the beginning of

each test hole. Location #8 is comprised mainly loose silty sands. The relatively clean sands extend throughout the CPT log to an approximate depth of 27 meters.

5.4.7 Development of Longitudinal-Direction Soil Profile

The longitudinal stratigraphy was developed by comparing data from the CPT's and the boreholes. Soil profiles vary along the length of the tunnel. (Figure 6.1 shows the longitudinal soil profile). Deposition processes along the river bed have resulted in two general contrasting profiles: those of the offshore locations (i.e., #2, #3, and #4) versus locations #7 and #8 at the south and north shores of the river, respectively. Loose sand is found to greater depths at the river banks, whereas along the course of the river, silts extend to greater depths.

Stratigraphies at the five analysis locations were developed as described in sections 5.4.2. to 5.4.6. Each of the cross-section stratigraphies were plotted on a profile drawing and the soil layers were extrapolated. The stratigraphies at the north and south boundaries were estimated from the 1956 borehole data. Though data from boreholes #3 and #10 were not used in the development of the cross-section stratigraphies, they aided in determining the soil types at the north and south ends of the tunnel. (Refer to figure 2.5 for a profile view of the test hole locations).

CHAPTER 6

RESULTS: LIQUEFACTION TRIGGERING & POST-EARTHQUAKE STABILITY

6.1 Introduction

Results corresponding to the analyses described in sections 4.2 and 4.3 are presented in this chapter. Initially, results of the liquefaction assessments at each of the five locations are presented. Post-liquefaction stability is then assessed, outlining the flow slide analyses. Input parameters critical to the analyses are summarized, also.

Results are discussed in chapter 7. Each of the upcoming sections points out the corresponding section in chapter 7 that should be referred to while reviewing the individual result summaries in this chapter.

6.2 Liquefaction Assessment and Associated Parameters

6.2.1 Zones of Liquefaction

At each of the five locations (refer to figure 6.1), soil columns were analyzed for liquefaction resistance. Points of discussion relating to the liquefaction assessment are presented in section 7.2. Refer to section 4.2 for the liquefaction assessment procedure. Appendix B.5 contains detailed information (CSR, CRR, etc.) from the liquefaction assessment at each location. For reference, ground motion amplification factors are summarized in appendix B.4.

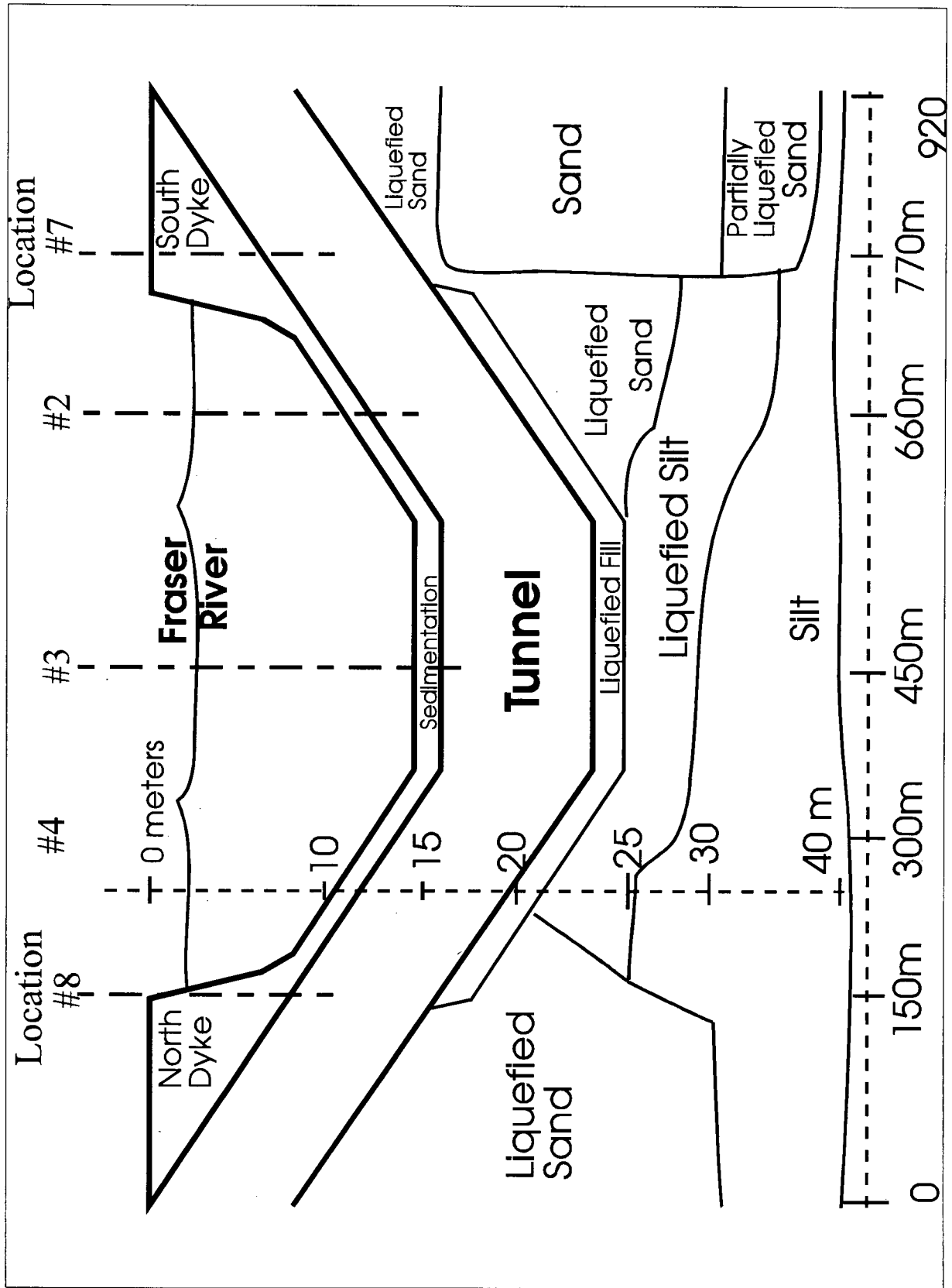


Figure 6.1 Zones of Liquefaction in Profile View

Figure 6.1 shows the zones of liquefaction on a soil profile parallel to the axis of the tunnel. Table 6.1 summarizes the depths to liquefaction both before and after construction of the tunnel. As the table shows, the largest zone of liquefaction extends to a depth of about 11 meters below the tunnel at location #8. Amongst the offshore locations, location #2 is of greatest concern, where the depth to liquefaction is approximately 8 meters. The zones of liquefaction extend no more than about 3 meters at the remaining locations. At the south shore (location #7), the depth to liquefaction coincides with the point at which the tunnel excavation ends.

Location	Depth to Tunnel Invert (meters)	Total Thickness of Liquefied Zone (meters)	Thickness of Liquefied Zone Below Tunnel (meters)
#2	4	11.7	7.7
#3	6.4	9.1	2.7
#4	8	10.5	2.5
#7	20	20	0
#8	16	27.2	11.2

Table 6.1 - Depth of Liquefaction at Each Location

Figures 6.2 to 6.9 graphically summarize the CSR's, CRR's, and Factors of Safety at each location. The liquefaction assessment results at the three offshore locations (#2, #3, #4) are summarized first, followed by the summaries for the south (#7) and north (#8) shores.

In the tables in sections 6.2.1.1 to 6.2.1.5, V_{s1} is the normalized shear wave velocity, and G_{\max} is the maximum (initial) shear modulus. $(N_1)_{60}$ is the corrected blow count as estimated using the program CPTINT, which uses a Q_c/N ratio that varies according to soil type, as described by Robertson & Campanella (1986). 'Fines content' is the percentage of fines passing a no.200 U.S. standard sieve, and K_o is the overburden correction factor for the liquefaction analyses. 'Criteria' is the liquefaction assessment criteria used to assess the triggering potential of the soil layer, and 'status' refers to the outcome of the liquefaction analysis for that particular layer. In the tables, where 'N.A' is found it means that the data for that entry was not available. It should be noted that for soil layers where 'Seed & Robertson' is shown as the liquefaction criteria, both the Seed (1984) and Robertson (1990) criteria were individually applied, and then the results were compared.

Key liquefaction parameters are summarized in table 6.2 to 6.6. Refer to appendix B.5 for detailed summaries of ground motion parameters at each location.

6.2.1.1 Location #2

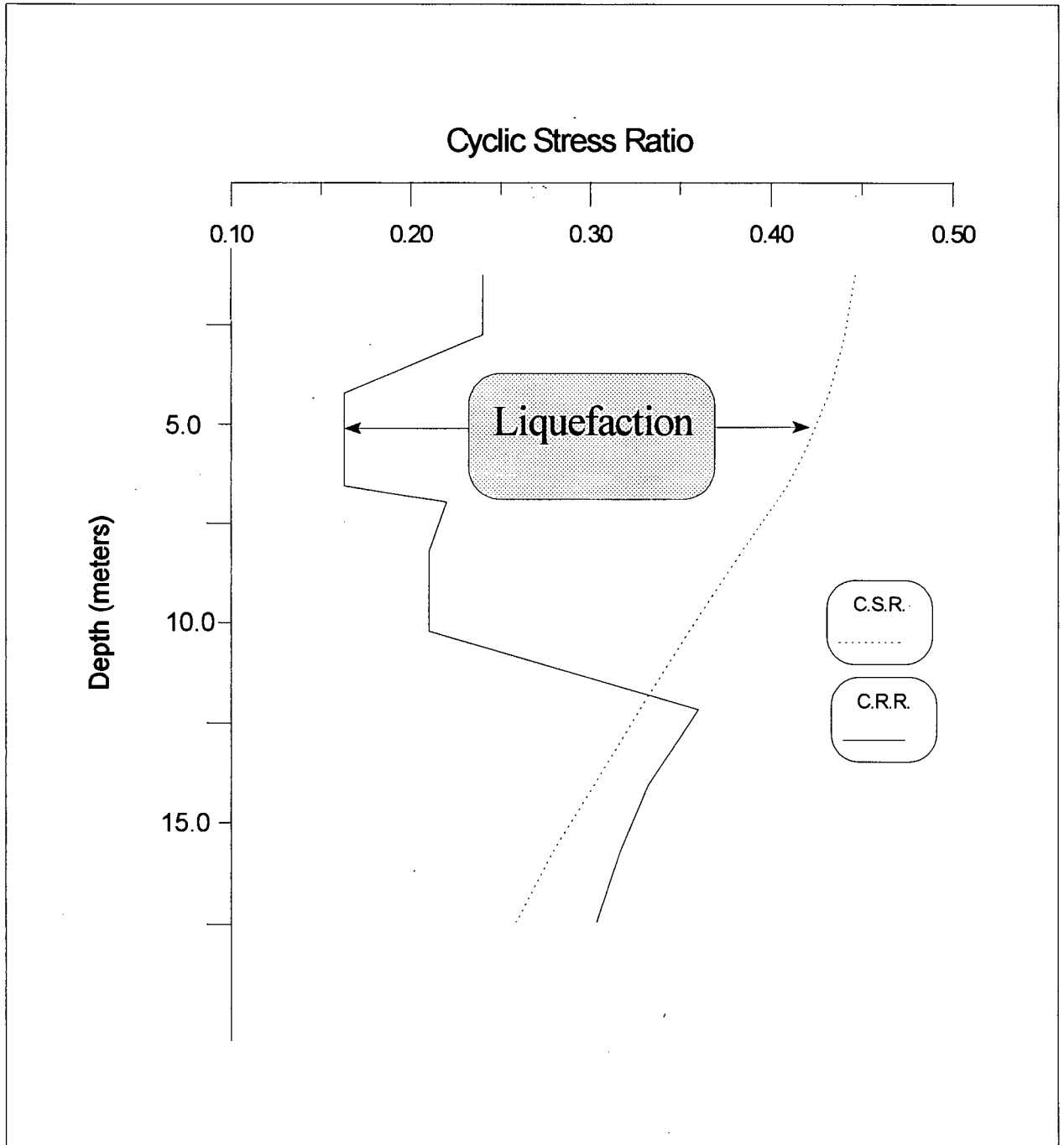


Figure 6.2 - Comparison of Cyclic Stress and Cyclic Resistance Ratios at Location #2

Layer	Soil Type	Depth (m)	$(V_s)_1$ (m/s)	$(N_1)_{60}$	Fines Content (%)	K_σ	Criteria	Status
No data from first 3 meters of CPT log								
1	Sand	3 - 4.5	185	N.A.	5	1	Seed & Robertson	Liquefied
* Tunnel Invert Location (excavation ends at 4 meters below the original ground surface)								
2	Sand	4.5 - 6	185	N.A.	5	1	Seed & Robertson	Liquefied
3	Sand	6 - 7.4	160	13	5	1	Seed	Liquefied
4	Sand	7.4 - 8.8	160	13	5	1	Seed	Liquefied
5	Sandy Silt	8.8 - 9.2	160	7	45	1	Seed	Liquefied
6	Silty Sand	9.2 - 9.7	160	18	45	1	Seed	Liquefied
7	Clayey Silt	9.7 - 13.7	175	5	45	1	Seed & Robertson	** top 2 meters is Liquefied
8	Clayey Silt	13.7 - 17.5	185	5	95	N.A.	Chinese	Not Liquefied
9	Sand	17.5 - 18.9	240	17	5	0.96	Seed	Not Liquefied
10	Sand	18.9 - 21	240	17	5	0.92	Seed	Not Liquefied
11	Silt	21 - 50	150	N.A.	N.A.	N.A.	N.A.	Not Liquefied
12	Silt	50 - 75	150	N.A.	N.A.	N.A.	N.A.	Not Liquefied
13	Silt	75 - 100	150	N.A.	N.A.	N.A.	N.A.	Not Liquefied
14	Silt	100 - 125	150	N.A.	N.A.	N.A.	N.A.	Not Liquefied
15	Silt	125 - 150	150	N.A.	N.A.	N.A.	N.A.	Not Liquefied
16	Silt	150 - 175	150	N.A.	N.A.	N.A.	N.A.	Not Liquefied
17	Silt	175 - 200	150	N.A.	N.A.	N.A.	N.A.	Not Liquefied

Table 6.2 - Soil Parameters for Liquefaction Assessment at Location #2

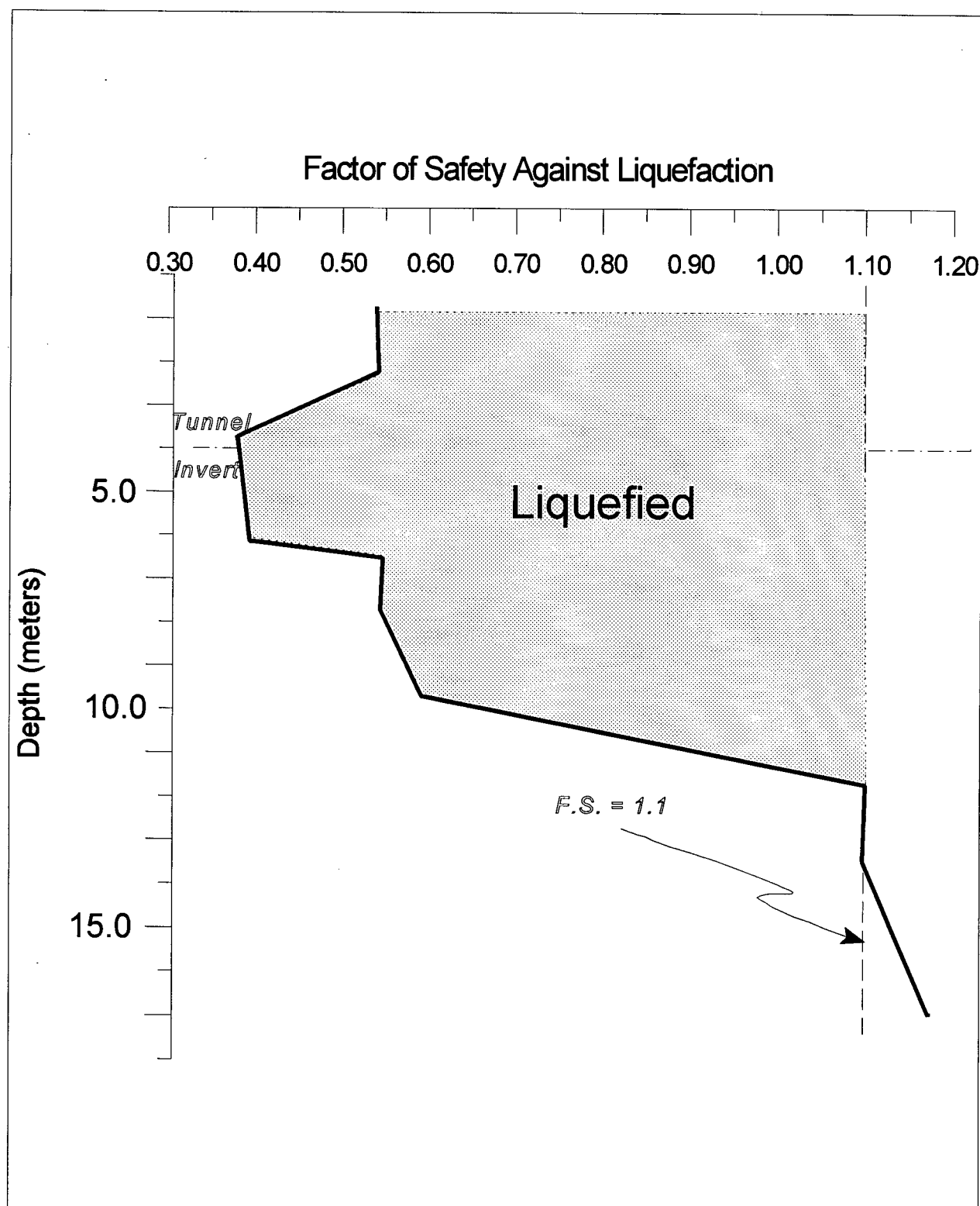


Figure 6.3 - Factor of Safety Against Liquefaction (FS_L) -- Location #2

6.2.1.2 Location #3

The comparison of CRR's and CSR's is not shown for location #3. CRR's could not be estimated in the plastic silts (which are predominant at this location).

Layer	Soil Type	Depth (m)	$(V_s)_1$ (m/s)	$(N_1)_{60}$	Fines Content (%)	K_o	Criteria	Status
No CPT data over the first 3.4 meters								
1	Silty Sand	3.4 - 5	142	11	15	1	Seed	Liquefied
2	Sand	5 - 6.4	142	14	5	1	Seed	Liquefied
* Tunnel Invert Location (excavation ends at 6.4 meters below the original ground surface)								
3	Silt	6.4 - 9.1	143	8	80	1	Seed	Liquefied
4	Silt	9.1 - 12	155	5	85	N.A.	Chinese	Not Liquefied
5	Silt	12 - 17.9	150	5	85	N.A.	Chinese	Not Liquefied
6	Sand	17.9 - 22	240	17	N.A.	0.93	Seed	Not Liquefied
7	Silt	22 - 40	150	N.A.	N.A.	N.A.	N.A.	Not Liquefied
8	Silt	40 - 60	150	N.A.	N.A.	N.A.	N.A.	Not Liquefied
9	Silt	60 - 80	150	N.A.	N.A.	N.A.	N.A.	Not Liquefied
10	Silt	80 - 100	150	N.A.	N.A.	N.A.	N.A.	Not Liquefied
11	Silt	100 - 125	150	N.A.	N.A.	N.A.	N.A.	Not Liquefied
12	Silt	125 - 160	150	N.A.	N.A.	N.A.	N.A.	Not Liquefied
13	Silt	160 - 200	150	N.A.	N.A.	N.A.	N.A.	Not Liquefied

Table 6.3 - Soil Parameters for Liquefaction Assessment at Location #3

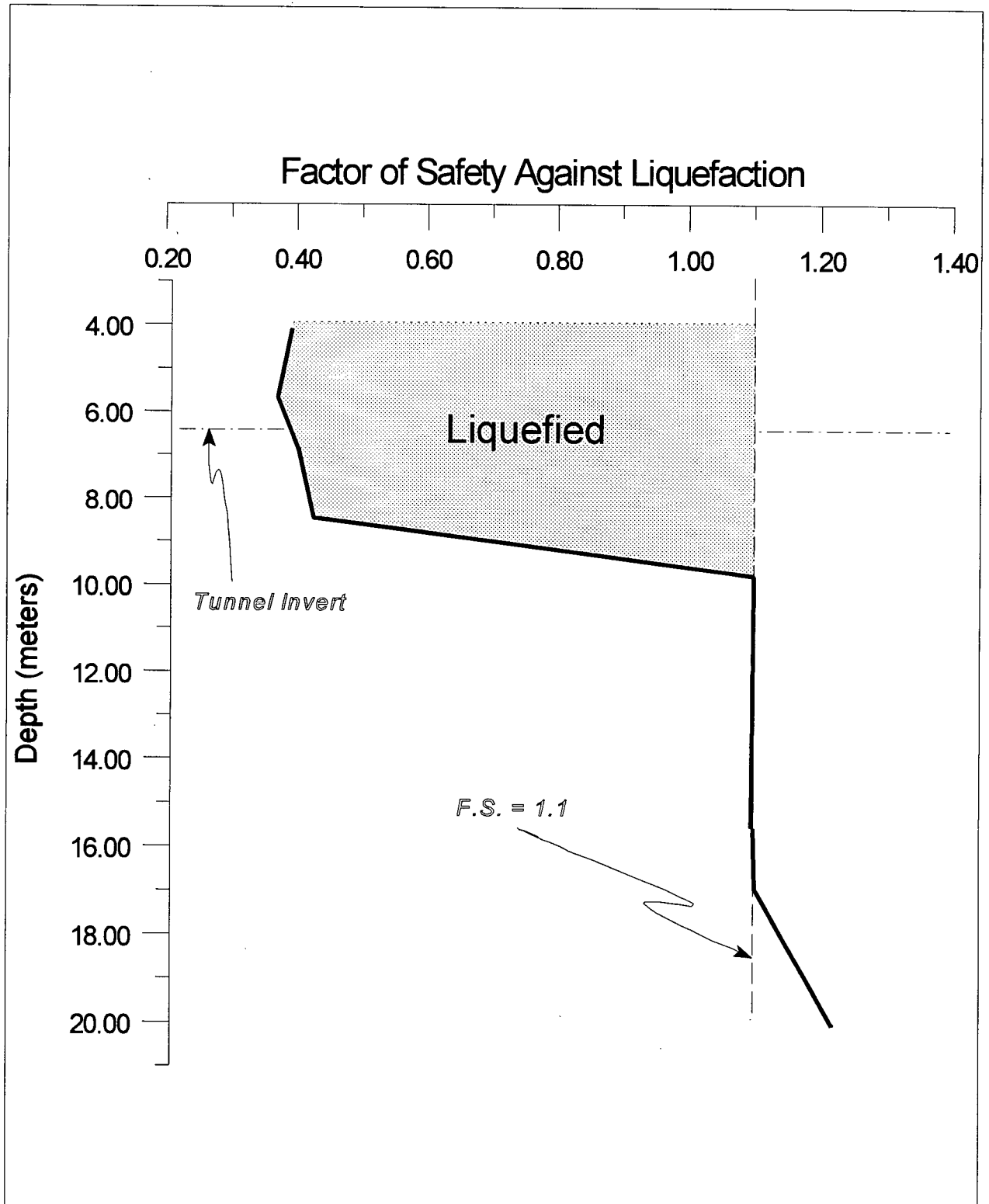


Figure 6.4 - Factor of Safety Against Liquefaction -- Location #3

6.2.1.3 Location #4

The comparison of CRR's and CSR's is not shown for location #4 because plastic silts were predominant at that location; therefore, the CRR's could not be estimated.

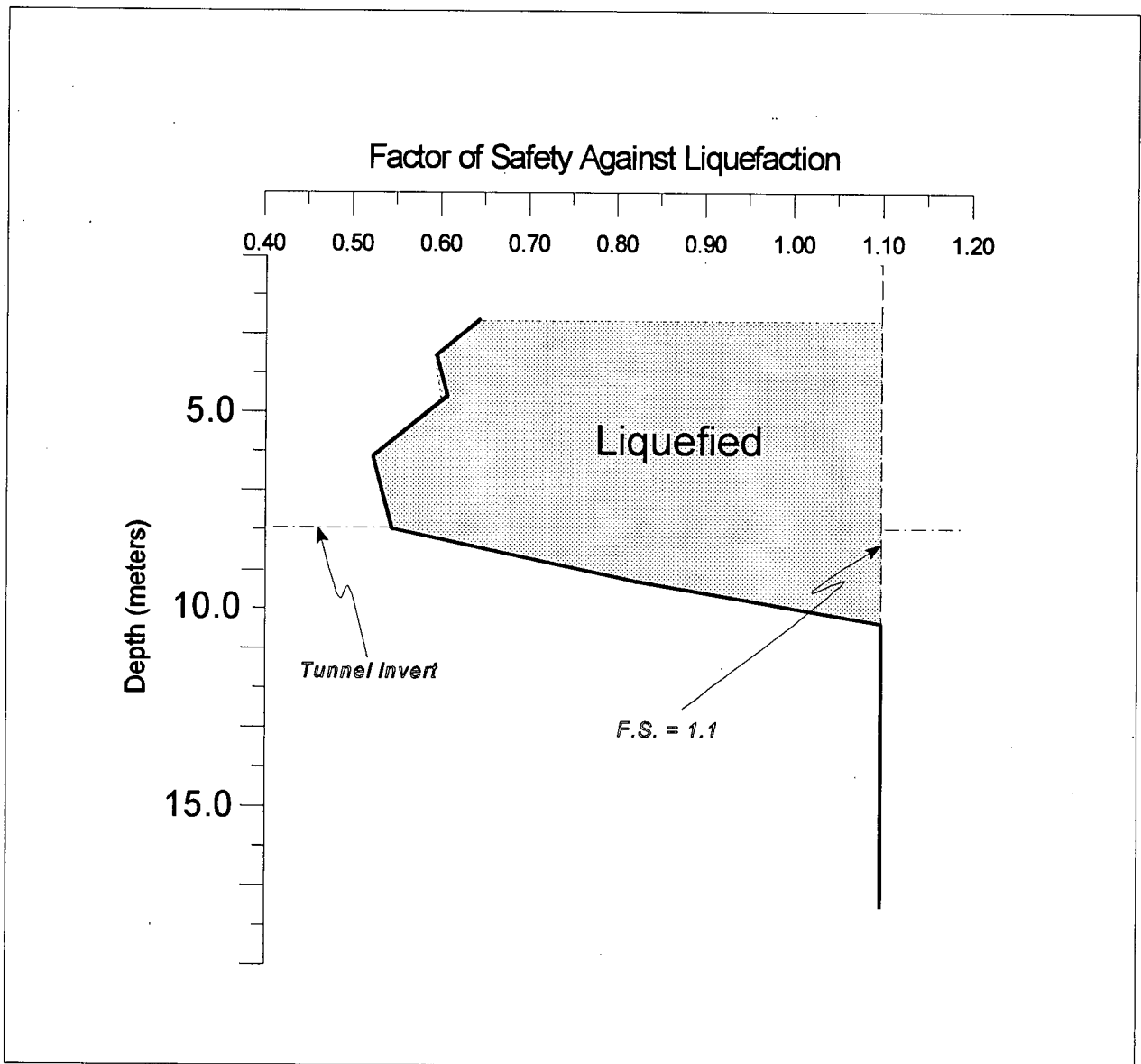


Figure 6.5 - Factor of Safety Against Liquefaction (FS_L) -- Location #4

Layer	Soil Type	Depth (m)	$(V_s)_1$ (m/s)	$(N_1)_{60}$	Fines Content (%)	K_o	Criteria	Status
No CPT data over the first 3.5 meters depth								
1	Sand	3.5 - 4	184	23	5	1	Seed	Liquefied
2	Sand	4 - 6.25	160	22	5	1	Seed	Liquefied
3	Sandy Silt	6.25 - 8	150	12	35 - 50	1	Seed	Liquefied
* Tunnel Invert Location (excavation ends at 8 meters below the original ground surface)								
4	Sandy Silt	8 - 9.9	150	12	35 - 50	1	Seed	Liquefied
5	Silty Sand	9.9 - 10.5	160	20	15	1	Seed	Liquefied
6	Sandy Silt	10.5 - 14	182	6	85	N.A.	Chinese	Not Liquefied
7	Sandy Silt	14 - 17	151	5	85	N.A.	Chinese	Not Liquefied
8	Sandy Silt	17 - 22	202	4	85	N.A.	Chinese	Not Liquefied
9	Sandy Silt	22 - 24.1	140	5	85	N.A.	Chinese	Not Liquefied
11	Silt	24.1 - 50	150	N.A.	N.A.	N.A.	N.A.	Not Liquefied
12	Silt	50 - 75	150	N.A.	N.A.	N.A.	N.A.	Not Liquefied
13	Silt	75 - 100	150	N.A.	N.A.	N.A.	N.A.	Not Liquefied
14	Silt	100 - 125	150	N.A.	N.A.	N.A.	N.A.	Not Liquefied
15	Silt	125 - 150	150	N.A.	N.A.	N.A.	N.A.	Not Liquefied
16	Silt	150 - 175	150	N.A.	N.A.	N.A.	N.A.	Not Liquefied
17	Silt	175 - 200	150	N.A.	N.A.	N.A.	N.A.	Not Liquefied

Table 6.4 - Soil Parameters for Liquefaction Assessment at Location #4

6.2.1.4 Location #7

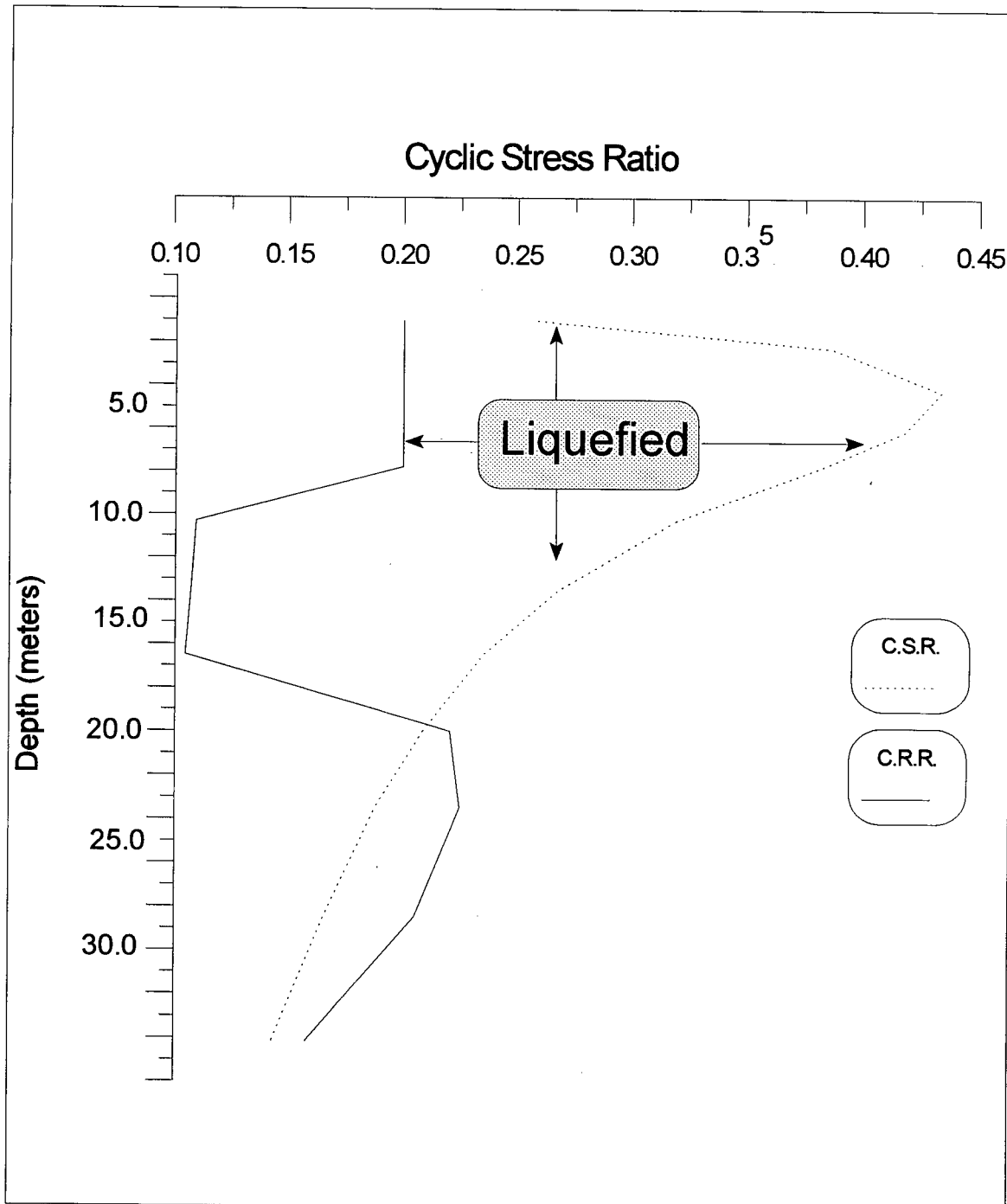


Figure 6.6 - Comparison of Cyclic Stress and Cyclic Resistance Ratios at Location #7

CHAPTER 6 *Results: Liquefaction Assessment*

Layer	Soil Type	Depth (m)	$(V_s)_1$ (m/s)	$(N_1)_{60}$	Fines Content (%)	K_o	Criteria	Status
No CPT data over first 2.7 meters								
1	Silty Sand	2.7 - 3.3	110	12	16	1	Seed	Liquefied
* Watertable located at 3.3 meters depth								
2	Silty Sand	3.3 - 7.25	110	12	16	1	Seed	Liquefied
3	Sand	7.25 - 11	110	9	6	1	Seed	Liquefied
4	Sand	11 - 14	160	9	5	1	Seed	Liquefied
5	Sand	14 - 17	160	9	10	0.98	Seed	Liquefied
6	Silty Sand	17 - 20	140	7	10	0.96	Seed	Liquefied
* Tunnel Invert Location (excavation ends at 20 meters below the original ground surface)								
7	Sand	20 - 24	220	11	9	0.9	Seed	Not Liquefied
8	Sand	24 - 27	190	11	9	0.89	Seed & Robertson	Not Liquefied
9	Sand	27 - 34	230	13	9	0.85	Seed & Robertson	Not Liquefied
10	Silty Sand	34 - 38.3	170	10	52	0.8	Seed	Not Liquefied
11	Silt	38.3 - 50	150	N.A.	N.A.	N.A.	N.A.	Not Liquefied
12	Silt	50 - 75	150	N.A.	N.A.	N.A.	N.A.	Not Liquefied
13	Silt	75 - 100	150	N.A.	N.A.	N.A.	N.A.	Not Liquefied
14	Silt	100 - 125	150	N.A.	N.A.	N.A.	N.A.	Not Liquefied
15	Silt	125 - 150	150	N.A.	N.A.	N.A.	N.A.	Not Liquefied
16	Silt	150 - 175	150	N.A.	N.A.	N.A.	N.A.	Not Liquefied
17	Silt	175 - 200	150	N.A.	N.A.	N.A.	N.A.	Not Liquefied

Table 6.5 - Soil Parameters for Liquefaction Assessment at Location #7

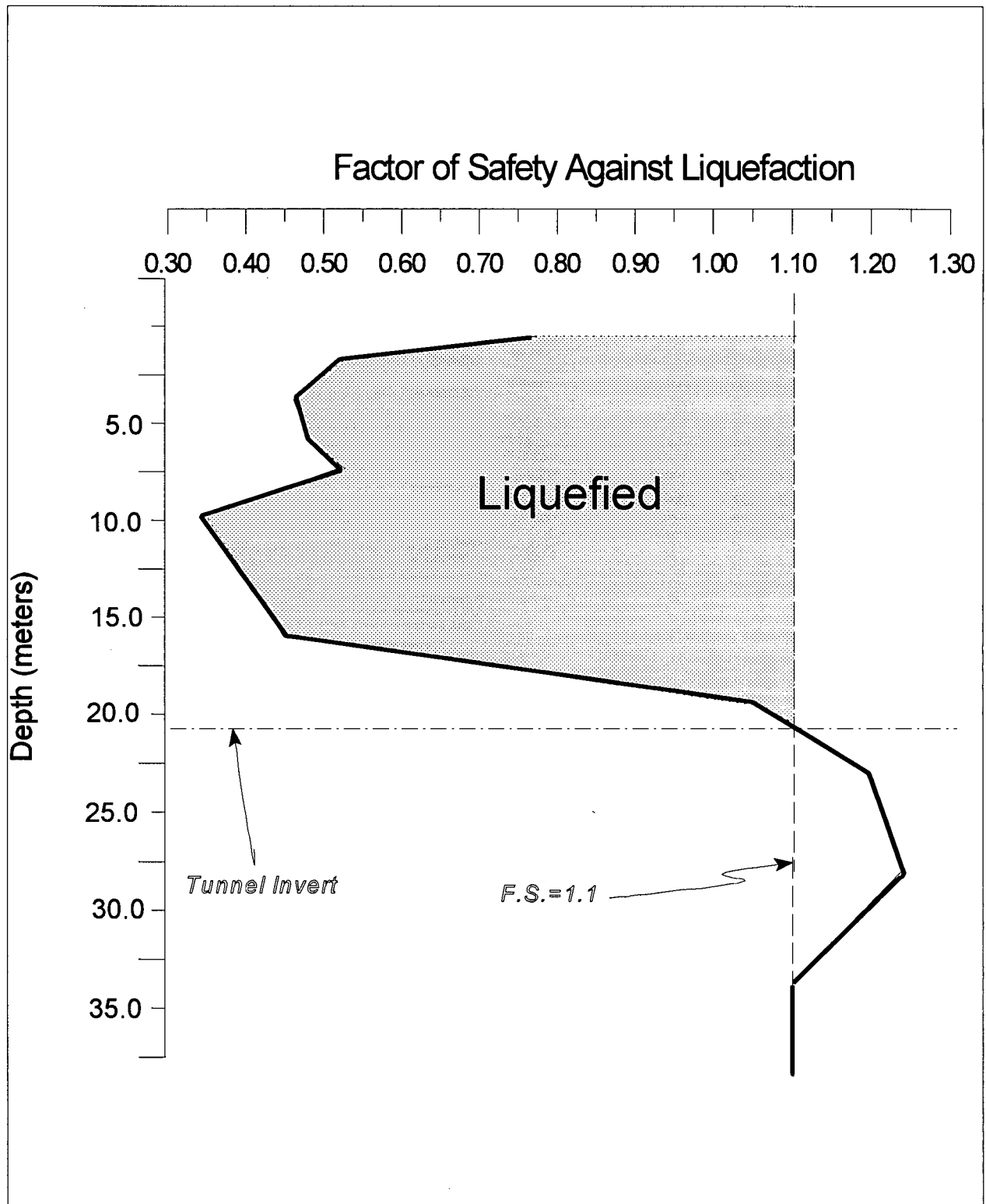


Figure 6.7 - Factor of Safety Against Liquefaction (FS_L) -- Location #7

6.2.1.5 Location #8

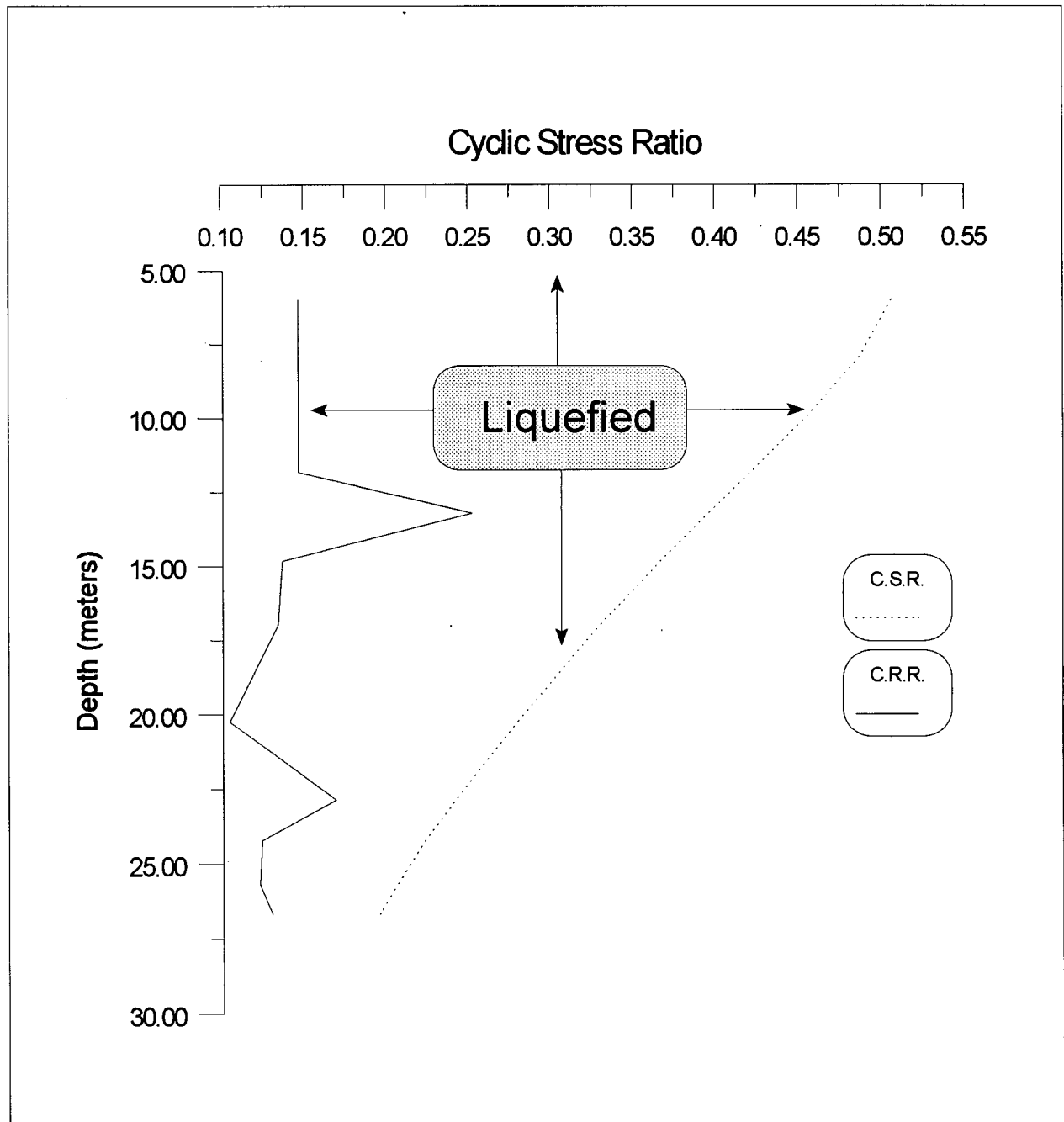


Figure 6.8 - Comparison of Cyclic Stress and Cyclic Resistance Ratios at Location #8

CHAPTER 6 Results: Liquefaction Assessment

Layer	Soil Type	Depth (m)	$(V_s)_1$ (m/s)	$(N_1)_{60}$	Fines Content (%)	K_o	Criteria	Status
No CPT data over the first 5 meters								
* Watertable located at 4.2 meters depth								
1	Sand	5 - 7	170	12	10	1	Seed	Liquefied
2	Sand	7 - 9	150	12	3	1	Seed	Liquefied
3	Sand	9 - 11	170	12	3	1	Seed	Liquefied
4	Sand	11 - 12.8	170	12	4	1	Seed	Liquefied
5	Silty sand	12.8 - 13.6	170	16	4	1	Seed	Liquefied
6	Sand	13.6 - 16	190	11	4	1	Seed	Liquefied
* Tunnel Invert Location (excavation ends at 16 meters below the original ground surface)								
7	Sand	16 - 18	190	11	4	0.98	Seed	Liquefied
8	Sand	18 - 22.5	160	9	4	0.96	Seed	Liquefied
9	Silty sand	22.5 - 23.3	170	8	30	0.92	Seed	Liquefied
10	Sand	23.3 - 25.2	170	11	4	0.91	Seed	Liquefied
11	Silty sand	25.2 - 26.2	170	7	30	0.9	Seed	Liquefied
12	Sand	26.2 - 27.2	170	12	4	0.89	Seed	Liquefied
13	Silt	27.2 - 50	150	N.A.	N.A.	N.A.	N.A.	Not Liquefied
14	Silt	50 - 75	150	N.A.	N.A.	N.A.	N.A.	Not Liquefied
15	Silt	75 - 100	150	N.A.	N.A.	N.A.	N.A.	Not Liquefied
16	Silt	100 - 125	150	N.A.	N.A.	N.A.	N.A.	Not Liquefied
17	Silt	125 - 150	150	N.A.	N.A.	N.A.	N.A.	Not Liquefied
18	Silt	150 - 175	150	N.A.	N.A.	N.A.	N.A.	Not Liquefied
19	Silt	175 - 200	150	N.A.	N.A.	N.A.	N.A.	Not Liquefied

Table 6.6 - Soil Parameters for Liquefaction Assessment at Location #8

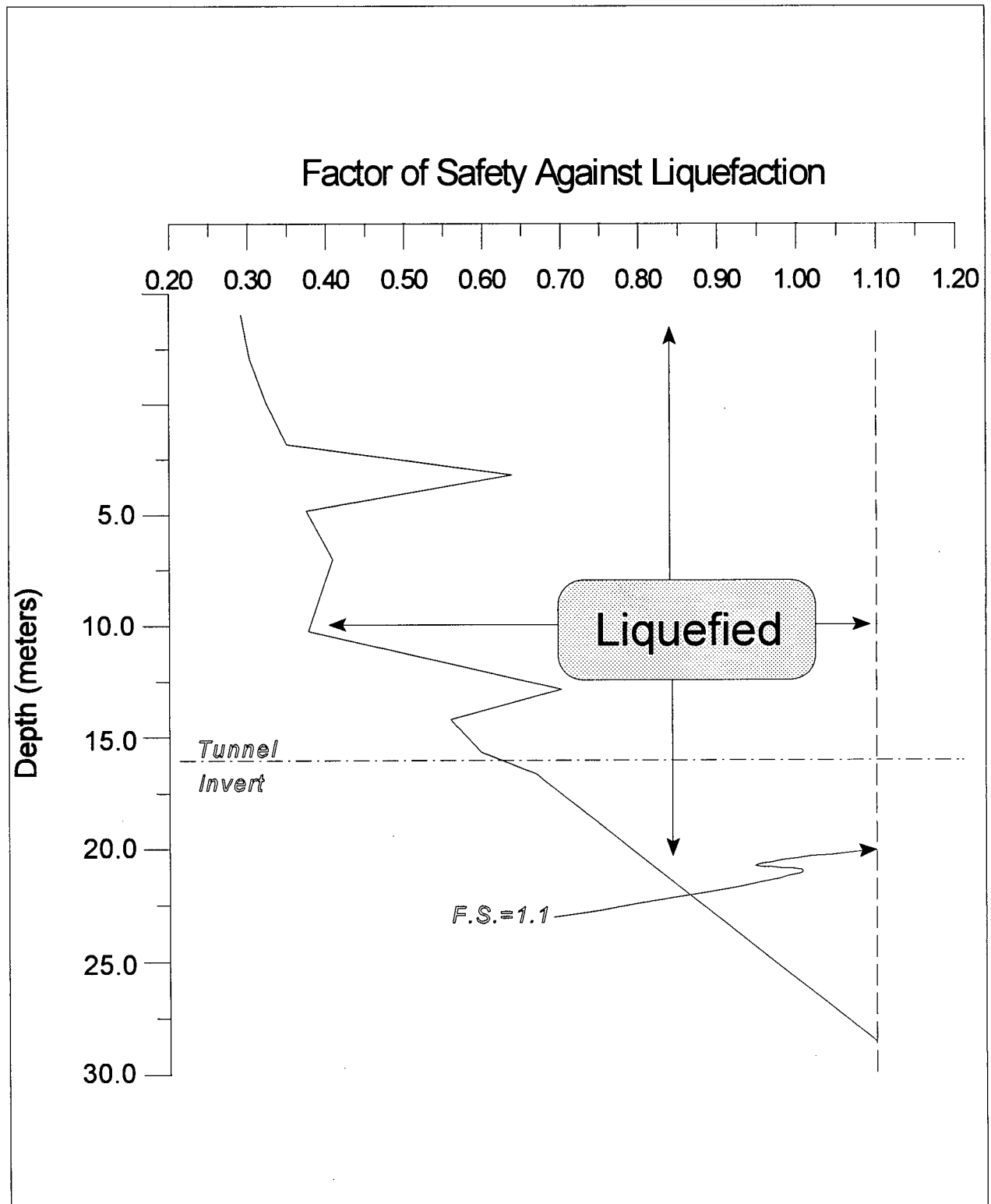


Figure 6.9 - Factor of Safety Against Liquefaction (FS_L) -- Location #8

6.3 Post-liquefaction Stability -- Flow Slides, Residual Strength (S_r), and Limiting Strains (γ_{Lim})

Refer to section 4.3 for descriptions of the procedures used in the post-liquefaction stability analyses. The results in this section should be reviewed in conjunction with the material in section 7.3.

Section 6.3.1 presents the results of the post-liquefaction limit equilibrium analyses, and section 6.3.2 presents summaries of two key post-liquefaction stress-strain parameters. Post-earthquake strength properties for each of the locations are listed on the graphic output (figures 6.10 and 6.11). Tables 6.7 and 6.8 summarize the residual strength (S_r) and limiting strain (γ_{lim}) magnitudes for each liquefied layer (at each location).

6.3.1 Flowslide Potential

Two separate types of analyses were done. At locations #7 and #8 (south and north river banks, respectively) the stability of the overlying dykes was analyzed; the analyses correspond to the plane parallel to the axis of the tunnel (i.e., longitudinal-direction). The offshore locations, on the other hand, were analyzed in the transverse section view.

In the limit equilibrium analyses at the river banks (locations #7 and #8), the failure surface was confined to the overlying dyke material (refer to figures 6.10 and 6.11). A lower bound residual strength was estimated for the dyke sands. As figure 6.10

shows, the estimated residual strength of the dyke material can be as low as 9 kPa at the south shore (location #7) and still remain stable (under the $F.S_{FL} > 1.3$ criteria). At location #8 (north shore) the dyke material could have a residual strength as low as 10 kPa. Appendix C.2 contains graphic output using a more realistic residual strength estimate of 26 kPa. Based on the results of these analyses, it can be concluded that the north and south shores are stable.

The graphic output from the flowslide analyses at the offshore locations (#2, #3, and #4) are shown in appendix C.1. Since the tunnel is founded on a level excavation, the tunnel is very stable in the direction transverse to the roadway (i.e., cross-section view). Refer to appendix C.1 for a description of the results of the analyses at the offshore locations.

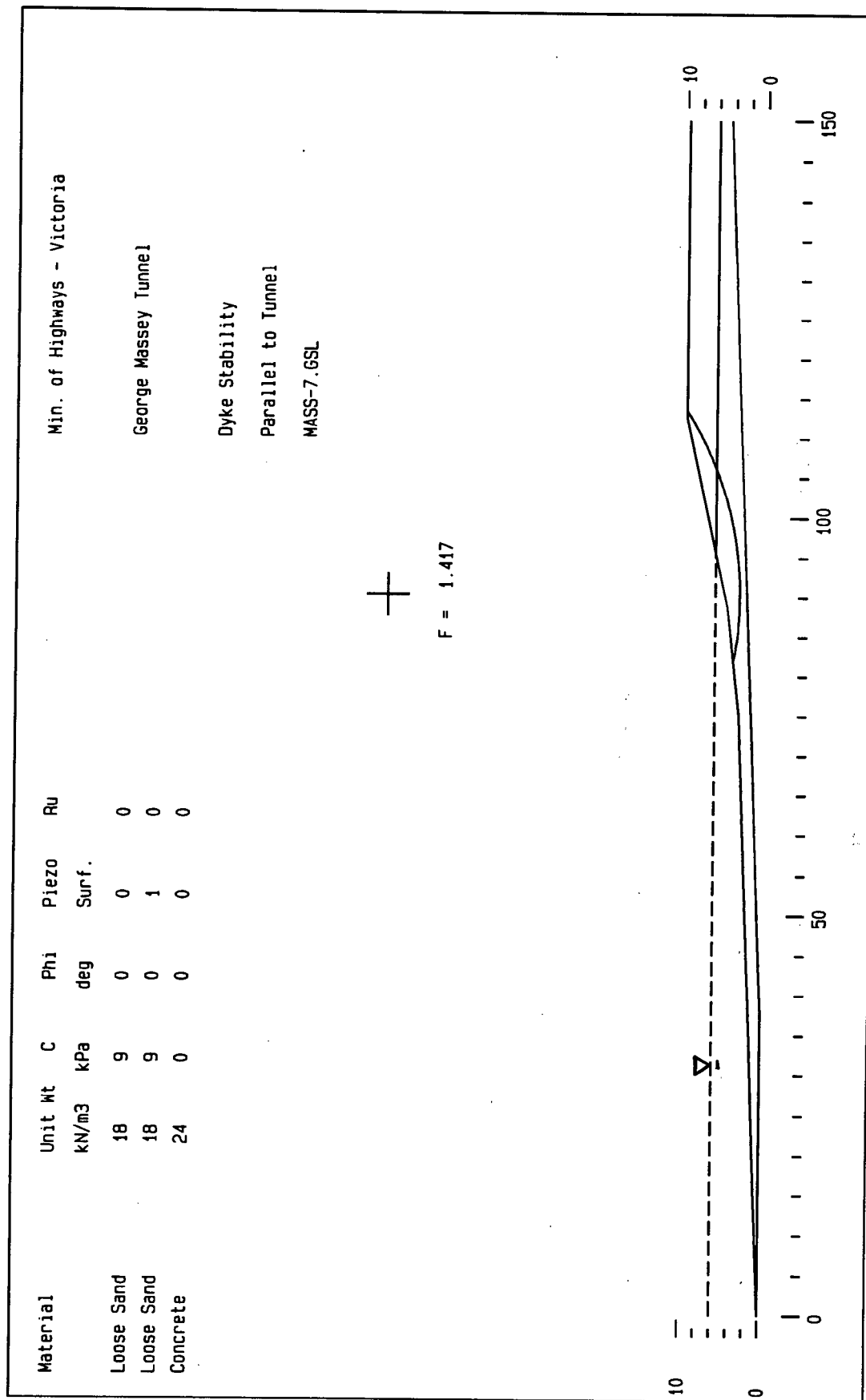


Figure 6.10 - Post-liquefaction Limit Equilibrium Stability Analysis at Location #7 (South Shore Dyke)

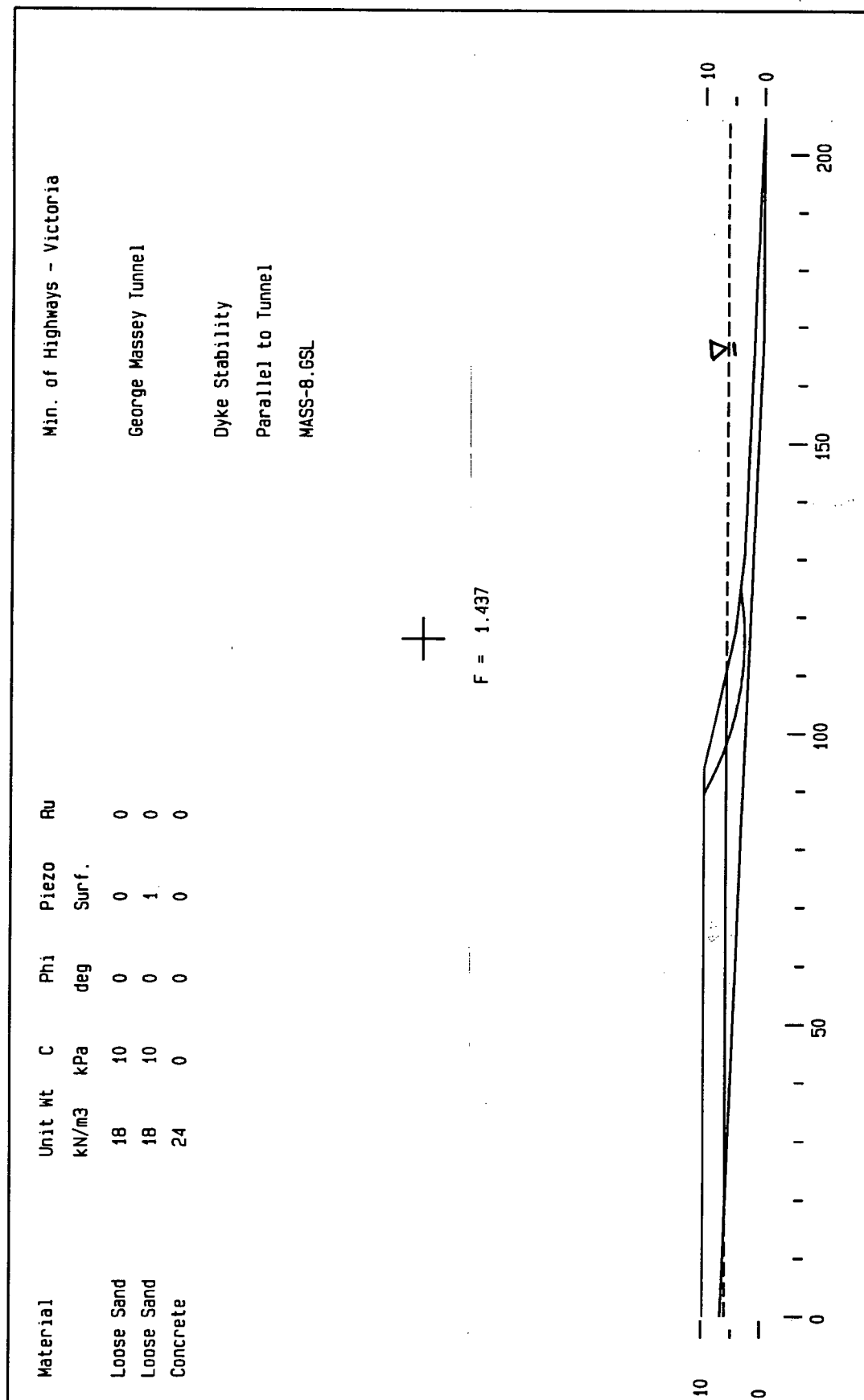


Figure 6.11 - Post-liquefaction Limit Equilibrium Stability Analysis at Location #8 (North Shore Dyke)

6.3.2 Residual Strength (S_r) and Limit Strain (γ_{lim}) Summaries

The summaries in this section should be reviewed when analyzing the SOILSTRESS results (in chapter 8). Residual strength (S_r) and limit strain (γ_{lim}) estimates for each of the analyzed locations are summarized in tables 6.7 and 6.8. The

Location	Material Type	Material Number	$(N1)_{60}$	Factor of Safety Against Liquefaction (FS_L)	S_u/σ'_{vo}	γ_{Lim} (%)	S_r (kPa)
#2	Sand	5	13	0.5	0.2	30	12
	Sand	6	13	0.5	0.2	30	12
	Silt	7	Not App.	Not App.	0.4	27	40
#3	Silt	5	Not App.	Not App.	0.4	27	30
#4	Silt	5	Not App.	Not App.	0.4	27	30
#8	Sand	5	10	0.7	0.2	25	40
	Sand	6	10	0.7	0.2	25	46
	Sand	7	10	0.7	0.2	25	56
	Sand	8	10	0.7	0.2	25	56
	Sand	10	10	0.5	0.2	30	26
#2, #3, & #4	Sand	3	4	Not Available	0.07	30	7
All	Sand	4	9	0.5	0.18	30	11

Table 6.7 - Residual Strength (S_r) and Limiting Strain (γ_{Lim}) Estimates for Transverse Direction Analyses

material numbers corresponding to the liquefied materials in table 6.7 are graphically shown in figures 6.12 and 6.13. The material numbers corresponding to the liquefied materials in table 6.8 are graphically shown in figure 6.14.

Material Number	Material Type	(N1) ₆₀	Factor of Safety Against Liquefaction (FS _L)	Su/σ' _{vo}	γ _{Lim} (%)	S _r (kPa)
2	Silt	N.A.	Not Available	0.4	27	30
3	Sand	4	Not Available	0.07	30	7
4	Sand	10	0.7	0.2	25	46
6	Sand	9	0.5	0.18	30	11
10	Sand	10	0.5	0.2	30	26
13	Sand	10	0.7	0.2	25	56

Table 6.8 - Residual Strength (S_r) and Limiting Strain (γ_{Lim}) magnitudes for Longitudinal Direction Analyses

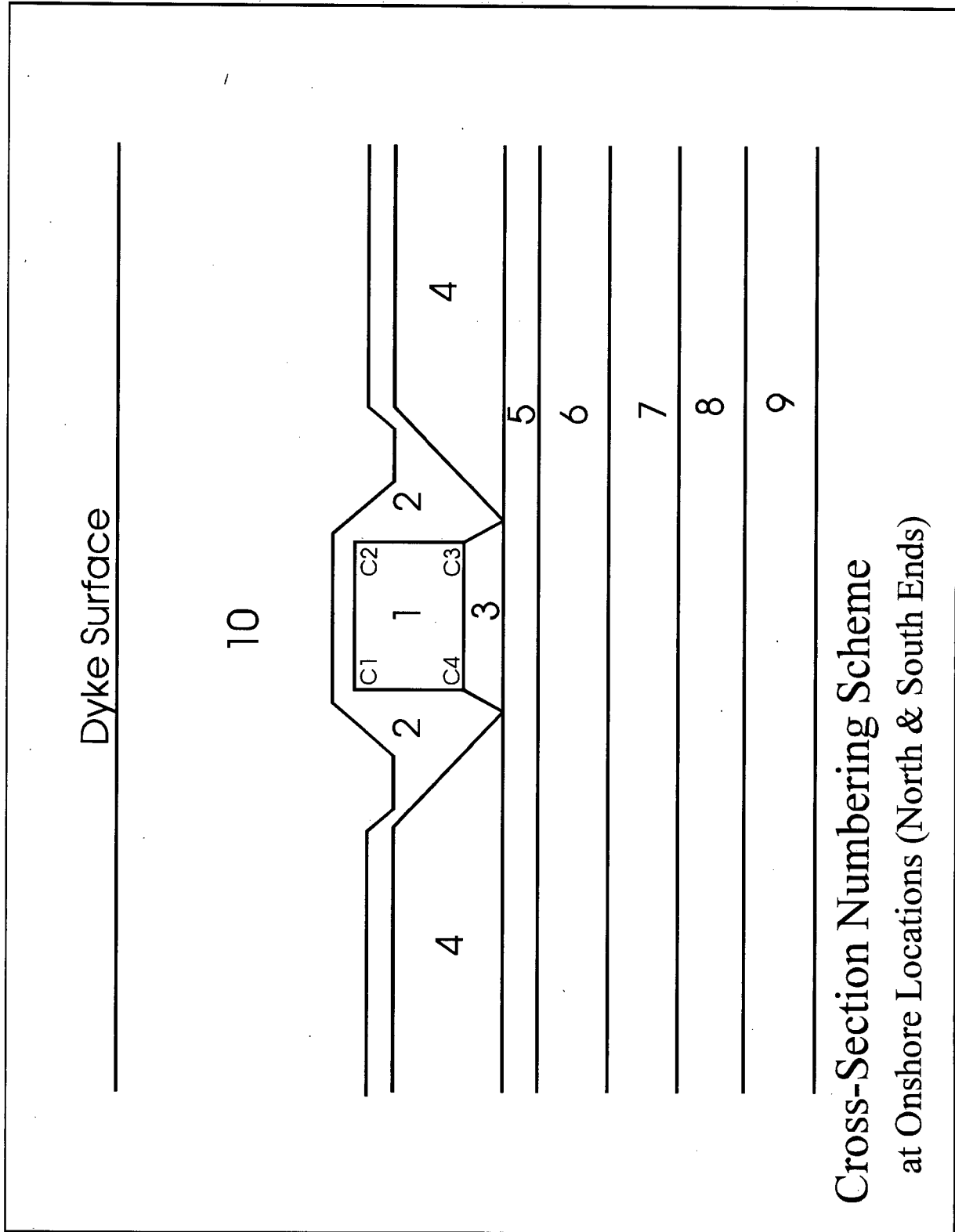


Figure 6.12 - Material Numbering Scheme at Onshore Locations (#7 and #8)

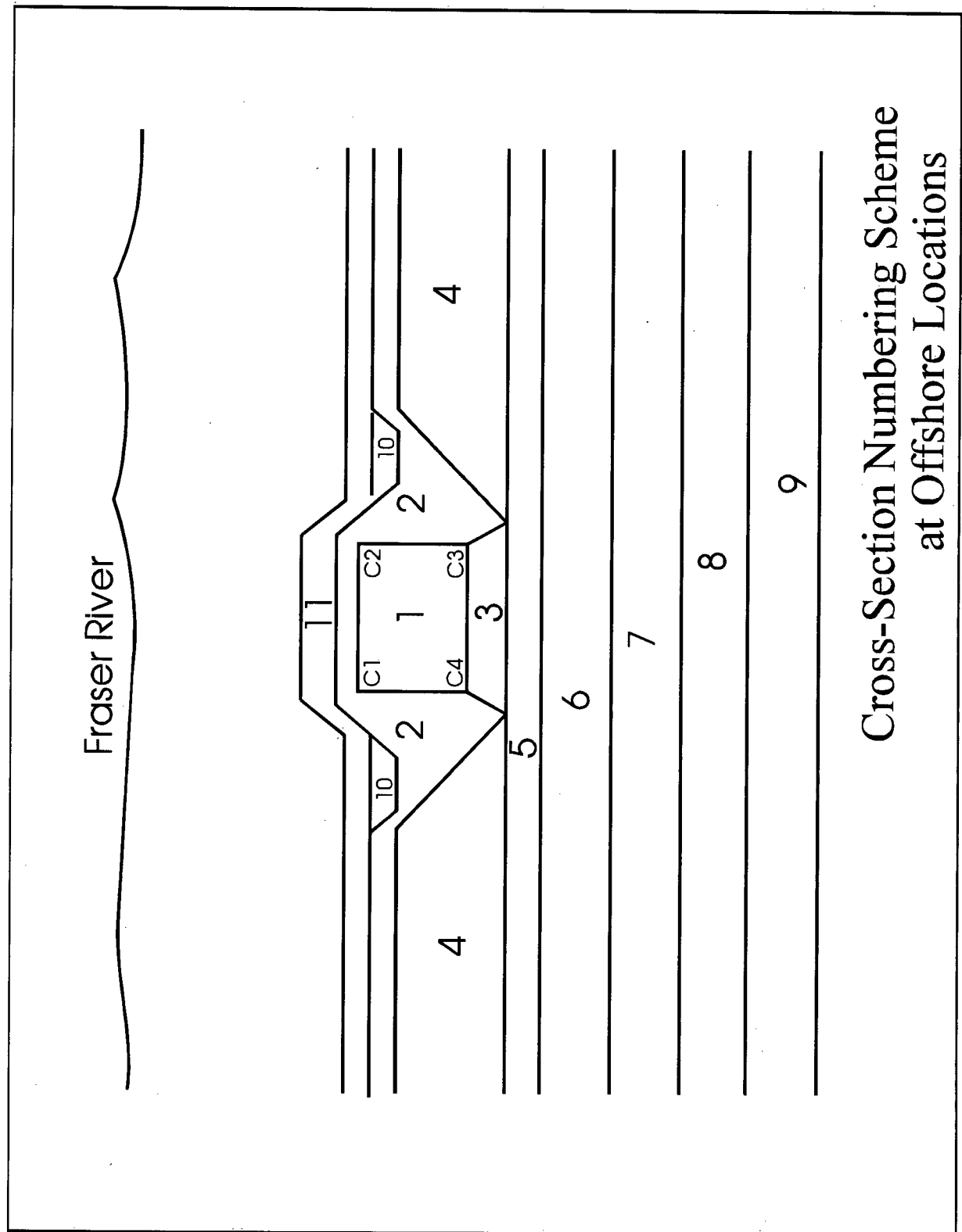


Figure 6.13 - Material Numbering Scheme at Offshore Locations (#2, #3, and #4)

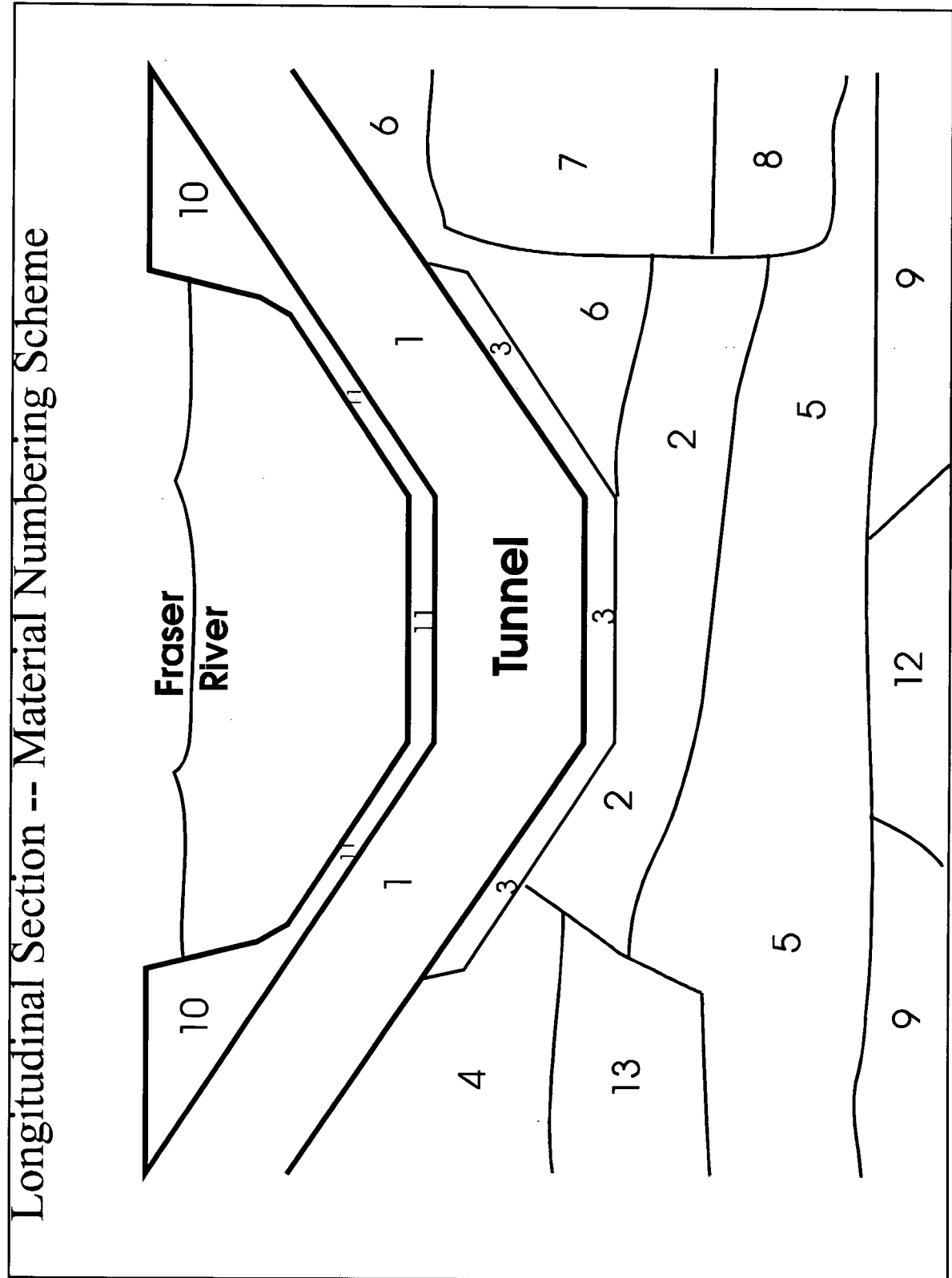


Figure 6.14 - Material Numbering Scheme for Longitudinal Section

CHAPTER 7

DISCUSSION OF CHAPTER 6 RESULTS

7.1 Introduction

This chapter presents interpretations of the results that are summarized in chapter 6. Interpretations focus on how the results compare with expectations, and why, in some cases, they differ. The information in each upcoming section should be reviewed with the corresponding section in chapter 6.

7.2 Liquefaction Assessment

7.2.1 Zones of Liquefaction

The discussion material in this section corresponds to the results of section 6.2. Refer to section 4.2 for a description of the liquefaction assessment procedures. In this section, the points of discussion are segregated by headings.

i.) Methods of Liquefaction Assessment:

The stratigraphy (soil layers and thicknesses) vary along the length of the tunnel. As table 6.1 shows, depths to liquefaction vary along the length of the tunnel. Directly beneath the tunnel, the soils comprise sands and silts. As described in section 4.2, the liquefaction resistance of sands was based solely on the available CPT data. In plastic silts, the Chinese criteria (Wang, 1979) was used, whereas both penetration data and shear wave velocity data were used to assess liquefaction potential of non-plastic silts.

Non-plastic silts were analyzed using both the Robertson (1990) and Seed (1984) criteria. The Robertson correlation is based on data from sands with fines contents ranging from 10% (Niigata) to 35%. It is assumed that the generally higher fines contents of the silts at the tunnel site will mean that the CRR estimates using the Robertson correlation are lower. The Robertson correlation is limited because it is derived from a small data base.

As mentioned earlier, direct testing of undisturbed samples is the best method for estimating the CRR of a soil.

ii.) Soil Profile at Location #7:

One additional point of concern was highlighted by the CPT data at location #7. Because of the homogeneous nature of the sand at location #7, it was thought that it may be post-excavation backfill. But the Canadian Liquefaction Experiment (CANLEX) test data (in the vicinity of location #7) aren't as uniform, yet they're of similar cone resistance; therefore, the ----sands were assumed to be natural. CANLEX did some CPT's and sample retrievals at the south end of the tunnel. Though some of the CANLEX data is detailed, it was judged to be in sufficient agreement with CPT #91-7, so that there was no need to distinguish it in this study.

7.2.2 Cyclic Loading and Spectral Response -- SHAKE

The discussion material in this section corresponds to the results of section 6.2. Refer to section 4.2.3 for a description of the ground response analyses.

i.) Ground-Motion Amplification Factors:

Appendix B.4 contains a tabular summary of the amount of amplification of ground motions from the soil profile base to the surface. In general, there is a great deal of amplification through the surface layers. There is significant decoupling of ground motions at the interfaces between surficial loose sands and underlying silts. Ground-motions were amplified by a factor of 1.5 to 2 from base to surface, in most cases. These amplification factors are in agreement with the Fraser Delta ground response study by Sy et al. (1991). For instance, location #7 shows an increase in predicted acceleration from 0.28g to 0.38g within the top three surface layers. This generally occurs at the site, at locations where there is a transition from silt up to loose sand.

ii.) Soil Damping & Modulus Reduction:

As discussed in section 4.2.3, to account for soil damping and modulus reduction (versus shear strain), data published by Sy et al. (1991) for Fraser Delta sands and silts was applied in the SHAKE analyses. Ground response is strongly dependent on these parameters. For comparison purposes, SHAKE analyses were performed using other damping and modulus reduction estimations (Idriss 1990, Vucetic 1991, etc.), but they

provided amplifications which were inconsistent with amplification factors published by Lo et al.(1991) and Byrne & Anderson (Fraser Delta Task Force, 1991) for the Fraser Delta.

iii.) Response Spectra:

Figures B.3.1 to B.3.5 (in appendix B.3) depict the surface spectral response at the five locations. Spectral shapes depend upon earthquake magnitude and site conditions. The frequency content of the records used is also illuminated by the shape of the response spectra. Softer soils often increase the spectrum response values in the long period range. In general, soils tend to attenuate low period motions and amplify high period ground motions. It has been estimated that the tunnel has a fundamental period of vibration in the range of 0.5 and 4.0 seconds (Ker Priestmann, 1989), though it is most likely in the longer period range. As the figures show, amplification of ground motions within the lower period range is low. The possibility of a magnified response (approaching resonance) between the tunnel and soil is limited.

iv.) Depth to Firm Ground:

As discussed in section 5.3, firm ground (presumed to be Pleistocene) was encountered at a depth of 200 meters in a seismic reflection survey. Though many past ground response analyses in the Fraser Delta (i.e., Wallis, 1979; Sy et al., 1991, etc.) incorporate both bedrock and the Pleistocene within the soil column estimate, it is known

that SHAKE is not designed for simulating the movement of shear waves through a dense layer (i.e., Pleistocene). Instead, it can be presumed that strong ground motions travel along the surface of a dense layer, and then propagate up through the surficial layers (Byrne, 1994b). Consequently, it was considered appropriate not to use the bedrock depth estimate of 700 meters in this study. A shear wave velocity of 3500 ft/s was applied in the base material for all of the SHAKE analyses. A graphic comparison of results at location #2 using velocities of 1000 ft/s, 3500 ft/s, and 8000 ft/s is shown in appendix B.2. As expected, figure B.2.1 shows that there is a noticeable increase in peak parameters as the firm ground velocity estimate is increased.

v.) Potential Structural Influence and Multi-dimension Dynamic Analyses:

The effect of the tunnel has not been incorporated in the ground response analyses. It can be speculated that, since the relatively stiff tunnel could not be included as part of the soil columns, the peak parameter estimates are conservative. An alternative would have been to use rigorous two- or three-dimensional dynamic analyses, but they are, in general, complex and require extensive evaluation of parameters. Due to the lack of detailed soil data at this site, the use of two-dimension analyses would have been inappropriate. Additionally, since the tunnel is founded within a shallow excavation in the river bed, it was deemed unnecessary to account for tunnel-structure effects within the free-field, so multi-dimension dynamic analyses were considered unnecessary.

Because SHAKE lacks the ability to account for two- or three-dimensional effects, cyclic shear stress magnitudes are likely under-estimated. SHAKE'S one dimensional method has been compared with a two dimensional approach (2-D FLUSH -- Jong, 1988). Jong found that the one-dimensional analysis peak cyclic shear stress estimations were up to 15% lower than those of the two-dimensional analysis. On the other hand, it should be noted that when the tunnel was constructed, the excavation resulted in a decrease in the overburden stresses (below the tunnel). This change in σ'_{vo} cannot be accounted for in the CPT results, so this contributes a little to the uncertainty. A decrease in effective stress decreases the liquefaction potential of a soil, consequently, the underlying soil's resistance to liquefaction has been increased due to the placement of the tunnel, whose average unit weight is approximately one-half that of the original overburden soil.

7.3 Post-Earthquake Stability -- Flow Slides, Residual Strength, and Limiting Strains

The discussion material in this section corresponds to the results of section 6.3.

Refer to section 4.3 for a description of the post-earthquake stability inputs and analyses.

i.) Estimation of Residual Strengths in Sands:

As described in section 4.3.2, the principal relation used to estimate residual strengths was the procedure suggested by Stark & Mesri (1992).

It should be noted that Stark & Mesri (1992) stated that post-liquefaction stability analyses cannot assume drainage and must be based on a constant volume critical strength -- as opposed to the assumption of some other published relations, in which drainage has obviously occurred, causing the peak strength to rise. Consequently, the Stark & Mesri (1992) estimates tend to be lower than those estimates based on typical case-history back-calculations.

ii.) Estimation of Residual Strength and Limiting Strains in Silts:

As described in section 4.3.2, data from the BC Hydro Transmission Tower study (summarized in appendix G.2) was used to estimate residual strengths in silts. The data from sample #HSS1 indicates an S_u/p ratio of 0.4 at an effective confining stress of 80kPa. This ratio was applied to obtain the results shown in tables 6.7 and 6.8. Additionally, stress-strain data (figure G.2.1 in appendix G.2) was used to estimate the

limit strain (the strain required to mobilize the residual strength) in the silts. An estimate of $\gamma_{\text{lim}} = 27\%$ was obtained from the figure.

Additionally, for comparison, the method proposed by Senneset et al.(1981) was applied to estimate undrained strengths in the silts. CPT penetration resistances varied between 600 kPa and 900 kPa. So, using an average $N_c'=15$, the undrained strength estimates ranged between 40 kPa and 60 kPa; therefore, this method was in agreement with the BC Hydro data-based residual strength estimates. Furthermore, a lower-bound undrained strength of 40 kPa was estimated using data from the Chatfield Dam & Birch Dam sites (Duncan & Byrne, 1980).

7.4 Future Work

i.) Soil Data:

Test data is limited, and a larger data base would benefit any future studies. More in-situ testing on the upstream side of the tunnel should be done. Preferably cone penetration tests (CPT) would be done at points between the 1991 CPT locations. To confirm the validity of this study's assumption -- that soil layers can be extended horizontally (i.e., to both sides of the tunnel) -- an adjacent CPT could be performed on the opposite side of the tunnel. Additionally, since the loose sand extends deeper as the north river bank is approached, another CPT should be done between location #4 and the north river bank (location #8). Seismic shear wave velocity data should be collected.

ii.) Ground Response Analyses:

The acceleration time-histories used in this study are from the San Fernando strike-slip type earthquake. The anticipated major earthquake in British Columbia is a subduction type event. A future assessment could be based solely on records from subduction events.

CHAPTER 8

RESULTS: POST-EARTHQUAKE DISPLACEMENTS

8.1 Introduction

Results from the empirical and numerical method displacement analysis methods are summarized graphically and in tabular form in this chapter.

It should be noted that, the results of the various analyses are independently summarized in this chapter, but are compared in section 9.2 (in chapter 9). All results are discussed in chapter 9. Each of the upcoming sections points out the corresponding section in chapter 9 that should be referred to while reviewing the individual result summaries in this chapter.

8.2 Empirical Methods -- Displacement Predictions

Refer to section 4.4.2 for descriptions of the procedures used in the empirical method displacement analyses. Section 9.3 discusses the results in this section, and appendix D contains detailed summaries of the inputs used.

Table 8.1 summarizes the lateral displacement predictions using the Bartlett-Youd (1992) and Hamada (1987) methods. The total liquefied layer thickness at location #2 is approximately 10 meters, and at locations #3 and #4, there is approximately 3 meters of liquefied sandy silt. At location #8, there is approximately 14 meters of liquefied sand. Both sets of analyses correspond to ground slopes of 1% and 3%. The Bartlett-Youd

Location	Bartlett - Youd (meters)		Hamada (meters)	
	1%	3%	1%	3%
#2	0.5	0.8	3.4	4.8
#3	Not Applicable	Not Applicable	1.1	1.5
#4	Not Applicable	Not Applicable	1.1	1.5
#8	0.6	1.0	4.0	5.7

Table 8.1 - Empirical Method Displacement Estimates

predictions are based on a horizontal epicentral distance of 30 kilometers. These inputs are discussed in section 4.4.2.2. As the table shows, the Bartlett-Youd predictions are much lower than the corresponding Hamada estimates. Bartlett-Youd analyses were not done at locations #3 and #4 due to the high fines content of the liquefied soils.

As discussed in section 4.4.2.4, the method developed by Tokimatsu and Seed (1987) was used to estimate liquefaction induced settlements. Table 8.2 summarizes the predictions. As expected, the locations with the greatest depth to liquefaction (i.e., locations #2 and #8) show the largest magnitudes.

As discussed in section 4.4.3.2, the Tokimatsu/Seed correlation was used to estimate volumetric strains for the SOILSTRESS analyses. The estimates in table 8.2 have been provided only as a reference for the SOILSTRESS vertical displacement estimates, which include both movement due to undrained distortion, and consolidation

due to excess pore-pressure dissipation.

Location	Cumulative thickness of Liquefied Layers (meters)	Settlement	
		(centimeters)	(feet)
#2	10	29	1.0
#3	2	6	0.2
#4	2	5	0.2
#8	14	35	1.1

Table 8.2 - Tokimatsu/Seed Method Post-Liquefaction Settlement Estimates

8.3 Numerical Methods -- Displacement Predictions

8.3.1 Introduction

Section 8.3 consists of two general parts: summaries of the SOILSTRESS predictions, followed by the LIQDISP predictions. Both sections 8.3.2 and 8.3.3 summarize the input parameters and the displacement estimates for each particular analysis.

Section 8.3.2 contains graphic output and tabular summaries of the lateral and vertical SOILSTRESS displacement predictions for all five locations.

The discussion material in section 9.4 should be reviewed in conjunction with the results in this section.

8.3.2 Finite Element Method (SOILSTRESS) Displacements

The procedures used to perform the SOILSTRESS analyses are described in section 4.4.3. Results correspond to a peak ground velocity (v_{\max}) of 0.30m/s. The choice of this value is discussed in section 9.4.1.

First, transverse-direction (cross-section) displacements at the north and south shores are summarized. Those analyses are followed by summaries for the offshore locations. At the offshore locations, the sediment loading (on top of the tunnel) is varied, and the effects of increasing the peak ground velocity are analyzed, also. Finally, displacements in the plane parallel to the axis of the tunnel ('longitudinal direction') are

assessed (in section 8.3.2.2).

Section 8.3.3 summarizes the results of the single-degree-of-freedom LIQDISP analyses. SOILSTRESS analyses showing the effects of remedial measures are summarized and discussed in chapter 10.

8.3.2.1 Transverse-Direction SOILSTRESS Analyses

Figures 6.12 and 6.13 show the material numbering schemes for the tunnel cross-section at the onshore and offshore locations, respectively. Figures 8.3 to 8.15 show the displacement pattern and displacement vector graphics for the transverse section analyses. The displacement vector images have been provided to aid in interpreting the displacement patterns. As shown in figures 6.12 and 6.13, "C1" and "C3" correspond to the top left and bottom right corners of the tunnel's concrete section. The displacements at the two corners are provided to show the magnitude of tunnel rotation and differential movement between the sides of roadway. In the tabular displacement summaries, a negative vertical displacement indicates a downward movement.

For each particular SOILSTRESS analysis, the pre- and post-earthquake parameters are presented in tables that precede the corresponding displacement summaries. Table 8.3 presents inputs for materials which were applied in all of the transverse section analyses (Eg. concrete roadway). Figures 6.12 and 6.13 show the relative locations of the materials.

Because of the seasonal sediment load variation, two separate analyses have been performed at each of the offshore locations. The first (Case #1 -- section 8.3.2.1.2) of the two sets of analyses corresponds to a case of two meters of sediment loading on top of the tunnel, and the second case (Case #2 -- appendix A.1.1) corresponds to the condition of no sediment loading.

All Locations									
Material Number	Soil Type	K_a	n	K_b	m	R_f	ϕ (deg)	$\Delta\phi$ (deg)	C (kPa)
1	Concrete	50000 (50000)	0.5	200000	0.25	0.5	50	0	1000
2	Compact Gravel	1200 (600)	0.5	1800	0.25	0.6	47	7	0
3	Liquefied Sand Fill	181 (0.1)	0.5 (0)	2000	0.25	0.9 (0)	32 (0)	0	0
4	Loose Sand	505 (0.4)	0.4	2000	0.25	0.8 (0)	33 (0)	0	0
10*	Sand (overburden)	200 (0.9)	0.5 (0)	2000	0.25	0.8 (0)	33 (0)	0	0

Table 8.3 - SOILSTRESS Pre- and Post-liquefaction Inputs For Transverse (Cross-section) Analyses at All Locations

Notes: - values in parentheses are post-earthquake estimates

- * Material #10 is the sand overburden at the north and south dykes (i.e., Locations #8 and #7, respectively)

Case #3 (appendix A.1.2) shows the effects of increasing the sediment load on top of the tunnel, and Case #4 (appendix A.1.3) shows the effects of increasing the peak ground velocity (v_{max}) from 0.30 m/s to 0.38 m/s.

8.3.2.1.1 Displacements at North and South Shores (Dykes)

Tables 8.4 to 8.6 summarize input parameters for the SOILSTRESS analyses at the onshore locations. (Refer to figure 6.12 for the material numbering scheme). Figures 8.1 and 8.2 show the final stratigraphies used in the analyses.

For post-earthquake conditions, a 50% reduction in stiffness was applied to all non-liquefied materials due to the severity of shaking (i.e., $v_{\max} = 0.3$ m/s). Table 8.4 contains key stiffness and strength parameters. Refer to section 6.3 for more detailed results of post-liquefaction parameters.

Location (Dyke)	Material Type	Material Number	Shear Modulus (G_{\max} in kPa)	$(k_g)_i$ (Initial)	γ_{Lim} (%)	S_r (kPa)	$(k_g)_f$ (final)
#8	Sand	4	51170	505	30	11	0.3
	Sand	5	72170	712	25	40	1.6
	Sand	6	51200	505	25	46	1.8
	Sand	7	57770	570	25	56	2.2
	Sand	8	57770	570	25	56	2.2

Table 8.4 - SOILSTRESS Inputs for Liquefied Materials at North Shore

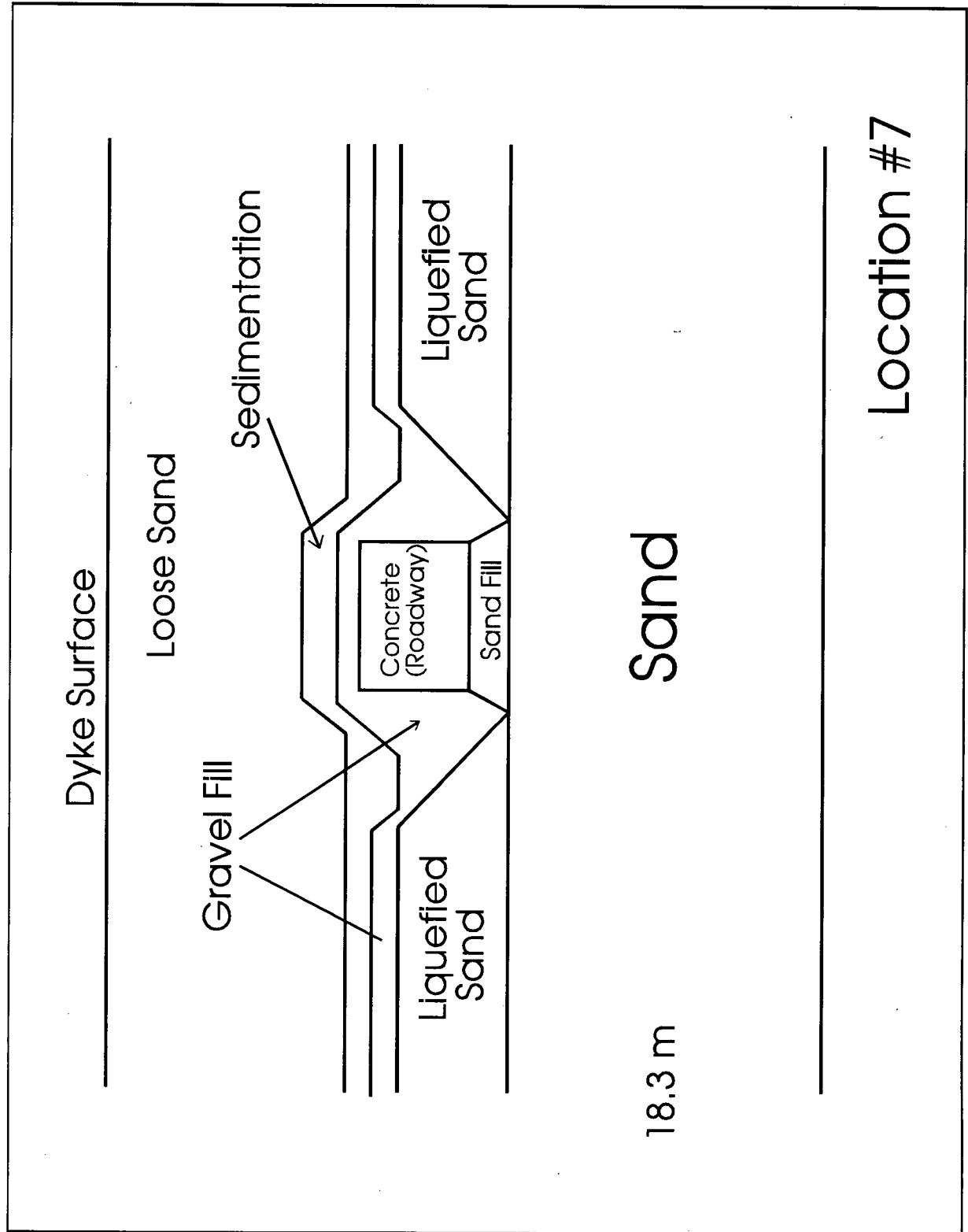


Figure 8.1 - Final Stratigraphy at Location #7

Location #7									
Material Number	Soil Type	K_g	n	K_b	m	R_r	ϕ (deg)	$\Delta\phi$ (deg)	C (kPa)
5	Partially Liquefied Sand	955 (100)	0.5	2000	0.25	0.7	37	2	0
6	Partially Liquefied Sand	712 (100)	0.5	2000	0.25	0.7	37	2	0
7	Partially Liquefied Sand	1044 (100)	0.5	2000	0.25	0.7	37	2	0
8	Partially Liquefied Sand	1044 (100)	0.5	2000	0.25	0.7	37	2	0
9	Partially Liquefied Sand	570 (100)	0.5	2000	0.25	0.7	31	0	0

Table 8.5 - SOILSTRESS Pre- and Post-earthquake Inputs -- Location #7

Note: values in parentheses are post-earthquake estimates

Location #8									
Material Number	Soil Type	K_g	n	K_b	m	R_r	ϕ (deg)	$\Delta\phi$ (deg)	C (kPa)
5	Liquefied Sand	712 (1.6)	0.5 (0)	2000	0.25	0.8 (0)	35 (0)	0	0
6	Liquefied Sand	505 (1.8)	0.5 (0)	2000	0.25	0.8 (0)	35 (0)	0	0
7	Liquefied Sand	570 (2.2)	0.5 (0)	2000	0.25	0.8 (0)	35 (0)	0	0
8	Liquefied Sand	570 (2.2)	0.5 (0)	2000	0.25	0.8 (0)	35 (0)	0	0
9	Silt	747 (374)	0.5	2000	0.25	0.6	34	0	40

Table 8.6 - SOILSTRESS Pre- and Post-earthquake Inputs -- Location #8

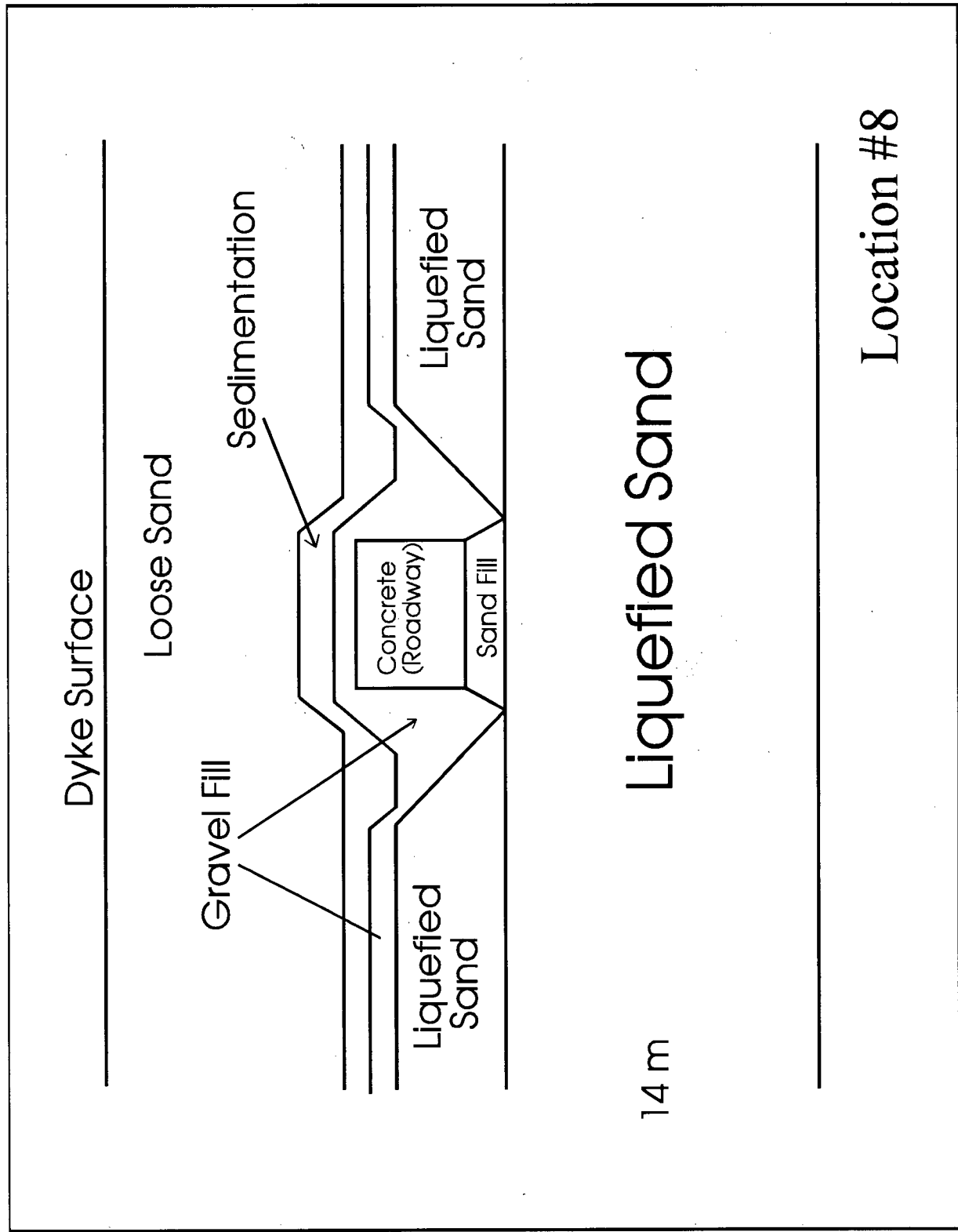


Figure 8.2 Final Stratigraphy at Location #8

Table 8.7 summarizes the horizontal and vertical displacement predictions at locations #7 and #8. The 'pre-consolidation vertical displacement' is the movement due to undrained distortion, and the '2-Dimension vertical displacement' is the total predicted vertical movement in which settlement due to dissipation of excess pore-pressures is also included. The Tokimatsu/Seed method (1987) was applied (refer to section 4.4.2.4) to determine the volumetric strain inputs for the settlement calculations in all of the SOILSTRESS analyses. The 'total vertical displacement' (in the final column of the table) represents the full 3-dimensional effect by incorporating the undrained vertical distortion estimates from the longitudinal analyses. (Refer to section 8.3.2.2 for longitudinal pre-consolidation estimates).

Location	Corner	HORIZONTAL Displacement (meters)	Pre - Consolidation Vertical Displacement (centimeters)	2-Dimension VERTICAL Displacement (centimeters)	TOTAL (3-Dimension) VERTICAL Displacement (centimeters)
#7	C1	0.021	-0.8	-5.9	-6.5
	C3	0.021	-0.6	-5.6	-6.2
#8	C1	0.82	7.9	-33.5	-31.3
	C3	0.84	14.5	-27.0	-24.8

Table 8.7 - Displacements at North & South Shore Locations

Note: - A negative vertical displacement indicates a downward movement

Figures 8.3 to 8.6 show the displacement pattern and displacement vector

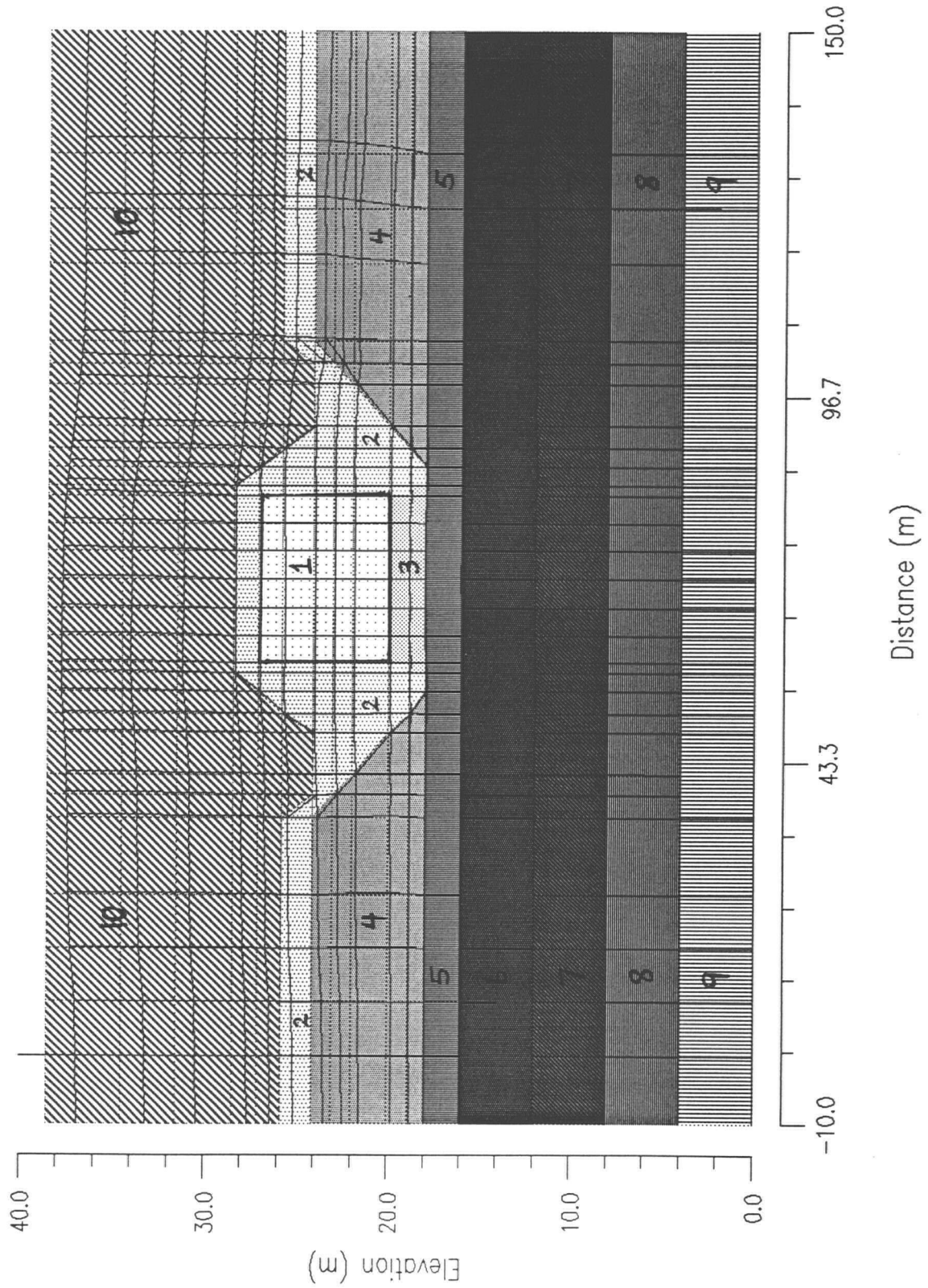


Figure 8.3 - Displacement Pattern -- Location #7

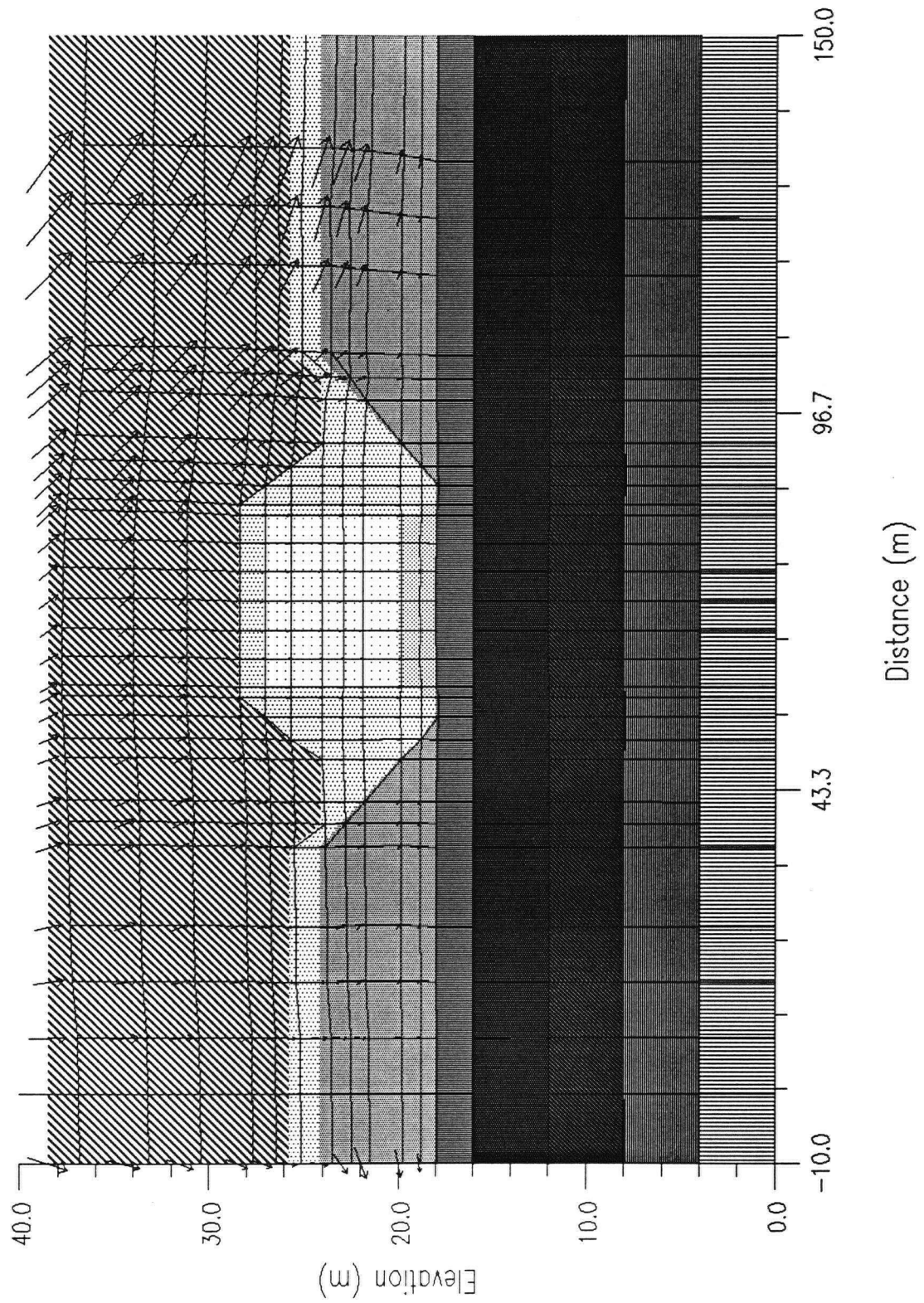


Figure 8.4 - Displacement Vectors -- Location #7

graphics for locations #7 and #8. The dashed lines represent the initial state, and the solid lines show the post-earthquake position of the nodes. The displacements are magnified by a factor of two.

At location #7, no liquefaction was predicted in the underlying soil units, but at location #8, soil units #5 to #8 liquefy. Location #7 (south river bank) shows very small horizontal and vertical movements because no liquefaction was predicted to occur below the tunnel invert. The overlying loose sand (dyke) deforms noticeably, but it has little influence on the underlying movements. Refer to section 9.4.1.1 for a discussion of the similarities between locations #7 and #8.

Figure 8.5 shows the magnitude and pattern of displacement at location #8. As summarized in table 8.7, the horizontal movements are approximately 0.8 meters, and the total vertical displacement is approximately 0.3 meters. The displacement pattern shows that the movement of the concrete section is controlled by the underlying unit #5 and #6 sands.



Figure 8.5 - Displacement Pattern -- Location #8

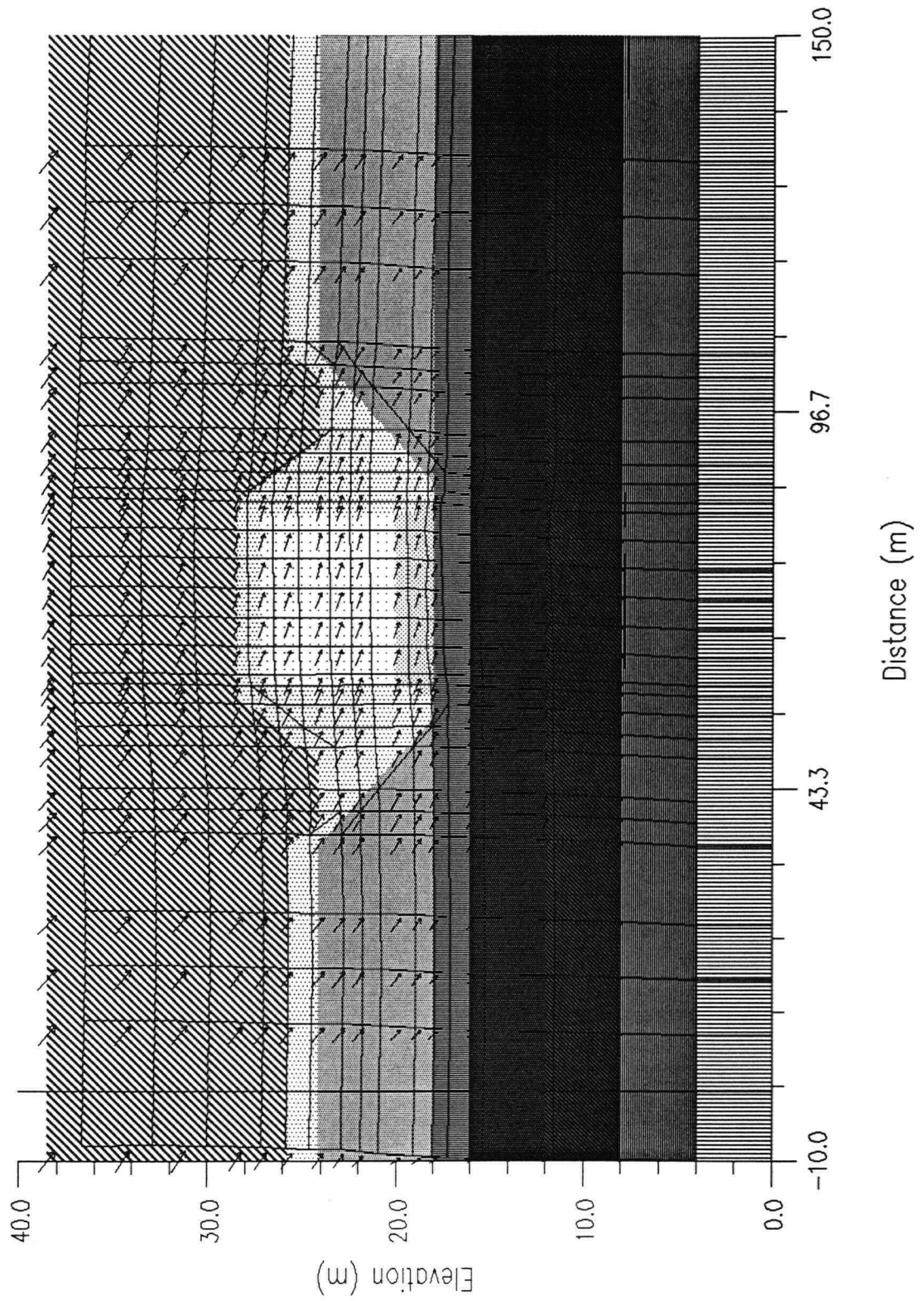


Figure 8.6 - Displacement Vectors -- Location #8

8.3.2.1.2 Displacements at Offshore Locations

The analyses in this section are referred to as the 'Case #1 analyses'. Cases #2 and #3 are analyses with different levels of sediment on top of the tunnel, and case #4 shows the effect of increasing the earthquake ground velocity. The results of the case #2 to #4 analyses are summarized in appendix A.1. Case #1 represents the most realistic representation of the current sediment conditions at the tunnel. Figures 8.7 to 8.9 show cross-section summaries for the location #2, #3, and #4 analyses. Tables 8.8 to 8.11 summarize input parameters for the analyses at the offshore locations. (Refer to figure 6.13 for the material numbering scheme). Table 8.11 contains key stiffness and strength parameters. Refer to section 6.3 for more detailed results of post-liquefaction parameters.

Location #2									
Material Number	Soil Type	K_r	n	K_b	m	R_r	ϕ (deg)	$\Delta\phi$ (deg)	C (kPa)
5	Liquefied Sand	675 (0.4)	0.5 (0)	2000	0.25	0.7 (0)	35 (0)	0	0
6	Liquefied Sand	505 (0.4)	0.5 (0)	2000	0.25	0.7 (0)	34 (0)	0	0
7	Liquefied Silt	605 (1.5)	0.5 (0)	2000	0.25	0.7 (0)	34 (0)	0	40
8	Silt	675 (338)	0.5	2000	0.25	0.7	34	0	40
9	Silt	712 (356)	0.5	2000	0.25	0.6	34	0	40

Table 8.8 - SOILSTRESS Pre- and Post-earthquake Inputs -- Location #2

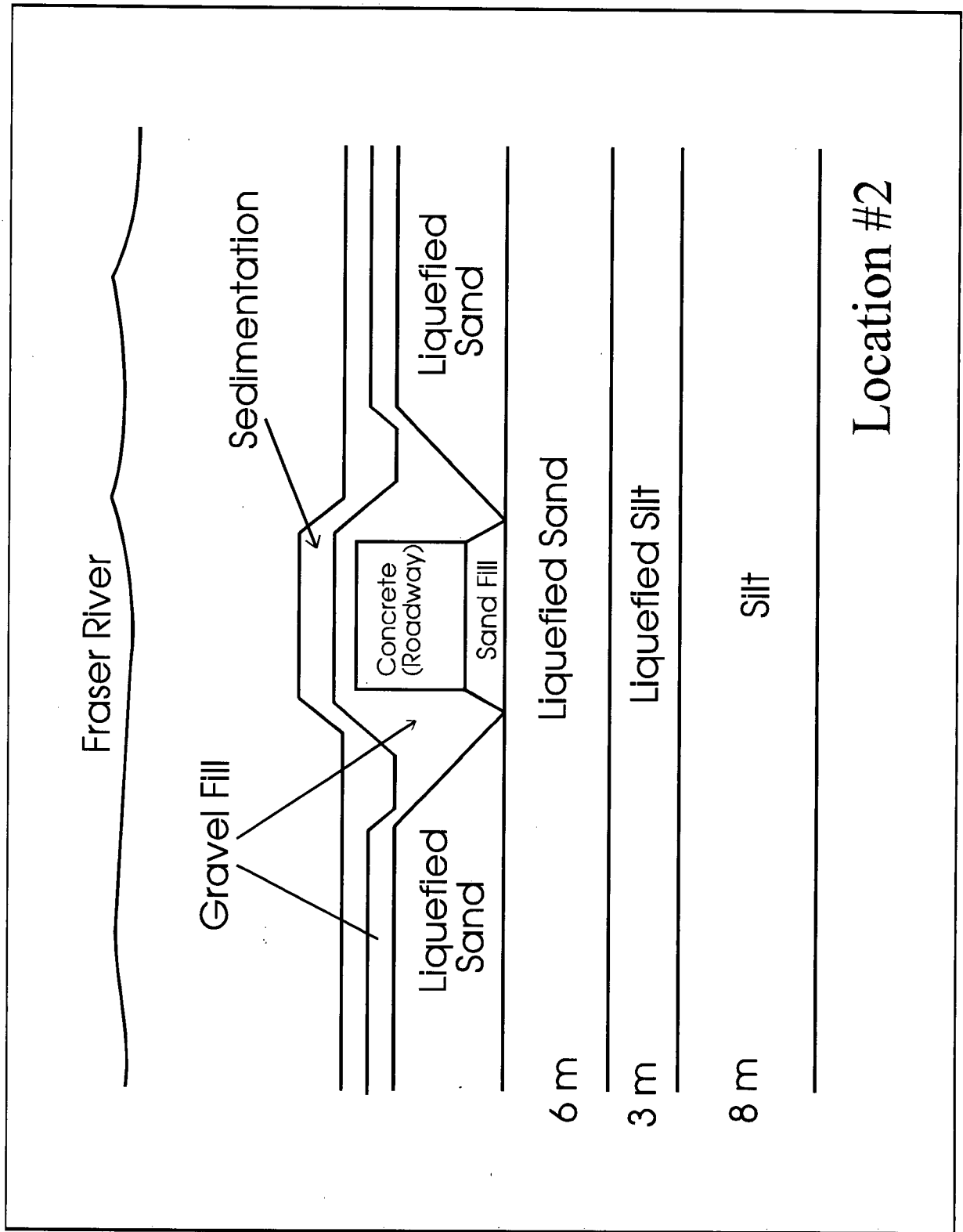


Figure 8.7 Final Stratigraphy at Location #2

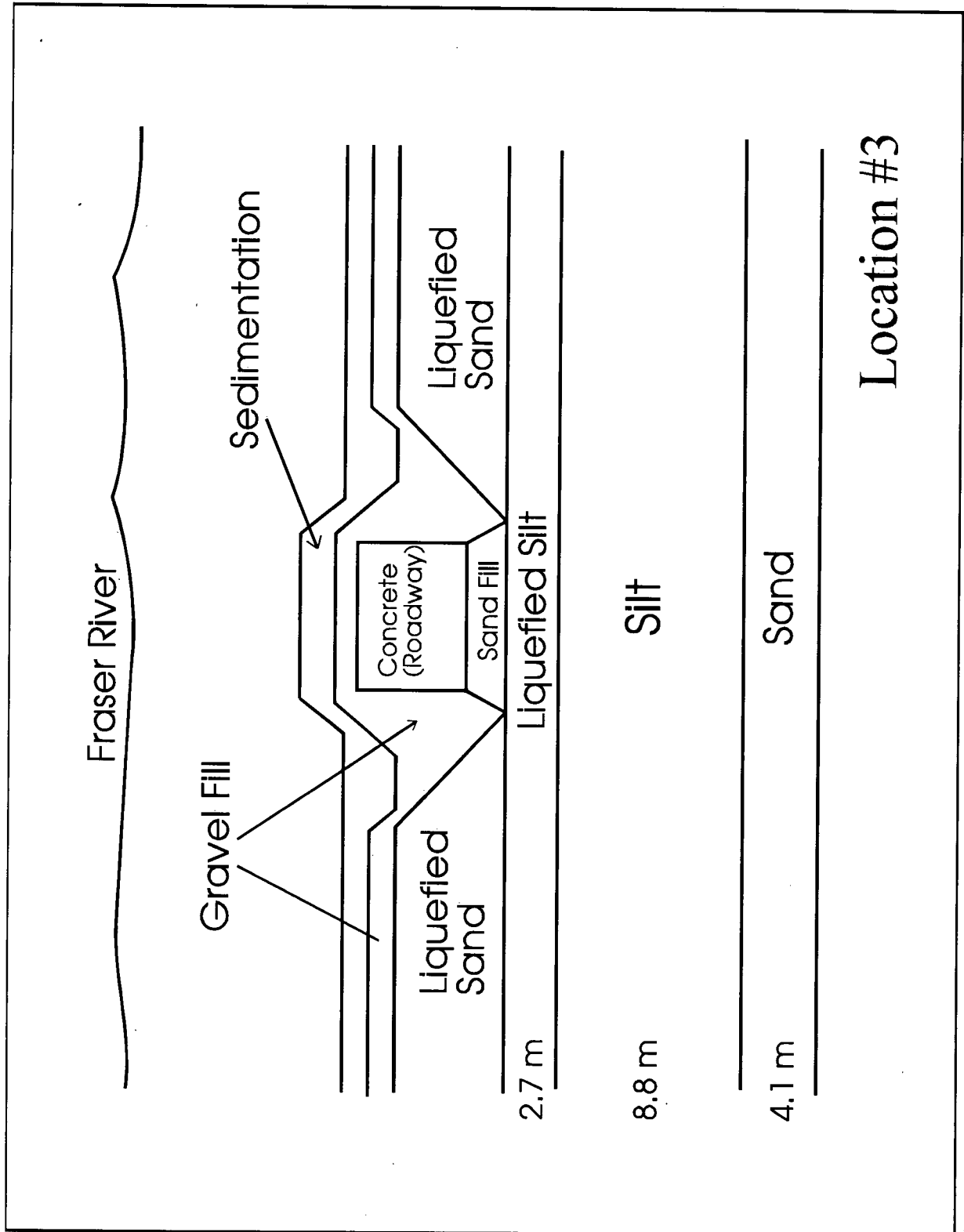


Figure 8.8 Final Stratigraphy at Location #3

Location #3									
Material Number	Soil Type	K_g	n	K_b	m	R_r	ϕ (deg)	$\Delta\phi$ (deg)	C (kPa)
5	Liquefied Silt	387 (1.1)	0.5 (0)	2000	0.25	0.7 (0)	34 (0)	0	30
6	Silt	474 (237)	0.5	2000	0.25	0.6	34	0	40
7	Silt	444 (222)	0.5	2000	0.25	0.6	34	0	40
8	Silt	444 (338)	0.5	2000	0.25	0.6	34	0	40
9	Dense Sand	712 (356)	0.5	2000	0.25	0.6	37	7	0

Table 8.9 - SOILSTRESS Pre- and Post-earthquake Inputs -- Location #3*Note: values in parentheses are post-earthquake estimates*

Location #4									
Material Number	Soil Type	K_g	n	K_b	m	R_r	ϕ (deg)	$\Delta\phi$ (deg)	C (kPa)
5	Liquefied Silt	444 (1.1)	0.5 (0)	2000	0.25	0.7 (0)	34 (0)	0	30
6	Silt	647 (323)	0.5	2000	0.25	0.6	34	0	40
7	Silt	450 (225)	0.5	2000	0.25	0.6	34	0	40
8	Silt	805 (402)	0.5	2000	0.25	0.6	34	0	40
9	Silt	738 (369)	0.5	2000	0.25	0.6	34	0	40

Table 8.10 - SOILSTRESS Pre- and Post-earthquake Inputs -- Location #4*Note: values in parentheses are post-earthquake estimates*

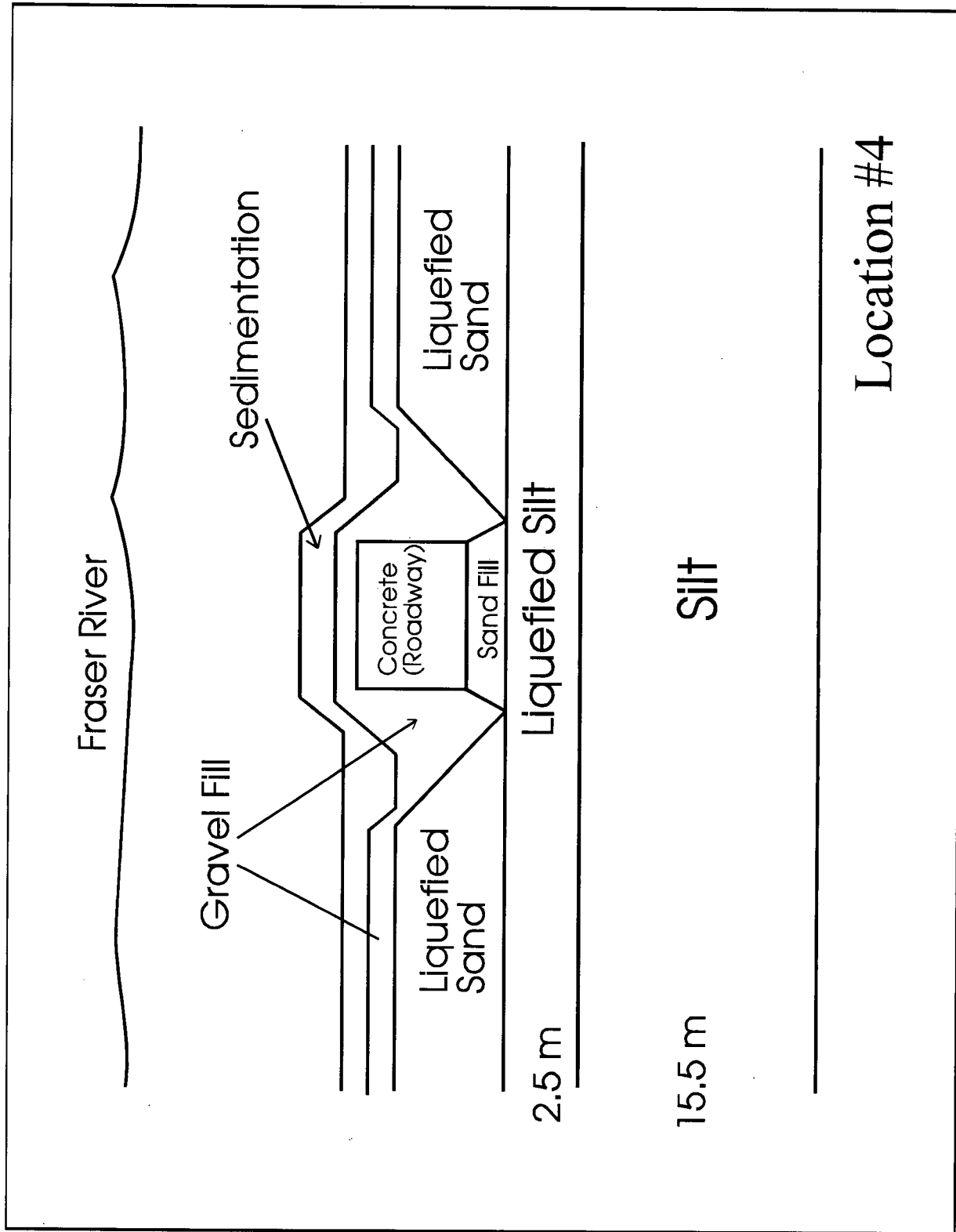


Figure 8.9 Final Stratigraphy at Location #4

Figures 8.10 to 8.15 show the displacement patterns and displacement vectors for the analyses at locations #2, #3, and #4. In all of the figures, the displacements are magnified by a factor of two. The estimates for the Case #1 analyses are summarized in table 8.12.

Offshore Location	Material Type	Material Number	Shear Modulus (G_{max} in kPa)	$(k_g)_i$ (Initial)	γ_{Lim} (%)	S_r (kPa)	$(k_g)_f$ (final)
#2	Sand	5	68380	675	30	12	0.8
	Sand	6	51170	505	30	12	0.8
	Silt	7	61300	605	27	40	1.5
#3	Silt	5	39190	387	27	30	1.1
#4	Silt	5	44990	444	27	30	1.1
All	Sand (Fill)	3	18300	180	30	7	0.1
	Sand	4	51170	505	30	11	0.3

Table 8.11 - SOILSTRESS Soil Input Parameters for Liquefied Materials at Offshore Locations

At location #2, soil units #5 to #7 are liquefied, and at locations #3 and #4, soil unit #5 is liquefied. As table 8.12 shows, the horizontal displacement of the roadway at location #2 is approximately 1 meter. The displacement pattern for location #2 (figure 8.10) is uniform. The displacement vectors (figure 8.11) show the effect of the compression of the loose sand directly beneath the tunnel. The movement of the unit #4 loose sand causes a slight undercutting of the gravel backfill (unit #2), thereby pushing the concrete section slightly upward.

Location	Corner	HORIZONTAL Displacement (meters)	Pre - Consolidation Vertical Displacement (centimeters)	2-Dimension VERTICAL Displacement (centimeters)	TOTAL (3-Dimension) VERTICAL Displacement (centimeters)
#2	C1	0.96	8.9	-26.5	-22.6
	C3	0.96	8.3	-26.4	-22.5
#3	C1	0.24	-1.4	-14.4	-15.6
	C3	0.23	-1.7	-14.0	-15.2
#4	C1	0.20	-1.3	-11.7	-17.7
	C3	0.19	-2.3	-12.8	-18.8

Table 8.12 - SOILSTRESS Displacements at Offshore Locations

Note: - A negative vertical displacement indicates a downward movement

Locations #3 and #4 show significantly lower displacements than location #2. The only difference between the locations is in the depth to liquefaction. Even though the adjacent liquefied sand (unit #4) is the same in all three analyses, the depth to liquefaction apparently controls the amount of movement of the concrete section.

In most of the displacement pattern graphics there is a noticeable outward movement of the elements at the left and right boundaries. Refer to section 9.4.1 for a discussion of this phenomenon.

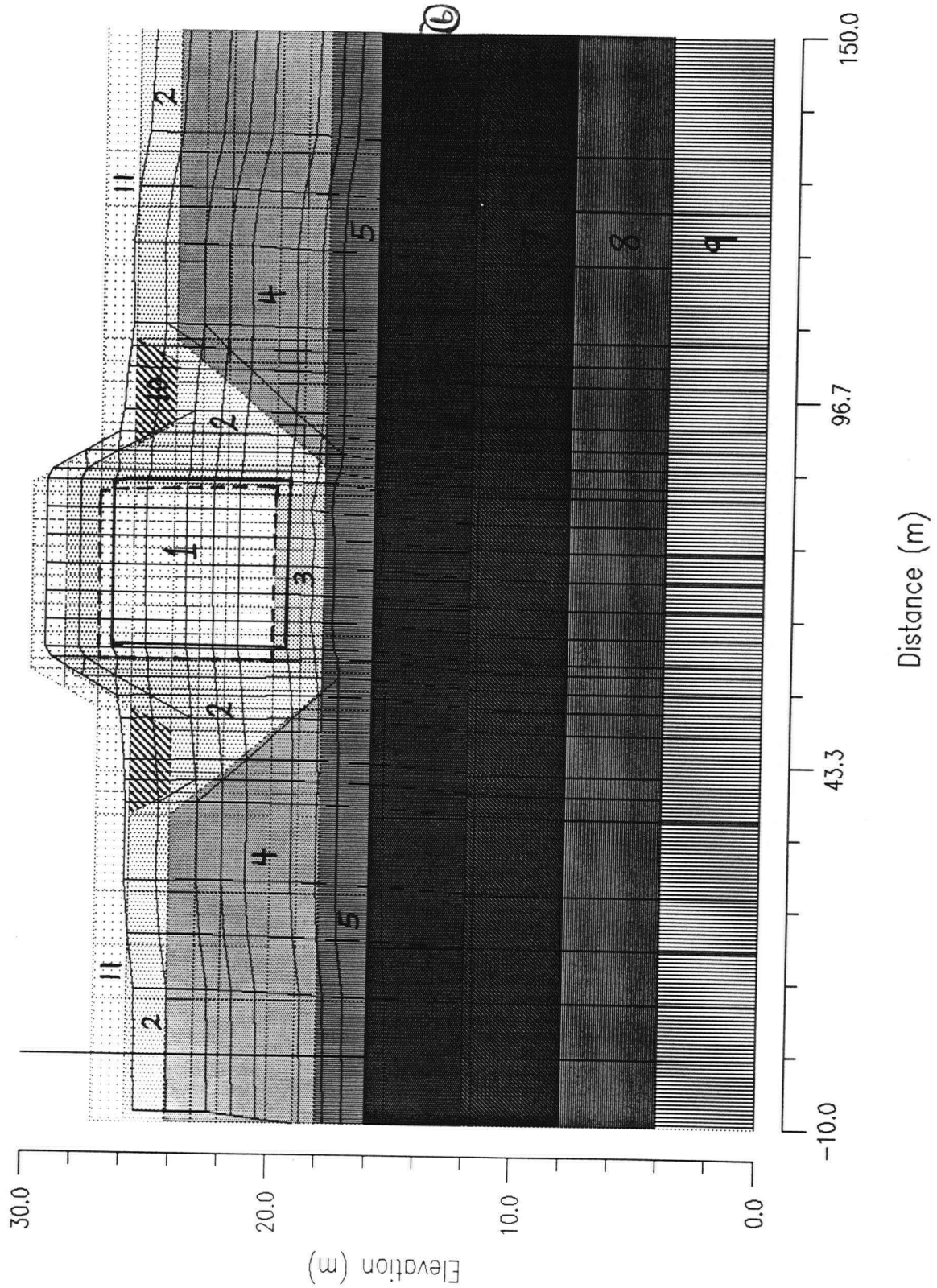


Figure 8.10 - Displacement Pattern -- Location #2

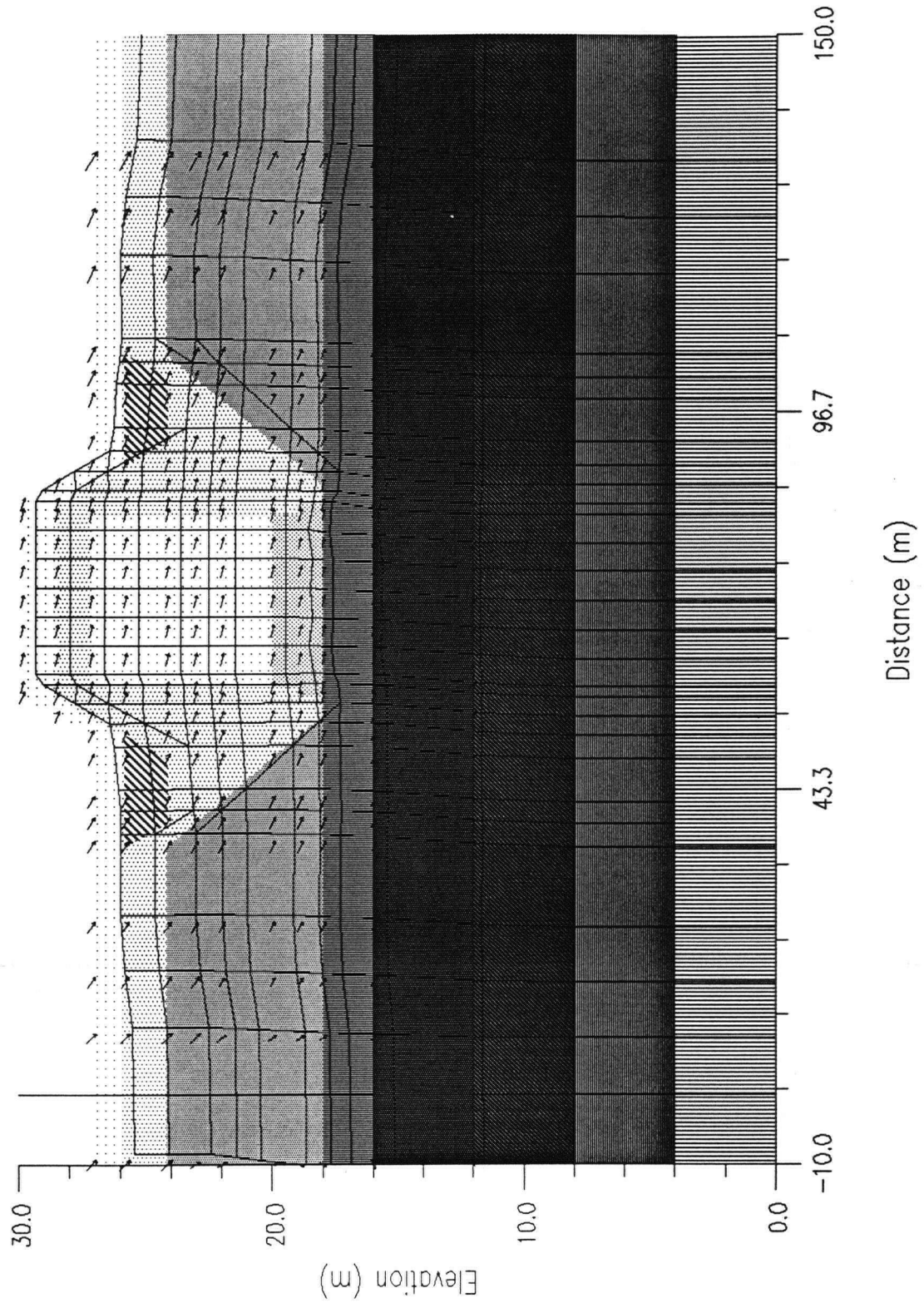


Figure 8.11 - Displacement Vectors -- Location #2

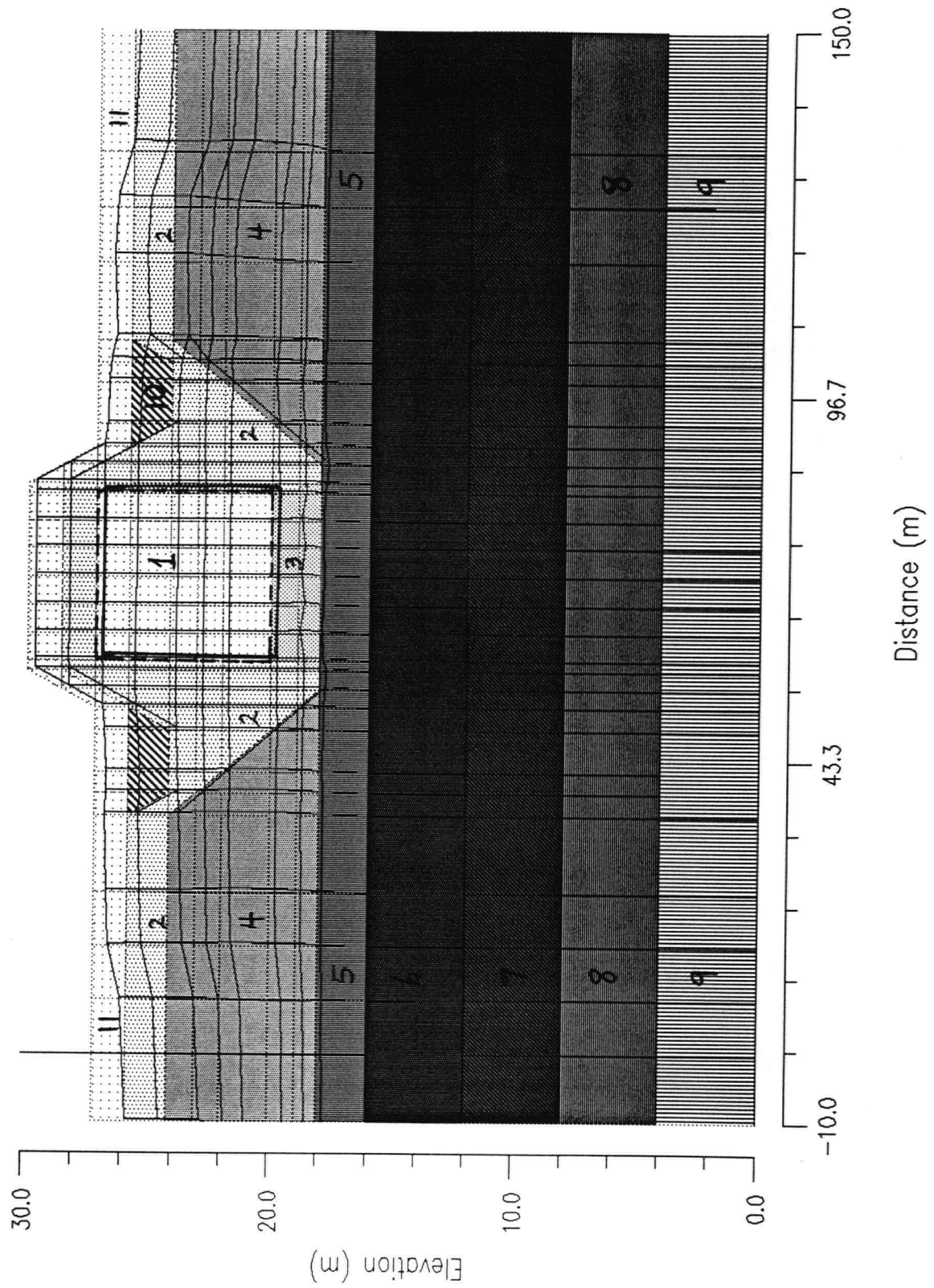


Figure 8.12 - Displacement Pattern -- Location #3

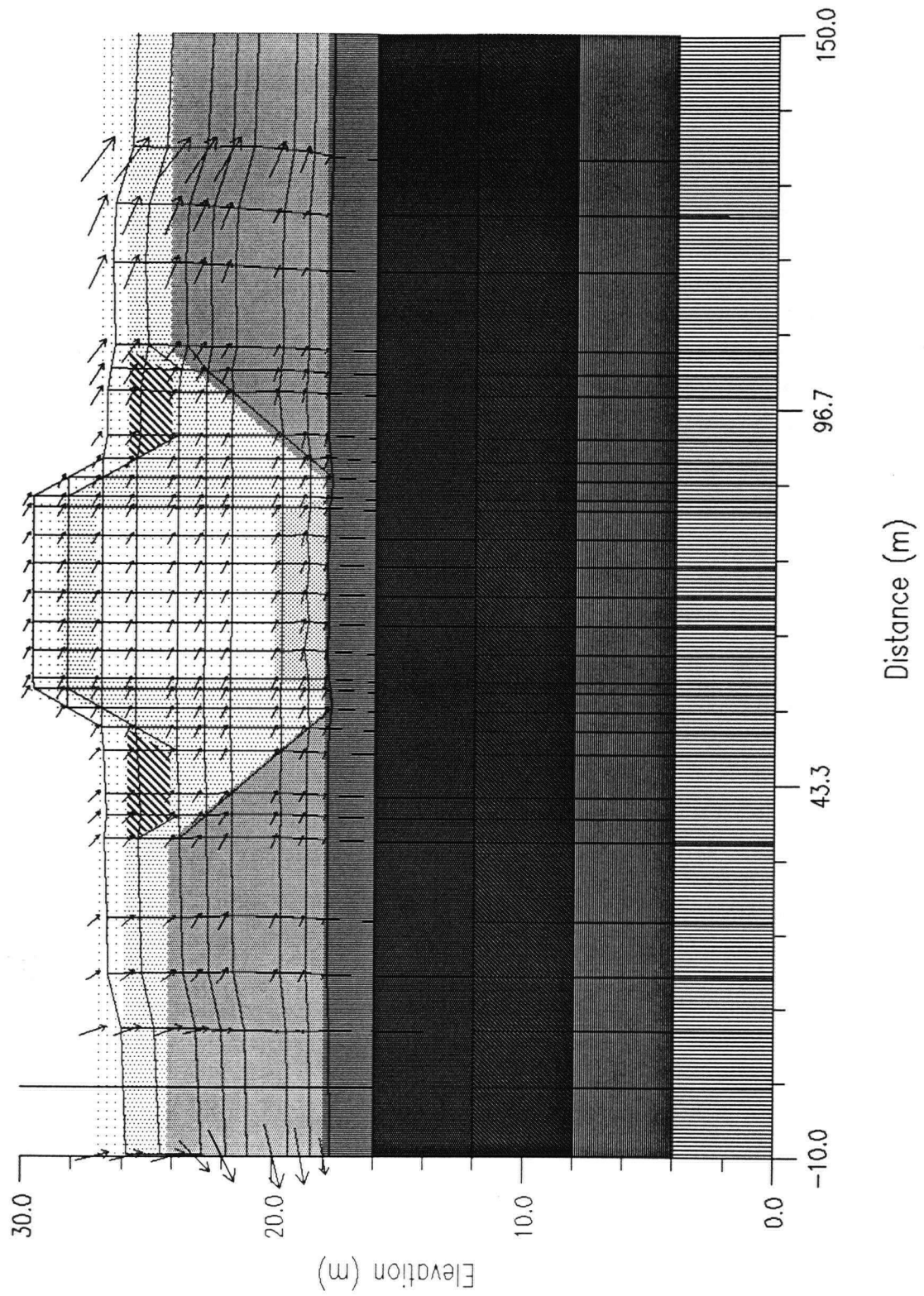


Figure 8.13 - Displacement Vectors -- Location #3

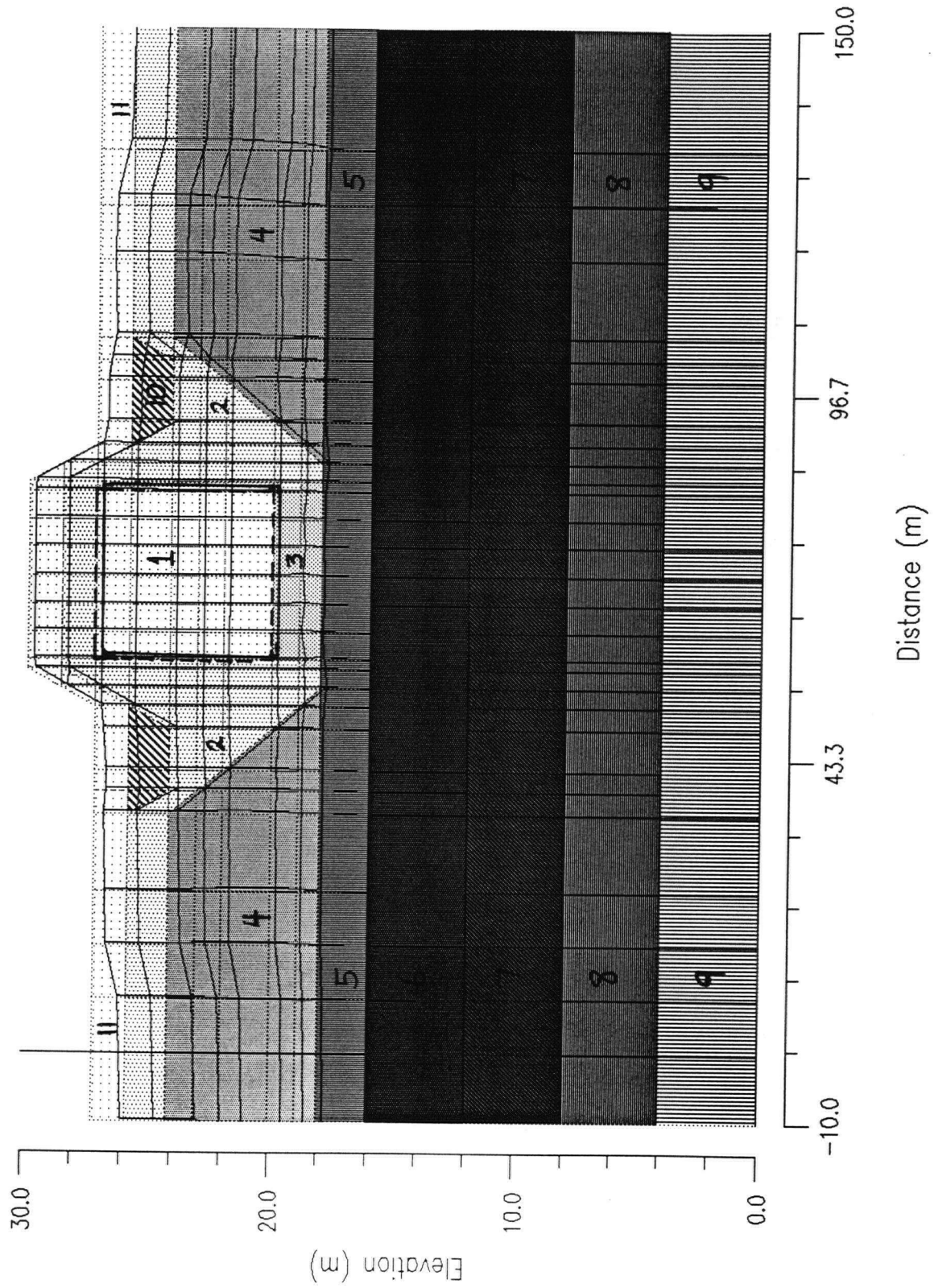


Figure 8.14 - Displacement Pattern -- Location #4

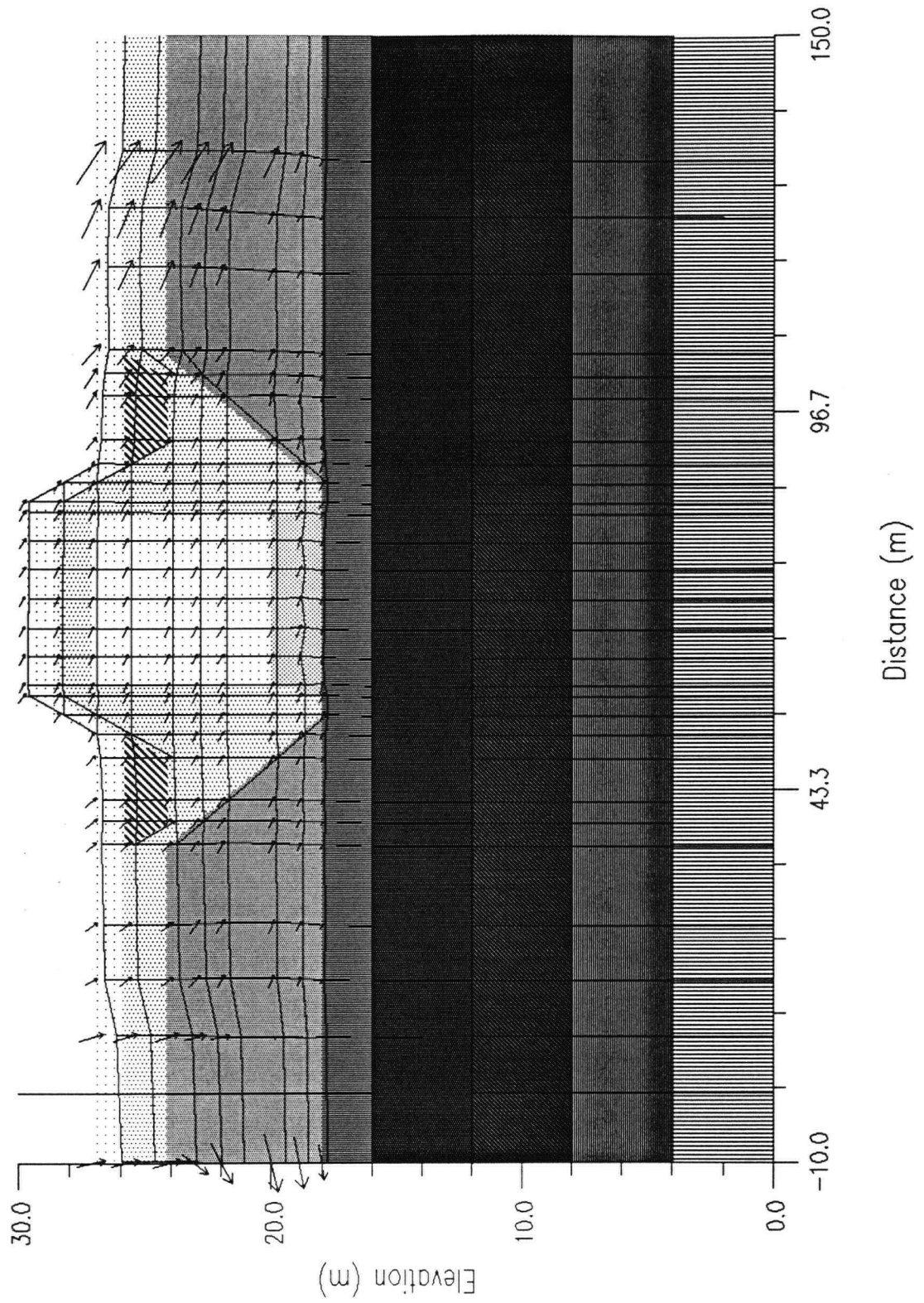


Figure 8.15 - Displacement Vectors -- Location #4

Movements are smaller at locations #3 and #4. In the SOILSTRESS analyses, the total energy dissipated at each of the three locations is the same, but more energy is dissipated in the stronger non-liquefied units (#6 and #7) at locations #3 and #4. Refer to section 9.4.1 for a discussion of differences in kinetic energy dissipation at the offshore locations.

The displacement estimates at the two corners show how much differential movement occurs between the opposite sides of the tunnel's concrete section. Differential movements are discussed in section 9.4.1.1.

8.3.2.2 Longitudinal-direction Displacements

Displacements in the plane parallel to the axis of the tunnel ('longitudinal-direction') are summarized in this section. Figure 6.1 shows the estimated soil profile along the length of the tunnel, and the distance between the analyzed locations. Refer to section 9.4 for a discussion of the SOILSTRESS results.

Figures 8.16 to 8.19 show the displacement patterns and displacement vectors for the longitudinal-direction analyses. The dashed lines represent the initial state, and the solid lines show the post-earthquake position of the nodes. The displacements are magnified by a factor of three.

Pre- and post-earthquake inputs for the SOILSTRESS analyses are

Longitudinal Section Analysis									
Material Number	Soil Type	K_r	n	K_b	m	R_f	ϕ (deg)	$\Delta\phi$ (deg)	C (kPa)
1	Concrete	50000 (50000)	0.5	200000	0.25	0.5	50	0	1000
2	Liquefied Silt	444 (1.1)	0.5 (0)	2000	0.25	0.7 (0)	34 (0)	0	30
3	Liquefied Sand Fill	181 (0.1)	0.5 (0)	2000	0.25	0.9 (0)	32 (0)	0	0
5	Silt	444 (222)	0.5	2000	0.25	0.6	34	0	40

Table 8.13 - SOILSTRESS Pre- and Post-liquefaction Inputs For Materials Common to Both Longitudinal Section Halves

Note: - values in parentheses indicate post-liquefaction estimates

summarized in tables 8.13 to 8.15. For post-earthquake conditions, a 50% reduction in stiffness was applied to all non-liquefied materials due to the severity of shaking (i.e., v_{\max}

= 0.3 m/s). Residual strength and limit strain estimates that were applied in the transverse-direction analyses were also applied in the longitudinal analyses. (Section 6.3 summarizes the post-liquefaction parameters).

Longitudinal Section Analysis									
Material Number	Soil Type	K_g	n	K_b	m	R_f	ϕ (deg)	$\Delta\phi$ (deg)	C (kPa)
4	Liquefied Sand	505 (1.8)	0.5 (0)	2000	0.25	0.8 (0)	35 (0)	0	0
6	Silt	747 (374)	0.5	2000	0.25	0.6	34	0	40
7	Liquefied Sand	200 (0.5)	0.5 (0)	2000	0.25	0.8 (0)	33 (0)	0	0
8	Sand (Sediment)	200	0.5	2000	0.25	0.6	33	0	0
9	Dense Sand Lens	1137 (568)	0.5	2000	0.25	0.6	37	7	0
10	Liquefied Sand	570 (2.2)	0.5 (0)	2000	0.25	0.8 (0)	35 (0)	0	0

Table 8.14 - SOILSTRESS Pre- and Post-liquefaction Inputs For North-End -- Longitudinal Section Analysis

Notes: - values in parentheses indicate post-liquefaction estimates

Tables 8.16 and 8.17 summarize the displacements at the base of the concrete section in the vicinity of the five locations at which the transverse analyses were done. The 'pre-consolidation vertical displacement' is the movement due to undrained distortion, and the '2-Dimension vertical displacement' is the total vertical movement in which settlement due to dissipation of excess pore-pressures is also included. The 'total vertical displacement' (in the final column of each displacement summary table) represents the full 3-dimensional effect by incorporating the undrained vertical distortion estimates from

Longitudinal Section Analysis									
Material Number	Soil Type	K_g	n	K_b	m	R_r	ϕ (deg)	$\Delta\phi$ (deg)	C (kPa)
6	Liquefied Sand	505 (0.4)	0.5 (0)	2000	0.25	0.8 (0)	33 (0)	0	0
7	Partially Liquefied Sand	955 (100)	0.5	2000	0.25	0.7	37	2	0
8	Partially Liquefied Sand	570 (100)	0.5	2000	0.25	0.7	31	0	0
9	Silt	747 (374)	0.5	2000	0.25	0.6	34	0	40
10	Liquefied Sand	200 (0.5)	0.5 (0)	2000	0.25	0.8 (0)	33 (0)	0	0
11	Sediment (Sand)	200	0.5	2000	0.25	0.6	33	0	0
12	Dense Sand Lens	1137 (568)	0.5	2000	0.25	0.6	37	7	0

Table 8.15 - SOILSTRESS Pre- and Post-liquefaction Inputs For South-End -- Longitudinal Section Analysis

Notes: - values in parentheses indicate post-liquefaction estimates

the onshore and offshore (i.e., Case #1) transverse analyses. (Refer to sections 8.3.2.1.1 and 8.3.2.1.2 for transverse-section pre-consolidation estimates).

As figure 8.16 shows, there is a noticeable outward movement of the elements at the left boundary of the northern section. This phenomenon is explained in section 9.4. The vertical displacement estimates at the five locations show how much differential movement occurs along the length of the tunnel. Differential movements are discussed in section 9.4.1.2.

The displacement vectors (figures 8.17 and 8.19) show the uneven effect of the transitions from liquefied to non-liquefied soils. For instance, the unit #7 sands in the south section were not predicted to liquefy; consequently, the liquefied unit #6 and #2 soils experience slightly greater distortion as the horizontal velocity impulse is applied.

All locations show small displacement at the roadway. In zones of liquefaction, more noticeable deformations occur, but those zones do not have much effect on the movements of the concrete section.

The central boundary is fixed in the horizontal direction in both analyses. This fixed condition is meant to simulate the effect of the northern and southern slopes counteracting each other horizontally. Refer to appendix A.1.4 for a description of the full length longitudinal analysis.

Location	HORIZONTAL Displacement (centimeters)	Pre - Consolidation Vertical Displacement (centimeters)	2-Dimension VERTICAL Displacement (centimeters)	TOTAL (3-Dimension) VERTICAL Displacement (centimeters)
#8	5.4	3.8	- 28.2	- 20.3
#4	3.3	- 0.4	- 13.6	- 15.9
#3	0.8	- 0.6	- 11.9	- 13.6

Table 8.16 - Northern Half -- Longitudinal-direction Displacement Predictions

Note: - A negative vertical displacement indicates a downward movement

Location	HORIZONTAL Displacement (centimeters)	Pre - Consolidation Vertical Displacement (centimeters)	2-Dimension VERTICAL Displacement (centimeters)	TOTAL (3-Dimension) VERTICAL Displacement (centimeters)
#3	0.3	0.7	- 10.0	- 11.7
#2	2.0	5.1	- 31.2	- 22.9
#7	0.03	- 7.5	- 28.2	- 29.0

Table 8.17 - Southern - half -- Longitudinal-direction Displacement Predictions

Note: - A negative vertical displacement indicates a downward movement

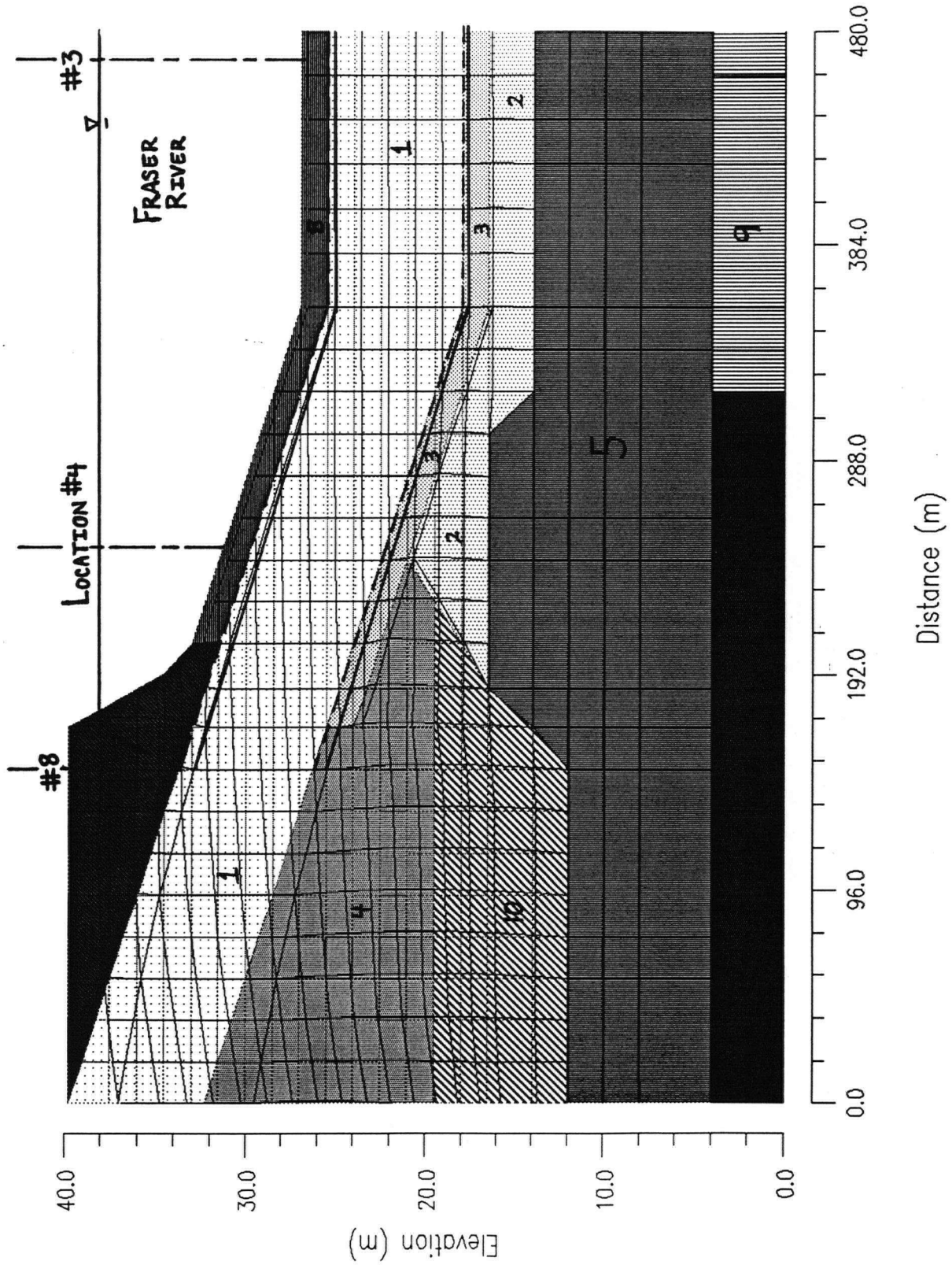


Figure 8.16 - Displacement Pattern for Northern Half of Tunnel

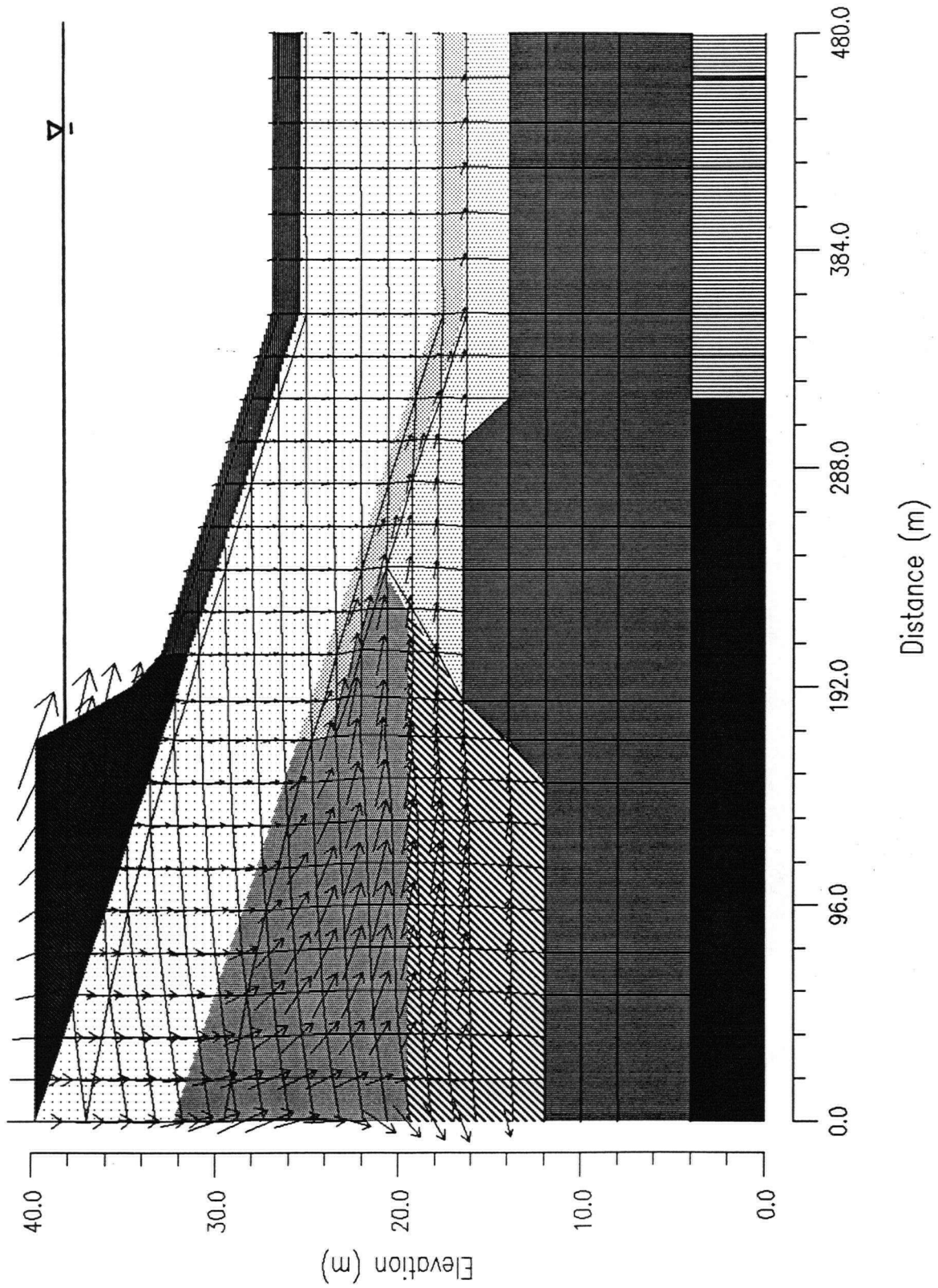


Figure 8.17 - Displacement Vectors for Northern Half of Tunnel

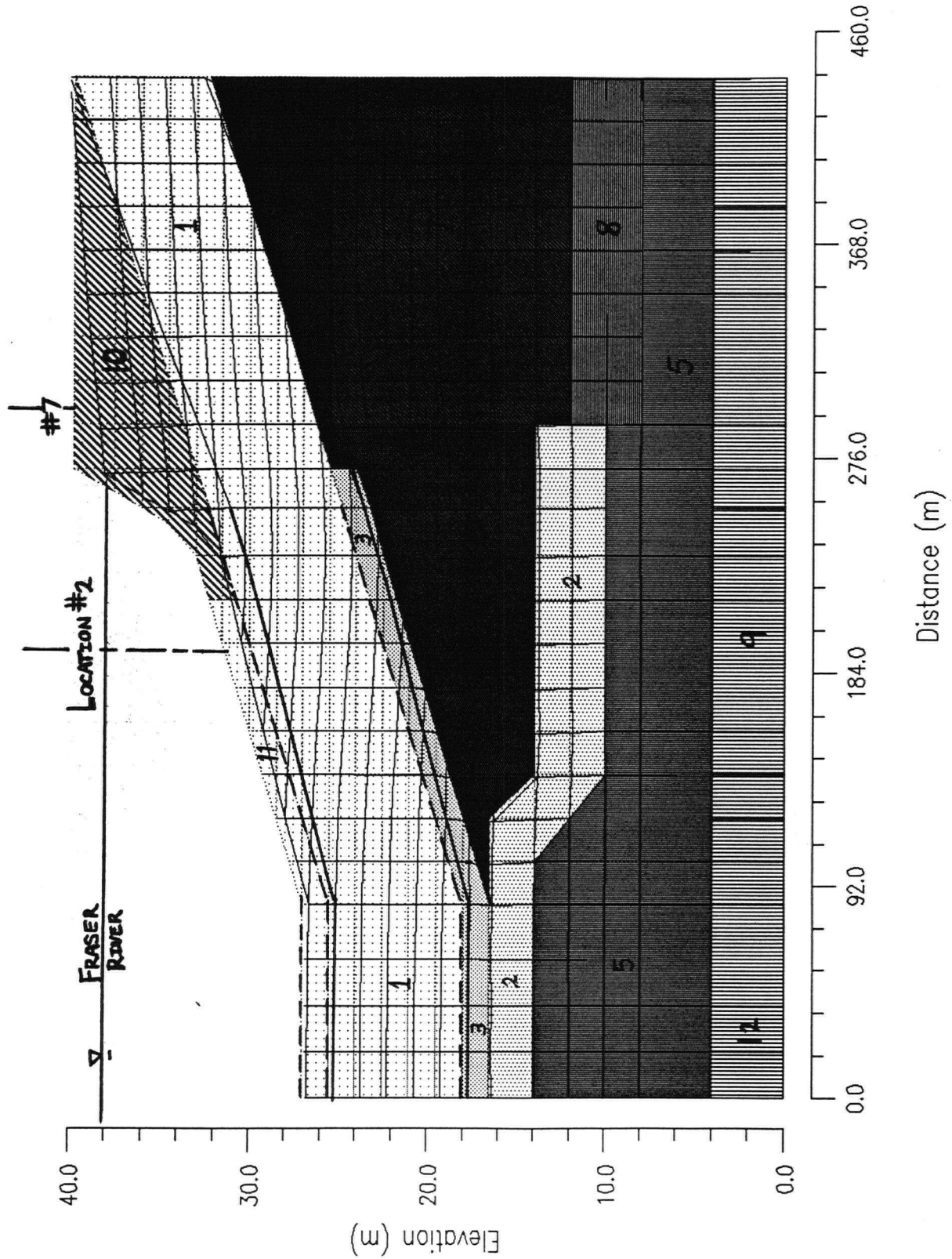


Figure 8.18 - Displacement Pattern for Southern Half of Tunnel

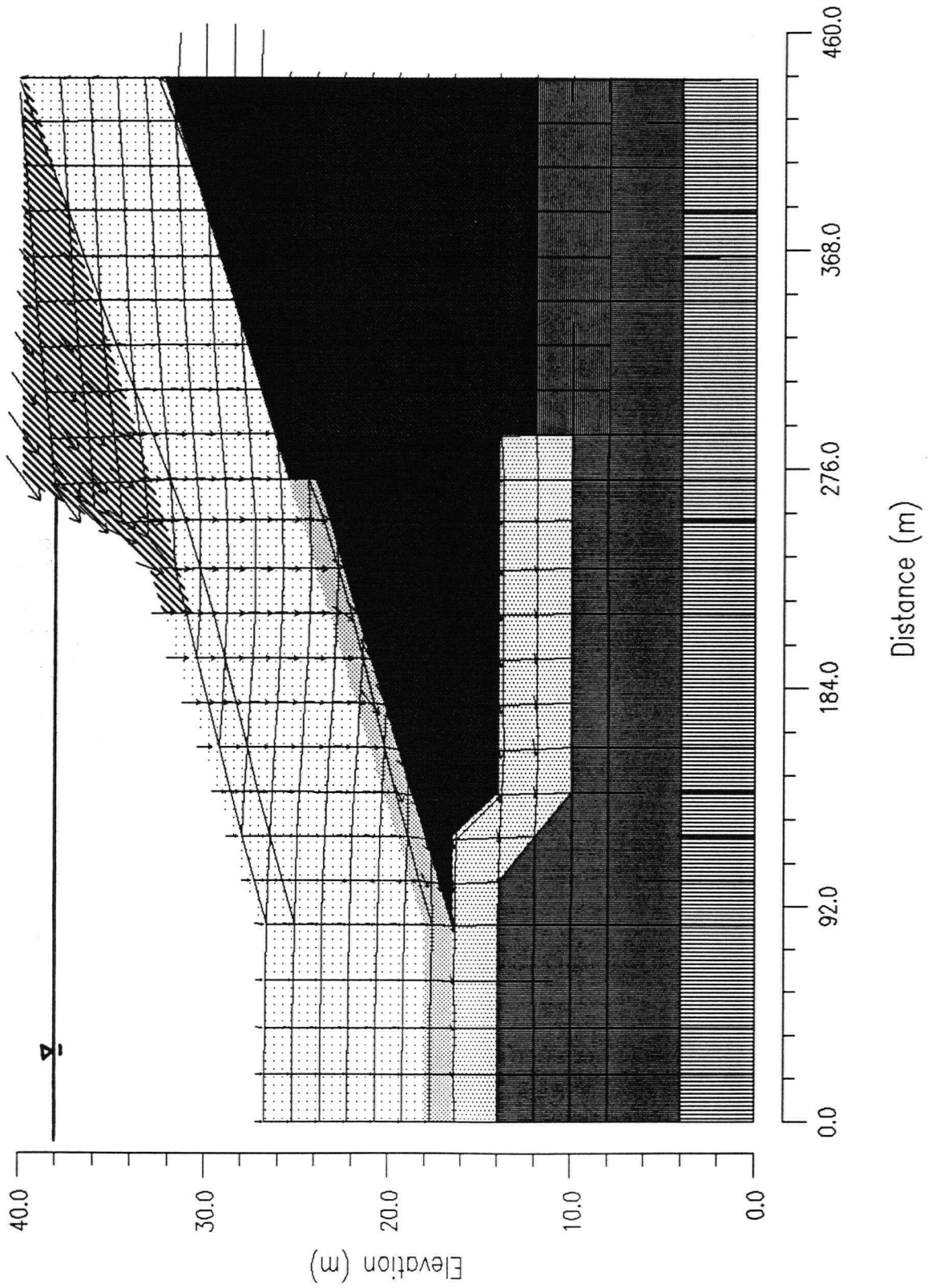


Figure 8.19 - Displacement Vectors for Southern Half of Tunnel

8.3.3 LIQDISP -- Single-degree-of-freedom Displacements

Refer to section 9.4.2 for a discussion of the results summarized in this section. Section 9.2 contains a comparison of the LIQDISP results and the other displacement methods. The LIQDISP analysis procedure is discussed in section 4.4.3.3. In all analyses, residual strengths and limiting strains were estimated as described in section 4.3.

Location	Liquefied Layer Thickness (meters)	Residual Strength (S_r) (kPa)	Limiting Strain (%)	Factor of Safety	Linear Modulus Prediction (meters)	Non-Linear Modulus Prediction (meters)
#2	10	12	30	1.63	4.18	5.47
#3	2.5	30	27	2.04	0.74	0.96
#4	2.5	30	27	1.90	0.79	1.03

Table 8.18 - LIQDISP: Input Parameters and Displacements at Offshore Locations

LIQDISP's slope failure model was applied at the offshore locations. The slope failure model uses a limit equilibrium stability factor of safety to approximate the static driving stress, which is used to estimate the static displacement. As table 8.18 shows, the estimations are influenced strongly by liquefied layer thickness. The soil inputs in table 8.18 show that, amongst the offshore locations the main difference is in the liquefied layer thickness; consequently, location #2 shows significantly larger displacements than locations #3 and #4.

Location	Liquefied Layer Thickness (meters)	Residual Strength (S_r) (kPa)	Limiting Strain (%)	Slope (%)	Linear Modulus Prediction (meters)	Non-Linear Modulus Prediction (meters)
#8	16	57	30	1	1.18	2.68
				2	1.91	3.61
				3	2.70	4.36
				4	3.52	5.02

Table 8.19 - LIQDISP: Input Parameters and Displacements at Onshore Location

Since no liquefaction occurs below the tunnel invert at location #7, it was not analyzed using LIQDISP. LIQDISP's infinite slope model was used to analyze the north shore (location #8), since the overlying level dyke material resembles an infinite slope. As table 8.19 shows, the estimations are influenced strongly by the ground slope input.

CHAPTER 9

DISCUSSION OF CHAPTER 8 RESULTS

9.1 Introduction

This chapter presents interpretations of the results that are summarized in chapter 8. Interpretations focus on how the results compare with expectations, and why, in some cases, they differ. The information in each upcoming section should be reviewed with the corresponding section in chapter 8.

9.2 Comparison of Displacement Predictions

Section 9.2.1 compares the displacement predictions from the empirical and numerical methods. Section 9.2.2 briefly provides a review of past seismic performance of underground structures (within the context of this study).

9.2.1 Comparison of Empirical and Numerical Method Predictions

Table 9.1 summarizes the empirical and numerical method horizontal displacement estimates at each location. The detailed inputs and results from all methods are independently summarized in chapter 8 (the Bartlett-Youd and Hamada results are summarized in table 8.1, the LIQDISP results are in tables 8.18 and 8.19, and the SOILSTRESS results (for Case #1) are compiled in table 8.12).

The Bartlett-Youd method was not applied at locations #3 and #4, where silts are predominant. The empirical method results in table 9.1 correspond to ground slopes of

1% and 3%. Both linear and nonlinear modulus LIQDISP predictions are provided in the table. The SOILSTRESS results represent the Case #1 (i.e., 2-meter sediment loading -- refer to section 8.3.2.1.2) horizontal displacement prediction at corner #1 ('C1').

Location	Bartlett - Youd (meters)		Hamada (meters)		LIQDISP (meters)		SOILSTRESS (Case #1) (meters)
	1%	3%	1%	3%	Linear	Non - Linear	
#2	0.5	0.8	3.4	4.8	4.2	5.5	0.94
#3	Not App.	Not App.	1.1	1.5	0.8	1.0	0.18
#4	Not App.	Not App.	1.1	1.5	0.8	1.1	0.19
#8	0.6	1.0	4.0	5.7	1%	1.2	0.82
					3%	2.7	

Table 9.1 - Horizontal Displacement Predictions from Empirical and Numerical Methods

At location #2, there is approximately 6 meters of liquefied sand and 4 meters of liquefied silt below the tunnel invert. At locations #3 and #4, there is approximately 3 meters of liquefied silt beneath the tunnel. Location #7 was not analyzed using LIQDISP or the empirical methods because liquefaction was not predicted to occur beneath the tunnel. At location #8, there is a thick segment (approximately 18 meters) of liquefied sand beneath the tunnel.

Upon comparing the results, it should be noted that, since the empirical methods

are derived from case-histories, they are generally meant to provide a range within which the numerical predictions should lie. As table 9.1 shows, the Bartlett-Youd results compare well with the SOILSTRESS results, and the Hamada results are in good agreement with the LIQDISP predictions.

In table 9.1, the LIQDISP predictions at location #8 correspond to ground slopes of 1% and 3%. The relatively high nonlinear modulus LIQDISP predictions compare well with the Hamada values at corresponding ground slopes. At all locations, the Hamada predictions are approximately 5 times as large as the corresponding SOILSTRESS estimates. Since the Hamada calculation is strongly dependent upon liquefied layer thickness, its predictions at locations #2 and #8 are high. Similarly, when using LIQDISP's slope failure model (i.e., in which a limit equilibrium stability factor of safety is used to estimate the static shear stress) at the offshore locations, the estimations were strongly dependent upon liquefied layer thickness. As the soil inputs in table 8.18 show, amongst the offshore locations the main difference is in the liquefied layer thickness; consequently, location #2 shows significantly larger displacements than locations #3 and #4.

Since the surficial deposits are susceptible to liquefaction (upon the 475-year earthquake), it was important to be able to include the structural influence (i.e., stiffness of the tunnel) within the deformation analyses. The simplified methods were limited by their inability to acknowledge the amount of submergence of the tunnel at the offshore

locations; consequently, those methods should be cautiously acknowledged in a study such as this. As discussed in section 4.4.3.2, the SOILSTRESS analyses were the only ones in which the tunnel could be included. Because SOILSTRESS properly considers the 2-dimensional nature of the problem, the results can be considered more accurate than those obtained by the simplified methods. LIQDISP handles the 2-dimensional nature of the problem using a "trick" similar to that of Newmark (1965); whereas SOILSTRESS captures the 2-dimensional response, providing a range of displacements over a discretized (finite element) grid. LIQDISP models the embankment as a single-degree-of-freedom system and assumes uniform block movement along a failure surface, thereby providing a single maximum displacement. In this study, it was presumed that the maximum displacement (LIQDISP prediction) occurs in the liquefying layers beneath the tunnel.

It should be noted that the Hamada equation was derived from data on clean medium-grained sands, and earthquake magnitudes of $M = 7.5$ and 7.7 . Youd et al. (1988) compared historical earthquake-induced displacements from earthquakes in Japan and the United States, and found that displacements in Japan tended to be larger than those in the U.S. The generally coarser and cleaner sands in Japan were hypothesized to be the cause of the difference. Because the Hamada data base consists of such sands, the predictions provided for the sandy silt liquefied layers at the #3 and #4 locations should be acknowledged as being very conservative (low). The estimates have been provided for

reference purposes only.

9.2.2 Underground Structure Case-histories

In general, underground structures are less severely affected by seismic motions than surface structures (Owen & Scholl, 1981). The response of the tunnel will be dependent upon post-earthquake stiffness of the foundation soils. If the soil does not liquefy, then the tunnel can be expected to deform according to the free-field motions of the soil. This phenomenon has been documented in post-earthquake analyses of other underground structures (i.e, subways, pipelines, foundation piles). If, on the other hand, the soil liquefies, then the stiffness of the tunnel will have more of an influence on the extent of deformation. It should be noted that the submerged portion of the tunnel comprises six segments, so the connections between those segments will influence the movement.

In the event of an earthquake smaller than the one addressed in this study, the surface soils may retain their integrity. In that case, the stiffness of the tunnel may reduce the soil stiffness-dependent free-field motions. For example, the Trans-Bay subway in San Francisco was estimated to have reduced the free-field motions within the soft surface clays by approximately 15% (Kuesel, 1969).

9.3 Empirical Method Displacements

This section consists of two separate discussions. Discussion of the Bartlett-Youd (1992) and Hamada (1987) methods is followed by the Tokimatsu-Seed method. In this section, the individual points of discussion are segregated by headings.

i.) Bartlett-Youd and Hamada Methods:

The discussion material in this section corresponds to the results of section 8.2. Refer to section 4.4.2 for a description of the empirical method procedures.

The Hamada (1987) predictions (summarized in table 8.1) are relatively high. Hamada's method is commonly acknowledged for overestimating displacements. The Bartlett-Youd (1992) approach proved to be sensitive to fines contents (F_{15}) and distance (R) from the earthquake source. A higher fines content decreases a prediction significantly. Contained in appendix D.1 are estimates using an earthquake distance of 60 kilometers. These displacements were approximately one-fifth those obtained using a distance of 30 kilometers. The magnitudes in table 8.1 were estimated using an earthquake distance of 30 kilometers. This distance was applied to maintain consistency with the attenuation distance input which was used to develop the target spectrum for the ground response analyses (refer to section 3.2.1). (All empirical method inputs and calculations are provided in appendix D).

To estimate post-earthquake displacements, both methods require liquefied layer

data. The liquefied layers acknowledged in the analyses were those that were below the tunnel invert. The Bartlett-Youd and Hamada methods allow each liquefied layer to be treated separately, so that the displacements in each layer can be summed. The loose sand layers adjacent to the excavation (i.e., material #4 in figure 6.12) and the pump sand fill (material #3 in figure 6.12) were not acknowledged in the empirical analyses because they are presumed to have little effect on the magnitude of the tunnel displacements. (This is verified in the remediation analyses in chapter 10). The sand fill (material #3) which was pumped in beneath the tunnel wasn't included in the analyses because it is constrained by the coarse gravel and rockfill at the sides of the excavation.

Since the liquefied layers at locations #3 and #4 consist of sandy silts containing fines contents (F_{15}) beyond the recommended limit ($F_{15}=50\%$) of the Bartlett-Youd data base, these locations were not analyzed using the Bartlett-Youd method (1992). Since location #7 doesn't show any liquefaction below the tunnel invert, it wasn't possible to analyze it using either of the empirical methods. But, the analysis results of location #8 can be applied to location #7, in the event liquefaction does occur at location #7. (The similarities between locations #7 and #8 are discussed in section 9.4.1).

The Bartlett-Youd and Hamada method predictions were derived using ground slopes of 1% and 3%. Although the tunnel is constructed on a level excavation, the underlying liquefied stratum are assumed, to be sloping approximately parallel to the river bed. The river bed slope varies considerably in both the north-south and east-west

directions, but estimates of downstream stratum slope at the tunnel site were obtainable using seismic reflection survey data (Monaghan, 1995). The reflections indicate approximate dips varying between 1% and 3%.

The Bartlett-Youd model is advantageous over the Hamada model in that it takes into account earthquake and soil parameters as well as the topographical and geological factors. But, the use of either of these methods at the offshore locations is questionable because of the inability to account for the amount of submergence, and the structural influence within the surficial soil. The ground displacements computed using the simplified formulae are approximate, and are valid for free-field conditions only (i.e. without interaction with the tunnel).

The Bartlett-Youd model was developed from Japanese and western U.S. data, so it is most applicable to regions in which significant ground motion attenuation can be expected to occur. This may explain the relatively low estimates obtained using this method. Furthermore, none of the case histories used to derive this model showed liquefied layers deeper than 15 meters; there is an 18-meter thick segment of liquefied sand at location #8. Additionally, the case histories showed a depth to the top of the liquefied layer which was generally within a few meters of the ground surface.

ii.) Tokimatsu/Seed Post-liquefaction Settlements:

As discussed in section 4.4.2.4, the method developed by Tokimatsu and Seed (1987) was used to estimate liquefaction-induced settlements. The post-liquefaction volumetric strain inputs for the SOILSTRESS analyses were estimated using the Tokimatsu/Seed correlation. Additionally, table 8.2 provides a summary of the estimated post-liquefaction settlements based on the Tokimatsu/Seed methodology. These values are provided only as a reference, since the pre-consolidation SOILSTRESS vertical displacement estimates indicate that noticeable vertical movements do occur at all of the locations before dissipation of pore pressures. The use of these estimates is limited because partial buoyant uplift of the tunnel (upon generation of excess pore pressures) can not be accounted for.

It should be noted that at locations #3 and #4, the liquefied material is silt. Additionally, 4 meters of the liquefied material at location #2 is silt. The Tokimatsu/Seed method was developed for use in liquefied sands, so the tabulated predictions (at those locations) should be acknowledged cautiously.

9.4 Numerical Method Displacements

The discussion material in this section corresponds to the results of section 8.3. Section 9.4.1 discusses the general factors common to all (i.e., transverse and longitudinal) SOILSTRESS analyses in this study. Sections 9.4.1.1 and 9.4.1.2 discuss the specific transverse- and longitudinal-direction analyses. Section 9.4.2 discusses the LIQDISP analyses. In each section, the individual points of discussion are segregated by headings.

9.4.1 Finite Element (SOILSTRESS) Displacements

i.) Outward Movement of Elements at Left and Right Boundaries:

In all SOILSTRESS analyses there was some degree of outward movement of elements at the left and right boundaries. Because a fixed boundary condition would not properly represent conditions in the field, the nodes at those boundaries were, instead, constrained by forces equivalent in magnitude to in situ horizontal soil pressures. (Horizontal pressure boundaries are also discussed in section 4.4.3.2). The displacement vector graphics (in chapter 8) show the boundary effect, which is due to insufficient lateral resistance required to confine the vertical seismic coefficient (k_v) force application on the softened soil. For comparison, the boundary forces were increased at two of the offshore locations, but the high pressure magnitudes caused unacceptable distortions at the mesh boundaries. Although the displacement estimates at the nodes close to the left

and right boundaries are inaccurate, the critical central portion of the mesh is unaffected (i.e., a large enough mesh width was chosen to negate boundary effects).

ii.) Application of Horizontal (k_H) and Vertical (k_v) Seismic Coefficients:

All SOILSTRESS analyses were done using the method in which both vertical and horizontal seismic coefficients can be applied (i.e., 'option 0'). (The use of seismic coefficients, k_v and k_H , to provide an additional force (ΔF) to satisfy the energy balance is discussed in appendix A.3). As discussed in section 4.4.3, seismic-induced displacements occur due to:

- i.) softening caused by liquefaction, and
- ii.) kinetic energy due to the earthquake-induced velocity pulse.

Displacements due to strain-softening are best computed using a $\{\Delta F\}$ based on a vertical seismic coefficient (k_v), since it is mainly the (vertical) gravitational force that causes the displacements. The displacements due to the velocity pulse are best computed using a $\{\Delta F\}$ based on a horizontal seismic coefficient (k_H), since the velocity is assumed to be in the horizontal direction. When using option 0, first, k_v is used to compute displacements that satisfy the convergence criterion for overall energy balance of the system due to strain-softening (i.e., due to gravity and boundary forces acting on the softened soil). Then, the additional displacements due to kinetic energy are accounted for by applying k_H . The net work (N.W.) is estimated as: $N.W. = (W_{int} - W_{ext}) / W_{ext}$. When N.W is

negative, the seismic coefficient must be increased to increase the internal work (i.e., increase the strains) to achieve the energy balance of the system.

The longitudinal profile was analyzed as two separate halves. The longitudinal analyses are described in section 8.3.2.2. One of the points of concern when assessing the validity of the SOILSTRESS results is in the horizontal displacement estimates when the profile is analyzed as one continuous section. When the profile is analyzed as such, the whole system 'lurches' in the direction of the horizontal velocity impulse. (The results from the full-section longitudinal analyses are presented in appendix A.1.4). In reality, this simultaneous movement will not likely occur. The vertical movements, on the other hand, can be considered reliable. To alleviate concerns about the validity of using option 0, comparison analyses were performed for all SOILSTRESS analyses (i.e., longitudinal and transverse sections) using the options in which only one of the two seismic coefficients is applied (i.e., 'option 1' for horizontal seismic coefficient only, and 'option 2' for vertical coefficient only). When k_H alone (option 1) was applied, the horizontal displacements were very similar to the horizontal magnitudes estimated when using option 0, and, as expected, the vertical displacement estimates of option 1 were very low. Similarly, when k_v alone (option 2) was applied, the vertical displacements were very similar to the vertical magnitudes estimated when using option 0. So, in effect, the vertical and horizontal SOILSTRESS displacements (estimated in this study) can be distinguished somewhat, in the event of a future comparison of displacement estimates

using a different method such as FLAC (Fast Lagrangian Analysis of Continua).

Additionally, the stratigraphy was taken to only 18 meters below the tunnel (at its lowest point -- i.e., halfway across the river) in the SOILSTRESS analyses because of the system mass. If the soil depth was increased, the system mass would increase, and this would result in an increase in the kinetic inertia of the system (when the earthquake impulse is applied). Since external work is proportional to the displacements, the displacements will have to be too large to achieve an energy balance. The work-energy concepts are discussed in appendix A.2.

iii.) Validation of the SOILSTRESS Method:

The SOILSTRESS finite element analysis has been found to give exact agreement with Newmark when a rigid-plastic single-degree-of-freedom system has been assumed (Byrne et al., 1992). Additionally, it corroborates well with the observations of Hamada et al. (1987); furthermore, it predicts the failure of the Lower San Fernando dam, and provides accurate displacement predictions of pattern and magnitude of deformations for the Upper San Fernando dam (Byrne et al., 1992).

9.4.1.1 Transverse-direction Analyses

i.) Comparison of Soil Response at the South and North Shores (Locations #7 & #8):

The liquefaction assessment for location #7 indicated that the sands were 'partially-liquefied' (i.e., they could experience noticeable softening). Since the stratigraphies at locations #7 and #8 consist of very similar soil types and thicknesses, the response at location #7 would have been nearly identical to that of location #8; therefore, it was considered most expedient to do the SOILSTRESS analyses at location #7 with contrasting (i.e., more stiff) post-earthquake shear modulus inputs to those of location #8. The response could then be considered representative of how both the north and south shores would perform should a smaller earthquake occur (and the underlying sands do not liquefy to the degree predicted at location #8). On the other hand, the predicted displacements at location #8 could be considered applicable to those at #7 should an event equal to the design earthquake be considered. Consequently, it is recommended that the displacement predictions for location #8 be conservatively considered applicable to location #7.

ii.) Varying Loading Conditions (Cases #1 to #3):

Appendix A.1.2 ('Case #3') summarizes the results of analyses at location #2 with increased sediment loading on top of the tunnel. These analyses were carried out for two reasons:

- i.) the depth of sediment on top of the tunnel varies with season, and
- ii.) increasing or decreasing the sediment load was presumed to be a potential remedial measure (to decrease displacements, or prevent buoyant uplift).

<i>Displacement</i>	Case #1	Case #2	Case #3a
HORIZONTAL (m)	1.0	1.0	1.1
VERTICAL (cm)	-23	-20	-25

Table 9.2 - Comparison of SOILSTRESS Results -- Varying Sediment Loads

Table 9.2 summarizes the displacement estimates for Cases #1 to #3. As outlined in section 8.3.2, Case #1 represents a 2-meter river sediment load, Case #2 represents the removal of the sediment, and Case #3a is the 4-meter sediment load. As expected, when the sediment load increases, the displacement predictions increase slightly, due to the increase in the gravity-driven deformations of the liquefied soil. Since the differences are small, and buoyant uplift of the tunnel was not significant, there is no need to perform any such remediation (i.e., removal or addition of sediment).

iii.) Increased Earthquake Ground Velocity (Case #4):

Peak ground accelerations estimated by SHAKE varied from 0.32 m/s to 0.38 m/s. An A/V ratio of 1 was applied at this site (Byrne, 1994), where 'A' is the acceleration in gravity units and 'V' is the maximum velocity in m/sec. Consequently, a peak ground velocity (v_{\max}) of 0.30 m/s was applied in all transverse and longitudinal SOILSTRESS analyses. The maximum velocity parameter, v_{\max} , is used to compute the kinetic inertia

of the system. (Refer to appendix A.2 for a description of the incorporation of kinetic inertia within the Extended Newmark procedure). Since all the liquefied soil cannot be expected to trigger at the same time, it was considered appropriate to slightly decrease the ground velocity input from the maximums (i.e., $v_{\max} = 0.32$ m/s to 0.38 m/s) inferred from SHAKE. For comparison, location #2 was analyzed with an increased velocity input of $v_{\max} = 0.38$ m/s. The results of that analysis are summarized in appendix A.1.3 ('Case 4'). As expected, horizontal displacements increased proportionally to the increase in the velocity input.

iv.) Differences in Kinetic Energy Dissipation:

Amongst the offshore locations, locations #3 and #4 show smaller movements than location #2. There is an 8-meter thick segment of liquefied soils below the tunnel at location #2; the other two locations have approximately 3 meters of liquefied soil beneath the tunnel. The total kinetic energy to be dissipated is approximately the same for all three cases, but more energy is dissipated in the stronger non-liquefied materials at locations #3 and #4; consequently, the displacements are smaller -- since less energy is dissipated in the surrounding and underlying liquefied soils.

v.) Differential Movements in Transverse Direction:

The SOILSTRESS results depict differential movements along the width of the tunnel. The displacements at opposite corners ('C1', and 'C3') are provided to highlight

the differential movements at the vital concrete roadway section of the tunnel. These differing levels of movement are due to variations in the surficial geology. Locations and thicknesses of liquefied layers, as well as variations in residual strength and stiffness are key causes of the uneven movements. This proves to be a key advantage of using the SOILSTRESS finite element method -- post-earthquake stress-strain variations can be accounted for, in addition to the irregularities in geometry and geology.

9.4.1.2 Longitudinal-direction Analyses

Differential Movements:

Differential movements are accounted for in the longitudinal SOILSTRESS analyses. These differential movements are very important when considering post-earthquake structural effects, especially at the connections between the subaqueous tunnel elements.

When the pre-consolidation vertical movements from the Case #1 analyses are added to the total ('2-D') longitudinal vertical displacement, the ('3-D') vertical displacement predictions are very close in magnitude. Location #3 shows a vertical displacement which is about 9 centimeters lower than the other locations, yet the closest location (#4) is 140 meters away; consequently, the differential value is of little significance in terms of post-earthquake structural stability. If the Case #1 transverse analysis vertical displacement estimates are not added to the longitudinal prediction, then the largest differential movement occurs between locations #3 and #2. The two locations

are approximately 220 meters apart, and location #2 moves approximately 20 centimeters (8 inches) further down than location #3. Again, this magnitude of differential displacement is insignificant when considering the distance between locations.

9.4.2 LIQDISP -- Single-Degree-of-Freedom Analyses

i.) General Discussion:

LIQDISP is a simple method of analysis that incorporates the Extended Newmark methodology (Byrne, 1990). The closed form LIQDISP code is ideal for simple (infinite) slopes. For complex geometries, the program is limited to predicting free-field movements. Although LIQDISP is a simple program, it is advantageous over many procedures since it incorporates a model which takes into account nonlinear stress-strain behaviour of soil. (Refer to appendix A.2 for a description of the Extended Newmark model).

Because of the simplified nature of the program, it is not possible to include the effect of the tunnel interaction with the crust. The properties of the non-liquefied surface (crust) layers were averaged and input as one equivalent layer, and the same technique was applied to the underlying liquefied layers.

ii.) Analysis of Offshore Locations:

One of the difficulties in using LIQDISP at the offshore locations was the inability to acknowledge the water table location. Additionally, the weight of the overlying water could not be input, unless some form of averaging (i.e., additional weight) was incorporated in the crust mass.

The offshore locations (#2, #3, #4) were analyzed using the slope failure model, in

which a limit equilibrium stability factor of safety is used to approximate the static driving stress. The displacements are summarized in table 8.18.

Only a non-liquefied ('crust') material, and an underlying liquefied material can be input, regardless of the interbedded nature of a soil column. The method considers the crust (i.e., non-liquefied layer) and liquefied soil to be a single-degree-of-freedom elastic-plastic system. All liquefied layer thicknesses are accumulated, and then average soil parameter inputs must be used to represent the liquefied layer. Location #2 comprises 6 meters of liquefied sand and 4 meters of liquefied silt. When preparing the LIQDISP analyses, the sand and silt were combined, and average residual strength (S_r) and blow count magnitudes were applied to create one liquefied layer. The discrepancy between the silt and sand values wasn't significant, hence the LIQDISP estimates at location #2 can be considered crudely applicable.

It should be noted that the loose sand layers adjacent to the excavation (i.e., material #4 in figure 6.12) and the pump sand fill (material #3 in figure 6.12) were not applied in the LIQDISP analyses because they are presumed to have little effect on the magnitude of the tunnel displacements.

iii.) Analysis of Onshore Locations:

Since no liquefaction occurs below the tunnel invert at location #7, it was not analyzed using LIQDISP. The north shore (location #8) was analyzed as an infinite

slope, since the overlying dyke material resembles a continuous slope. Slopes varying from 1% to 4% were analyzed. Results and input parameters are summarized in table 8.19.

Since liquefaction of the overlying dyke sands will not have much influence on the underlying displacements, the thickness of that segment of liquefied sand was included as part of the crust (i.e., non-liquefied layer) thickness (t_c) to account for the added inertia.

CHAPTER 10

REMEDIAL MEASURES

10.1 Introduction

This chapter presents the results of SOILSTRESS analyses that simulate the effects of ground improvement on post-earthquake displacements. The location #2 analyses in section 8.3.2.1.2 should be referred to when reviewing the information in this chapter.

Potential remedial options were analyzed at location #2 because it is the offshore location determined to be the most susceptible to liquefaction. As table 8.15 shows, horizontal and vertical displacements for the original configuration were approximately 1 meter and 0.2 meters, respectively. (Figures 8.10 and 8.11 graphically depict the movements).

The zones of improvement represent soil which has been densified. As with other non-liquefied materials, only a two-fold degradation in post-earthquake stiffness of the densified zones was applied in these analyses. Soil units #3 to #7 are liquefied. The pre- and post-earthquake soil properties of all other materials were not changed from their original values. Tables 8.3, 8.8, and 8.11 summarize the pre- and post-earthquake SOILSTRESS inputs, and figure 6.13 provides the material numbering scheme (for location #2).

10.2 Presentation and Discussion of Results

Six densification schemes were analyzed. Table 10.1 summarizes the ground improvements that were simulated.

Densification Case Number	Description of Densification Scheme
D1	- densify sides of tunnel only -- not underneath
D2	- densify directly beneath tunnel
D3	- densify outside of excavation and go to 6 meters below excavation
D4	- same as D3 but go to 10 meters below excavation
D5	- densify closer to roadway and go to 6 meters below excavation
D6	- same as D5 but increase width of densified zone; and increase depth by 4 meters

Table 10.1 - Descriptions of Densification Schemes

Table 10.2 summarizes the results of the analyses for each case. As in previous analyses, C1 is the top left corner of the concrete section and C3 is the bottom right corner. (Figure 6.13 shows the locations on a transverse-section drawing). The displacements at opposite corners are provided so that differential displacements can be reviewed.

i.) Case #D1:

Figures 10.1 to 10.10 are graphic SOILSTRESS output depicting the magnitude

and pattern of displacement for each densification scheme. In the graphics, the dashed lines represent the initial state, and the solid lines show the post-earthquake position of the nodes. Densification Case #D1 shows the effects of densifying the 16-meter wide (at

Remediation Case Number	Corner	HORIZONTAL Transverse Displacement (meters)	VERTICAL Displacement (meters)
D1	C1	1.0	-0.27
	C3	1.0	-0.29
D2	C1	0.31	-0.22
	C3	0.31	-0.22
D3	C1	0.60	-0.10
	C3	0.51	-0.40
D4	C1	0.37	-0.40
	C3	0.42	-0.26
D5	C1	0.43	-0.36
	C3	0.43	-0.35
D6	C1	0.18	-0.65
	C3	0.31	-0.18

Table 10.2 - Modelling of Remediation Schemes -- Transverse Displacements at Location #2

base) loose sand segment adjacent to the tunnel. As table 10.2 shows, there isn't any mitigation of displacements at the concrete section.

The displacement pattern is shown in figure 10.1. The displacements are

magnified by a factor of two. Although the stiffness of the unit #4 loose sand will degrade significantly upon liquefaction, it has little influence on the horizontal movement of the concrete section. Figure 10.1 shows that the underlying liquefied materials control the movement. As table 10.2 shows, there is no benefit in densifying the small zones close to the tunnel centerline.

Cases #D2 to #D6 show that the extent of lateral movement is controlled by the underlying unit #5, #6, and #7 soils.

ii.) Case #D2:

The next option, Case #D2, represents the densification of a 57-meter segment of loose sand (units #5 and #6) directly beneath the tunnel. Figure 10.2 shows the displacement pattern. (The displacements are magnified by a factor of two). As expected, this option is very effective in decreasing horizontal movement. Vertical displacements are similar to those in the original (no ground improvement) analyses, but the horizontal displacements are only one-third the original predictions. It is apparent that the magnitude of the horizontal movement is controlled by the underlying liquefied layers. Although this densification scheme accomplishes its objective, accessing the zones directly beneath the tunnel may be very difficult. The remaining (more practical) schemes assess the effects of densifying zones adjacent to the tunnel.

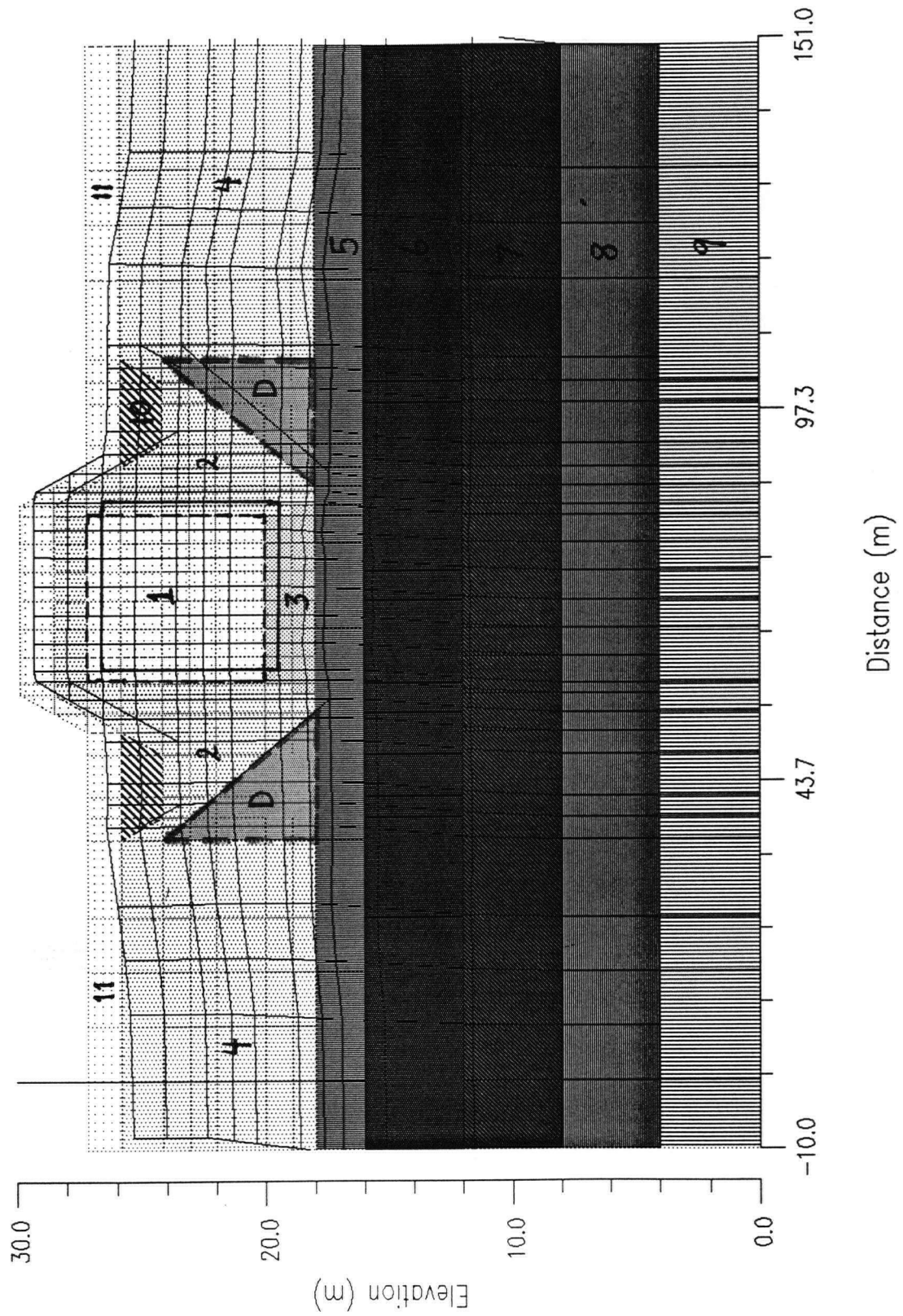


Figure 10.1 - Displacement Pattern -- Case #D1

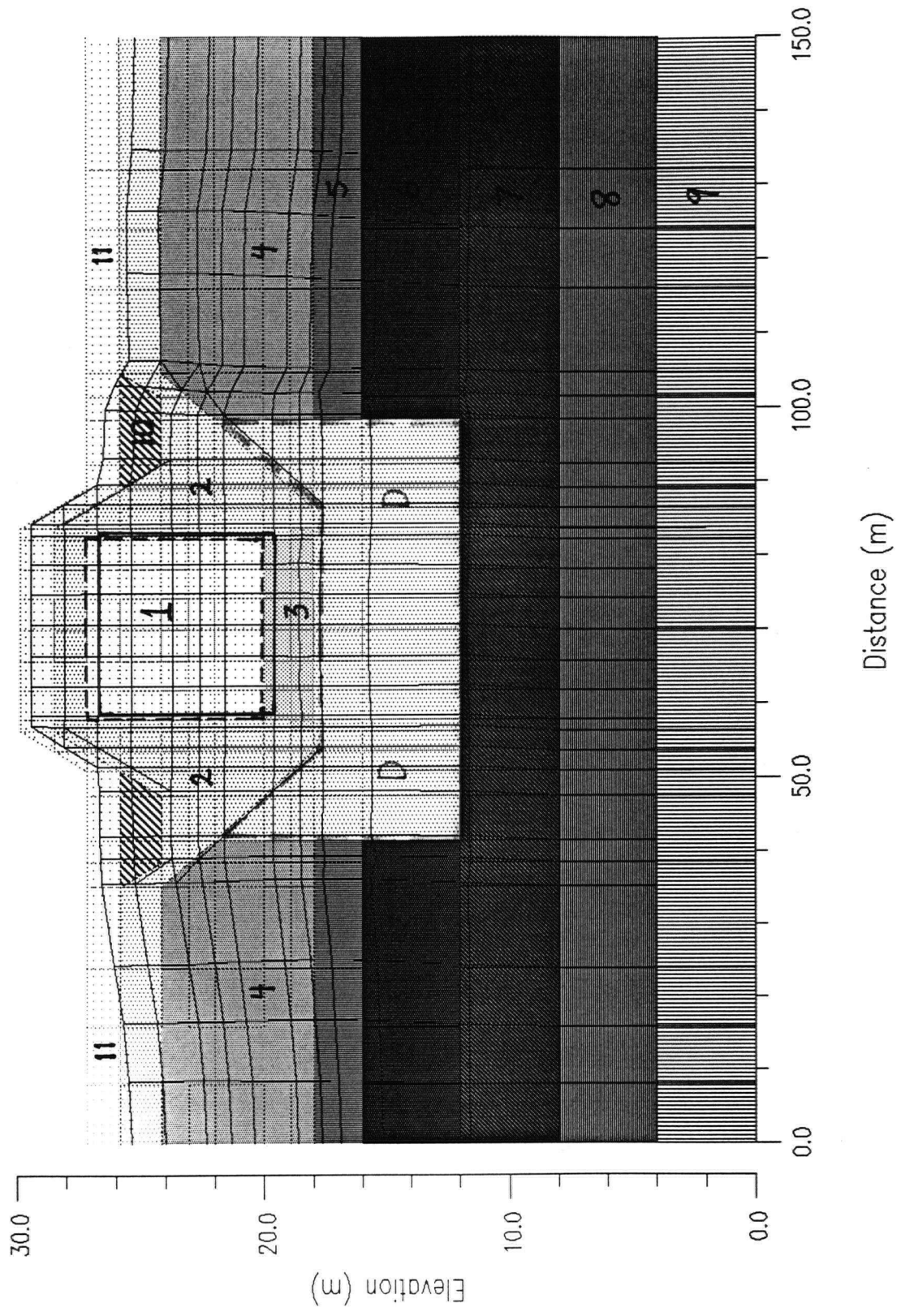


Figure 10.2 - Displacement Pattern -- Case #D2

iii.) Case #D3:

Case #D3 represents the densification of two 29-meter width zones that extend from the ground surface to the base of the 6-meter segment of loose sand (unit #6). The densification is initiated 35 meters from the tunnel centerline. Figures 10.3 and 10.4 show the displacement pattern and vectors, respectively. The displacements in figures 10.3 and 10.4 are to scale (i.e., not magnified). The densified zones cause a slight clockwise rotation of the concrete section. As summarized in table 10.2, the horizontal displacements decrease by forty to fifty percent. The decrease in vertical displacement at corner #1 is simply due to the upward rotation. The displacement vectors of figure 10.4 show the uneven effect of the transitions from liquefied to non-liquefied soils. The rotation of the concrete section is most likely due to the restriction caused by the second (right side) densified zone.

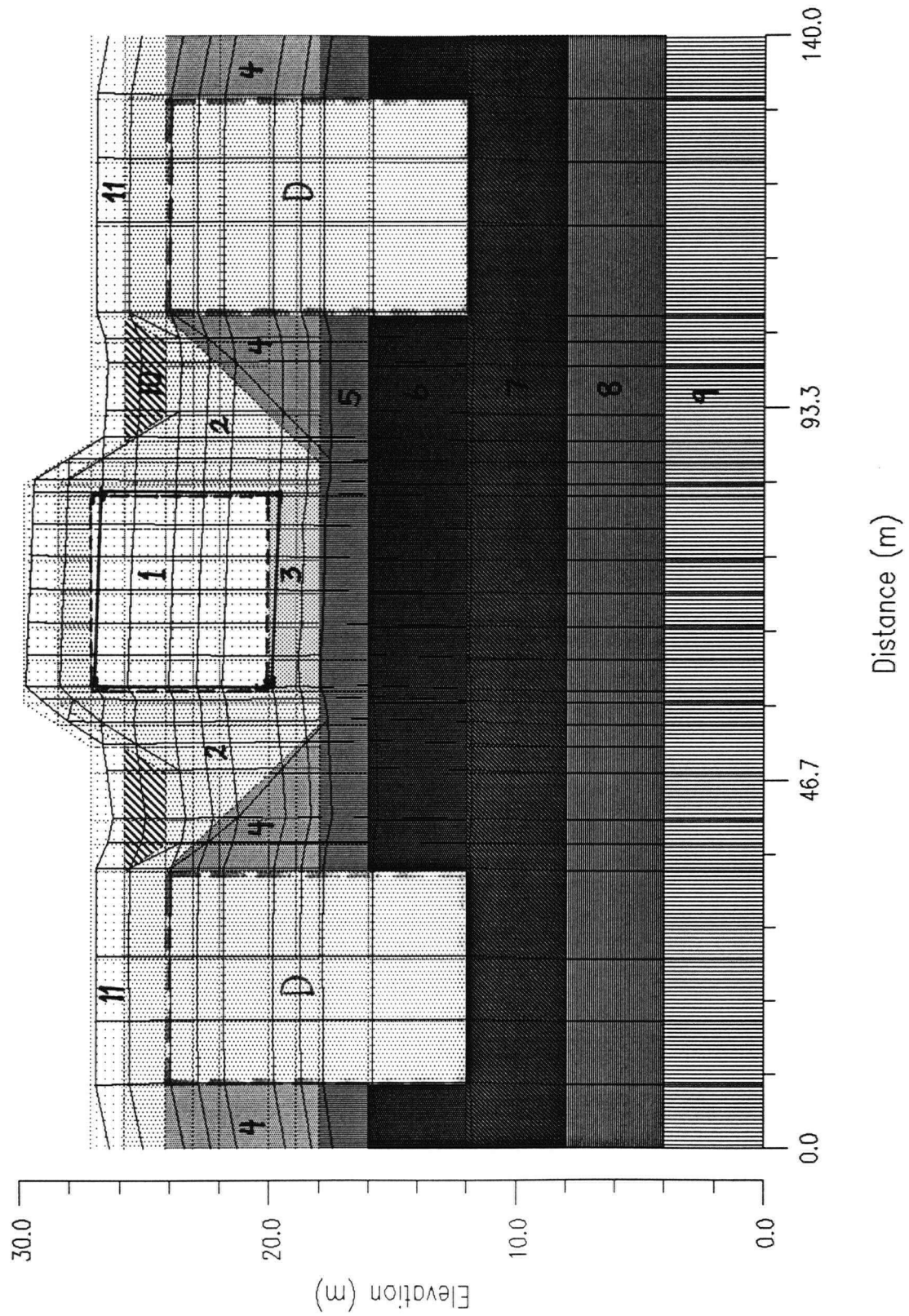


Figure 10.3 - Displacement Pattern -- Case #D3

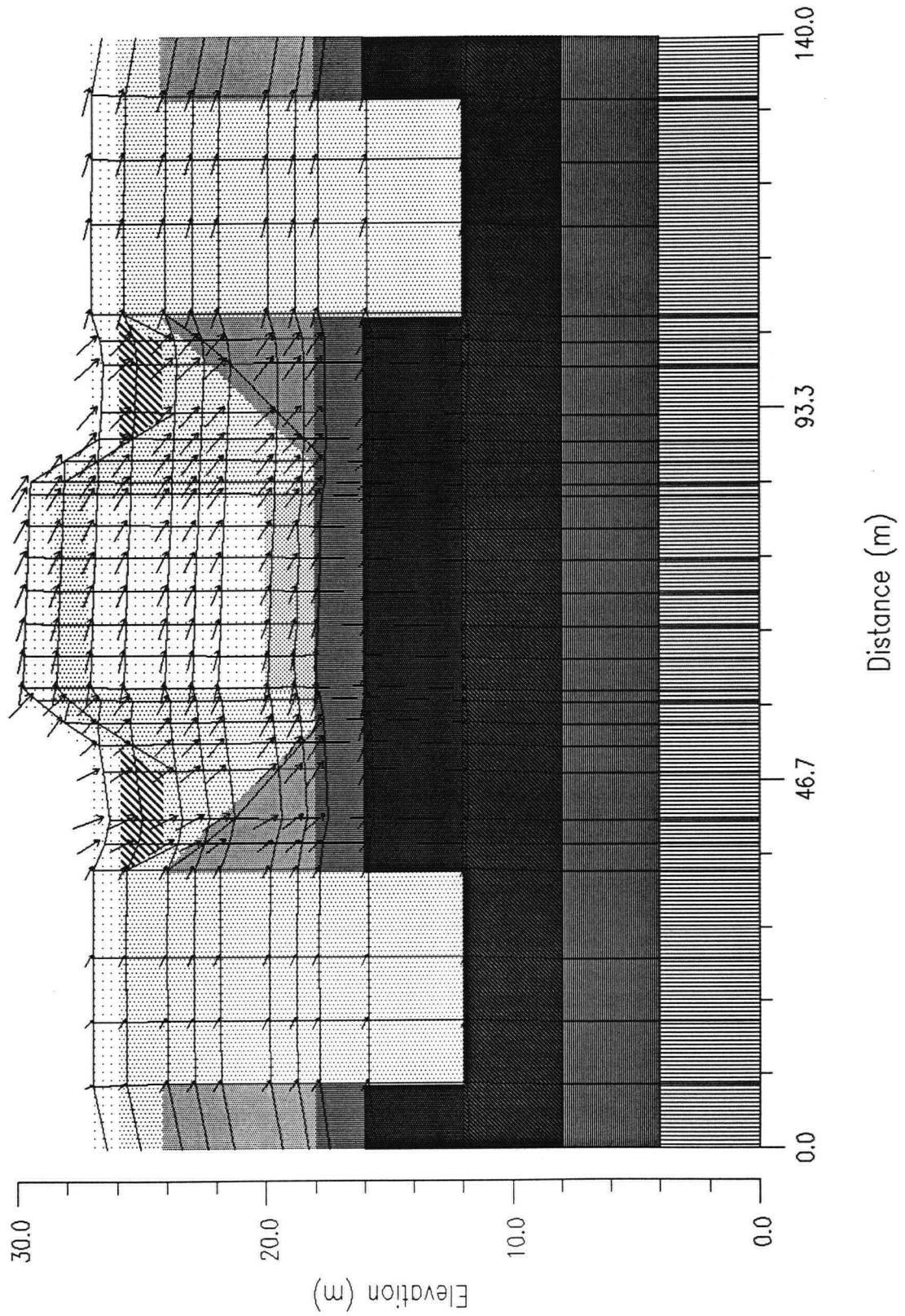


Figure 10.4 - Displacement Vectors -- Case #D3

iv.) Case #D4:

Case #D4 is very similar to Case #D3; the only difference is that the zone of densification extends to a depth 10 meters below the tunnel invert. The two 29-meter width densified zones extend from the ground surface to the base of the liquefied silt (unit #7). The densification is initiated 35 meters from the tunnel centerline.

As discussed earlier, the underlying layers control the lateral movement of the concrete section. Figures 10.5 and 10.6 show the displacement pattern and vectors, respectively. (The displacements in figures 10.5 and 10.6 are magnified by a factor of two). Comparing with Case #D3, the further restriction of the movement in the underlying layers results in an additional decrease in the horizontal movement of the concrete section. As shown in table 10.2, this configuration reduces horizontal movement by approximately sixty percent. Like Case #D3, the concrete rotates, except in this configuration, it rotates counter-clockwise. The same amount of energy has to be dissipated in all the cases. The unit #5 liquefied sand dissipates more kinetic energy in Case #D4 (versus Case #D3) because of the lateral restriction in the deepest liquefied layer (unit #7); consequently, this results in greater deformation in the unit #5 sand.

v.) Case #D5:

Case #D5 is similar to Case #D3, except the zones of densification are closer to the tunnel centerline. The densification is initiated 22 meters from the tunnel centerline.

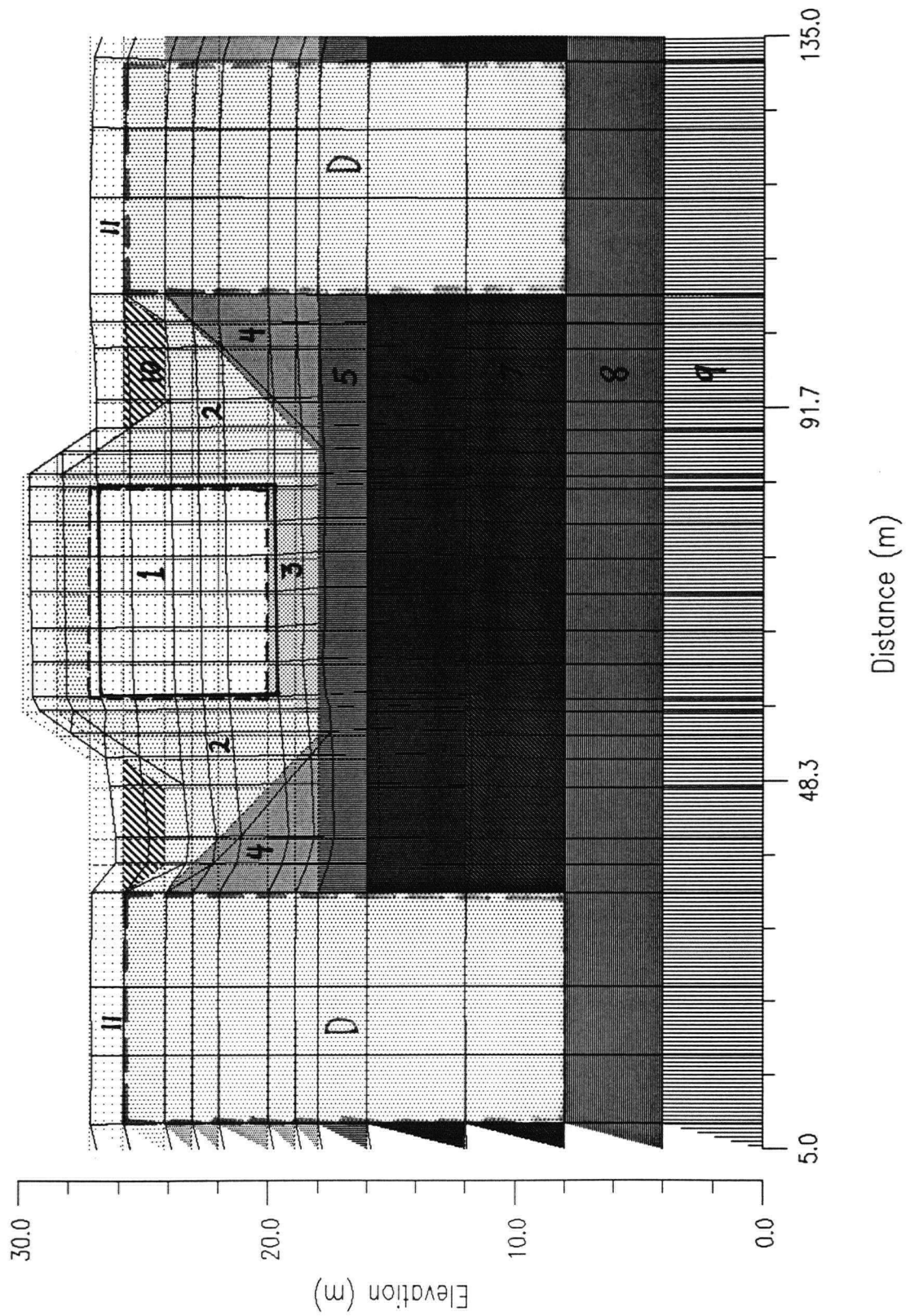


Figure 10.5 - Displacement Pattern -- Case #D4

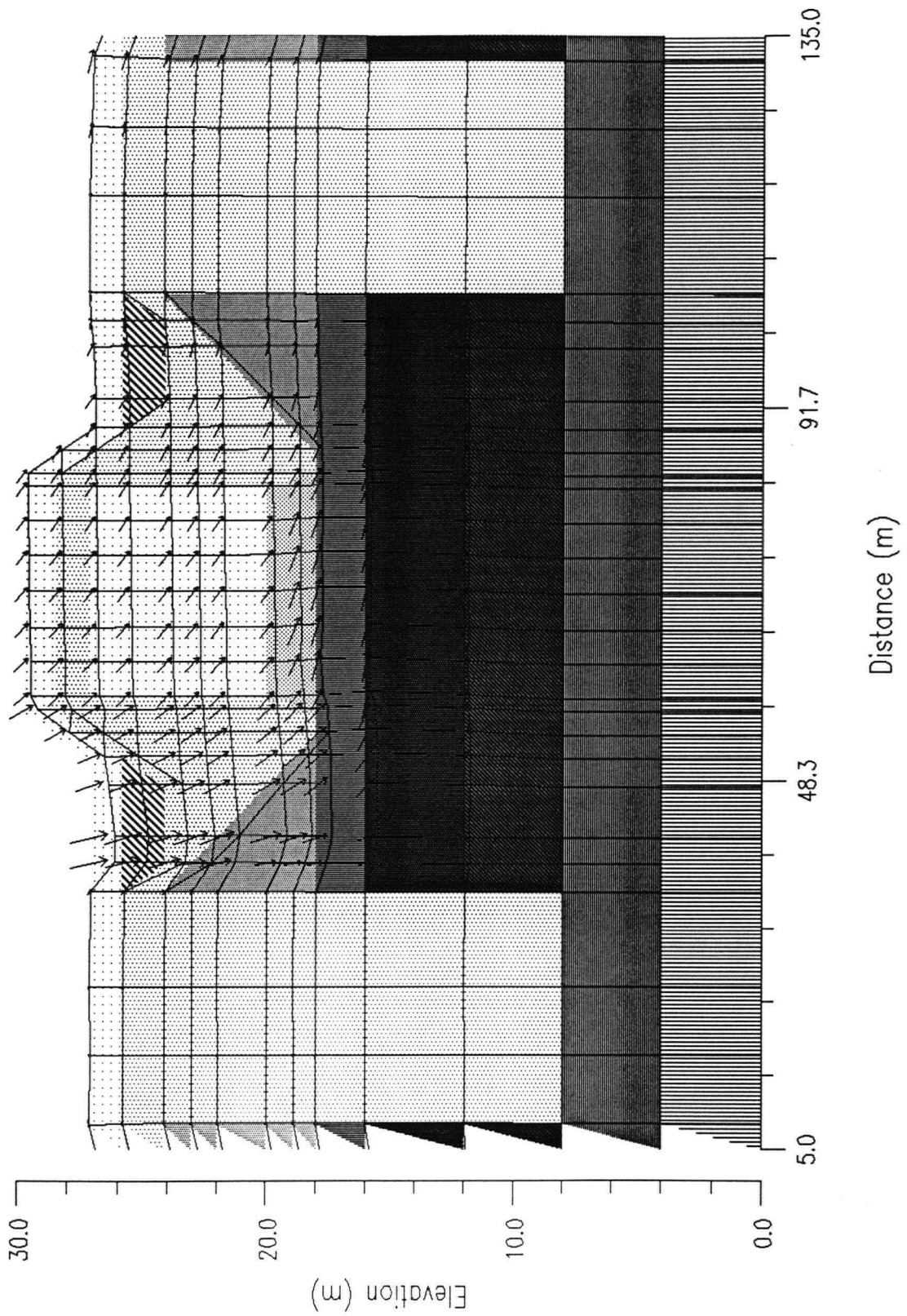


Figure 10.6 - Displacement Vectors -- Case #D4

Case #D5 represents the densification of two 36-meter wide segments that extend from the ground surface to a depth 6 meters below the tunnel invert. The densified zones initiate 25 meters from the centerline of the concrete section (tunnel roadway).

Figures 10.7 and 10.8 show the displacement pattern and vectors, respectively. (The displacements in figures 10.7 and 10.8 are magnified by a factor of two). The densified zones in configuration #D5 are effective in decreasing horizontal movement. In this configuration, the horizontal displacements are decreased by approximately sixty percent (refer to table 10.2). Additionally, the amount of rotation is very small; consequently, this densification scheme is mildly preferable to Cases #D3 and #D4. Since accessing the unit #4 sands directly beneath the gravel backfill (unit #2) will require temporary removal of the gravel, this may not be the most economical solution.

As figure 10.7 shows, there is significant outward movement of the elements at the left and right boundaries. This phenomenon is explained in section 9.4.1.

vi.) Case #D6:

Case #D6 is similar to Case #D5. There are two differences: the zone of densification extends to a depth 10 meters below the tunnel invert, and an additional 8-meter wide non-liquefied zone has been added. The two 29-meter width densified zones extend from the ground surface to the base of the non-plastic liquefied silt. Each zone is initiated 22 meters from the tunnel centerline. The additional width of the

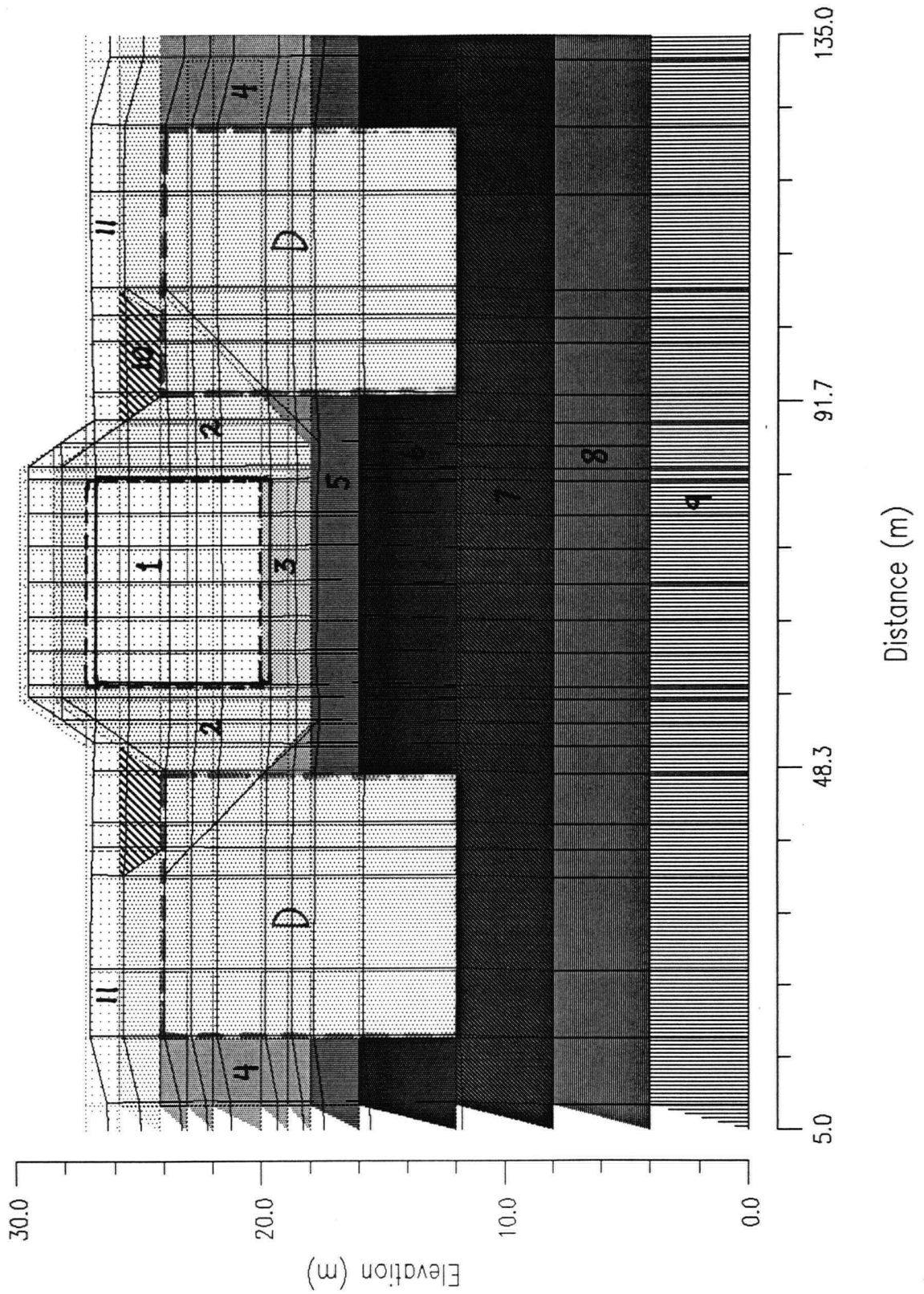


Figure 10.7 - Displacement Pattern -- Case #D5

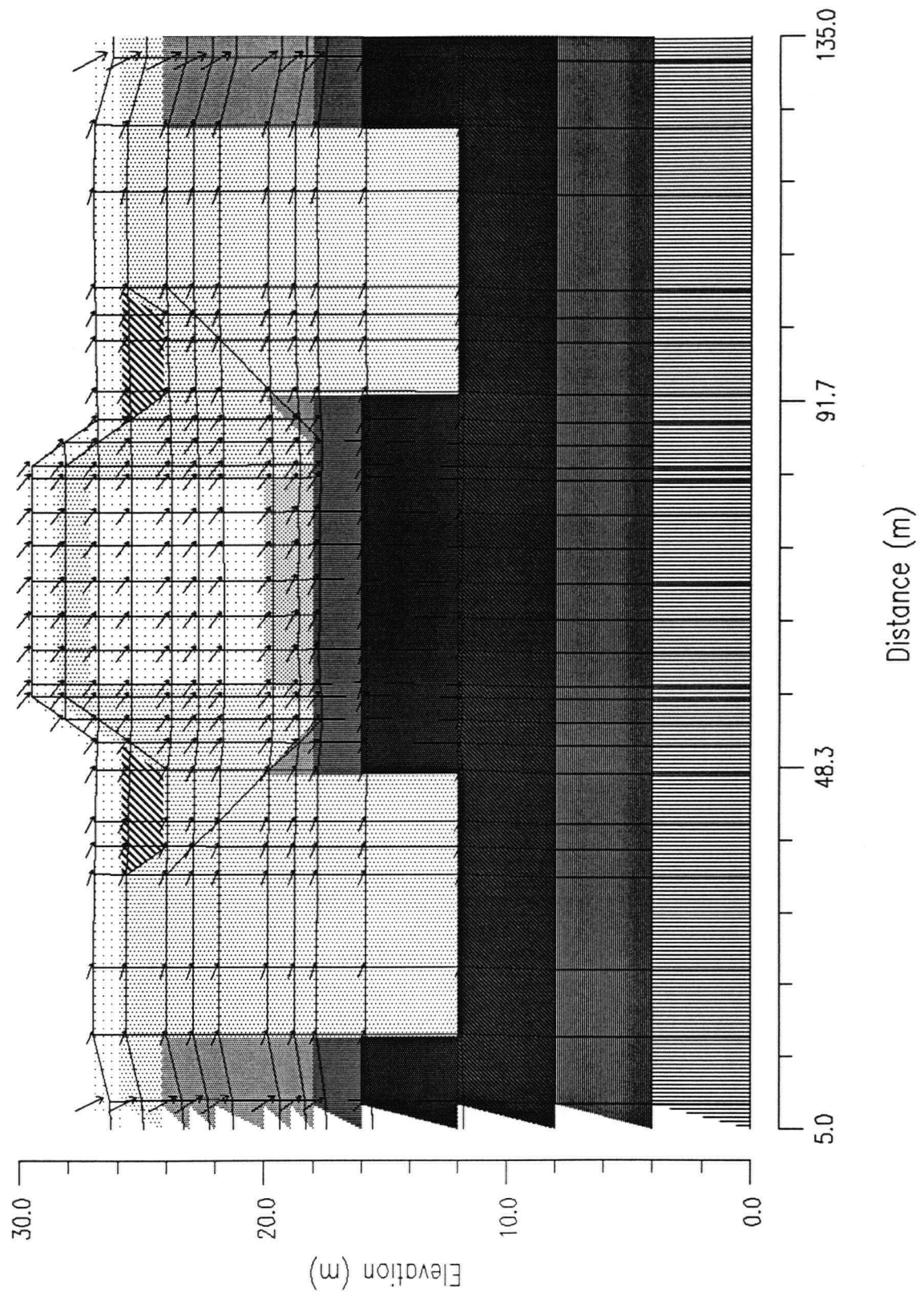


Figure 10.8 - Displacement Vectors -- Case #D5

densified zone represents a gradual densification scheme in which the additional width is a partially densified zone (referred to as 'P.D.' in figure 10.9). The partial densification is meant to simulate the gradual decrease in density as the perimeter of the radius of influence (of the outer-most timber piles) is approached.

This densification scheme is very effective in limiting horizontal movements, but there is significant rotation of the concrete section. Figures 10.9 and 10.10 show the displacement pattern and vectors, respectively. (The displacements in figures 10.9 and 10.10 are to scale). Comparing the displacement vector graphics of figures 10.8 and 10.10, the unit #5 sand dissipates more kinetic energy in Case #D6 (versus Case #D5) because of the restriction of flow in the deepest liquefied layer (unit #7). The gravel backfill (unit #2) restricts the deformations in the unit #4 liquefied sand; this leads to a downward movement into the unit #5 loose sand, and the consequent counter-clockwise rotation.

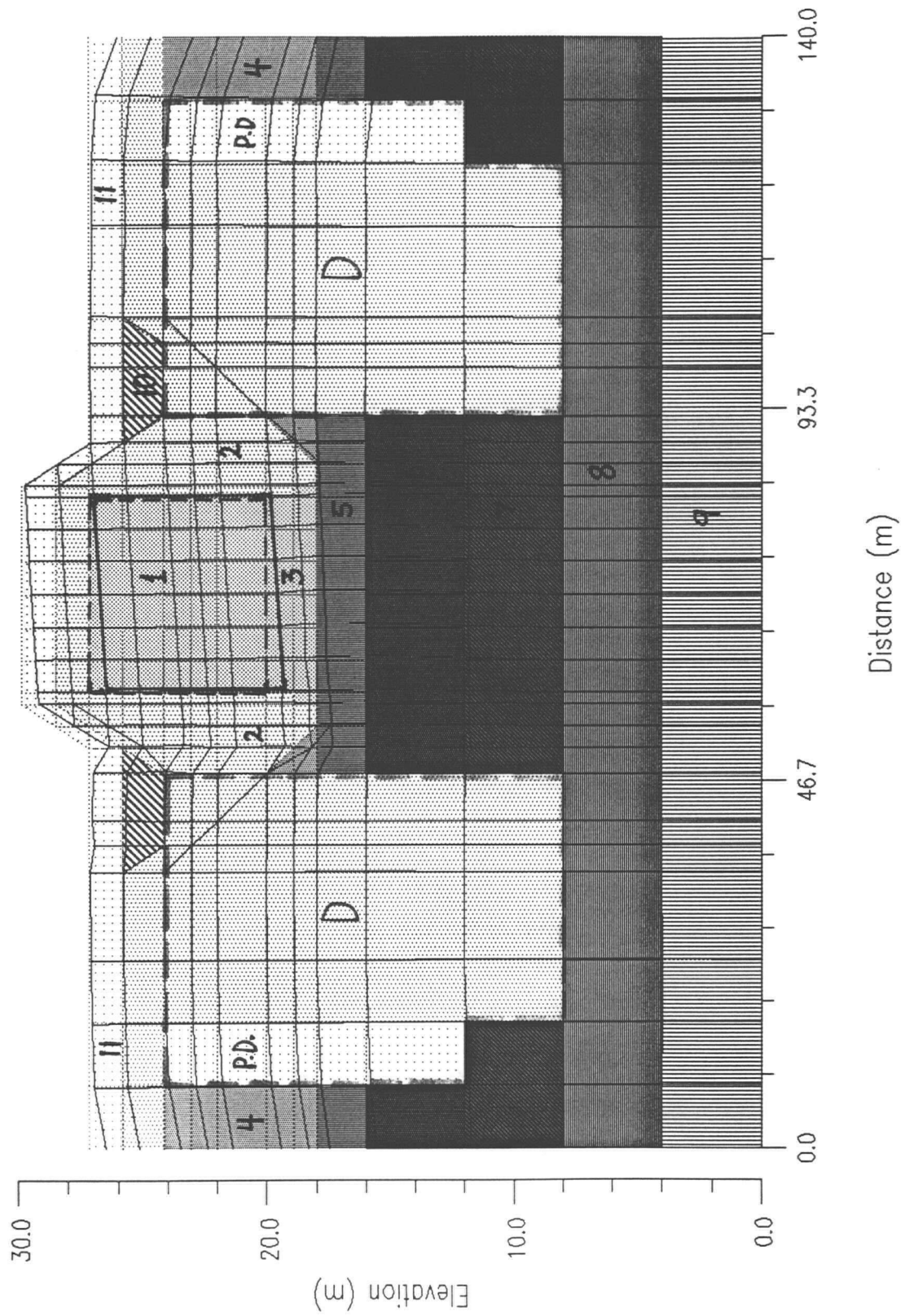


Figure 10.9 - Displacement Pattern -- Case #D6

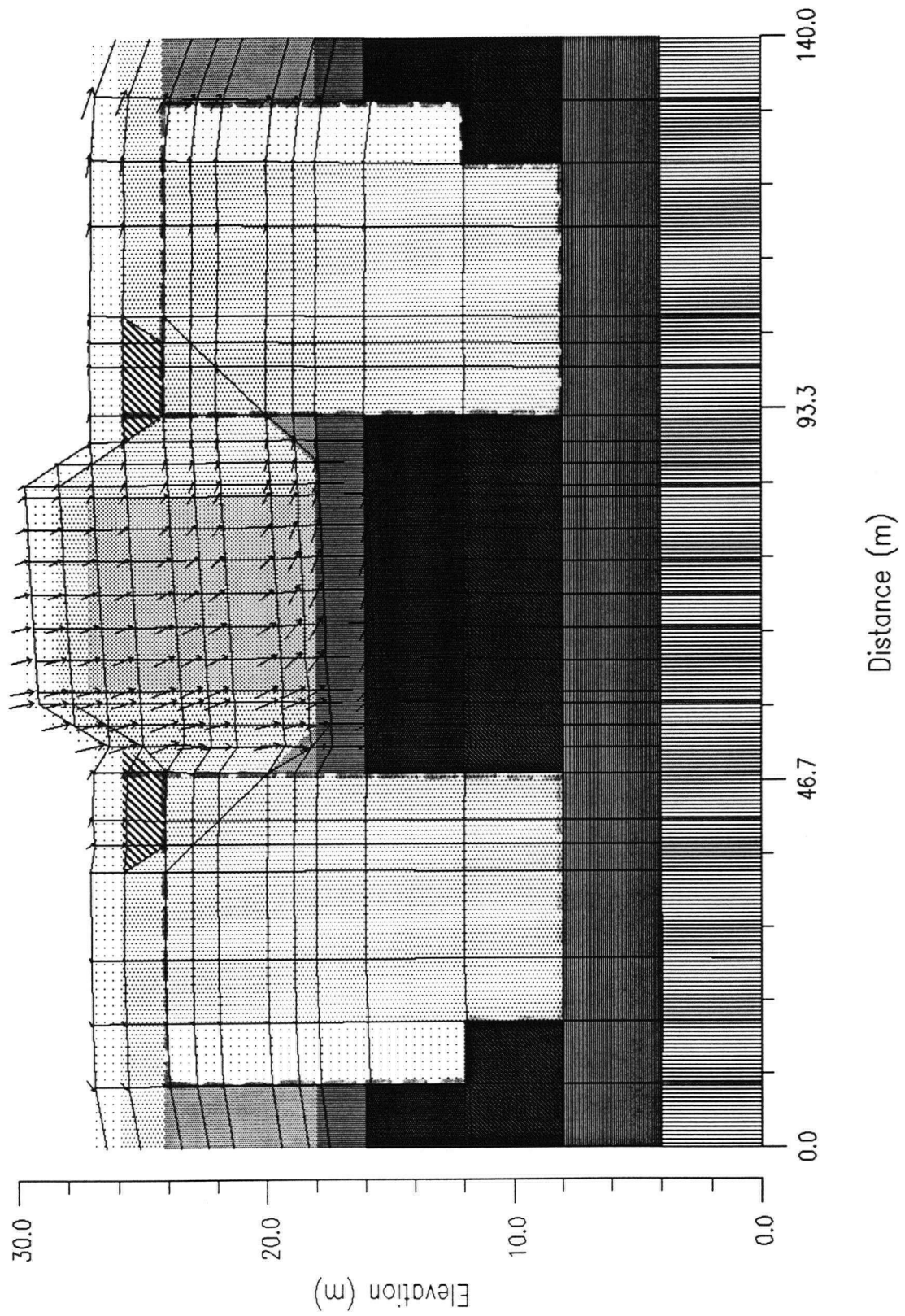


Figure 10.10 - Displacement Vectors -- Case #D6

10.3 Preliminary Remediation Recommendation

The most common method of foundation remediation is soil densification. The post-earthquake movements within foundation soils are a function of post-cyclic strength. Since residual strength is a function of void ratio, it can be increased by densifying the soil.

The analyses in section 10.2 assessed the effects of densification. Six densification schemes were analyzed. Although very effective in limiting displacements, densification beneath the tunnel would not be an economical solution due to lack of accessibility. Cases #D3 to #D6 assessed the effects of densification of zones adjacent to the tunnel. This general approach is the most efficient.

Location #2			
Depth (meters)	Soil Type	$[(N_1)_{60}]_{\text{Req'd}}$ (Blows/ft)	$(q_c)_{\text{Req'd}}$ (bar)
0 - 8	Sand	30	150
8 - 11.7	Sandy Silt	20	60

Table 10.3 - Required Densification to Prevent Liquefaction at Location #2

The depth of liquefaction along the length of the tunnel varies. Tables 10.3 to 10.7 summarize the remediation requirements for each location that has been analyzed in this study. A correlation published by Robertson et al. (1983) was employed to estimate q_c/N ratios to convert the $[(N_1)_{60}]_{\text{Req'd}}$ estimates to cone bearing (CPT) equivalents. In silty

sands, $q_c/N = 3.5$ was applied, and in silt $q_c/N = 3$. In sands, a q_c/N value of 5 was used.

Appendix F contains details of the calculations at each location.

Location #3			
Depth (meters)	Soil Type	$[(N_1)_{60}]_{\text{Req'd}}$ (Blows/ft)	$(q_c)_{\text{Req'd}}$ (bar)
0 - 6.4	Sand	30	150
6.4 - 9.1	Sandy Silt	20	60

Table 10.4 - Required Densification to Prevent Liquefaction at Location #3

Location #4			
Depth (meters)	Soil Type	$[(N_1)_{60}]_{\text{Req'd}}$ (Blows/ft)	$(q_c)_{\text{Req'd}}$ (bar)
0 - 6.5	Sand	30	150
6.5 - 10.5	Silt	23	69

Table 10.5 - Required Densification to Prevent Liquefaction at Location #4

Location #7			
Depth (meters)	Soil Type	$[(N_1)_{60}]_{\text{Req'd}}$ (Blows/ft)	$(q_c)_{\text{Req'd}}$ (bar)
0 - 3.5	Sand	20	100
3.5 - 7.2	Sand	23	115
7.2 - 11.0	Sand	30	150
11.0 - 17.0	Sand	28	140
17.0 - 20.0	Sand	26	130

Table 10.6 - Required Densification to Prevent Liquefaction at Location #7

Location #8			
Depth (meters)	Soil Type	$[(N_1)_{60}]_{\text{Req'd}}$ (Blows/ft)	$(q_c)_{\text{Req'd}}$ (bar)
0 - 10.0	Sand	20	100
10.0 - 12.0	Sand	19	95
12.0 - 15.8	Sand	18	90
15.8 - 21.6	Sand	17	85
21.6 - 23.0	Silty Sand	26	91
23.0 - 27.2	Sand	16	80

Table 10.7 - Required Densification to Prevent Liquefaction at Location #8

There is no headroom access restriction at this site, but due to the submergence of the structure, the choice of methods of remediation are limited. Timber piles would be a logical choice for a site such as this. Specifications of the remediation (i.e., densification method and relevant parameters, construction specifications, etc.) would be assessed after a confirmational study has been done.

CHAPTER 11

CONCLUSIONS

The George Massey Tunnel's response to the 1:475 year seismic event has been evaluated. The analyzed event is an *M* 7.0 causing a peak ground acceleration of 0.24g. Current research papers in the field of seismic response evaluation and geotechnical analysis reports for the Fraser Delta were reviewed. Structure and foundation geometry were assessed using as-built construction drawings. Available site-specific in-situ test data was applied to assess engineering parameters and the soil stratigraphy along the length of the tunnel.

The soils underlying the tunnel comprise loose to medium-dense sands and silts of low plasticity that could be triggered to liquefy in the event of a major earthquake. Liquefaction resistance of the predominant sands and non-plastic silts was based on the indirect approach using penetration test data together with charts based on performance during past earthquakes. Large zones of these underlying soils were predicted to liquefy for the *M* 7.0 event. The south-most offshore location (#2), and the northern river bank (location #8) are most susceptible to triggering.

Post-liquefaction stability analyses indicated that residual strengths were adequate to prevent flow slides at all locations. Because significant zones were predicted to trigger, empirical and numerical method deformation analyses were carried out. Analyses were done in directions transverse to and parallel to the tunnel alignment. Predictions using the most detailed empirical method (Bartlett/Youd, 1992) corroborated well with

those of the most rigorous numerical method (SOILSTRESS -- pseudo-dynamic finite element).

Since the predicted displacements were large in some cases, remedial measures were analyzed at location #2. A structural analysis should be carried out to determine structural tolerances; if foundation remediation is required, it is recommended that zones adjacent to the tunnel be densified to the predicted depth of liquefaction (at each analyzed location).

To affirm the results of this study, a seismic response analysis using a method such as F.L.A.C (Fast Lagrangian Analysis of Continua) should be carried out. Furthermore, it is recommended that, to decrease uncertainties in parameter estimates, more in-situ soil test data be acquired.

REFERENCES

- Anderson, D., and P.M. Byrne (1991). "Earthquake Design in the Fraser Delta", Task Force Report, June.
- Bartlett, S.F., and Youd, T.L. (1992). "Empirical Prediction of Lateral Spread Displacement", Proceedings, 4th US-Japan Workshop on Earthquake Resistant Design Lifeline Facilities and Countermeasures for Soil Liquefaction, NCEER, Honolulu, Hawaii, May.
- BC Hydro Priority Transmission Tower Study (1990). "Cyclic Testing of Silts Laboratory Test Results". Unpublished data.
- Bishop, A.W., (1955). "The Use of the Slip Circle in the Stability Analysis of Slopes". Geotechnique, Vol.5, No.1.
- Blunden, R.H., (1975). "Urban Geology of Richmond British Columbia", Adventures in Earth Science Series Number 15, B.C. Science Teachers' Association.
- Byrne, P.M., and Walter Janzen (1981). "SOILSTRESS: A Computer Program for Non-linear Analysis of Stresses and Deformations in Soil", Department of Civil Engineering, University of British Columbia, Soil Mechanics Series #52, December.
- Byrne, P., D. Anderson, and W. Janzen (1984). "Response of Piles and Casings to Horizontal Free Field Soil Displacements", Canadian Geotechnical Journal, Vol. 21, No. 4.
- Byrne, P.M., and U. Atukorala (1985). "A Report to the Ministry of Transportation & Highways on Seismic Stability of Bridge Abutments Underlain by Organic Soils, Annacis Island Project, January.
- Byrne, P.M. (1990). "A Model for Predicting Liquefaction Induced Displacements", Department of Civil Engineering, University of British Columbia, Soil Mechanics Series #147, September.
- Byrne, Peter M. & Hendra Jitno (1993). "Analysis of Earthquake Induced Displacements of the Intake Structures, John Hart Dam", Department of Civil Engineering, University of British Columbia, September.
- Byrne, P.M. (1993a). Civil 413 Class Notes -- University of British Columbia.

- Byrne, P.M. (1993b). Personal Communication.
- Byrne, P.M., A.S. Imrie, and N.R. Morgenstern (1994). "Results and Implications of Seismic Performance Studies for Duncan Dam", 46th Annual Canadian Geotechnical Conference Saskatoon, Saskatchewan, September 27-29, 1993, Canadian Geotechnical Journal Vol.31, pp.979-988.
- Byrne, P.M. (1994a). Civil 581 Class Notes -- University of British Columbia.
- Byrne, P.M. (1994b). Personal Communication.
- Byrne, P.M. (1994c). Memorandum to Ministry of Transportation & Highways -- Review of Seismic Liquefaction Analysis of Second Narrows Bridge. Report Reviewed: "Seismic Retrofit of Second Narrows Bridge" by Golder & Associates. June.
- Byrne, P.M. (1995). Personal Communication.
- Clague, John J., and J.L. Luternauer (1991). "Postglacial Deltaic Sediments, Southern Fraser River Delta, British Columbia"
- Craig, R.F. (1989). "Soil Mechanics", fourth edition, Van Nostrand Reinhold (International) Co. Ltd..
- Duncan, J.M., Peter Byrne, Kai S. Wong, and Phillip Mabry (1980). "Strength, Stress-strain and Bulk Modulus Parameters for Finite Element Analyses of Stresses and Movements in Soil Masses", Report No. UCB/GT/80-01, University of California at Berkeley, August.
- Ersoy, T. (1994). Private Communication.
- Ersoy, T. (1995). Private Communication.
- Finn, W.D.L., Byrne, P.M., and Martin, G., (1976). "Seismic Response and Liquefaction of Sands", Journal of Geotechnical Engineering, Vol.102, No.8, pp.841-856.
- Finn, W.D.L., (1988). "Dynamic Analysis in Geotechnical Engineering", Proceedings of Earthquake Engineering and Soil Dynamics II -- Recent Advances in Ground-Motion Evaluation Specialty Conference, ASCE, Geotechnical Special Publication #20, pp. 523-591.

- Finn, W.D. Liam, and Andrew M. Nichols (1988a). "Seismic Response of Long-Period sites: lessons from the September 19, 1985 Mexican Earthquake", *Canadian Geotechnical Journal*, Vol. 25.
- Finn, W.D.L., R.H. Ledbetter, R.L. Fleming Jr., A.E. Templeton, T.W. Forrest and S.T. Stacy (1990). "Dam on Liquefiable Foundation: Safety Assessment and Remediation", 17th International Congress on Large Dams, Vienna, June.
- Finn, W.D.L. (1993). "Evaluation of Liquefaction Potential", *Proceedings of the Seminar on Dynamics and Geotechnical Earthquake Engineering*, A.A. Balkema, pp. 127-157. Department of Civil Engineering -- University of British Columbia.
- Gillespie, D.G. (1993). Personal Communication.
- Hall, P. (1957). "Deas Island Tunnel"; *Journal of the Structural Division*, ASCE, ST6, November.
- Hamada, M., S. Yasuda, R. Isoyama, and K. Emoto (1986). "Study on Liquefaction Induced Permanent Ground Displacements", Published by the Association for the Development of Earthquake Prediction in Japan, p.87.
- Hamilton, Tark (1994). Personal Communication
- Hunter, J.A., J.L. Luternauer, K.G. Neave, S.E. Pullan, R.L. Good, R.A. Burns, and M.Douma (1993). "Shallow Shear Wave Velocity-Depth Data in the Fraser Delta from Surface Refraction Measurements, 1989, 1990, 1991". Geological Survey of Canada, Open File 2504.
- Idriss, I.M. (1991). "Procedures for Selecting Earthquake Ground Motions at Rock Sites", University of California at Davis, September 1991 (Revised March 1993).
- Jitno, Hendra, & Peter M. Byrne (1993). "A Procedure for Predicting Seismic Deformations of Earth Structures", Department of Civil Engineering, University of British Columbia, September.
- Jitno, H. (1994). Personal Communication.
- Jong, H., (1988). "A Critical Investigation of Post-liquefaction Strength and Steady-State Flow Behaviour of Saturated Soils", Ph.D. Thesis, Department of Civil Engineering, Stanford University, California.

- Kuesel, T.H. (1969). "Earthquake Design Criteria for Subways". *Journal of the Structural Division, ASCE*, ST6, June.
- Lambe, W.T., R.V. Whitman (1969). "Soil Mechanics", First Edition, Massachusetts Institute of Technology.
- Lo, Robert C., Alex Sy, Paul W. Henderson, David Y.Siu, W.D. Liam Finn, and Arthur C. Heidebrecht (1991). "Seismic Site Amplification Study for Fraser Delta, British Columbia", 6th Canadian Conference on Earthquake Engineering Toronto, June 12-14.
- Luternauer, J.L., and W.D. Liam Finn (1983). "Stability of the Fraser River Delta Front", *Canadian Geotechnical Journal*, V.20, pp. 603-616.
- Marcuson, W.F.III, M.E. Hynes and A.G. Franklin (1990). "Earthquake Spectra", Vol. 6, No. 3, August, pp. 529-572.
- Monaghan, Pat (1994). Personal Communication.
- Naumoski, N. (1985). "SYNTH Program: Generation of Artificial Acceleration Time History Compatible with a Target Spectrum", McMaster Earthquake Engineering Software Library, Department of Civil Engineering and Engineering Mechanics, McMaster University, Hamilton, Canada.
- Newmark, N.M. (1965). "Effects of Earthquakes on Dams & Embankments", Fifth Rankine Lecture, *Geotechnique*, Vol. 15, No. 2, June, pp.139-160.
- Owen, G. N. and R.E. Scholl (1981). "Earthquake Engineering of Large Underground Structures". Report No. FHWA/RD-80/195, Federal Highway Administration, January.
- Pillai, V.S., and R.A. Stewart (1994). "Evaluation of Liquefaction Potential of Foundation Soils at Duncan Dam", 46th Annual Canadian Geotechnical Conference Saskatoon, Saskatchewan, September 27-29, 1993, *Canadian Geotechnical Journal* Vol.31, pp.951-966.
- Pillai, V.S., and P.M. Byrne (1994). "Effect of Overburden Stress on Liquefaction Resistance of Sand", *Canadian Geotechnical Journal*, Vol.31, pp.53-60.

- Pillai, V.S., and F.M. Salgado (1994). "Post-Liquefaction Stability and Deformation Analysis of Duncan Dam", 46th Annual Canadian Geotechnical Conference Saskatoon, Saskatchewan, September 27-29, 1993, Canadian Geotechnical Journal Vol.31, pp.967-978.
- Plewes, Howard, V. Sitham Pillai, Michael R. Morgan, and Brian L. Kilpatrick (1994). "In situ Sampling, Density Measurements, and Testing of Foundation Soils at Duncan Dam", 46th Annual Canadian Geotechnical Conference Saskatoon, Saskatchewan, September 27-29, 1993, Canadian Geotechnical Journal Vol.31, pp.927-938.
- Poulos, S.J., G. Castro and J.W. France (1985). "Liquefaction Evaluation Procedures", Journal of the Geotechnical Engineering Division, ASCE, Vol. 111, No. 6, June, pp.772-792.
- Richter, K.J. (1991). "A Report to the Ministry of Transportation & Highways on the Seismic Retrofit of Structures in the Lower Mainland", September.
- Ripley & Associates Ltd. (1956). "Reports on Testing Program & Laboratory Test Data for Samples from holes 1 to 10 -- Deas Island Tunnel".
- Robertson, P.K., R.G. Campanella, D. Gillespie, and A. Rice (1986). "Seismic CPT to Measure In Situ Shear Wave Velocity", Journal of Geotechnical Engineering, Vol. 112, No. 8, August.
- Robertson, P., & R. Campanella (1989). "Guidelines for Geotechnical Design Using CPT and CPTU", Department of Civil Engineering, University of British Columbia, Soil Mechanics Series No. 120.
- Robertson, P.K. (1990). "Seismic Cone Penetration Testing for Evaluating Liquefaction Potential", Proceedings, Symposium on Recent Advances in Earthquake Design Using Laboratory and In Situ Tests, ConeTec Investigations Lt., Burnaby, BC, February 5.
- Schnabel, Per B., John Lysmer, and H. Bolton Seed, (1972). "SHAKE: A Computer Program for Earthquake Response Analysis of Horizontally Layered Sites", Report No. EERC 72-12, College of Engineering -- University of California at Berkeley, December.
- Seed, H., and Idriss, I. (1970). "Soil Moduli and Damping Factors for Dynamic Response Analyses", Earthquake Engineering Research Center Report, No. EERC 70-10, December, College of Engineering, University of California.

- Seed, H.B. (1979). "Considerations in the Earthquake-Resistant Design of Earth and Rockfill Dams", 19th Rankine Lecture, *Geotechnique*, Vol. 29, No. 3, pp.215-263.
- Seed, H.B., I.M. Idriss, & I. Arango (1983a). "Evaluation of Liquefaction Potential Using Field Performance Data", *Journal of Geotechnical Engineering Division, ASCE*, Vol. 109, GT3, pp. 458-482.
- Seed, H.B. (1983b). "Earthquake-Resistant Design of Earth Dams", in *Seismic Design of Embankments and Caverns*, Terry R. Howard, Editor, ASCE, pp. 41-64.
- Seed, H.B., Tokimatsu, K., Harder, L., and Chung, R. (1984). "The Influence of SPT Procedures in Soil Liquefaction Resistance Evaluations", Report No. UCB/EERC-84/15, College of Engineering, University of California, Berkeley, California.
- Seed, H.B. (1987). "Design Problems in Soil Liquefaction", *Journal of Geotechnical Engineering, ASCE*, Vol. 113, No. 7, August, pp. 827-845.
- Seed, H.B., R.B. Seed, L.F. Harder and H.L. Jong (1988). "Re-evaluation of the Slide in the Lower San Fernando Dam in the Earthquake of February 9, 1971", Report No. UCB/EERC-88/04, University of California, Berkeley, April.
- Seed, H.B., & L.F. Harder Jr. (1990). "SPT-Based Analysis of Cyclic Pore Pressure Generation and Undrained Residual Strength", *Proceedings, H. Bolton Seed Memorial Symposium, J. Michael Duncan (ed.)*, Vol. 2, May, pp.351-376.
- Sego, D.C., P.K. Robertson, S. Sasitharan, B.L. Kilpatrick, and V.S. Pillai (1994). "Ground Freezing and Sampling of Foundation Soils at Duncan Dam", 46th Annual Canadian Geotechnical Conference Saskatoon, Saskatchewan, September 27-29, 1993, *Canadian Geotechnical Journal* Vol.31, pp.939-950.
- Senneset, K., and N. Janbu (1981). "Shear Strength Parameters Obtained from Static Cone Penetration Tests", ASTM STP 883, Symposium, San Diego.
- Stark, T.D., and G. Mesri (1992). "Undrained Shear Strength of Liquefied Sands for Stability Analysis", *Journal of Geotechnical Engineering, ASCE*, Vol. 118, No.11, pp.1727-1747.

Supplement to the National Building Code of Canada (1990). National Research Council of Canada.

Sy, Alex, Paul W. Henderson, Robert C. Lo, David Y. Siu, W.D. Liam Finn, and Arthur C. Heidebrecht (1991). "Ground Motion Response for Fraser Delta, British Columbia", Fourth International Conference on Seismic Zonation, Stanford California, August 26-29.

Tokimatsu, K., H.B. Seed (1987). "Evaluation of Settlements in Sands Due to Earthquake Shaking", Journal of Geotechnical Engineering, ASCE, Vol. 113, No.8, pp. 861-878.

Vaid, Y.P., and J.C. Chern (1985). "Cyclic and Monotonic Undrained Response of Saturated Sands. ASCE National Convention, Session -- Advances in the Art of Testing Soils Under Cyclic Loading", Detroit, October 21-25, pp. 120-147.

Vaid, Y.P., E.K.F. Chung and R.H. Kuerbis (1989). "Stress Path and Steady State", Soil Mechanics Series No. 128, Dept. of Civil Engineering, University of British Columbia, Vancouver, BC, March.

Wang, W. (1979). "Some Findings in Soil Liquefaction", Water Conservancy and Hydroelectric Power Scientific Research Institute, Beijing, China, August.

Youd, T.L., and S.F. Bartlett (1988). "U.S. Case Histories of Liquefaction Induced Ground Displacement", Proceedings, First Japan-U.S. Workshop on Liquefaction, Large Ground Deformation and their Effects on Lifeline Facilities, pp. 22-31.

Youd, T.L., and D.M. Perkins (1987). "Mapping of Liquefaction Severity Index -- LSI", Journal of Geotechnical Engineering, Vol. 113, No. 11, pp. 1374-1392.

APPENDIX A

NUMERICAL METHOD DISPLACEMENTS

APPENDIX A.1 -- Additional SOILSTRESS Analyses

A.1.1 Displacements at Offshore Locations -- Case #2: No Sediment Loading

The Case #2 analyses are similar to the Case #1 analyses (refer to section 8.3.2.1.2); the only difference is that there is no sediment loading on top of the tunnel. The three load cases are compared in section 9.4.1.1. This case was analyzed to determine what effect the removal of sediment would have on the displacements.

Location	Corner	HORIZONTAL Displacement (meters)	2-Dimension VERTICAL Displacement (centimeters)	TOTAL (3-Dimension) VERTICAL Displacement (centimeters)
#2	C1	0.97	-22.1	-18.2
	C3	0.96	-23.9	-20.0
#3	C1	0.19	-13.4	-14.6
	C3	0.19	-14.3	-15.5
#4	C1	0.17	-11.9	-17.9
	C3	0.16	-13.0	-19.0

Table A.1.1 - Displacements at Offshore Locations -- No Sediment Loading

Figures A.1.1 to A.1.3 show the displacement patterns for the Case #2 analyses at locations #2, #3, and #4. The dashed lines represent the initial state, and the solid lines show the post-earthquake position of the nodes. The displacements are magnified by a factor of two.

The displacement estimates for the Case #2 analyses are summarized in table A.1.1. As described earlier, the 'total vertical displacement' (in the final column of the table) represents the full 3-dimensional effect by incorporating the undrained vertical distortion estimates from the longitudinal analyses.

The displacement patterns in the Case #2 analyses are very similar to the corresponding ones in the Case #1 analyses.

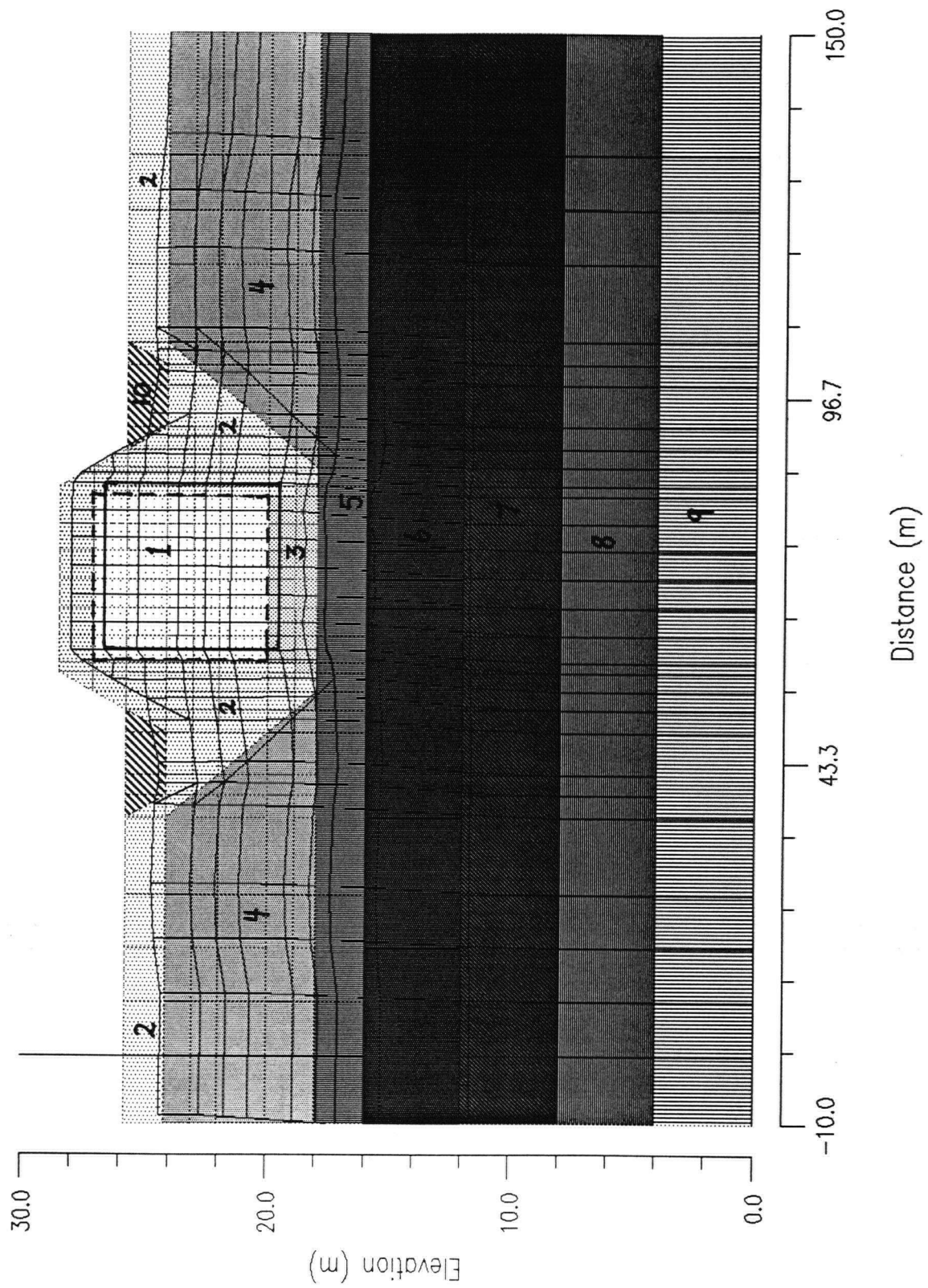


Figure A.1.1 - Displacement Pattern for Case #2 -- Location #2

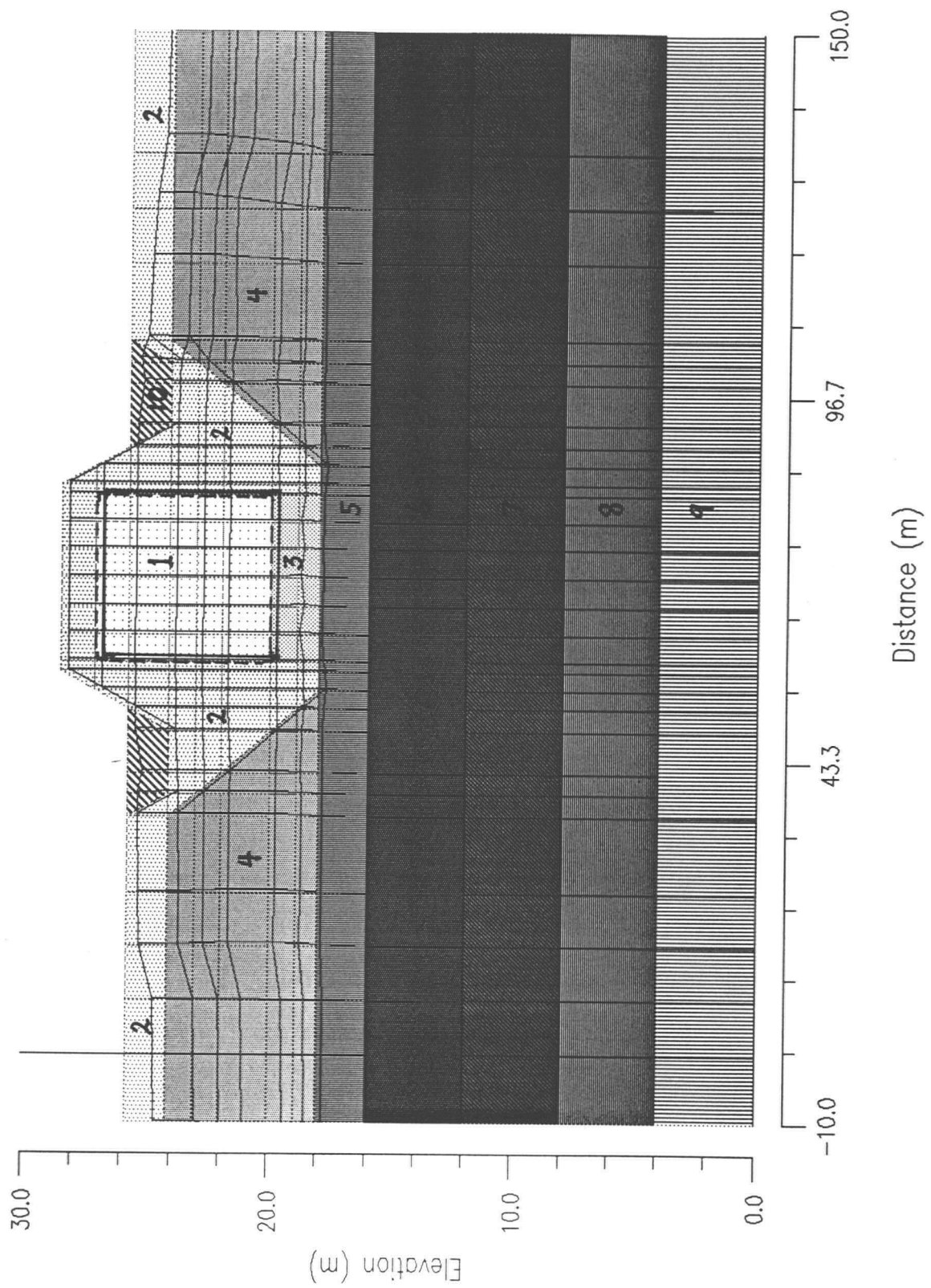


Figure A.1.2 - Displacement Pattern for Case #2 -- Location #3

A.1.2 Case #3: Displacements with Increased Sediment Loads

These analyses were done only at location #2. The Case #3 analyses were done to determine the effects of various sediment loads. As described earlier, Case #1 applied 2 meters of sediment loading on top of the tunnel, and Case #2 analyses were done using no sediment.

Thickness of Sediment	Corner	HORIZONTAL Displacement (meters)	2-Dimension VERTICAL Displacement (centimeters)	TOTAL (3-Dimension) VERTICAL Displacement (centimeters)
4 meters	C1	1.12	-30.7	-26.8
	C3	1.13	-27.8	-23.9
6 meters	C1	1.11	-32.0	-28.1
	C3	1.12	-28.0	-24.1

Table A.1.2 - Displacements at Location #2 -- Increased Sediment Loading

In this analysis, the sediment loading has been increased. A mass equivalent to 4 meters (Case #3a) of sediment was first incorporated in the finite element mesh, and then a sediment load case of 6 meters (Case #3b) was analyzed. Refer to section 9.4.1.1 for a discussion of the results using the various sediment loads.

Figures A.1.4 and A.1.5 show the displacement patterns for the Case #3 analyses at locations #2. The dashed lines represent the initial state, and the solid lines show the post-earthquake position of the nodes. The displacements are magnified by a factor of two.

Table A.1.2 summarizes the results of the analyses. Comparing the results in table 8.12 (i.e., Case #1) and table A.1.2, the horizontal displacements increase by approximately 20% (from 0.96 m to 1.12 m, at corner #1); the vertical displacements increase by 16% at corner #1, and at corner #3, they increase by 6%.

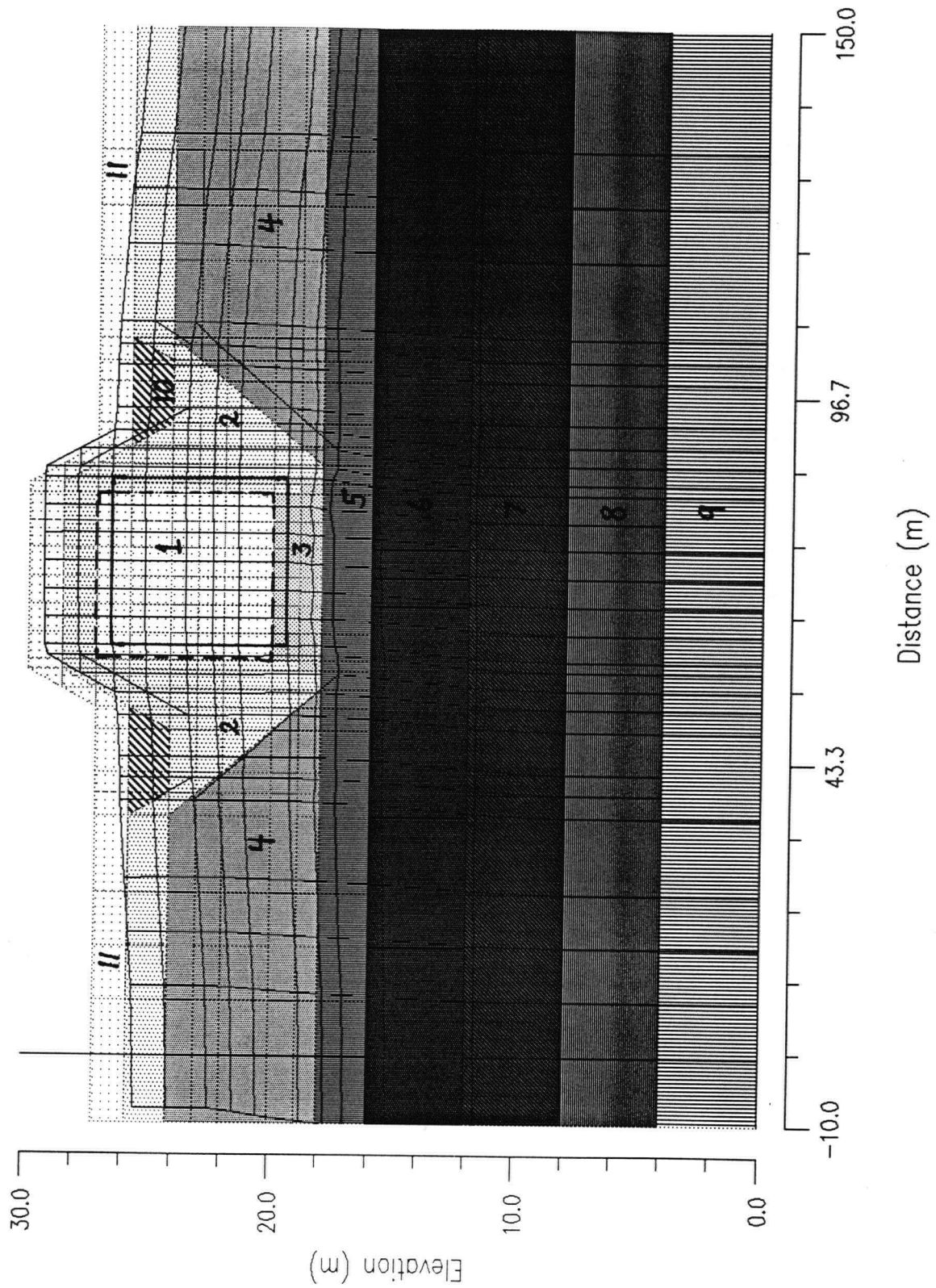


Figure A.1.4 - Displacement Pattern for Case #3a (4 meters of Sediment Loading)

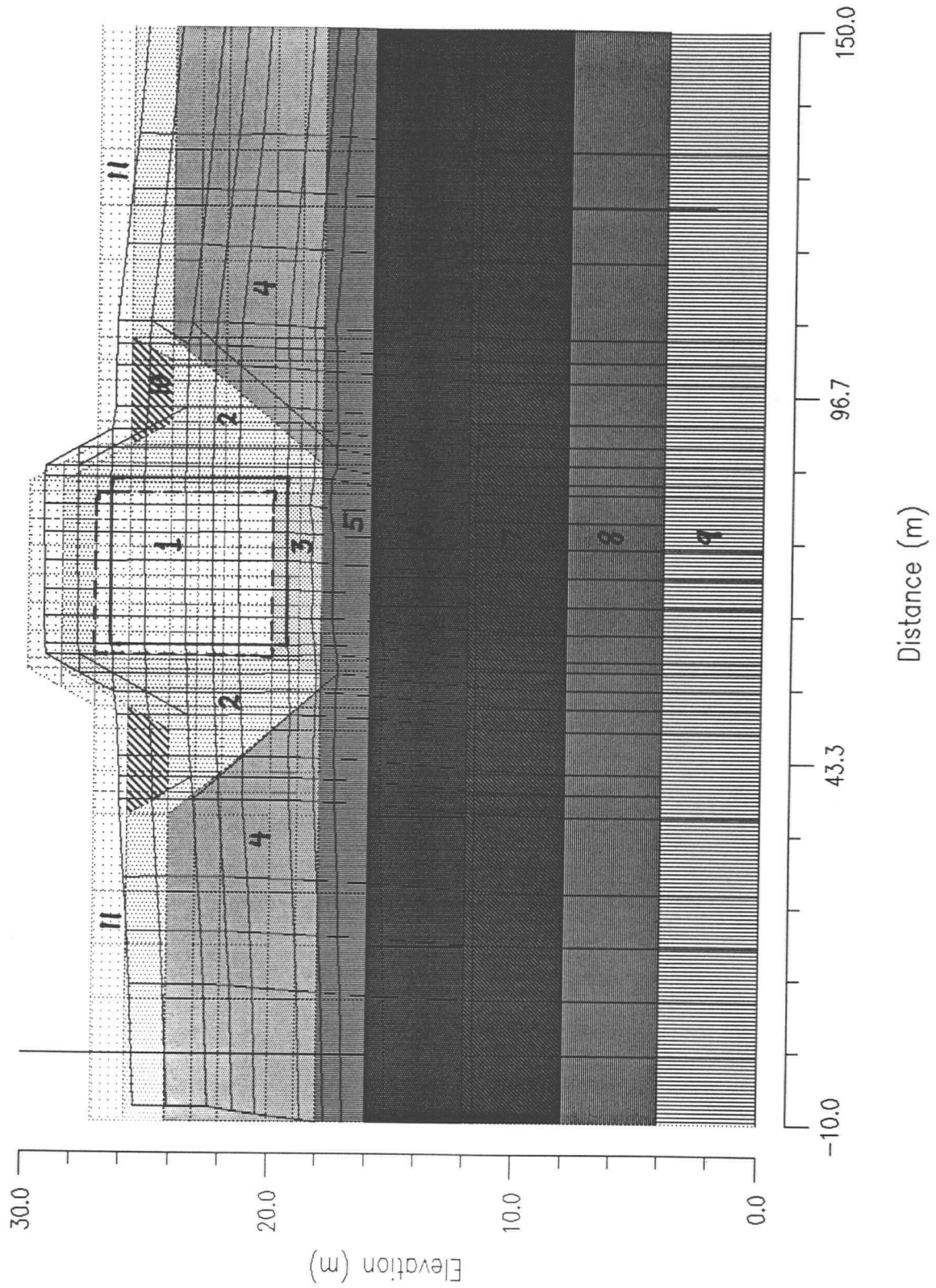


Figure A.1.5 - Displacement Pattern for Case #3b (6 meters of Sediment Loading)

A.1.3 Case #4: Displacements with Increased Ground Velocity

In this comparison analysis, the maximum velocity to compute kinetic inertia has been increased by 27% (from 0.30 m/s to 0.38 m/s) at location #2. Soil input parameters are summarized in tables 8.8 and 8.11. (The analysis is discussed in section 9.4).

Location	Corner	HORIZONTAL Displacement (meters)	2-Dimension VERTICAL Displacement (centimeters)	TOTAL (3-Dimension) VERTICAL Displacement (centimeters)
#2	C1	1.15	-26.4	-22.5
	C3	1.15	-26.7	-22.8

Table A.1.3 - Displacements at Location #2 -- Increased Ground Velocity

Table A.1.3 summarizes the case #4 results (of the increased velocity analyses at location #2). Comparing the results in table 8.12 (at location #2) and table A.1.3, the horizontal displacements increase by approximately 20%, and the vertical displacement estimates are very similar in both cases. Figure A.1.6 shows the displacement pattern for the Case #4 analysis at locations #2. The dashed lines represent the initial state, and the solid lines show the post-earthquake position of the nodes. The displacements are magnified by a factor of two.

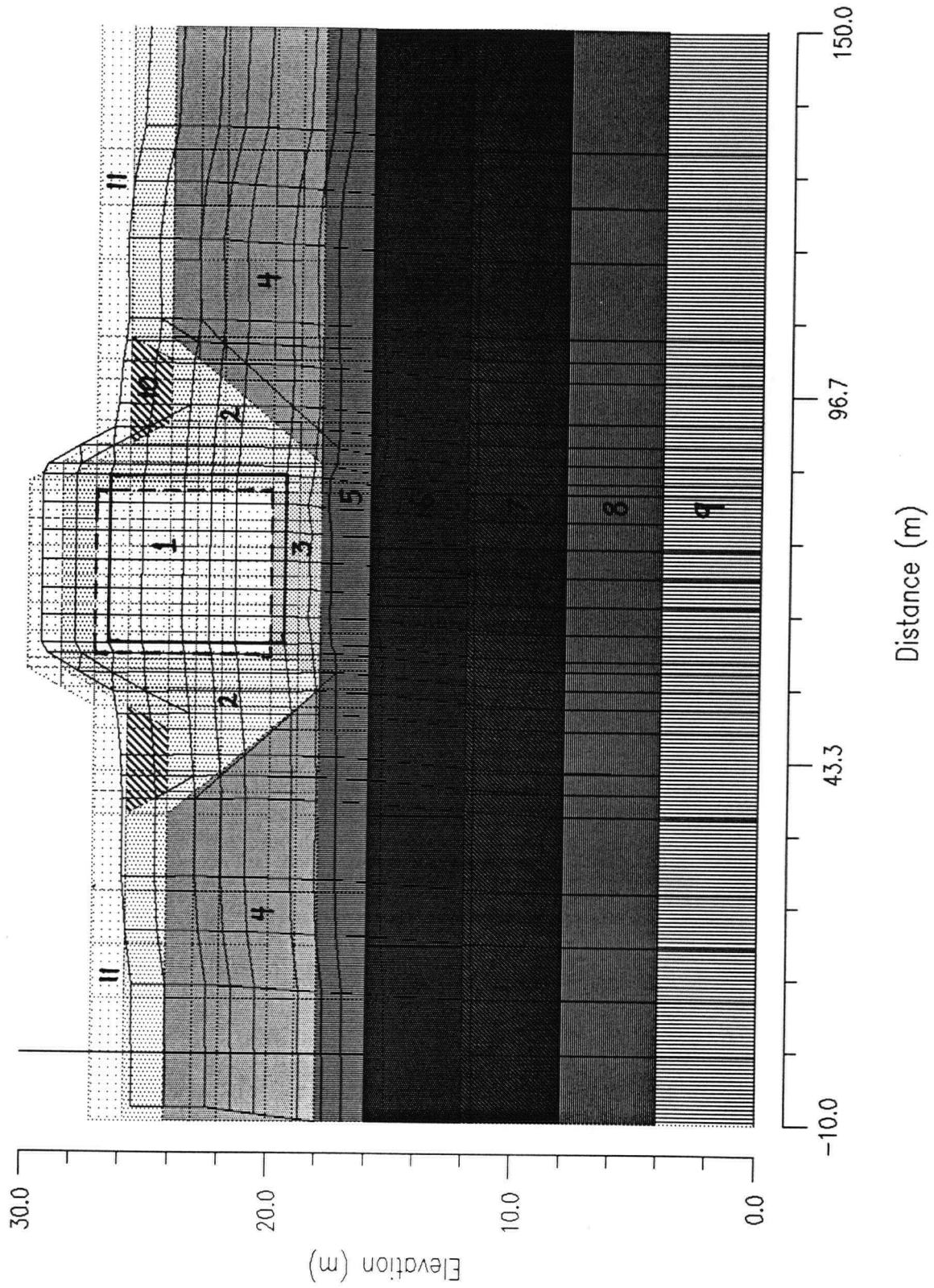


Figure A.1.6 - Displacement Pattern for Case #4 (Increased Ground Velocity)

Appendix A.1.4 -- Full-Section Longitudinal Displacements

Refer to section 4.4.3.2 for a description of the procedures used to do the SOILSTRESS analyses. Displacements in the plane parallel to the axis of the

Longitudinal Section Analysis									
Material Number	Soil Type	K_g	n	K_b	m	R_f	ϕ (deg)	$\Delta\phi$ (deg)	C (kPa)
1	Concrete	50000 (50000)	0.5	200000	0.25	0.5	50	0	1000
2	Liquefied Silt	444 (1.1)	0.5 (0)	2000	0.25	0.7 (0)	34 (0)	0	30
3	Liquefied Sand Fill	181 (0.1)	0.5 (0)	2000	0.25	0.9 (0)	32 (0)	0	0
4	Liquefied Sand	505 (1.8)	0.5 (0)	2000	0.25	0.8 (0)	35 (0)	0	0
5	Silt	444 (222)	0.5	2000	0.25	0.6	34	0	40
6	Liquefied Sand	505 (0.4)	0.5 (0)	2000	0.25	0.8 (0)	33 (0)	0	0
7	Partially Liquefied Sand	955 (100)	0.5	2000	0.25	0.7	37	2	0
8	Partially Liquefied Sand	570 (100)	0.5	2000	0.25	0.7	31	0	0
9	Silt	747 (374)	0.5	2000	0.25	0.6	34	0	40
10	Liquefied Sand	200 (0.5)	0.5 (0)	2000	0.25	0.8 (0)	33 (0)	0	0
11	Sandy Sediment	200	0.5	2000	0.25	0.6	33	0	0
12	Dense Sand Lens	1137 (568)	0.5	2000	0.25	0.6	37	7	0
13	Liquefied Sand	570 (2.2)	0.5 (0)	2000	0.25	0.8 (0)	35 (0)	0	0

Table A.1.4 - SOILSTRESS Pre- and Post-liquefaction Inputs For Longitudinal Section Analyses at All Locations

Notes: - values in parentheses indicate post-liquefaction estimates

tunnel ('longitudinal-direction') are summarized in this section. Residual strength and limit strain estimates are presented in section 6.3. Figure 6.1 shows the estimated soil profile along the length of the tunnel.

The material numbering scheme for the longitudinal section is summarized in figure 6.14. Figures A.1.7 and A.1.8 show the displacement pattern and displacement vector graphics for the longitudinal section SOILSTRESS analyses. The displacement vector images has been provided to aid in interpreting the displacement patterns along the full length of the tunnel.

Pre- and post-earthquake inputs for the SOILSTRESS analyses are summarized in table A.1.4. For post-earthquake conditions, a 50% reduction in stiffness was applied to all non-liquefied materials due to the severity of shaking (i.e., $v_{\max} = 0.3$ m/s). Residual strength and limit strain estimates that were applied in the transverse-direction analyses were also applied in the longitudinal analyses. (Section 6.3 summarizes the post-liquefaction parameter magnitudes).

Table A.1.5 summarizes the displacements at the base of the concrete section in the vicinity of each of the five locations at which the transverse-section analyses were done. The 'pre-consolidation vertical displacement' is the movement due to undrained distortion, and the '2-Dimension vertical displacement' is the total predicted vertical movement in which settlement due to dissipation of excess pore-pressures is also included. It should be noted that the Tokimatsu/Seed method (1987) was applied (refer to section 4.4.2.4) to determine the volumetric strain inputs for the settlement calculations in

Location	HORIZONTAL Displacement (meters)	Pre - Consolidation Vertical Displacement (centimeters)	2-Dimension VERTICAL Displacement (centimeters)	TOTAL (3-Dimension) VERTICAL Displacement (centimeters)
#8	1.20	2.2	-30.4	-22.5
#4	1.20	-6.0	-19.7	-22.0
#3	1.20	-1.2	-12.5	-14.2
#2	1.19	3.9	-31.1	-22.8
#7	1.21	-0.6	-23.2	-24.0

Table A.1.5 - Longitudinal-direction Analysis Displacement Predictions

all of the SOILSTRESS analyses. The 'total vertical displacement' (in the final column of each displacement summary table) represents the full 3-dimensional effect by incorporating the undrained vertical distortion estimates from the onshore and offshore (i.e., Case #1) transverse-section analyses. (Refer to sections 8.3.2.1.1 and 8.3.2.1.2 for transverse-section pre-consolidation estimates).

Figures A.1.7 and A.1.8 show the displacement pattern and displacement vector graphics for the longitudinal-direction analyses. The dashed lines represent the initial state, and the solid lines show the post-earthquake position of the nodes. The displacements are magnified by a factor of three.

Figure 6.1 (in section 6.2.) shows the zones of liquefaction along the length of the tunnel, and the distances between the analyzed locations. As table A.1.5 shows, the horizontal movements are predicted to be uniform over the length of the tunnel. The phenomenon is discussed in section 9.4.

The 3-dimension vertical displacement predictions are very similar along the length of the tunnel. As anticipated, location #3 shows the lowest vertical displacement, since the depth to liquefaction is least in the central segment of the tunnel.

The displacement vectors (figure A.1.8) shows the uneven effect of the transitions from liquefied to non-liquefied soils. For instance, the unit #7 sands were not predicted to liquefy; consequently, the liquefied unit #6 and #2 soils experience greater distortion as the horizontal velocity impulse is applied.

As figure A.1.7 shows, there is a noticeable outward movement of the elements at the left and right boundaries. This phenomenon is discussed in section 9.4.

The vertical displacement estimates at the five locations show how much differential movement occurs along the length of the tunnel. Differential movements are discussed in section 9.4.1.2.

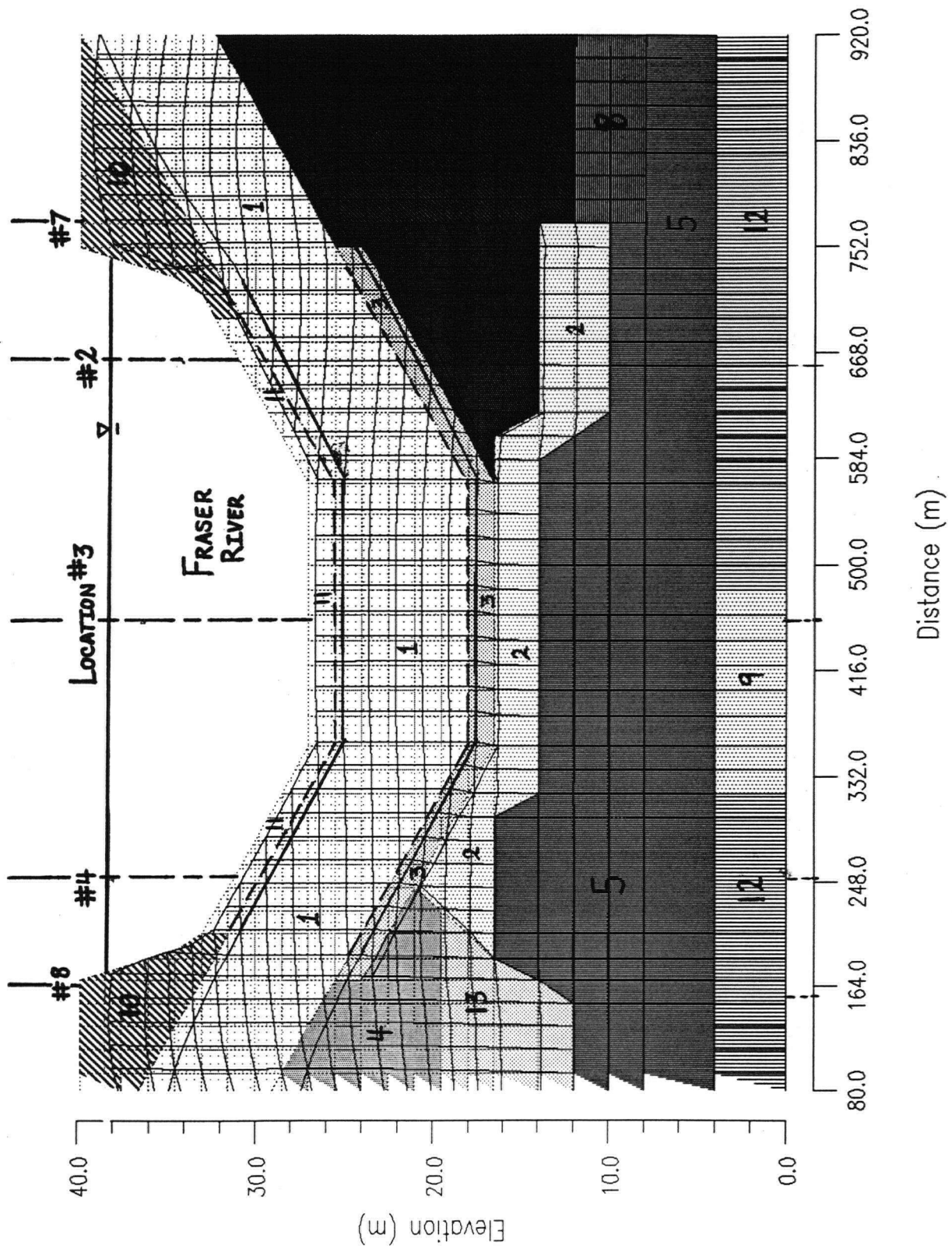


Figure A.1.7 - Displacement Pattern -- Parallel to the Axis of the Tunnel

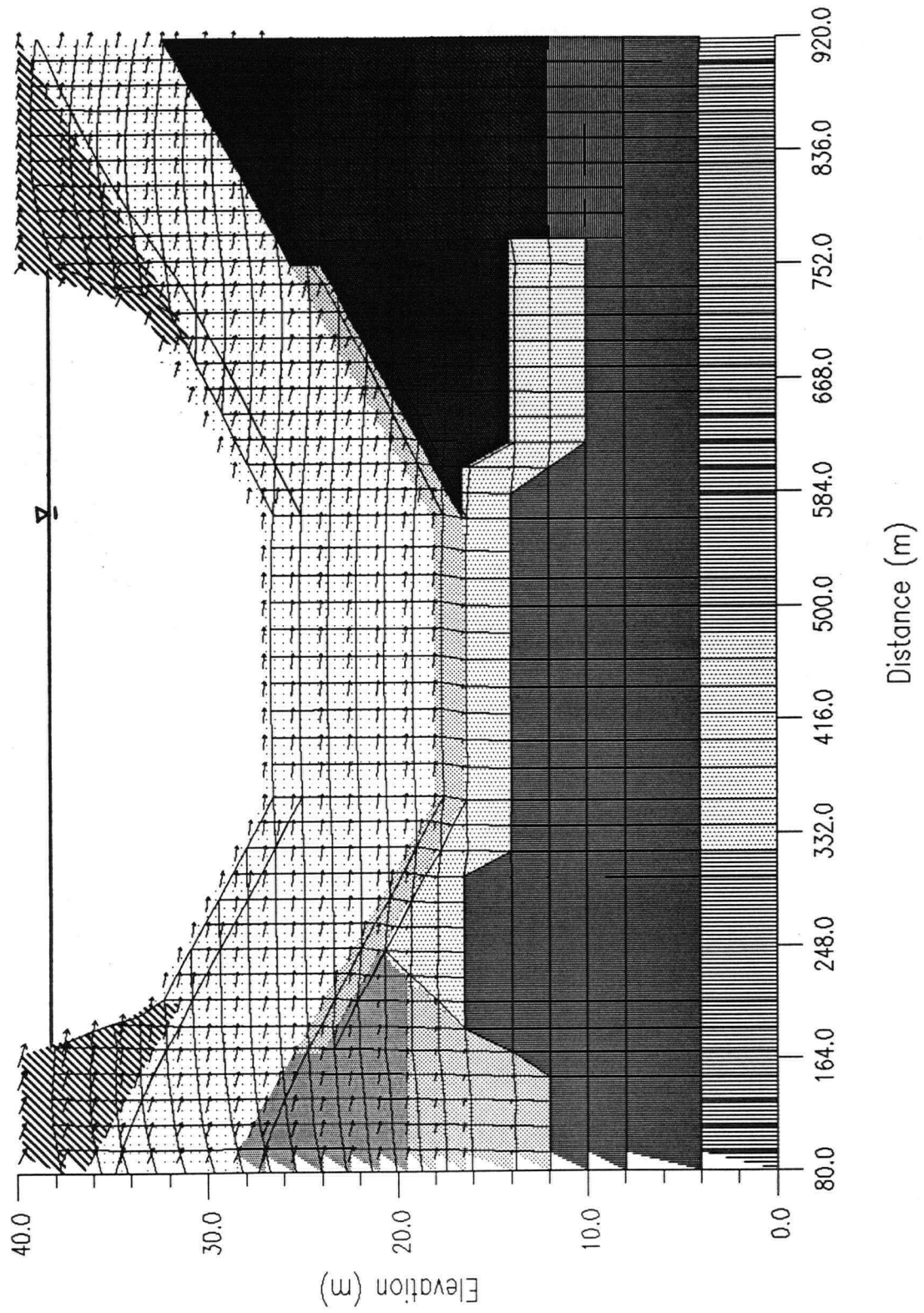


Figure A.1.8 - Displacement Vectors -- Parallel to the Axis of the Tunnel

APPENDIX A.2 -- Extended Newmark Model

Newmark's simplified (i.e., rigid-plastic single-degree-of-freedom) model is that of a block of mass M resting on an inclined plane of slope α . The mass is subjected to a velocity pulse (V) relative to the base (refer to figure A.2.1). The mass (block) will commence sliding along the plane when the base acceleration induces a driving force which together with the static driving force is equal to the sliding resistance of the block. The base acceleration at which movement is initiated is called the 'yield acceleration' or 'resistance coefficient' (N). The resistance coefficient (N) can be determined through limit equilibrium analysis. The product of the coefficient and the weight of the sliding mass is used to estimate the resistance to movement. Any prescribed time-history of acceleration can be applied at the base and the resulting

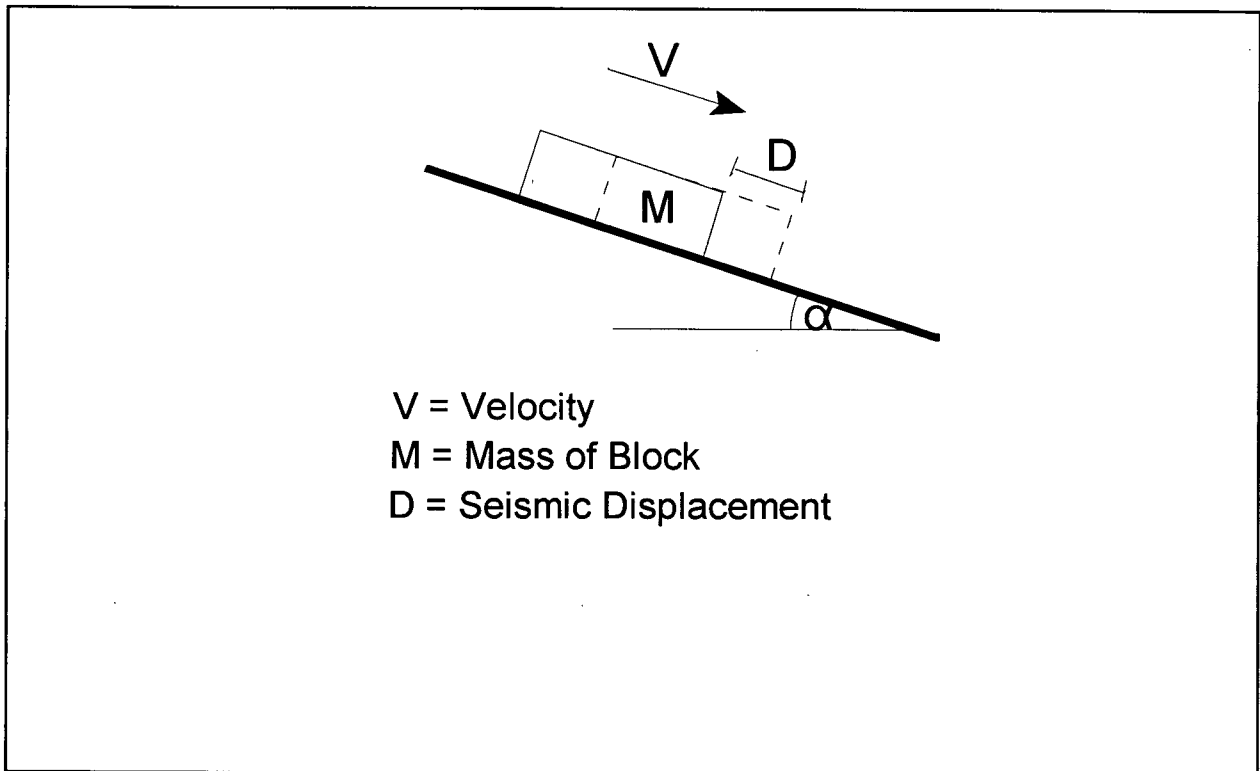


Figure A.2.1 - Block on an Inclined Plane Subjected to a Velocity Pulse -- Newmark Model
(After Newmark, 1965)

displacements can be computed by numerical integration. Alternatively, Newmark found that the maximum displacement (d) at the end of the shaking period could be estimated from simple formulae by considering the earthquake motion to be estimated by a chosen

number of pulses. The resulting displacement is given by:

$$d = \frac{6V^2}{2gN} \quad (\text{equation A.2.1})$$

where: d -- maximum displacement

V -- velocity pulse (taken to be equal to the peak ground velocity)

N -- yield acceleration (as a fraction of 'g') required to initiate yield and sliding

g -- acceleration of gravity

Newmark found agreement with the integrated records when six pulses of velocity (V) were considered and the ratio $N/A < 0.13$ (where 'A' is the peak ground acceleration). (The coefficient '6' in equation [A.2.1] reflects the six pulses). This ratio of N/A reflects the conditions in most practical cases. The number of pulses (in equation [A.2.1]) depends on the N/A ratio.

Underlying the Newmark procedure is the assumption that the stress-strain behaviour of soil is rigid-plastic. This implies that strains (deformations) will not occur until inertia forces exceed the failure loads. Consequently, displacements attributed to strain-softening are not accounted for. The Extended Newmark method (Byrne, 1990), on the other hand, extends the Newmark work-energy model to a general formulation and accounts for Newmark's discrepancy.

The essential difference between the Newmark (1965) and Byrne (1990) methods is in the way the post-liquefaction undrained shear stress-strain response of the soil is modelled. The characteristic post-liquefaction stress-strain curve is shown in figure A.2.2. The figure illustrates that if a shear stress is applied to a liquefied soil, it will undergo large deformations until the dilation of the soil skeleton results in a gradual gain in stiffness and strength. The key parameters that control the post liquefaction stress-strain response are the residual shear strength (S_r) and the limiting shear strain (γ_{lim}). (Refer to section 4.3 for a discussion of these parameters). It has been shown that the shear strains required to trigger liquefaction are generally small (approximately 0.1% to 1%) when compared with the ensuing strains caused by the earthquake and gravity loads acting on the liquefied soil; consequently Byrne (1990) proposed that the triggering strains be neglected. Post-liquefaction strains depend on the post-cyclic stress-strain characteristic behaviour of the soil and on the geometry of the structure (i.e., static bias). Consequently, liquefaction induced displacements can be adequately predicted by acknowledging both the gravity loads and earthquake-induced inertia forces, in conjunction with the appropriate post-liquefaction stress-strain relations.

The Extended Newmark model follows the work-energy theorem that states that the work done by the internal forces (W_{INT}) minus the work done by the external forces (W_{EXT}) must be equal to the change in kinetic energy of the system:

$$W_{INT} - W_{EXT} = \frac{1}{2}M(V^2 - V_f^2) = \frac{1}{2}MV^2 \quad (\text{equation A.2.2})$$

where: $\frac{1}{2}MV^2$ -- change in kinetic energy of the system
 V -- specified initial velocity of the system
 V_f -- final resting velocity (equal to zero)
 M -- mass of the system

Displacements caused by the gravity forces acting on the softened soil are depicted between points B and D in figure A.2.2. Upon liquefaction, the pore-pressure rise causes the stress in the soil to drop from its static value at point A to point B. As the soil dilates

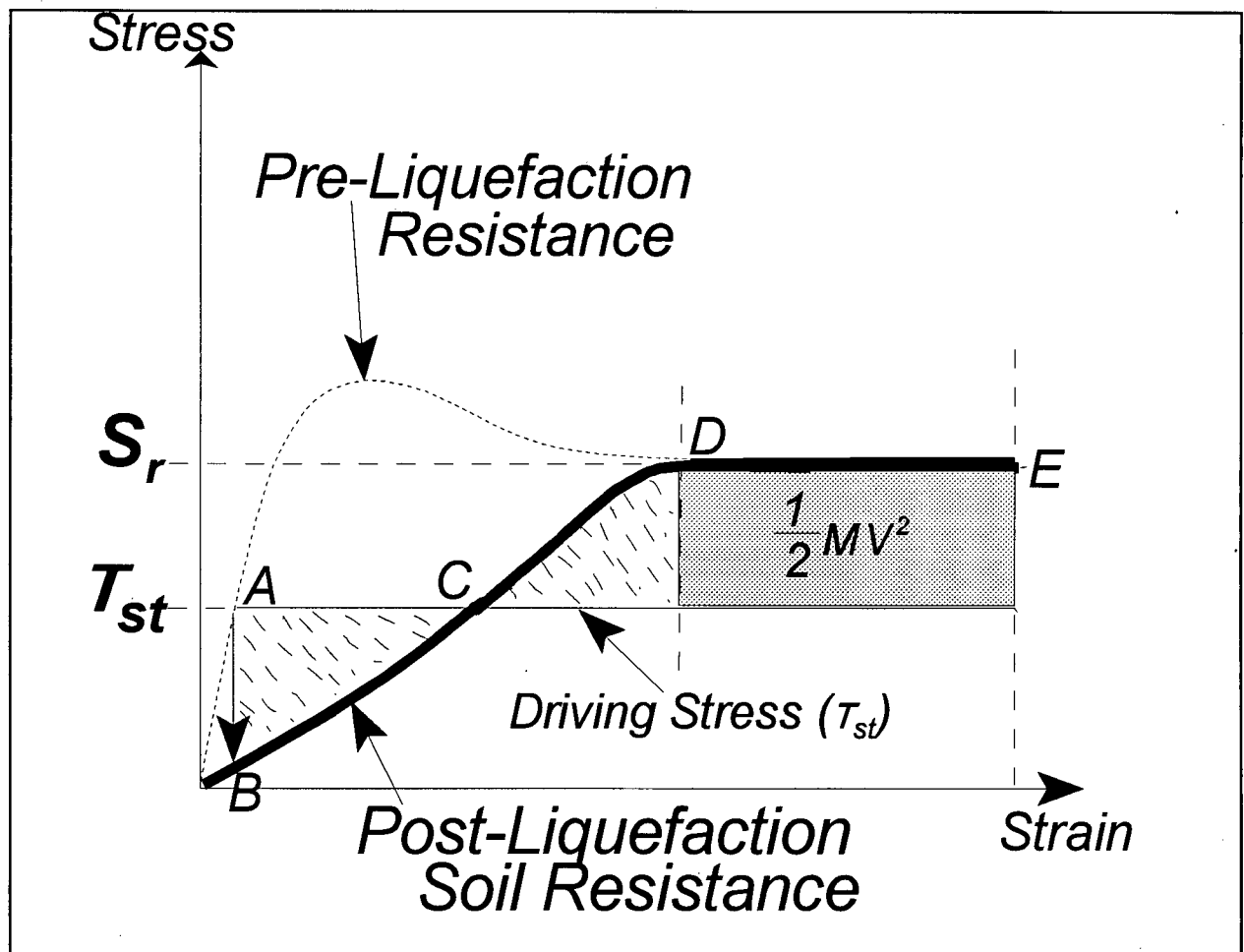


Figure A.2.2 - Work-energy principle -- Extended Newmark (Byrne, 1990)

and strains increase, it begins to regain stiffness to balance out the driving force (gravity loading). As depicted in figure A.2.1, the driving force from the static stresses remains constant. Because the soil's resistance had decreased upon the triggering of liquefaction (i.e., point A to B), the constant static driving force causes the system to accelerate as it deforms. When the strain reaches point C, the material has hardened sufficiently to counter the original driving force; however, the velocity developed by the system between points B and C causes the stress to increase until the resistance reaches the residual value (point D). (It should be noted, that if the driving stress exceeds the residual strength (S_r) of the soil, a flow slide will occur; refer to section 4.3 for a discussion of post-liquefaction stability). At point D, the net work, ($W_{INT} - W_{EXT}$) is equal to zero as depicted by the equal area portions ABC and CDE. The displacements between points A and D represent the strains that occur due to the static (gravity and boundary) loads acting on the softened soil. The earthquake-induced initial velocity (V_0) (developed at the time liquefaction is triggered) also contributes to the movement; it is represented by the movement from point D to E.

As mentioned earlier, the Newmark (1965) method is overly simplified. Newmark does not account for the displacements from point A to D (figure A.2.2). In cases where liquefaction occurs, this discrepancy results in a significant underestimation of displacements. Strains of approximately 20-50% are usually required to mobilize the residual strength (S_r); consequently, if Newmark's method is used, these strains aren't accounted for in the overall displacements.

For verification purposes, Newmark's (1965) method is now derived in terms of the work-energy principles. As illustrated in figure A.2.3, the external force that does work is the gravity (static) driving force ($= Mg \cdot \sin \alpha$), and is taken to be constant with displacement. Therefore, the work done is represented by the area beneath the driving force line. The work done by the internal forces, based on Newmark's assumption of rigid-plastic stress-strain behaviour of soil, is shown by the total area beneath the soil resistance line. As the figure shows, this internal force (resistance) is assumed to be constant with displacement. The net work done must equal the loss in kinetic energy ($1/2 MV^2$), and is illustrated as the difference between the two areas (i.e., the shaded area in figure A.2.3). The driving force is made up of both the static (gravity load) and earthquake pulse driving components. The static driving force is the self-weight vector component ($= Mg \cdot \sin \alpha$) driving the block down the inclined surface. External work (W_{EXT}) done by the gravity force, therefore, is approximated as:

$$W_{EXT} = (Mg \sin \alpha) \cdot d \quad (\text{equation A.2.3})$$

Opposing the static driving force is the residual strength (S_r) of the liquefied

layer that provides the sliding (internal) resistance; therefore, the work done by the residual shear resistance of the soil is approximated as:

$$W_{INT} = (S_r \cdot L \cdot b) \cdot d \quad (\text{equation A.2.4})$$

where S_r is the residual shear strength of the soil, and 'L' and 'b' are the length and width of the slide block, respectively. Consequently, equation [A.2.4] reduces to:

$$d \cdot (S_r \cdot L \cdot b - Mg \sin \alpha) = \frac{1}{2} MV^2 \quad (\text{equation A.2.5})$$

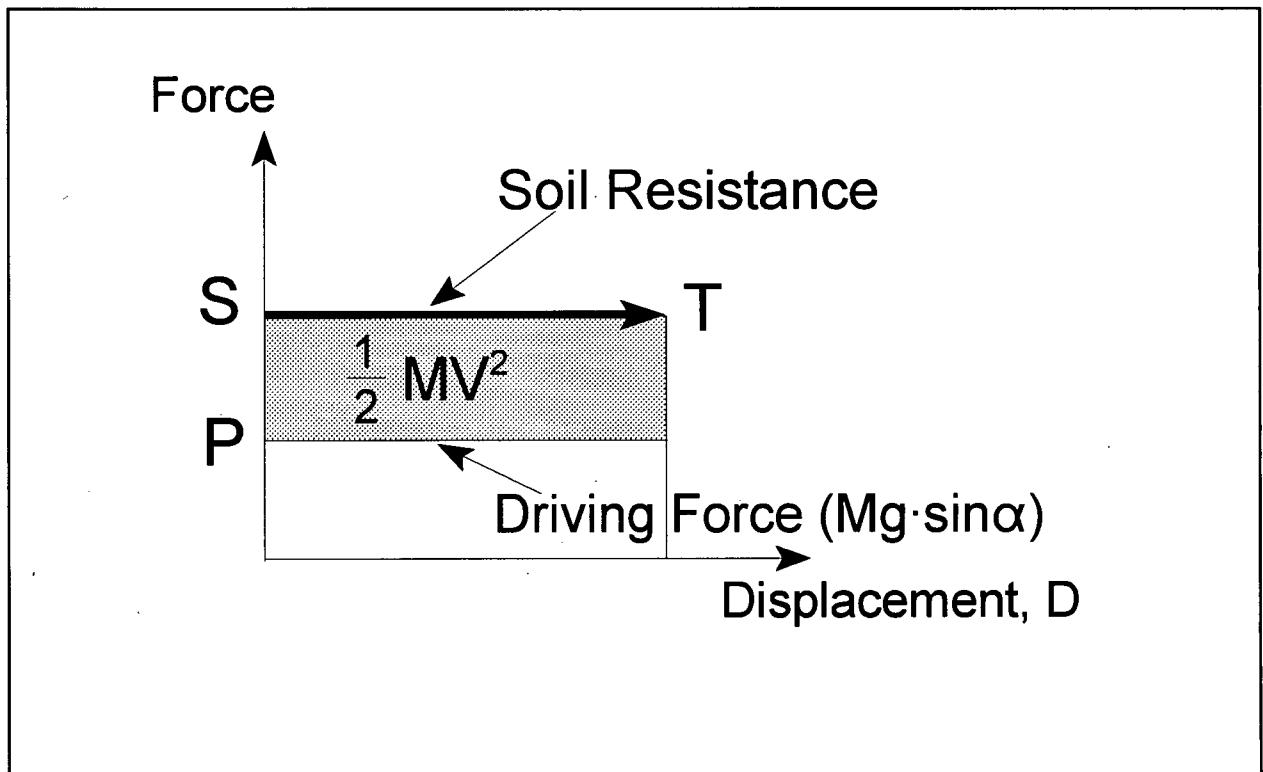


Figure A.2.3 - Work-energy (Rigid-plastic Stress-strain Behaviour) -- Newmark Method

Solving for the maximum displacement (d):

$$d = \frac{V^2}{2gN} \quad (\text{equation A.2.6})$$

where the yield acceleration (N) is given by:

$$N = \frac{Sr \cdot L \cdot b - Mg \cdot \sin \alpha}{Mg} \quad (\text{equation A.2.7})$$

Equation [A.2.6] represents a single velocity pulse; when six pulses are considered, a solution identical to Newmark's (equation [A.2.1]) is obtained. Therefore, if rigid-plastic stress-strain behaviour is assumed, Newmark's model is obtained in terms of the work-energy theorem.

It should be noted that, though Newmark simulated the effect of an earthquake by applying as many as six velocity pulses (depending upon the N/A ratio), Byrne (1990) considered only one pulse when dealing with liquefied soil. The displacements due to pulses prior to liquefaction will be, in general, small (i.e., strains of 0.1 to 1%) when compared to those which occur upon liquefaction; once liquefaction is triggered, it is assumed that no further major pulses would occur (Byrne, 1992).

APPENDIX A.3 -- Extended Newmark Model -- Integration with SOILSTRESS

A.3.1 Extended Newmark: Multi-degree-of-freedom Finite Element Analyses: SOILSTRESS

For the multi-degree-of-freedom system, the SOILSTRESS finite element approach computes displacements from the solution of:

$$[K]\{\delta\} = \{F + \Delta F\} \quad (\text{equation A.3.1})$$

where: $[K]$ -- global stiffness matrix of the system
 $\{\delta\}$ -- vector of nodal displacements
 $\{F\}$ -- static load (i.e., gravity and boundary load) vector acting on the system
 $\{\Delta F\}$ -- additional load applied to satisfy the energy balance

If $\{\Delta F\}$ equals zero, then for a single-degree-of-freedom analysis, a displacement corresponding to point C in figure A.2.2 would be predicted; therefore, an additional force is required to balance the energy and predict a displacement corresponding to point D or E. The additional force is applied using a seismic coefficient (k):

$$\{\Delta F\} = \{k \cdot w\} \quad (\text{equation A.3.2})$$

where: $\{\Delta F\}$ -- additional force vector (to satisfy the energy balance)
 k -- pseudo seismic coefficient
 w -- weight of soil element

It should be noted that 'k' is not related to the peak ground acceleration. The seismic coefficient is applied iteratively until the system energy is balanced according to equation[A.2.2]. For the multi-degree-of-freedom system, W_{INT} represents the work done by the element stresses, and W_{EXT} represents the work done by the static load vector:

$$W_{EXT} = \{F\} \cdot \{\Delta\}^T \quad (\text{equation A.3.3})$$

The seismic coefficient acts to adjust $\{\Delta F\}$ until displacements $\{\delta\}$ are obtained that balance the system energy. It should be noted that this additional force is not included as part of the external work (W_{EXT}) done by the static forces.

In developing the multi-degree-of-freedom system, the components of the Modified Newmark method analysis are applied to the elements. The internal work (W_{INT}) is represented by the work done by all the element stresses, the external work (W_{EXT}) is the work done by the static load vector ($\{F\}\{\Delta\}^T$), and the change in kinetic energy of the system is summed element by element:

$$\frac{1}{2}MV_{\max}^2 = \frac{1}{2} \sum [M_e \cdot V_{\max}^2] \quad e = 1, ne \quad (\text{equation A.3.4})$$

'e' represents a soil element and is defined by the limits $e=1,n$, where 'n' is the total number of elements used to define the mesh.

Hyperbolic stress-strain models are used to represent the shear modulus (G_s) and bulk modulus (B_s) in the SOILSTRESS program code. The soil is treated as equivalent isotropic elastic, and secant estimations are used to approximate the variations of the shear and bulk moduli with stress level as follows:

$$G_s = k_g \cdot P_a \cdot \left(\frac{\sigma'_m}{P_a}\right)^n \cdot \left(1 - \frac{T \cdot R_f}{T_f}\right) \quad (\text{equation A.3.5})$$

$$B_s = k_b \cdot P_a \cdot \left(\frac{\sigma'_m}{P_a}\right)^m \quad (\text{equation A.3.6})$$

Figures A.2.4 and A.2.5 show the shear and bulk moduli as secant estimations. Figure A.2.5 shows a graphical description of the bulk modulus as the ratio of the mean normal stress (σ'_m) to the volumetric strain (ϵ_v). Figure A.2.4(c) depicts the shear modulus and other related parameters as they are estimated and applied iteratively in the SOILSTRESS code. ' τ ' is the mobilized shear stress, τ_f is the failure strength, and R_f is the ratio of the strength at failure to the ultimate strength from the best-fit hyperbola. In figure A.2.4, ' G_m ' represents the initial maximum shear modulus estimate, and P_a is atmospheric pressure (to define the unit system being used). ' k_g ' and ' k_b ' are shear and bulk modulus numbers, and 'n' and 'm' are their respective modulus exponents. The determination of the hyperbolic parameters is described in detail by Byrne & Janzen (1989).

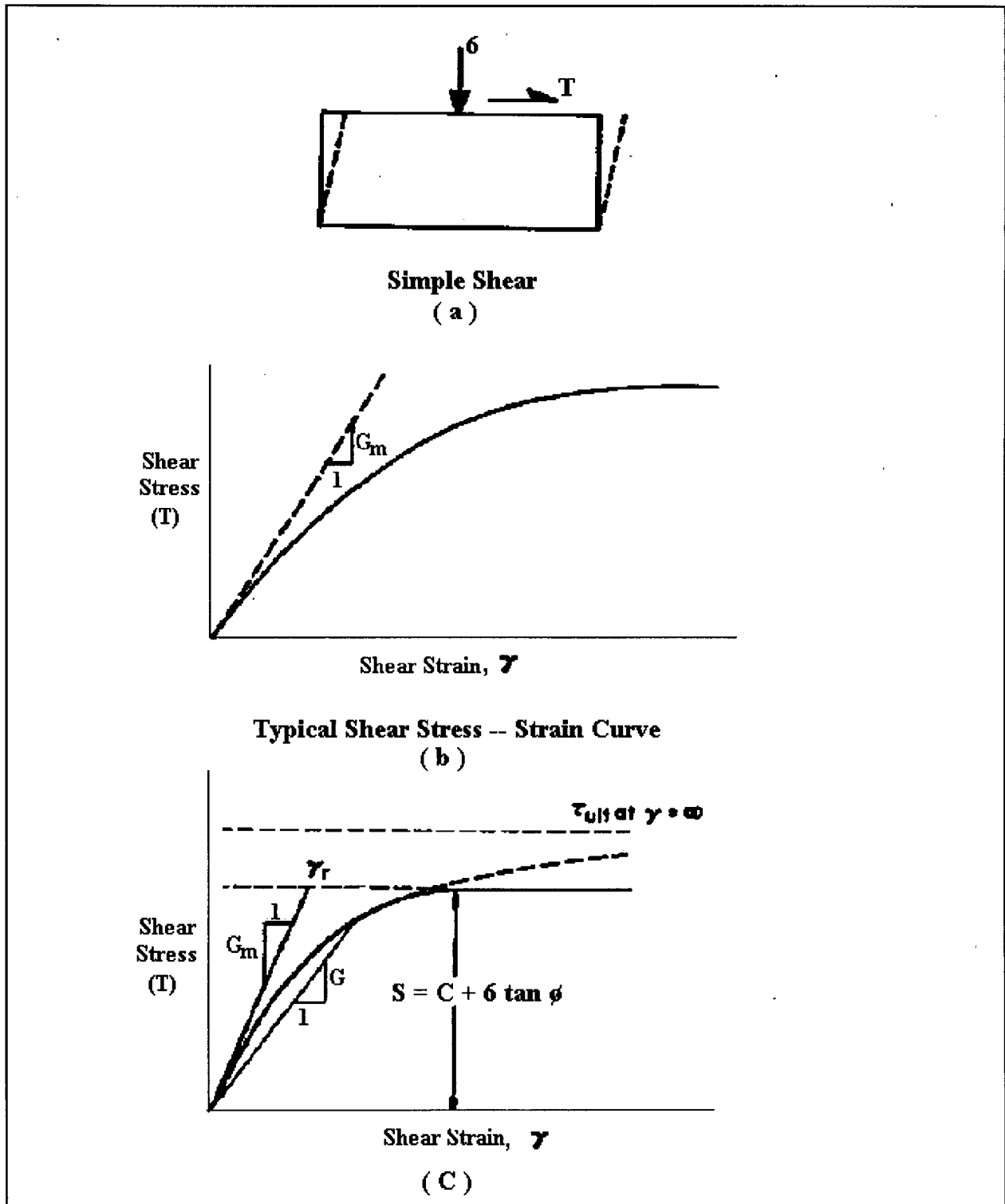


Figure A.2.4 - SOILSTRESS -- Idealized Nonlinear Shear Modulus Estimation (After Byrne & Janzen, 1989)

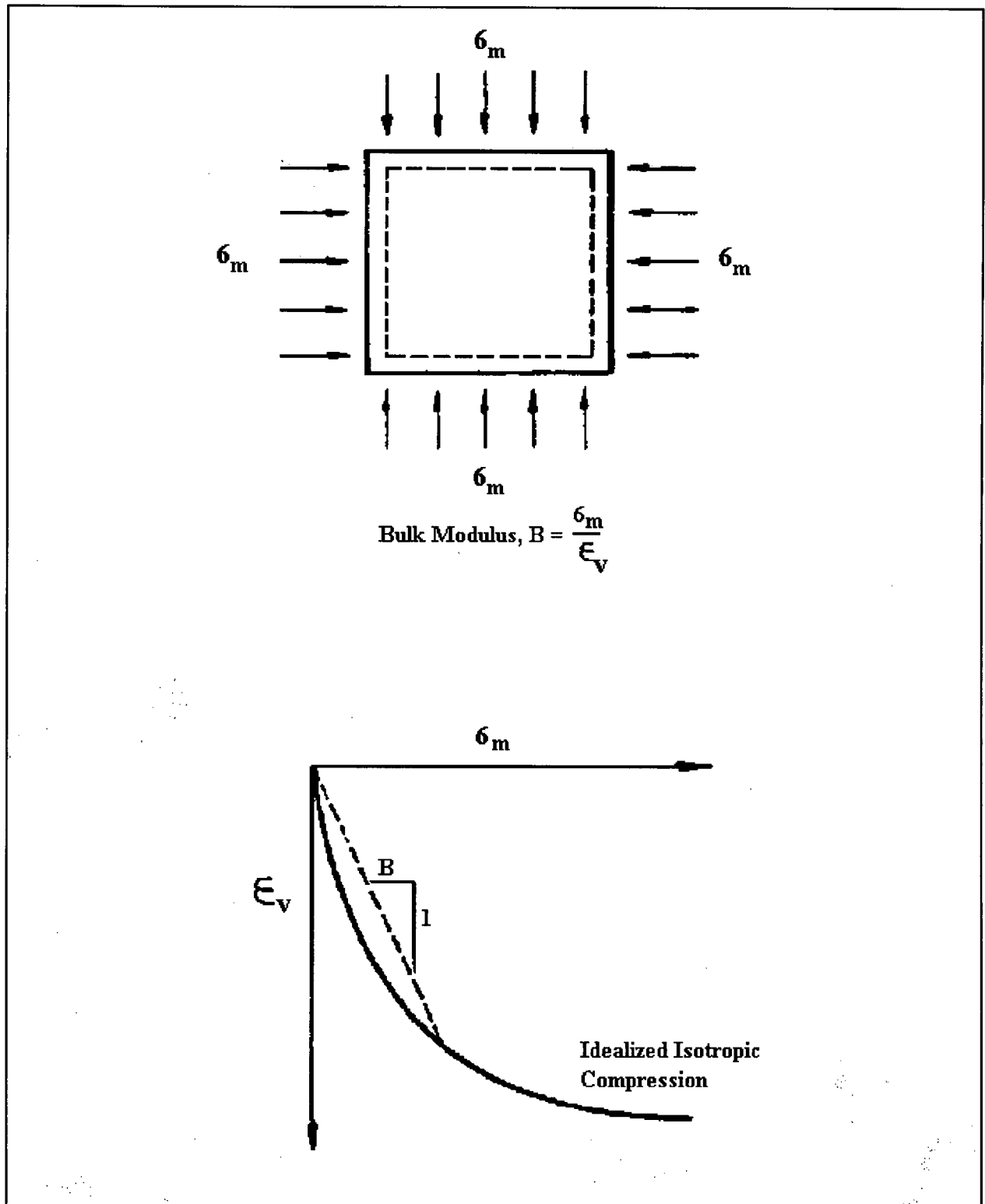


Figure A.2.5 - SOILSTRESS -- Idealized Nonlinear Bulk Modulus Estimation

APPENDIX B

SHAKE ANALYSES

B.1 SHAKE Analysis Method

To solve the nonlinear problem, SHAKE uses an iterative viscoelastic method of analysis. Soil, upon deforming, follows a hysteretic stress-strain path and the shape of the stress-strain path is dependent upon the stress-strain amplitude; therefore, to approximate the nonlinear soil behaviour, the program uses secant shear moduli and

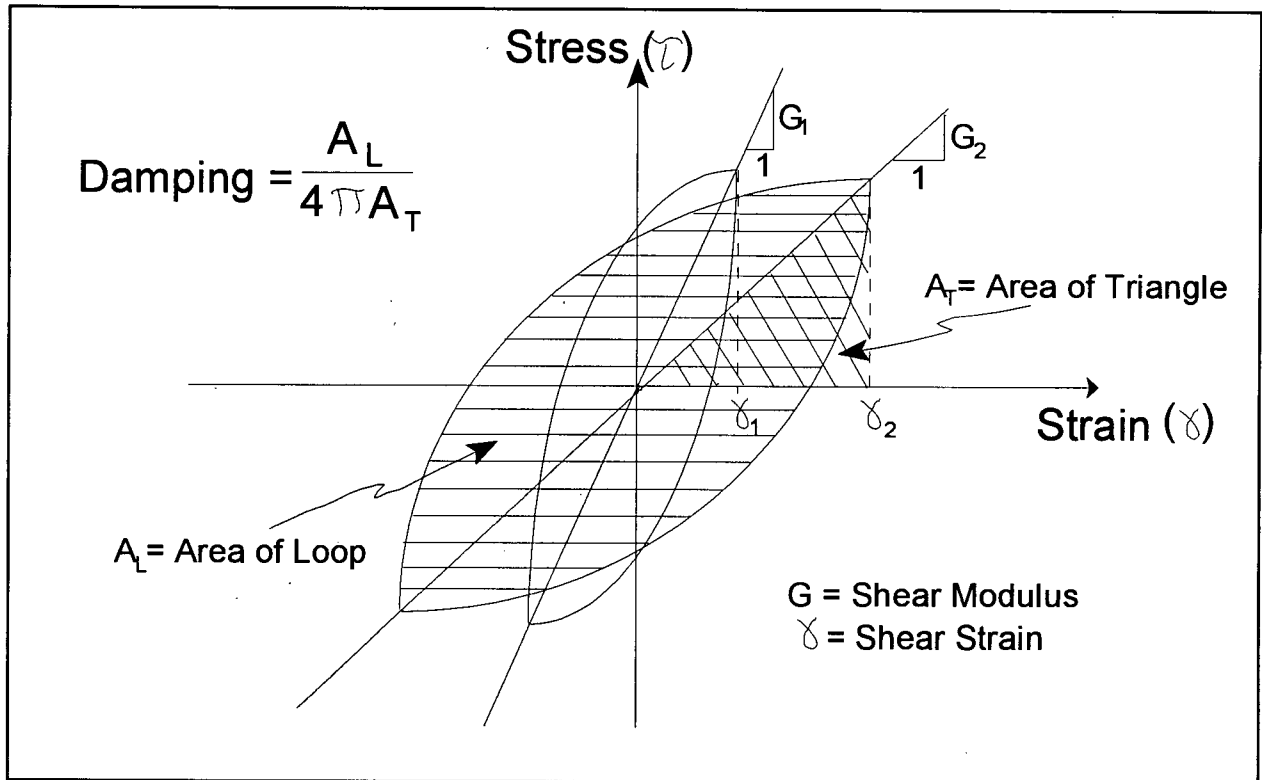


Figure B.1.1 - Estimation of Shear Modulus and Damping -- SHAKE

damping ratios. Figure B.1.1 shows the hysteretic stress-strain path. A straight line through the ends of the stress loop defines the shear modulus; the damping ratio is the ratio of the area of the hysteresis loop to the area of the triangle defined by the shear modulus and the endpoint of the loop. The iterative procedure is based on the assessment of this equivalent linear modulus and a viscous damping ratio to determine the strain amplitude, which will then lead to the designation of a new modulus and damping ratio. The iteration continues until stabilization of the solution is achieved.

B.2 Comparison of CSR's Using Various Bedrock Velocities

Figure B.2.1 shows the variation in the computed cyclic stress ratios if the firm ground velocity input is adjusted. Throughout this study, a firm ground velocity of 3500 m/s was applied. As expected, the CSR's increase as the firm ground input increases.

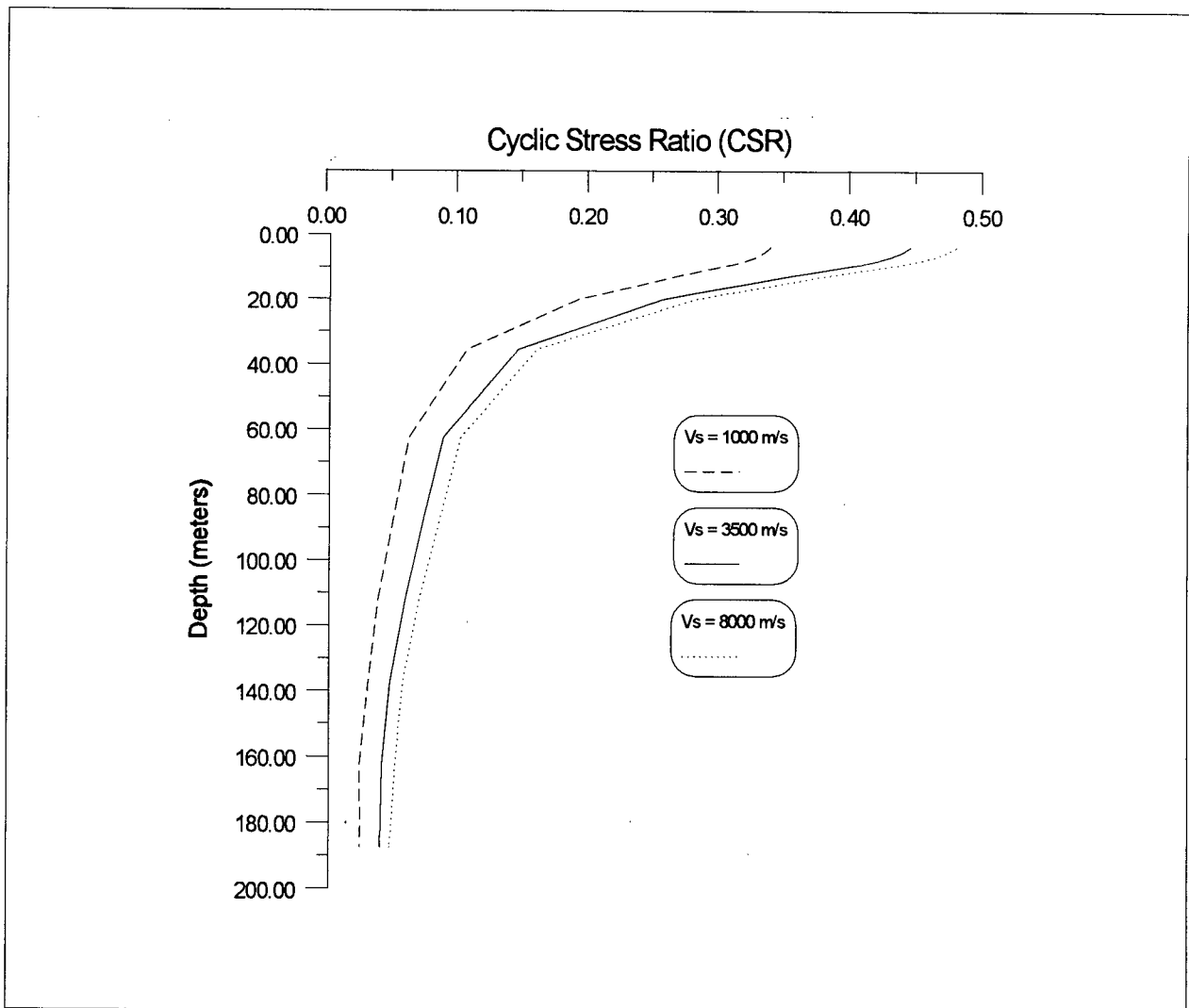


Figure B.2.1 - Comparison of C.S.R.'s Using Varying Bedrock Velocities at Location #2

B.3 Surface Spectral Response -- SHAKE

The computer program SHAKE was used to compute the response of the soil deposits to the selected input motions. The analysis procedure is discussed in section 4.2.3.2. The surface spectral response for the 475-year return period earthquake are graphically illustrated in figures B.3.1 to B.3.5. The results summaries (in this section) should be reviewed in conjunction with the discussion in section 7.2.2.

The surficial soils at the north and south river banks consist mostly of loose sands, whereas the offshore locations show more silt content. The peak surface response spectral values at the onshore and offshore locations are very similar. As figures B.3.1 to B.3.5 show, the surface response spectra for all locations show considerable amplifications at periods close to about 0.5 seconds.

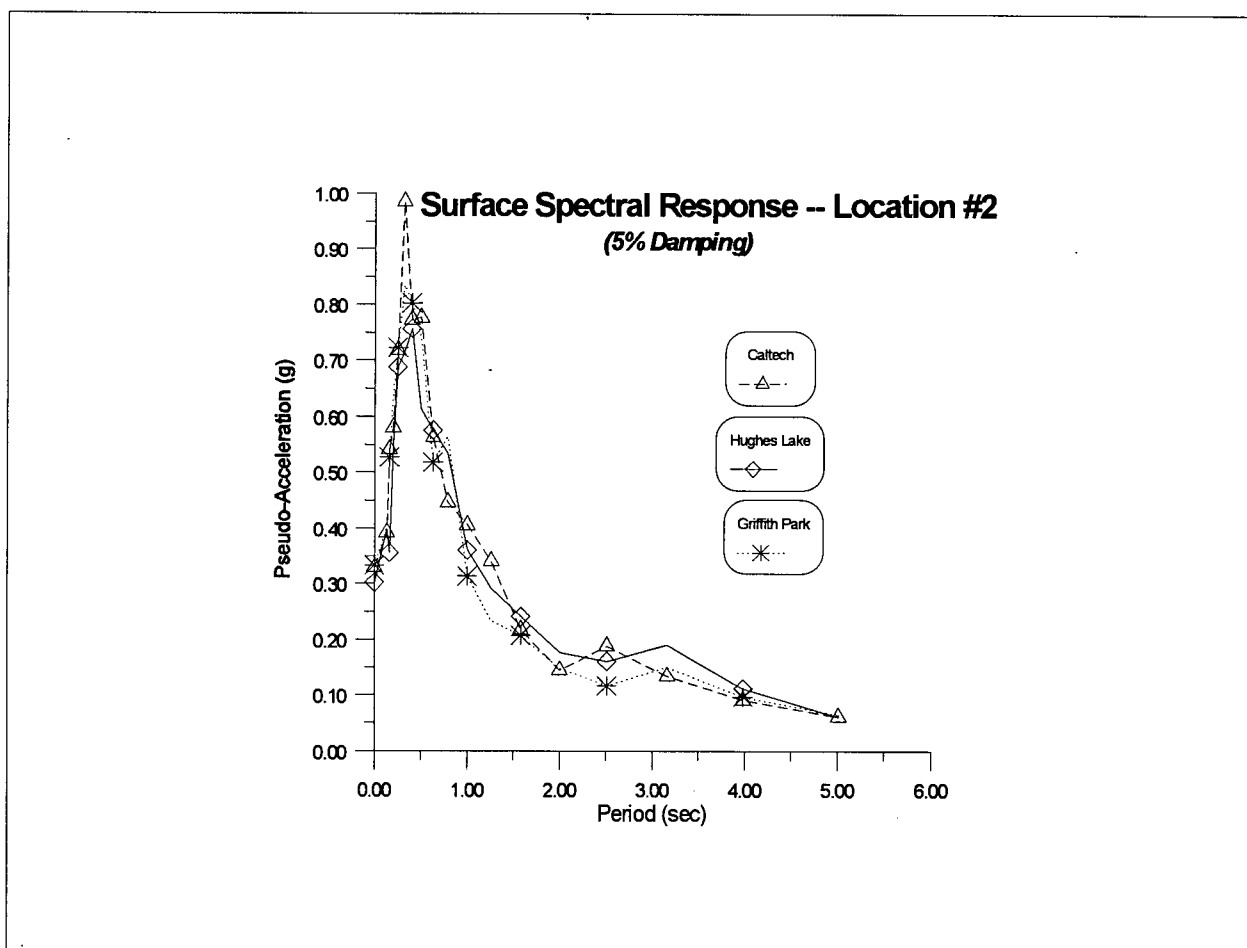


Figure B.3.1 - Ground Surface Spectral Response -- Location #2

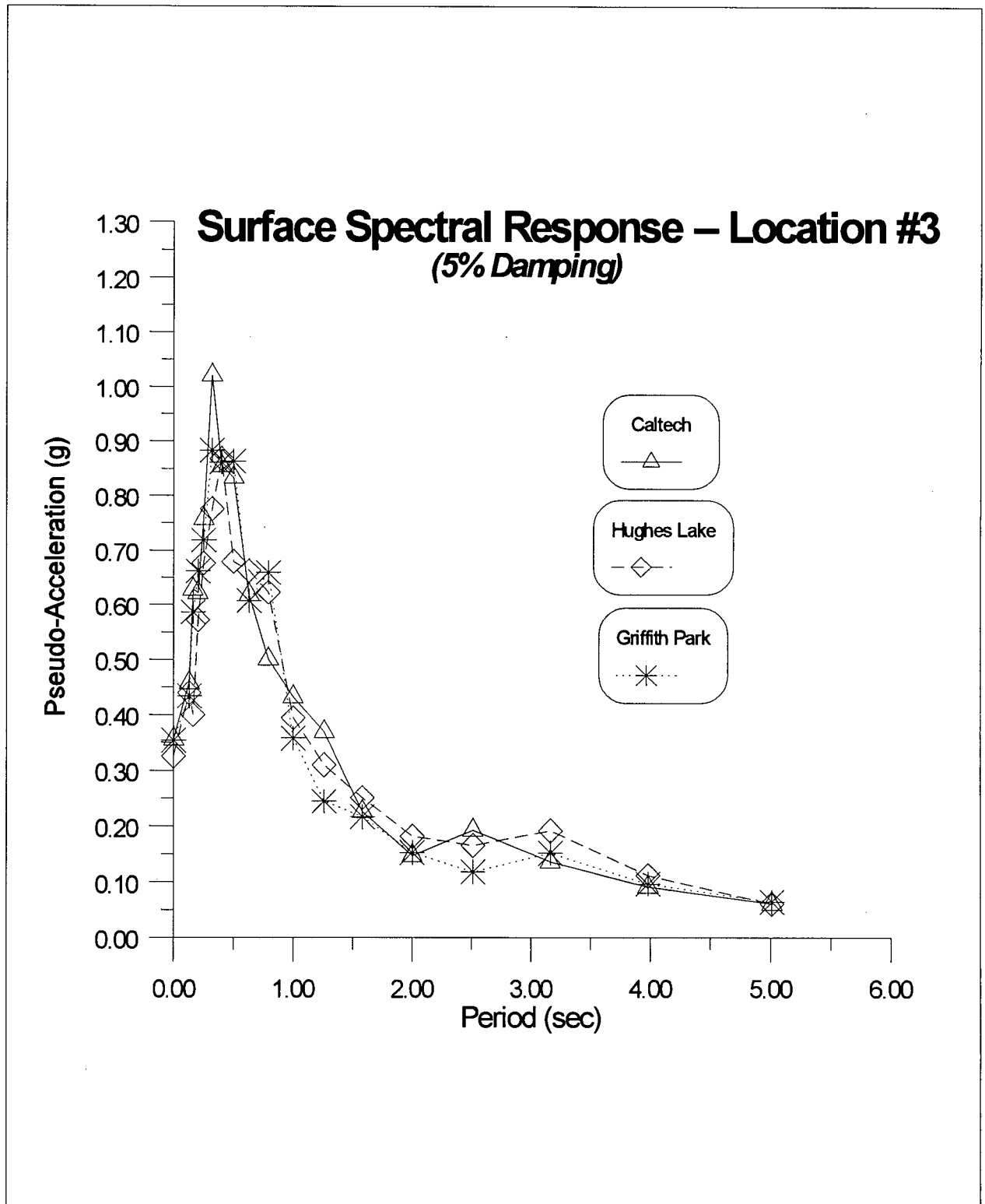


Figure B.3.2 - Ground Surface Spectral Response -- Location #3

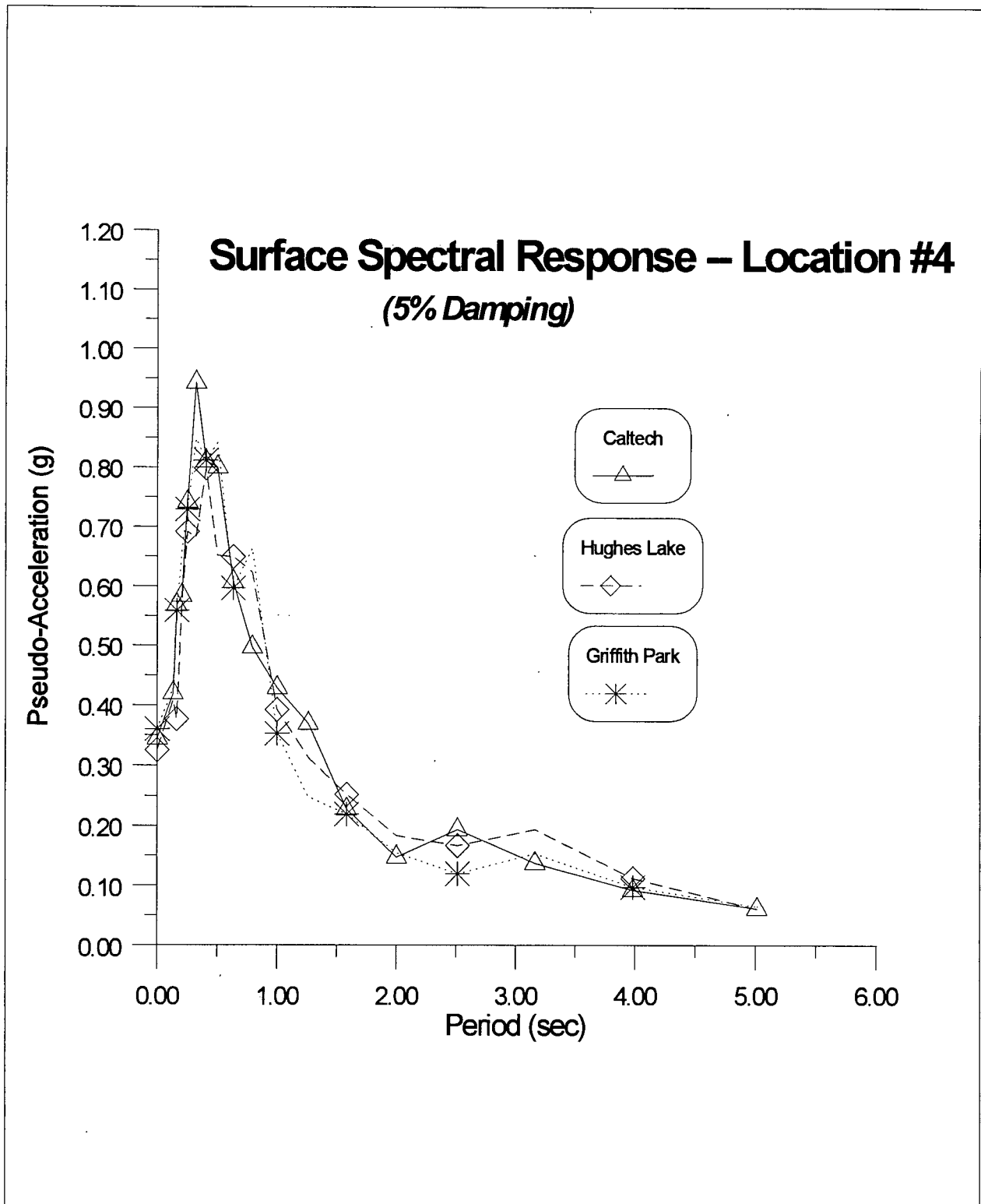


Figure B.3.3 - Ground Surface Spectral Response -- Location #4

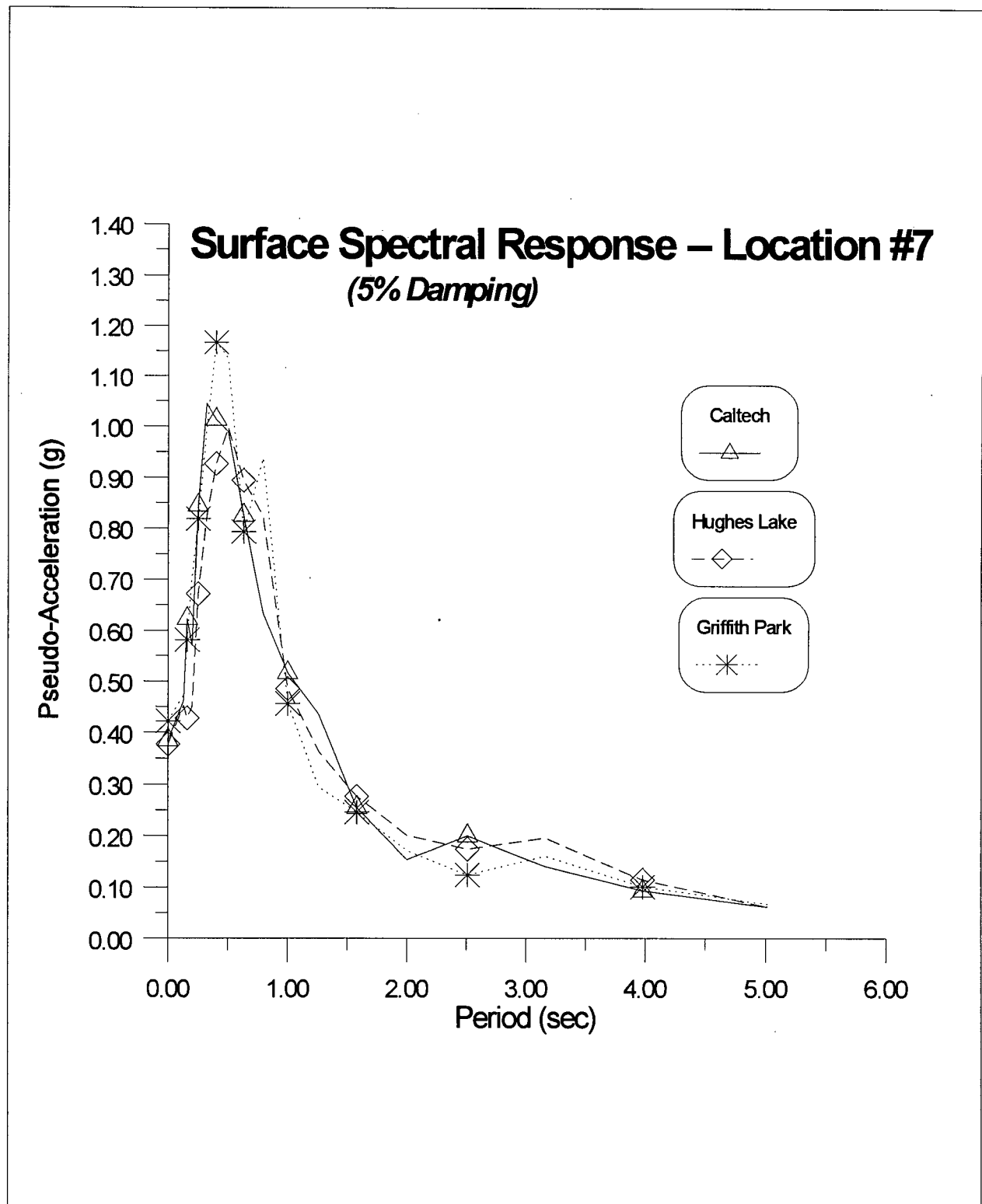


Figure B.3.4 - Ground Surface Spectral Response -- Location #7

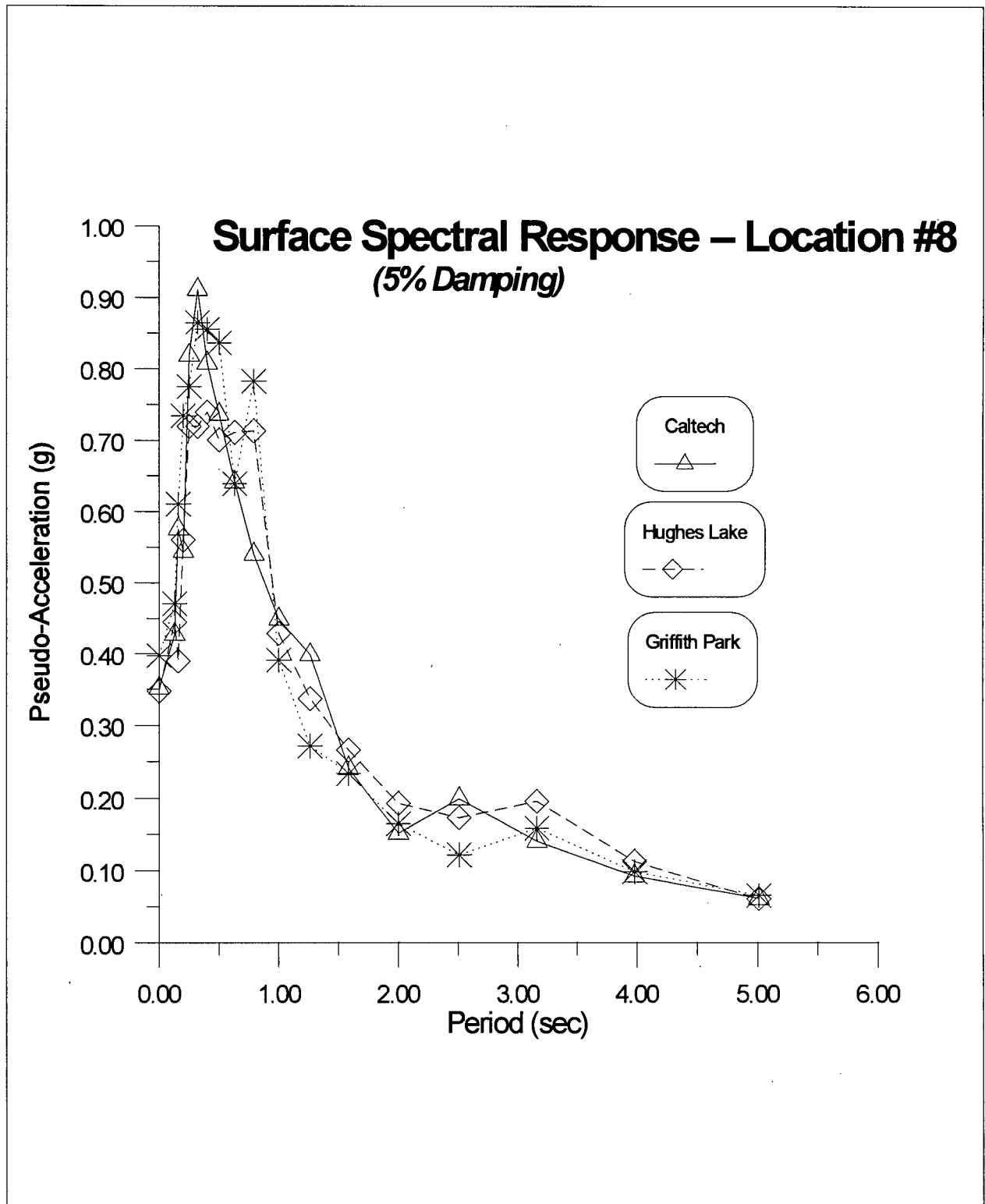


Figure B.3.5 - Ground Surface Spectral Response -- Location #8

B.4 Ground Motion Amplification Summary

Ground motion amplifications of peak horizontal firm ground accelerations (a_{\max}) were computed at each location. Amplifications varied between 40% (i.e., $a_{\text{surface}}/a_{\text{firm}} = 1.4$) and 60%. A firm ground design acceleration of 0.24g was applied in this study (as described in chapter 3). Peak surface accelerations varied between 0.33 g and 0.38 g.

Location #	Amplification Factor ($a_{\text{surface}}/a_{\text{firm}}$) (%)	Peak Surface Acceleration (g)
2	40	0.33
3	45	0.35
4	45	0.35
7	60	0.38
8	50	0.36

Table B.4.1 - Ground Motion Amplification at Each Location

Appendix B.5 -- Liquefaction Analysis Summaries**Appendix B.5.1 -- Location #2**

LIQUEFACTION ANALYSIS for CPT 91-2 Profile								
	Depth	Cyclic Stress Ratio (CSR)						
Layer #	(ft)	Caltech	Griffith	Hughes	Average	Standard	Mean + S	(CRR)1
			Park	Lake	CSR	Deviation	+ Sigma	
1	12.35	0.458	0.46	0.42	0.446	0.022539	0.468539	0.24
2	17.25	0.453	0.455	0.414	0.440667	0.023116	0.463782	0.24
3	22.05	0.444	0.447	0.405	0.432	0.023431	0.455431	0.148
4	26.75	0.433	0.433	0.392	0.419333	0.023671	0.443005	0.148
5	29.75	0.424	0.42	0.383	0.409	0.022605	0.431605	0.148
6	31.05	0.418	0.414	0.377	0.403	0.022605	0.425605	0.2
7	35.15	0.401	0.391	0.36	0.384	0.021378	0.405378	0.21
8	41.75	0.373	0.357	0.335	0.355	0.019079	0.374079	0.21
9	48.15	0.344	0.324	0.314	0.327333	0.015275	0.342609	Not App.
10	54.35	0.316	0.294	0.296	0.302	0.012166	0.314166	Not App.
11	59.75	0.29	0.267	0.281	0.279333	0.01159	0.290924	0.3
12	65.45	0.267	0.241	0.268	0.258667	0.015308	0.273975	0.3
13	116.45	0.139	0.125	0.178	0.147333	0.027465	0.174798	0.152
14	205.05	0.105	0.069	0.097	0.090333	0.018903	0.109237	0.152
15	287.05	0.072	0.061	0.092	0.075	0.015716	0.090716	0.152
16	369.15	0.065	0.058	0.06	0.061	0.003606	0.064606	0.152
17	451.15	0.043	0.052	0.054	0.049667	0.005859	0.055526	0.152
18	533.15	0.044	0.04	0.047	0.043667	0.003512	0.047179	0.152
19	615.15	0.041	0.043	0.043	0.042333	0.001155	0.043488	0.152

Table B.5.1 -- Triggering Summary for Location #2

Layer #	Cm	(K)sigma	CRR	F.o.S.	Depth	Soil	Criteria	Status
				CRR/CSR	(meters)	Type		
1	1.1	1	0.24	0.538117	3.76428	Sand	Robertson	Liquefy
2	1.1	1	0.24	0.544629	5.2578	Sand	Robertson	Liquefy
3	1.1	1	0.1628	0.376852	6.72084	Sand	Seed	Liquefy
4	1.1	1	0.1628	0.388235	8.1534	Sand	Seed	Liquefy
5	1.1	1	0.1628	0.398044	9.0678	Silt	Seed	Liquefy
6	1.1	1	0.22	0.545906	9.46404	Sand	Seed	Liquefy
7	1.1	1	0.21	0.546875	10.71372	Silt	Robertson	Liquefy
8	1.1	1	0.21	0.591549	12.7254	Silt	Robertson	Liquefy
9	1.1	0.98	0.360067	1.1	14.67612	Silt	Chinese	No Liq.
10	1.1	0.97	0.3322	1.1	16.56588	Silt	Chinese	No Liq.
11	1.1	0.96	0.3168	1.134129	18.2118	Sand	Seed	No Liq.
12	1.1	0.92	0.3036	1.173711	19.94916	Sand	Seed	No Liq.
13	1.1	0.8	0.152	1.031674	35.49396	Ext. Silt	Robertson	No Liq.
14	1.1	0.69	0.152	1.682657	62.49924	Ext. Silt	Robertson	No Liq.
15	1.1	0.62	0.152	2.026667	87.49284	Ext. Silt	Robertson	No Liq.
16	1.1	0.56	0.152	2.491803	112.51692	Ext. Silt	Robertson	No Liq.
17	1.1	0.52	0.152	3.060403	137.51052	Ext. Silt	Robertson	No Liq.
18	1.1	0.5	0.152	3.480916	162.50412	Ext. Silt	Robertson	No Liq.
19	1.1	0.5	0.152	3.590551	187.49772	Ext. Silt	Robertson	No Liq.

Table B.5.2 -- Triggering Summary for Location #2 -- Continued

Appendix B.5.2 -- Location #3

LIQUEFACTION ANALYSIS for CPT 91-3 Profile								
Cyclic Stress Ratio (CSR)								
Layer #	Depth (ft)	Caltech	Griffith Park	Hughes Lake	Average CSR	Standard Deviation	Mean + S + Sigma	(CRR)1
1	13.75	0.495	0.488	0.46	0.481	0.01852026	0.49952026	0.17
2	18.65	0.489	0.481	0.453	0.47433333	0.01890326	0.4932366	0.16
3	23.25	0.473	0.464	0.432	0.45633333	0.0215484	0.47788173	0.168
4	27.65	0.45	0.44	0.406	0.432	0.02306513	0.45506513	0.168
5	32.25	0.427	0.415	0.385	0.409	0.02163331	0.43063331	Not App.
6	36.95	0.402	0.389	0.365	0.38533333	0.01877054	0.40410388	Not App.
7	42.55	0.372	0.36	0.344	0.35866667	0.01404754	0.37271421	Not App.
8	49.05	0.334	0.323	0.32	0.32566667	0.00737111	0.33303778	Not App.
9	55.45	0.297	0.285	0.3	0.294	0.00793725	0.30193725	Not App.
10	65.45	0.253	0.232	0.272	0.25233333	0.02000833	0.27234166	0.3
11	86.95	0.196	0.164	0.228	0.196	0.032	0.228	0.152
12	116.45	0.144	0.127	0.178	0.14966667	0.02596793	0.1756346	0.152
13	147.65	0.125	0.094	0.137	0.11866667	0.02218859	0.14085525	0.152
14	180.45	0.117	0.079	0.11	0.102	0.02022375	0.12222375	0.152
15	229.65	0.097	0.066	0.1	0.08766667	0.01882374	0.10649041	0.152
16	295.25	0.071	0.062	0.086	0.073	0.01212436	0.08512436	0.152
17	369.05	0.065	0.06	0.064	0.063	0.00264575	0.06564575	0.152
18	467.55	0.039	0.051	0.05	0.04666667	0.00665833	0.05332499	0.152
19	590.55	0.042	0.042	0.045	0.043	0.00173205	0.04473205	0.152

Table B.5.3 -- Triggering Summary for Location #3

Layer #	Cm	(K)sigma	CRR	F.o.S.	Depth	Soil	Criteria	Status
				CRR/CSR	(meters)	Type		
1	1.1	1	0.187	0.38877339	4.191	Sand	Seed	Liquefy
2	1.1	1	0.176	0.37104708	5.68452	Sand	Seed	Liquefy
3	1.1	1	0.1848	0.40496713	7.0866	Silt	Seed	Liquefy
4	1.1	1	0.1848	0.42777778	8.42772	Silt	Seed	Liquefy
5	1.1	1	Not App.	1.1	9.8298	Silt	Chinese	No Liq.
6	1.1	1	Not App.	1.1	11.26236	Silt	Chinese	No Liq.
7	1.1	1	Not App.	1.1	12.96924	Silt	Chinese	No Liq.
8	1.1	0.99	Not App.	1.1	14.95044	Silt	Chinese	No Liq.
9	1.1	0.95	Not App.	1.1	16.90116	Silt	Chinese	No Liq.
10	1.1	0.93	0.3069	1.21624835	19.94916	Sand	Seed	No Liq.
11	1.1	0.86	0.152	1	26.50236	ext. silt	Robertson	No Liq.
12	1.1	0.8	0.152	1.0155902	35.49396	ext. silt	Robertson	No Liq.
13	1.1	0.75	0.152	1.28089888	45.00372	ext. silt	Robertson	No Liq.
14	1.1	0.72	0.152	1.49019608	55.00116	ext. silt	Robertson	No Liq.
15	1.1	0.66	0.152	1.7338403	69.99732	ext. silt	Robertson	No Liq.
16	1.1	0.61	0.152	2.08219178	89.9922	ext. silt	Robertson	No Liq.
17	1.1	0.56	0.152	2.41269841	112.48644	ext. silt	Robertson	No Liq.
18	1.1	0.51	0.152	3.25714286	142.50924	ext. silt	Robertson	No Liq.
19	1.1	0.5	0.152	3.53488372	179.99964	ext. silt	Robertson	No Liq.

Table B.5.4 -- Triggering Summary for Location #3 -- Continued

Appendix B.5.3 -- Location #4

LIQUEFACTION ANALYSIS for CPT 91-4 Profile								
Layer #	Depth (ft)	Cyclic Stress Ratio (CSR)			Average CSR	Standard Deviation	Mean + S + Sigma	(CRR)1
		Caltech	Griffith Park	Hughes Lake				
1	12.3	0.451	0.47	0.426	0.449	0.02206808	0.47106808	0.26
2	15	0.455	0.472	0.429	0.452	0.02165641	0.47365641	0.245
3	18.7	0.451	0.467	0.424	0.44733333	0.02173323	0.46906656	0.245
4	23.5	0.446	0.46	0.419	0.44166667	0.02084067	0.46250733	0.21
5	29.5	0.429	0.436	0.401	0.422	0.01852026	0.44052026	0.21
6	33.4	0.412	0.414	0.384	0.40333333	0.01677299	0.42010633	0.292
7	37.2	0.396	0.395	0.37	0.387	0.01473092	0.40173092	Not App.
8	43	0.372	0.365	0.351	0.36266667	0.01069268	0.37335934	Not App.
9	50.9	0.337	0.327	0.327	0.33033333	0.0057735	0.33610684	Not App.
10	59.9	0.292	0.276	0.303	0.29033333	0.01357694	0.30391027	Not App.
11	68.1	0.26	0.237	0.282	0.25966667	0.02250185	0.28216852	Not App.
12	75.6	0.238	0.209	0.263	0.23666667	0.02702468	0.26369135	Not App.
13	121.6	0.145	0.123	0.174	0.14733333	0.02557994	0.17291327	0.152
14	205.1	0.107	0.068	0.1	0.09166667	0.02079263	0.11245929	0.152
15	287.1	0.073	0.064	0.09	0.07566667	0.01320353	0.0888702	0.152
16	369.1	0.065	0.061	0.064	0.06333333	0.00208167	0.065415	0.152
17	451.2	0.042	0.054	0.053	0.04966667	0.00665833	0.05632499	0.152
18	533.2	0.044	0.04	0.051	0.045	0.00556776	0.05056776	0.152
19	615.2	0.04	0.042	0.04	0.04066667	0.0011547	0.04182137	0.152

Table B.5.5 -- Triggering Summary for Location #4

Layer #	Cm	(K)sigma	CRR	F.o.S. CRR/CSR	Depth (meters)	Soil Type	Criteria	Status
1	1.1	1	0.286	0.636971047	3.74904	Sand	Seed	Liquefy
2	1.1	1	0.2695	0.596238938	4.572	Sand	Seed	Liquefy
3	1.1	1	0.2695	0.602459016	5.69976	Sand	Seed	Liquefy
4	1.1	1	0.231	0.523018868	7.1628	Sandy Silt	Seed	Liquefy
5	1.1	1	0.231	0.547393365	8.9916	Sandy Silt	Seed	Liquefy
6	1.1	1	0.3212	0.796363636	10.18032	Silty Sand	Seed	Liquefy
7	1.1	1	Not App.	1.1	11.33856	Silt	Chinese	Not Liq.
8	1.1	1	Not App.	1.1	13.1064	Silt	Chinese	Not Liq.
9	1.1	0.98	Not App.	1.1	15.51432	Silt	Chinese	Not Liq.
10	1.1	0.97	Not App.	1.1	18.25752	Silt	Chinese	Not Liq.
11	1.1	0.94	Not App.	1.1	20.75688	Silt	Chinese	Not Liq.
12	1.1	0.91	Not App.	1.1	23.04288	Silt	Chinese	Not Liq.
13	1.1	0.8	0.152	1.031674208	37.06368	Ext. Silt	Robertson	Not Liq.
14	1.1	0.69	0.152	1.658181818	62.51448	Ext. Silt	Robertson	Not Liq.
15	1.1	0.62	0.152	2.008810573	87.50808	Ext. Silt	Robertson	Not Liq.
16	1.1	0.56	0.152	2.4	112.50168	Ext. Silt	Robertson	Not Liq.
17	1.1	0.52	0.152	3.060402685	137.52576	Ext. Silt	Robertson	Not Liq.
18	1.1	0.5	0.152	3.377777778	162.51936	Ext. Silt	Robertson	Not Liq.
19	1.1	0.5	0.152	3.737704918	187.51296	Ext. Silt	Robertson	Not Liq.

Table B.5.6 -- Triggering Summary for Location #4 -- Continued

Appendix B.5.4 -- Location #7

LIQUEFACTION ANALYSIS for CPT 91-7 Profile								
Layer #	Depth (ft)	Cyclic Stress Ratio (CSR)			Average CSR	Standard Deviation	Mean + S + Sigma	(CRR)I
		Caltech	Griffith Park	Hughes Lake				
1	9.86	0.252	0.277	0.247	0.25866667	0.01607275	0.27473942	0.182
2	14.06	0.378	0.414	0.369	0.387	0.02381176	0.41081176	0.182
3	20.56	0.427	0.461	0.413	0.43366667	0.02468468	0.45835134	0.182
4	26.56	0.414	0.439	0.402	0.41833333	0.01887679	0.43721013	0.182
5	32.06	0.375	0.394	0.377	0.382	0.01044031	0.39244031	0.182
6	40.36	0.309	0.308	0.34	0.319	0.01819341	0.33719341	0.1
7	50.86	0.262	0.236	0.307	0.26833333	0.03592121	0.30425454	0.1
8	60.66	0.228	0.2	0.278	0.23533333	0.03951371	0.27484704	0.1
9	72.16	0.196	0.183	0.248	0.209	0.03439477	0.24339477	0.223
10	83.66	0.176	0.166	0.223	0.18833333	0.03043572	0.21876906	0.23
11	100.06	0.16	0.145	0.193	0.166	0.02455606	0.19055606	0.22
12	118.66	0.141	0.128	0.162	0.14366667	0.01715615	0.16082281	0.18
13	144.86	0.131	0.097	0.13	0.11933333	0.0193477	0.13868103	0.152
14	205.06	0.103	0.071	0.107	0.09366667	0.01973153	0.1133982	0.152
15	287.06	0.075	0.066	0.088	0.07633333	0.01106044	0.08739377	0.152
16	369.16	0.067	0.064	0.07	0.067	0.003	0.07	0.152
17	451.16	0.043	0.051	0.057	0.05033333	0.00702377	0.0573571	0.152
18	533.16	0.04	0.041	0.052	0.04433333	0.00665833	0.05099166	0.152
19	615.16	0.04	0.038	0.045	0.041	0.00360555	0.04460555	0.152

Table B.5.7 -- Triggering Summary for Location #7

Layer #	Cm	(K)sigma	CRR	F.o.S.	Depth	Soil	Criteria	Status
				CRR/CSR	(meters)	Type		
1	1.1	1	0.2002	0.77396907	3.005328	Sand	Seed	Liquefy
2	1.1	1	0.2002	0.51731266	4.285488	Sand	Seed	Liquefy
3	1.1	1	0.2002	0.46164489	6.266688	Sand	Seed	Liquefy
4	1.1	1	0.2002	0.47856574	8.095488	Sand	Seed	Liquefy
5	1.1	1	0.2002	0.52408377	9.771888	Sand	Seed	Liquefy
6	1.1	1	0.11	0.34482759	12.301728	Sand	Seed	Liquefy
7	1.1	0.98	0.1078	0.40173913	15.502128	Sand	Seed	Liquefy
8	1.1	0.96	0.1056	0.44872521	18.489168	Sand	Seed	Liquefy
9	1.1	0.9	0.22077	1.05631579	21.994368	Sand	Seed	Partial Liq
10	1.1	0.89	0.22517	1.19559292	25.499568	Sand	Rob/Seed	Partial Liq
11	1.1	0.85	0.2057	1.23915663	30.498288	Sand	Rob/Seed	Partial Liq
12	1.1	0.8	0.1584	1.1025522	36.167568	Sand	Seed	Partial Liq
13	1.1	0.75	0.152	1.27374302	44.153328	Ext. Silt	Robertson	Not Liq.
14	1.1	0.69	0.152	1.6227758	62.502288	Ext. Silt	Robertson	Not Liq.
15	1.1	0.62	0.152	1.99126638	87.495888	Ext. Silt	Robertson	Not Liq.
16	1.1	0.56	0.152	2.26865672	112.519968	Ext. Silt	Robertson	Not Liq.
17	1.1	0.52	0.152	3.01986755	137.513568	Ext. Silt	Robertson	Not Liq.
18	1.1	0.5	0.152	3.42857143	162.507168	Ext. Silt	Robertson	Not Liq.
19	1.1	0.5	0.152	3.70731707	187.500768	Ext. Silt	Robertson	Not Liq.

Table B.5.8 -- Triggering Summary for Location #7 -- Continued

Appendix B.5.5 -- Location #8

LIQUEFACTION ANALYSIS for CPT 91-8 Profile								
	Depth	Cyclic Stress Ratio (CSR)						
Layer #	(ft)	Caltech	Griffith	Hughes	Average	Standard	Mean + S	(CRR)1
			Park	Lake	CSR	Deviation	+ Sigma	
1	19.6	0.489	0.547	0.483	0.50633333	0.03534591	0.54167924	0.134
2	26	0.474	0.523	0.465	0.48733333	0.03121431	0.51854765	0.134
3	32.4	0.448	0.485	0.438	0.457	0.02475884	0.48175884	0.134
4	38.8	0.418	0.44	0.409	0.42233333	0.01594783	0.43828116	0.134
5	43.3	0.393	0.408	0.389	0.39666667	0.01001665	0.40668332	0.23
6	48.6	0.363	0.372	0.368	0.36766667	0.00450925	0.37217592	0.125
7	55.8	0.323	0.325	0.343	0.33033333	0.01101514	0.34134847	0.125
8	66.4	0.272	0.261	0.308	0.28033333	0.02458319	0.30491653	0.1
9	75	0.237	0.214	0.277	0.24266667	0.03187998	0.27454665	0.168
10	79.5	0.217	0.194	0.261	0.224	0.03404409	0.25804409	0.125
11	84.3	0.2	0.176	0.245	0.207	0.03502856	0.24202856	0.125
12	87.5	0.187	0.167	0.235	0.19633333	0.03494758	0.23128091	0.134
13	126.6	0.144	0.116	0.164	0.14133333	0.02411086	0.16544419	0.152
14	205.1	0.109	0.072	0.106	0.09566667	0.02055075	0.11621742	0.152
15	287.1	0.079	0.067	0.088	0.078	0.01053565	0.08853565	0.152
16	369.1	0.064	0.063	0.068	0.065	0.00264575	0.06764575	0.152
17	451.1	0.044	0.053	0.054	0.05033333	0.00550757	0.0558409	0.152
18	533.2	0.044	0.041	0.053	0.046	0.006245	0.052245	0.152
19	615.2	0.039	0.039	0.041	0.03966667	0.0011547	0.04082137	0.152

Table B.5.9 -- Triggering Summary for Location #8

Layer #	Cm	(K)sigma	CRR	F.o.S.	Depth	Soil	Criteria	Status
				CRR/CSR	(meters)	Type		
1	1.1	1	0.1474	0.29111257	5.97408	Sand	Seed	Liquefy
2	1.1	1	0.1474	0.30246238	7.9248	Sand	Seed	Liquefy
3	1.1	1	0.1474	0.32253829	9.87552	Sand	Seed	Liquefy
4	1.1	1	0.1474	0.34901342	11.82624	Sand	Seed	Liquefy
5	1.1	1	0.253	0.63781513	13.19784	Sand	Seed	Liquefy
6	1.1	1	0.1375	0.37398005	14.81328	Sand	Seed	Liquefy
7	1.1	0.98	0.13475	0.40792129	17.00784	Sand	Seed	Liquefy
8	1.1	0.96	0.1056	0.37669441	20.23872	Sand	Seed	Liquefy
9	1.1	0.92	0.170016	0.70061538	22.86	Sand	Seed	Liquefy
10	1.1	0.91	0.125125	0.55859375	24.2316	Sand	Seed	Liquefy
11	1.1	0.9	0.12375	0.59782609	25.69464	Sand	Seed	Liquefy
12	1.1	0.89	0.131186	0.66817997	26.67	Sand	Seed	Liquefy
13	1.1	0.8	0.152	1.1	38.58768	Ext. Silt	Robertson	Not Liq.
14	1.1	0.69	0.152	1.1	62.51448	Ext. Silt	Robertson	Not Liq.
15	1.1	0.63	0.152	1.1	87.50808	Ext. Silt	Robertson	Not Liq.
16	1.1	0.57	0.152	1.1	112.50168	Ext. Silt	Robertson	Not Liq.
17	1.1	0.52	0.152	1.1	137.49528	Ext. Silt	Robertson	Not Liq.
18	1.1	0.5	0.152	1.1	162.51936	Ext. Silt	Robertson	Not Liq.
19	1.1	0.5	0.152	1.1	187.51296	Ext. Silt	Robertson	Not Liq.

Table B.5.10 -- Triggering Summary for Location #8 -- Continued

Appendix B.6 -- Idriss (1991) Ground Motion Attenuation

IDRISS ATTENUATION RELATIONSHIP (1991) :							
BETA1 =	2.475	BETA2 =	-0.286	M =	7	R =	31.4
PERIOD	ALPHA0	ALPHA1	ALPHA2	BETA0	ERROR	LN (PGA)	(m+1)
SEC					M<7.25		(PGA)
0	-0.05	3.477	-0.284	0	0.41	-1.4296761	0.23938644
0.03	-0.05	3.477	-0.284	0	0.41	-1.4296761	0.23938644
0.05	-0.278	3.426	-0.269	0.066	0.41	-1.1517156	0.31609401
0.075	-0.308	3.359	-0.252	0.07	0.41	-0.916233	0.40002308
0.1	-0.318	3.327	-0.243	0.072	0.44	-0.7331828	0.48037759
0.11	-0.328	3.289	-0.236	0.073	0.44	-0.683016	0.50509133
0.13	-0.338	3.233	-0.225	0.075	0.44	-0.5760612	0.56210805
0.15	-0.348	3.185	-0.216	0.076	0.44	-0.5027961	0.60483713
0.2	-0.358	3.1	-0.201	0.078	0.44	-0.3972815	0.67214482
0.25	-0.429	3.034	-0.19	0.08	0.44	-0.4002787	0.67013325
0.3	-0.486	2.982	-0.182	0.082	0.46	-0.4073719	0.66539672
0.35	-0.535	2.943	-0.177	0.087	0.46	-0.4587012	0.63210407
0.4	-0.577	2.906	-0.173	0.092	0.46	-0.5302441	0.5884613
0.5	-0.648	2.85	-0.169	0.099	0.48	-0.7040574	0.49457452
0.6	-0.705	2.803	-0.166	0.105	0.48	-0.8733475	0.41755145
0.7	-0.754	2.765	-0.165	0.111	0.5	-1.0362257	0.35479124
0.8	-0.796	2.728	-0.164	0.115	0.5	-1.2103226	0.2981011
0.9	-0.834	2.694	-0.163	0.119	0.5	-1.361894	0.25617511
1	-0.867	2.662	-0.162	0.123	0.5	-1.4958116	0.22406668
1.5	-0.97	2.536	-0.16	0.136	0.5	-2.035941	0.13055757
2	-1.046	2.447	-0.16	0.146	0.54	-2.3834324	0.09223346
3	-1.143	2.295	-0.159	0.16	0.54	-2.9341052	0.05317828
4	-1.177	2.169	-0.159	0.169	0.54	-3.3186894	0.03620025
5	-1.214	2.042	-0.157	0.177	0.54	-3.6313479	0.02648047

Table B.6.1 - Estimation of Target Spectrum for Modification of Time-Histories

Refer to Idriss (1991) for a general summary of spectral ordinates used in the calculation.

APPENDIX C

POST-EARTHQUAKE STABILITY

C.1 Flowslide Analyses: Limit Equilibrium Stability at Offshore Locations

Since the tunnel is founded on a level excavation, the tunnel is very stable in the direction transverse to the roadway (i.e., cross-section view). In each analysis at the offshore locations, the failure surface intersects an underlying liquefied layer. At location #2 (figure C.1.1), the failure surface intersects the unit #5 loose sand. (Refer to figure 6.13 for the material numbering scheme). A factor of safety of about 2.3 was estimated in the limit equilibrium analysis, in which a residual strength of 12 kPa was applied in the underlying liquefied sands. A flowslide type movement at location #2 is unlikely.

At location #3 (figure C.1.2), the failure surface intersects the unit #5 liquefied silt. A residual strength of 30 kPa was applied in the silt. A factor of safety against flowslide ($F.S_{FL}$) of about 1.3 was estimated in the stability analysis. A flowslide at location #3 is unlikely.

Similarly to location #3, the failure surface at location #4 intersects the unit #5 liquefied silt. A residual strength of 30 kPa was applied in the silt. A factor of safety against flowslide ($F.S_{FL}$) of about 1.6 was estimated in the stability analysis. Based on these analyses, it can be concluded that residual strengths are sufficient to prevent post-earthquake instability at all of the locations analyzed.

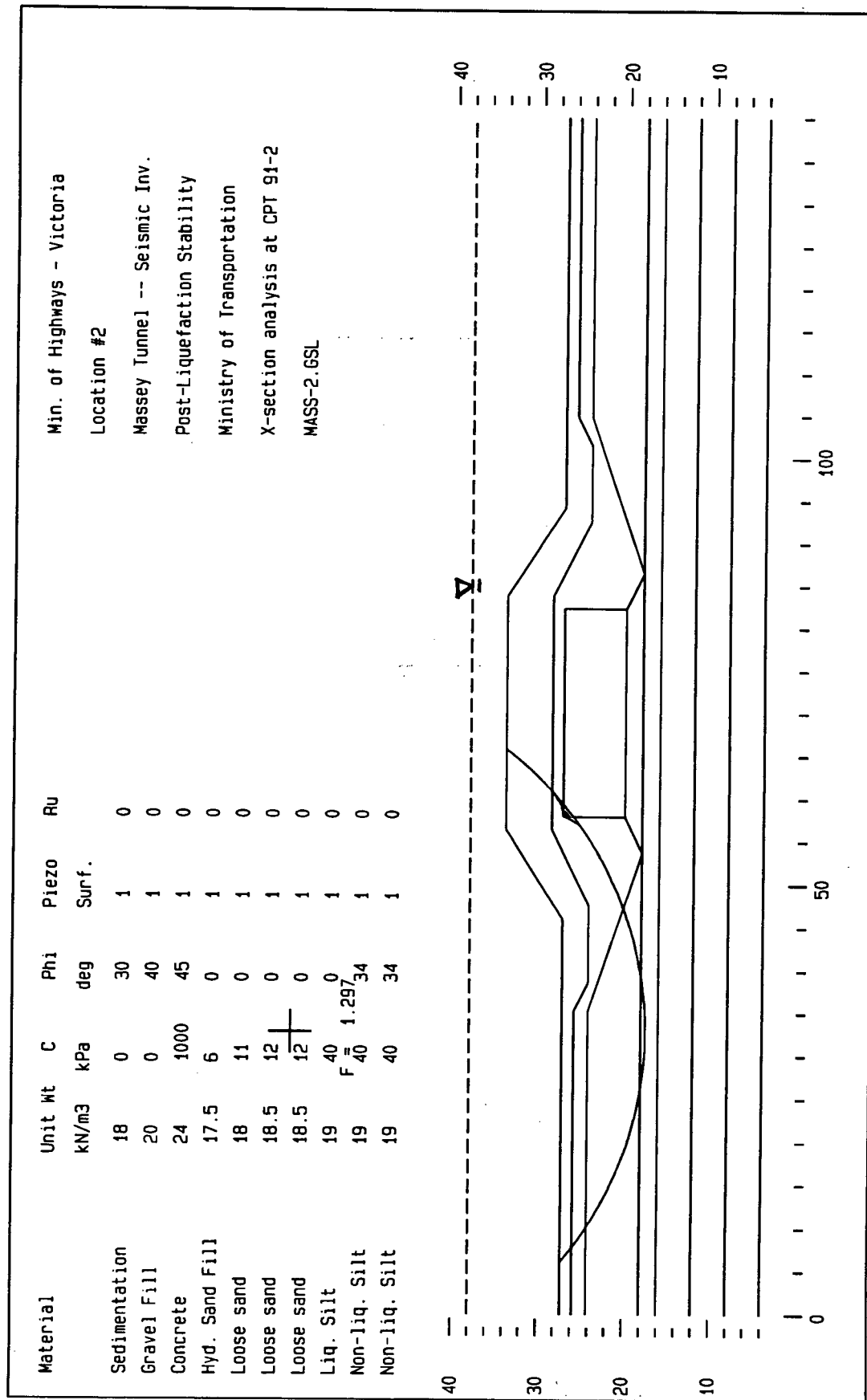


Figure C.1.1 - Post-liquefaction Limit Equilibrium Stability Analysis at Location #2

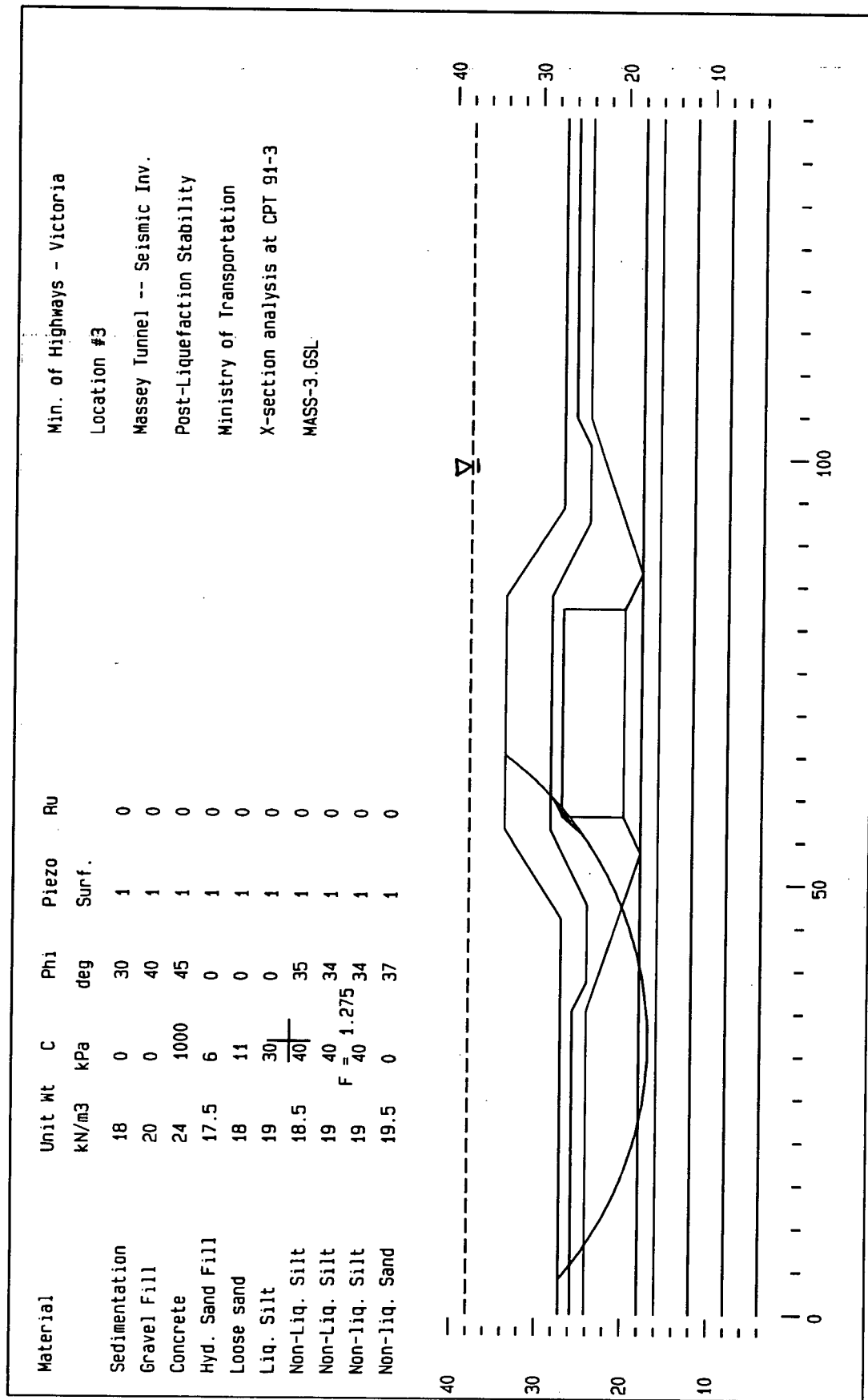


Figure C.1.2 - Post-liquefaction Limit Equilibrium Stability Analysis at Location #3

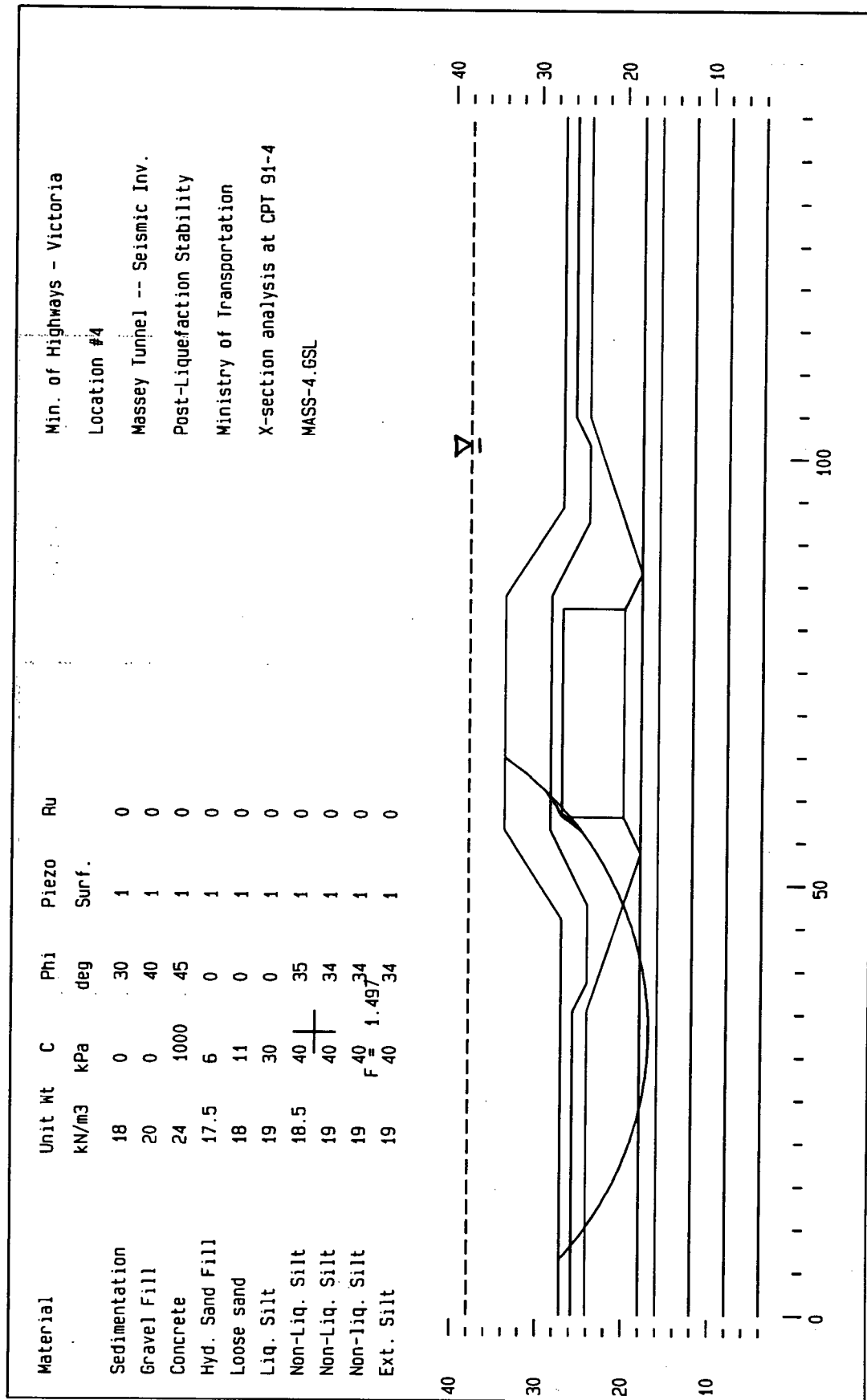


Figure C.1.3 - Post-liquefaction Limit Equilibrium Stability Analysis at Location #4

C.2 Flowslide Analyses with Higher Residual Strengths

This appendix summarizes the graphic output using a more realistic residual strength estimate of 26 kPa in the overlying dyke material at the north and south river banks (locations #8 and #7). Based on the results of these analyses, it can be concluded that the north and south shores are stable.

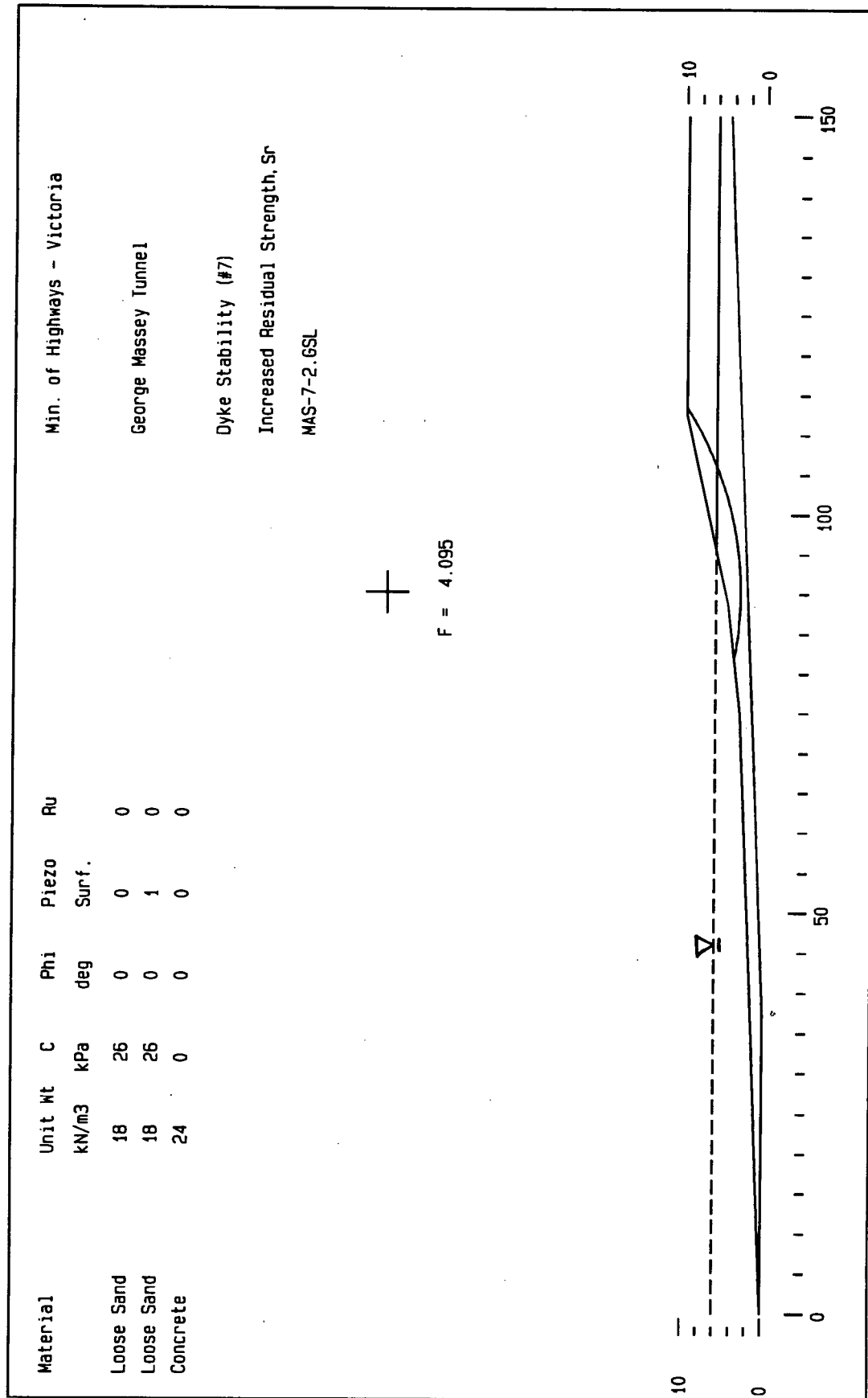


Figure C.2.1 - Post-liquefaction Stability Analysis at Location #7 with Increased Residual Strength

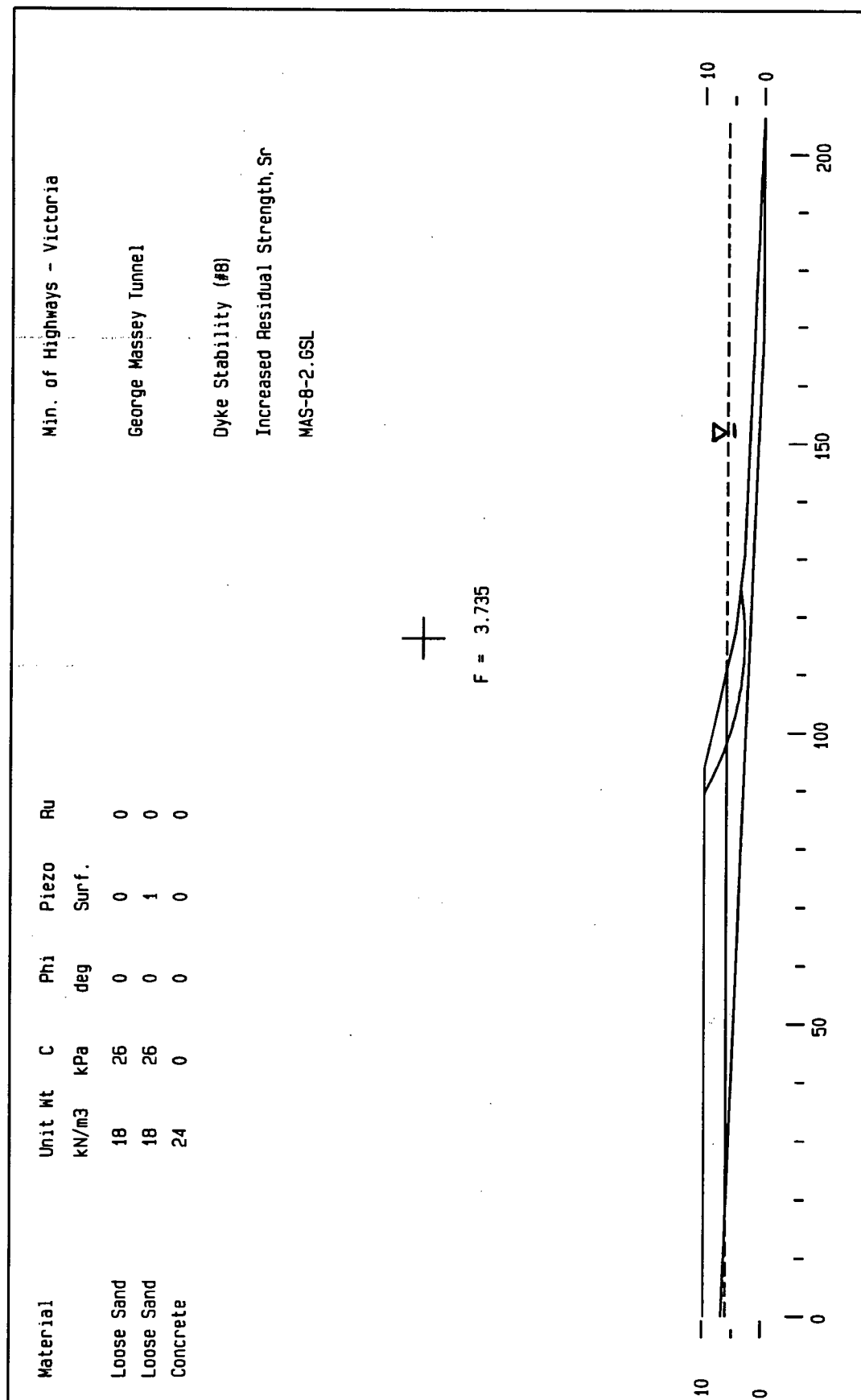


Figure C.2.2 - Post-liquefaction Stability Analysis at Location #8 with Increased Residual Strength

C.3 Residual Strength (S_r) in Sands -- Stark & Mesri (1992)

The Stark & Mesri method of estimating residual strength is discussed in section 4.3.2. This appendix provides more details about their procedure.

Stark & Mesri based their findings on comparison of:

- back-calculations of shear strength from case-histories (including the Seed & Harder (1990) data base) of liquefaction failure. (Back-calculated shear strengths were normalized with respect to pre-liquefaction overburden pressure.), and
- the cyclic shear stress, at 15 equivalent cycles (earthquake magnitude, $M=7.5$) causing liquefaction (i.e., yield strength of the soil) -- estimated using Seed's chart (Seed et al. 1984 -- refer to section 4.2.1).

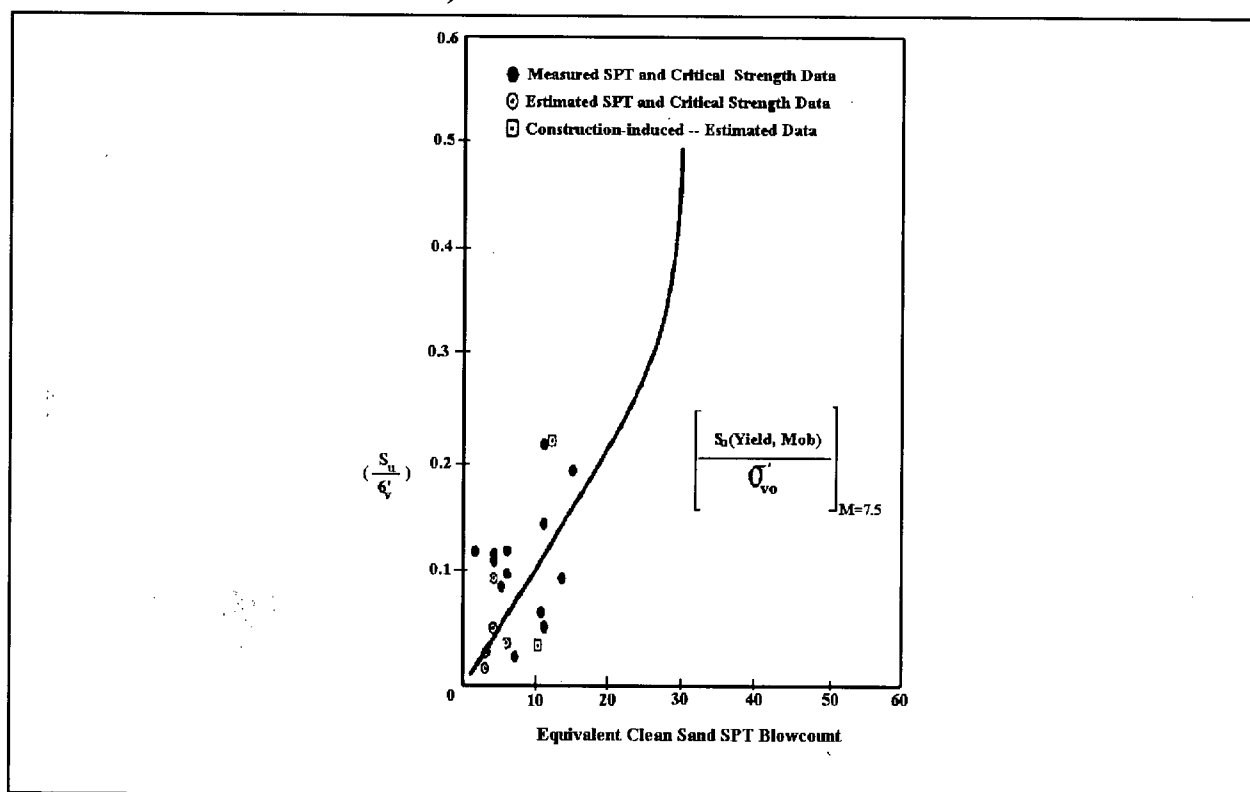


Figure C.3.1 - Comparison of Undrained Critical Strength Ratios and Yield Strength Ratios Back-calculated from Field Case-histories (after Stark & Mesri, 1992)

Some data used by Seed & Harder (1990) in developing their S_r - correlation (figure C.3.1) is based on soils that had enough time to drain after the post-liquefaction flow; therefore, by the time the liquefied mass came to rest, the residual strength was actually greater than the initial yield strength that controls the triggering of liquefaction (Stark & Mesri, 1992).

C.4 Residual Strength -- Seed & Harder (1990)

This approach is based on back-analysis of liquefaction case histories where values of the residual strength were calculated for soil zones in which Standard penetration test (SPT) results were available. The Seed & Harder (1990) residual strength magnitudes were back-calculated using limit equilibrium analyses, the final geometry of the slide mass, and varying failure surfaces to approximate the lower bound estimate of the residual strength. It shows a large scatter in its data, so at low blow count magnitudes (i.e., less than $(N_1)_{60} = 10$) there is significant uncertainty in the S_r estimates. Overall, blow count magnitudes at the tunnel site are low, so results from the Seed correlation can be considered unreliable and, therefore, have only been provided as a reference. The Seed & Harder (1990) (figure C.4.1) predictions for liquefied layers at larger depths will be conservative because the large confining stresses (at greater depths) will not be acknowledged.

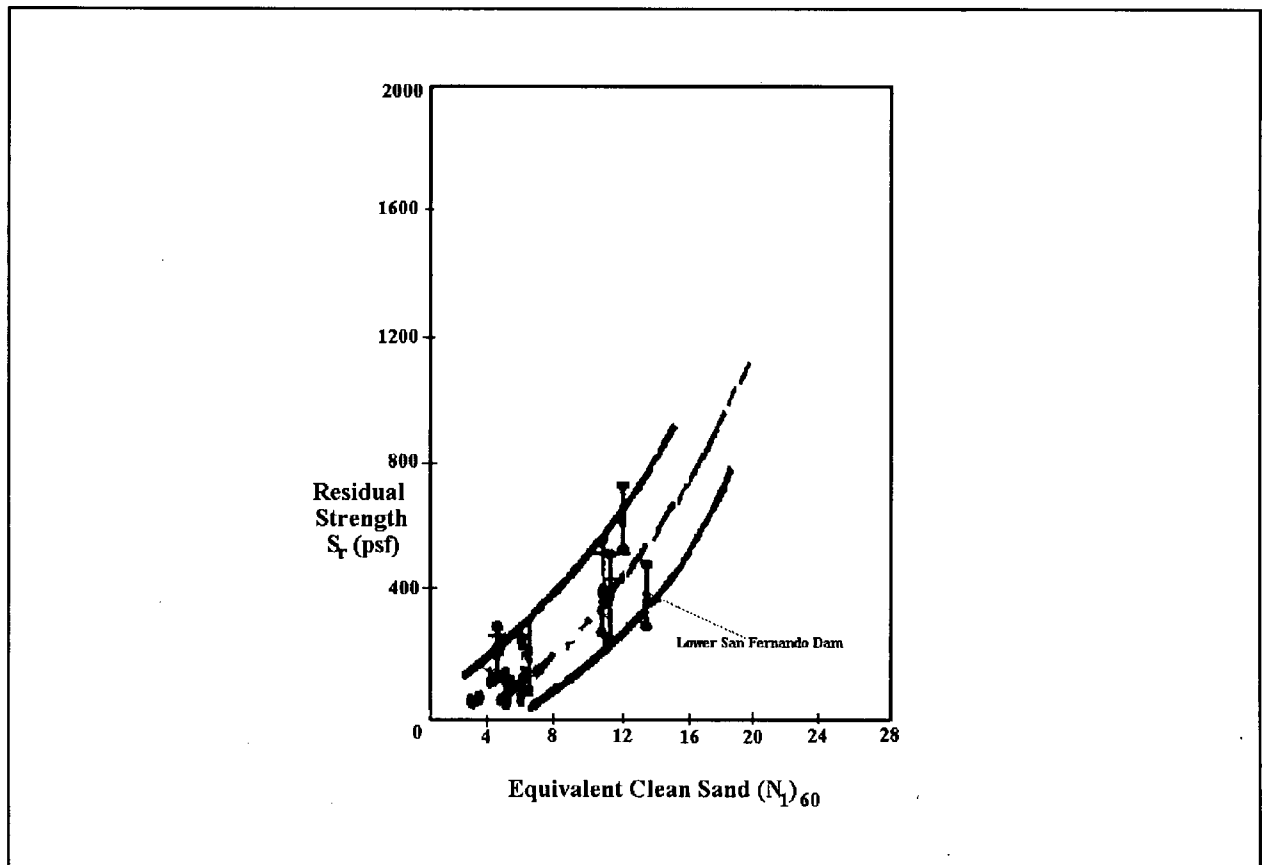


Figure C.4.1 - Relationship Between Residual Strength and $(N_1)_{60}$ (after Seed & Harder, 1990)

S_r - estimates using the Seed & Harder (1990) correlation are summarized in table C.4.1.

$(N_1)_{60}$	Corrected $(N_1)_{60}$			S_r (psf)			S_r (kPa)		
	5%	15%	35%	5%	15%	35%	5%	15%	35%
5	5	6	8	50 (0-225)	100 (25-325)	200 (75-425)	2.39 (0-10.8)	4.79 (1.2-15.6)	9.58 (3.6-20.4)
10	10	11	13	325 (175-525)	400 (200-625)	530 (325-800)	15.56 (8.4-25.2)	19.2 (9.6-30.0)	25.38 (15.6-38.4)
15	15	16	18	700 (450-925)	790 (500-1050)	1010 (760-1200)	33.52 (21.6-44.4)	37.83 (24.0-50.4)	48.36 (36.5-57.6)

Table C.4.1 - Residual Strength Estimates -- Seed & Harder (1990)

Note: Values in brackets indicate the upper and lower bounds of the S_r predictions

APPENDIX D

EMPIRICAL METHOD DISPLACEMENT PREDICTIONS

Appendix D.1 -- Bartlett/Youd: Analysis Details

Appendix D.1.1 -- Displacement Predictions with Epicentral Distance of 30km and Varying Ground Slopes

Layer #	M	R (km)	S (%)	T ₁₅ (m)	F ₁₅ (%)	(D ₅₀) ₁₅ (mm)	Log(D _h +0.01) (m)	D _h (m)
1	7	30	1	6	5	0.3	-0.353	0.434
2	7	30	1	4	45	0.1	-1.304	0.0497
							Total	0.484
1	7	30	3	6	5	0.3	-0.148	0.711
2	7	30	3	4	45	0.1	-1.100	0.0794
							Total	0.790

Table D.1.1 - Bartlett/Youd Parameters and Displacement Predictions at Location #2 -- R=30km

Layer #	M	R (km)	S (%)	T ₁₅ (m)	F ₁₅ (%)	(D ₅₀) ₁₅ (mm)	Log(D _h +0.01) (m)	D _h (m)
1	7	30	1	2	80	0.3	-3.582	2.6e-4
1	7	30	3	2	80	0.3	-3.378	4.2e-4

D.1.2 - Bartlett/Youd Parameters and Displacement Predictions at Location #3 -- R=30km

Layer #	M	R (km)	S (%)	T ₁₅ (m)	F ₁₅ (%)	(D ₅₀) ₁₅ (mm)	Log(D _h +0.01) (m)	D _h (m)
1	7	30	1	2	80	0.3	-1.781	0.0166
1	7	30	3	2	80	0.3	-1.576	0.0265

D.1.3 - Bartlett/Youd Parameters and Displacement Predictions at Location #4 -- R=30km

Layer #	M	R (km)	S (%)	T ₁₅ (m)	F ₁₅ (%)	(D ₅₀) ₁₅ (mm)	Log(D _h +0.01) (m)	D _h (m)
1	7	30	1	6	5	0.3	-0.353	0.434
2	7	30	1	8	30	0.17	-0.790	0.162
							Total	0.596
1	7	30	3	6	5	0.3	-0.148	0.711
2	7	30	3	8	30	0.17	-0.585	0.250
							Total	0.961

Table D.1.4 - Bartlett/Youd Parameters and Displacement Predictions at Location #8 -- R=30km

Appendix D.1.2 -- Displacement Predictions with Epicentral Distance of 60km and Varying Ground Slopes

Layer #	M	R (km)	S (%)	T ₁₅ (m)	F ₁₅ (%)	(D ₅₀) ₁₅ (mm)	Log(D _h +0.01) (m)	D _h (m)
1	7	60	1	6	5	0.3	-1.022	0.0095
2	7	60	1	4	45	0.1	-1.973	0.0106
							Total	0.1056
1	7	60	3	6	5	0.3	-0.817	0.152
2	7	60	3	4	45	0.1	-1.769	0.017
							Total	0.169

Table D.1.5 - Bartlett/Youd Parameters and Displacement Predictions at Location #2 -- R=60km

Layer #	M	R (km)	S (%)	T ₁₅ (m)	F ₁₅ (%)	(D ₅₀) ₁₅ (mm)	Log(D _h +0.01) (m)	D _h (m)
1	7	60	1	2	80	0.3	-4.251	6e-5
1	7	60	3	2	80	0.3	-4.047	9e-5

D.1.6 - Bartlett/Youd Parameters and Displacement Predictions at Location #3 -- R=60km

Layer #	M	R (km)	S (%)	T ₁₅ (m)	F ₁₅ (%)	(D ₅₀) ₁₅ (mm)	Log(D _h +0.01) (m)	D _h (m)
1	7	60	1	2	80	0.3	-2.450	0.0035
1	7	60	3	2	80	0.3	-2.245	0.0057

D.1.7 - Bartlett/Youd Parameters and Displacement Predictions at Location #4 -- R=60km

Layer #	M	R (km)	S (%)	T ₁₅ (m)	F ₁₅ (%)	(D ₅₀) ₁₅ (mm)	Log(D _h +0.01) (m)	D _h (m)
1	7	60	1	6	5	0.3	-1.022	0.095
2	7	60	1	8	30	0.17	-1.459	0.035
							Total	0.13
1	7	60	3	6	5	0.3	-0.817	0.152
2	7	60	3	8	30	0.17	-1.254	0.056
							Total	0.21

Table D.1.8 - Bartlett/Youd Parameters and Displacement Predictions at Location #8 -- R=60km

Appendix D.2 -- Hamada: Analysis Details**Appendix D.2.1 -- Model Details**

The Hamada model was developed using pre- and post-earthquake aerial photographs. From these, vector maps of liquefaction induced ground displacements were developed based on ground deformation patterns within areas of similar surface topography. Figure D.2.1 shows a displacement vector map for part of the Niigata site.

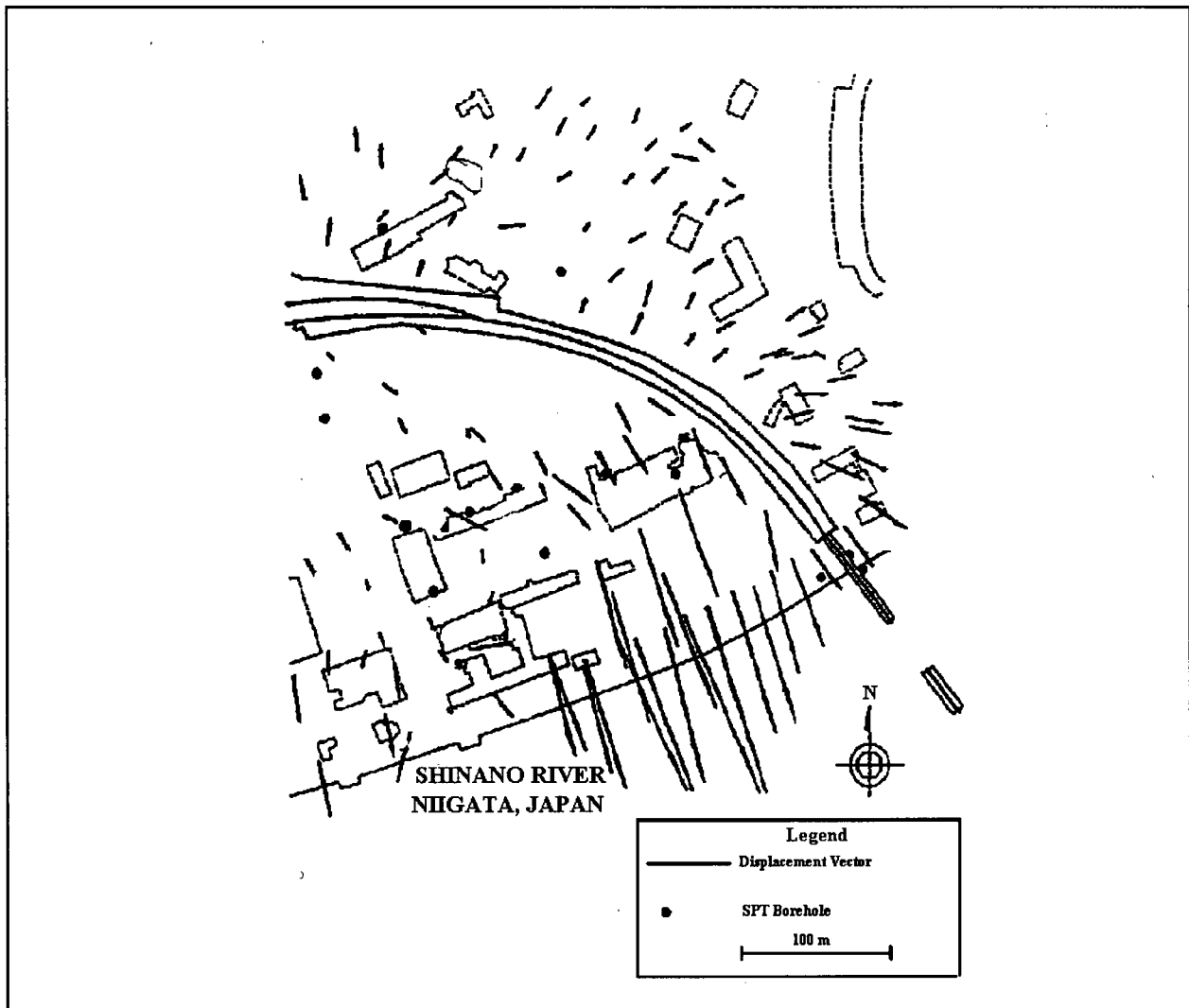


Figure D.2.1- Displacement Vectors and SPT Boreholes for Part of Niigata, Japan Analysis by Hamada (From Bartlett & Youd, 1992)

Appendix D.2.2 -- Hamada Displacement Predictions with Varying Ground Slopes

Layer #	Thickness (m)	Slope (%)	Displacement (m)
1	6	1	1.84
2	8	1	1.5
		Total	3.34
1	6	3	2.64
2	8	3	2.16
		Total	4.80

Table D.2.1 -- Hamada Parameters and Predictions at Location #2

Layer #	Thickness (m)	Slope (%)	Displacement (m)
1	2	1	1.06
1	2	3	1.52

Table D.2.2 -- Hamada Parameters and Predictions at Location #3

Layer #	Thickness (m)	Slope (%)	Displacement (m)
1	2	1	1.06
1	2	3	1.52

Table D.2.3 -- Hamada Parameters and Predictions at Location #4

Layer #	Thickness (m)	Slope (%)	Displacement (m)
1	6	1	1.84
2	8	1	2.12
		Total	3.96
1	6	3	2.64
2	8	3	3.05
		Total	5.69

Table D.2.4 -- Hamada Parameters and Predictions at Location #8

Appendix D.3 -- Tokimatsu/Seed: Analysis Details

Layer #	Thickness (m)	CSR	$(N_1)_{60}$	Volumetric Strain (%)	Settlement (m)
1	2	0.403	13	2.1	0.042
2	4	0.327	13	2.1	0.084
3	4	0.259	5	4	0.16
				Total	0.286

Table D.3.1 - Tokimatsu/Seed Parameters and Predictions at Location #2

Layer #	Thickness (m)	CSR	$(N_1)_{60}$	Volumetric Strain (%)	Settlement (m)
1	2	0.41	8	2.9	0.058

Table D.3.2 - Tokimatsu/Seed Parameters and Predictions at Location #3

Layer #	Thickness (m)	CSR	$(N_1)_{60}$	Volumetric Strain (%)	Settlement (m)
1	2	0.42	12	2.2	0.044

Table D.3.3 - Tokimatsu/Seed Parameters and Predictions at Location #4

Layer #	Thickness (m)	CSR	$(N_1)_{60}$	Volumetric Strain (%)	Settlement (m)
1	2	0.33	11	2.4	0.048
2	4	0.28	9	2.7	0.108
3	4	0.22	11	2.4	0.096
4	4	0.2	11	2.4	0.096
				Total	0.348

Table D.3.4 - Tokimatsu/Seed Predictions at Location #8

APPENDIX E

Additional Figures & Charts Used in Analyses

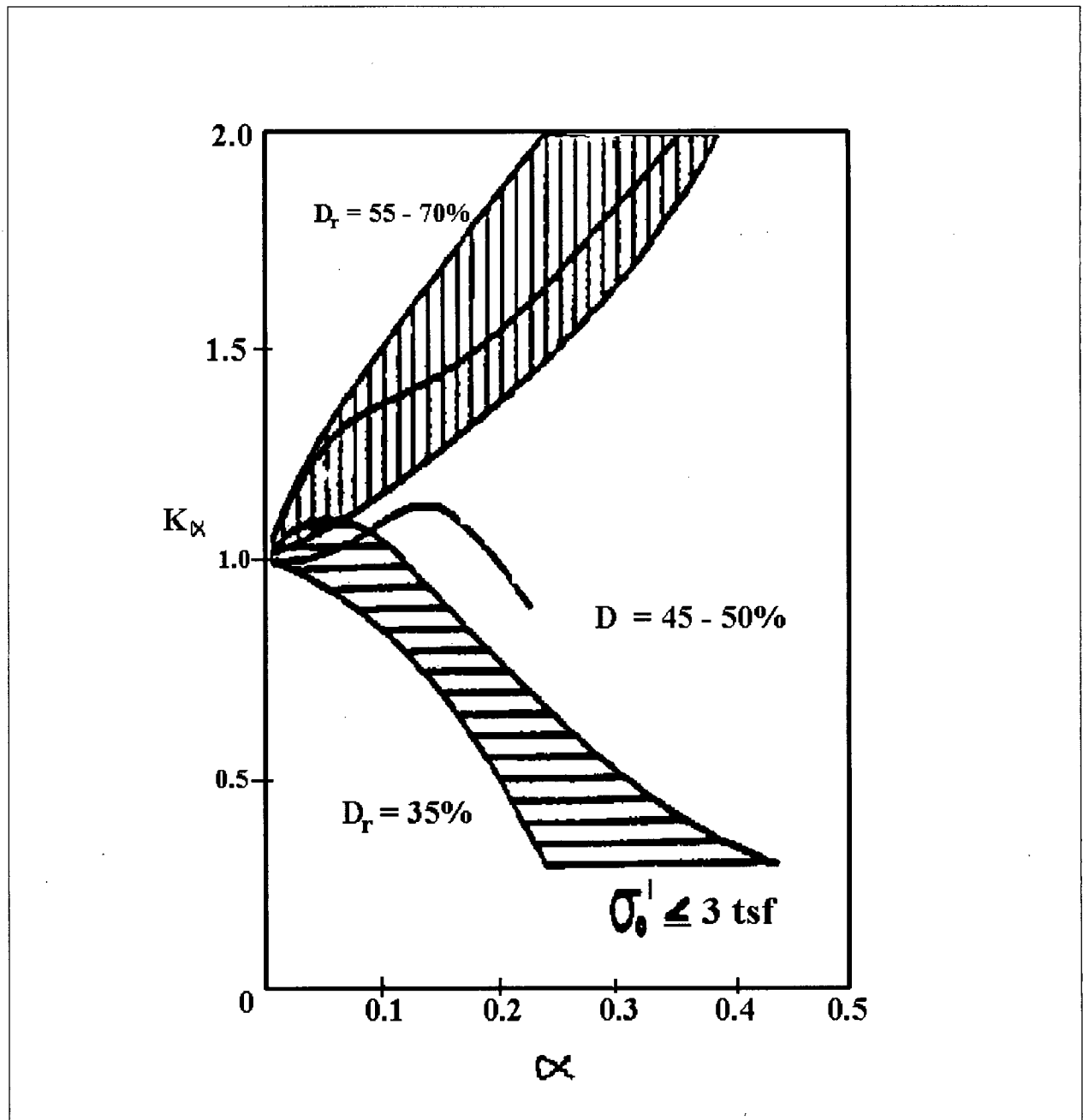


Figure E.1: Ranges in K_α Factors (Seed & Harder, 1990)

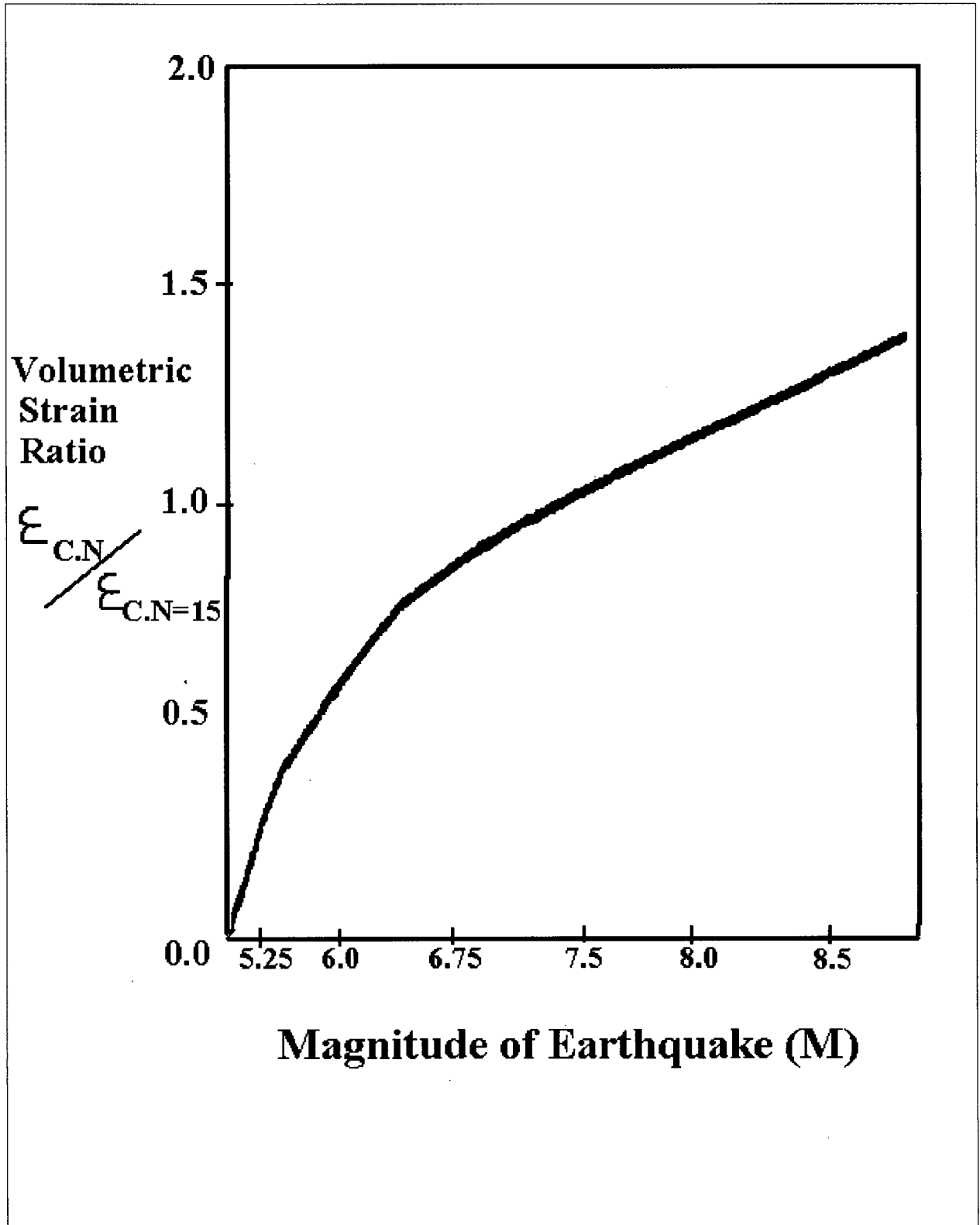


Figure E.2: Relationship between Volumetric Strain Ratio and Number of Cycles (Earthquake Magnitude) (After Tokimatsu and Seed, 1984)

Earthquake Magnitude (M)	No. of Representative Cycles at $0.65 \tau_0$	Magnitude or Duration Correction Factor: K_M
8.5	26	0.89
7.5	15	1.0
6.75	10	1.13
6.0	5 - 6	1.32
5.25	2 - 3	1.5

Table E.1: Correction Factors for Magnitude (after Seed et al., 1984)

APPENDIX F

Remediation Estimations For Each Location

Depth (meters)	SOIL TYPE	CSR	Ksig	Km	(CRR)req	[(N1)60]req		
						5%	15%	35%
0.8	Sand	0.47	1	1.1	0.51272727	<u>30</u>	23	20
2.3	Sand	0.46	1	1.1	0.50181818	<u>30</u>	23	20
3.7	Sand	0.46	1	1.1	0.50181818	<u>30</u>	23	20
5.2	Sand	0.44	1	1.1	0.48	<u>30</u>	23	20
6.1	Silt	0.43	1	1.1	0.46909091	30	23	<u>20</u>
6.5	Sand	0.43	1	1.1	0.46909091	30	23	<u>20</u>
7.7	Silt	0.41	1	1.1	0.44727273	30	23	<u>20</u>
9.7	Silt	0.38	1	1.1	0.41454545	29	22	19

Table F.1 -- Estimation of Blowcounts Required to Prevent Liquefaction at Location #2

Depth (meters)	SOIL TYPE	CSR	Ksig	Km	(CRR)req	[(N1)60]req		
						5%	15%	35%
0.8	Sand	0.5	1	1.1	0.54545455	30	<u>23</u>	20
2.3	Sand	0.49	1	1.1	0.53454545	<u>30</u>	23	20
3.7	Silt	0.48	1	1.1	0.52363636	30	23	<u>20</u>
5.0	Silt	0.46	1	1.1	0.50181818	30	23	<u>20</u>

Table F.2 -- Estimation of Blowcounts Required to Prevent Liquefaction at Location #3

Depth (meters)	SOIL TYPE	CSR	Ksig	Km	(CRR)req	[(N1)60]req		
						5%	15%	35%
0.3	Sand	0.47	1	1.1	0.51272727	<u>30</u>	23	20
1.1	Sand	0.47	1	1.1	0.51272727	<u>30</u>	23	20
2.2	Sand	0.47	1	1.1	0.51272727	<u>30</u>	23	20
3.7	Silt	0.46	1	1.1	0.50181818	30	23	<u>20</u>
5.5	Silt	0.44	1	1.1	0.48	30	23	<u>20</u>
6.7	Silt	0.42	1	1.1	0.45818182	30	<u>23</u>	20

Table F.3 -- Estimation of Blowcounts Required to Prevent Liquefaction at Location #4

APPENDIX F Remediation Estimations

Depth (meters)	SOIL TYPE	CSR	Ksig	Km	(CRR)req	[(N1)60]req		
						5%	15%	35%
0.3	Sand	0.28	1	1.1	0.30545455	26	<u>20</u>	17
1.6	Sand	0.41	1	1.1	0.44727273	30	<u>23</u>	20
3.6	Sand	0.46	1	1.1	0.50181818	30	<u>23</u>	20
5.4	Sand	0.44	1	1.1	0.48	<u>30</u>	23	20
7.1	Sand	0.39	1	1.1	0.42545455	<u>30</u>	23	20
9.6	Sand	0.34	1	1.1	0.37090909	<u>28</u>	21	18
12.8	Sand	0.31	0.98	1.1	0.34508349	<u>28</u>	21	18
15.8	Sand	0.28	0.96	1.1	0.31818182	<u>26</u>	20	17
19.3	Sand	0.25	0.9	1.1	0.3030303	<u>26</u>	20	17
22.8	Sand	0.22	0.89	1.1	0.26966292	<u>24</u>	19	16
27.8	Sand	0.19	0.85	1.1	0.24385027	<u>22</u>	17	14
33.5	Sand	0.16	0.8	1.1	0.21818182	<u>20</u>	15	13

Table F.4 -- Estimation of Blowcounts Required to Prevent Liquefaction at Location #7

Depth (meters)	SOIL TYPE	CSR	Ksig	Km	(CRR)req	[(N1)60]req		
						5%	15%	35%
1.0	Sand	0.54	1	1.1	0.58909091	<u>30</u>	23	20
2.9	Sand	0.52	1	1.1	0.56727273	<u>30</u>	23	20
4.9	Sand	0.48	1	1.1	0.52363636	<u>30</u>	23	20
6.8	Sand	0.44	1	1.1	0.48	<u>30</u>	23	20
8.2	Sand	0.41	1	1.1	0.44727273	<u>30</u>	23	20
9.8	Sand	0.37	1	1.1	0.40363636	<u>29</u>	22	19
12.0	Sand	0.34	0.98	1.1	0.37847866	<u>29</u>	22	19
15.2	Sand	0.31	0.96	1.1	0.35227273	<u>28</u>	21	18
17.9	Sand	0.28	0.92	1.1	0.33201581	<u>28</u>	21	18
19.2	Sand	0.26	0.91	1.1	0.31168831	<u>26</u>	20	17
20.7	Sand	0.24	0.9	1.1	0.29090909	<u>26</u>	20	17
21.7	Sand	0.23	0.89	1.1	0.28192033	<u>25</u>	19	18

Table F.5 -- Estimation of Blowcounts Required to Prevent Liquefaction at Location #8

APPENDIX G

Available Soil Data

APPENDIX G.1

CPT & Borehole Soil Profiles and Summaries

Massey Tunnel

Operator : GILLESPIE

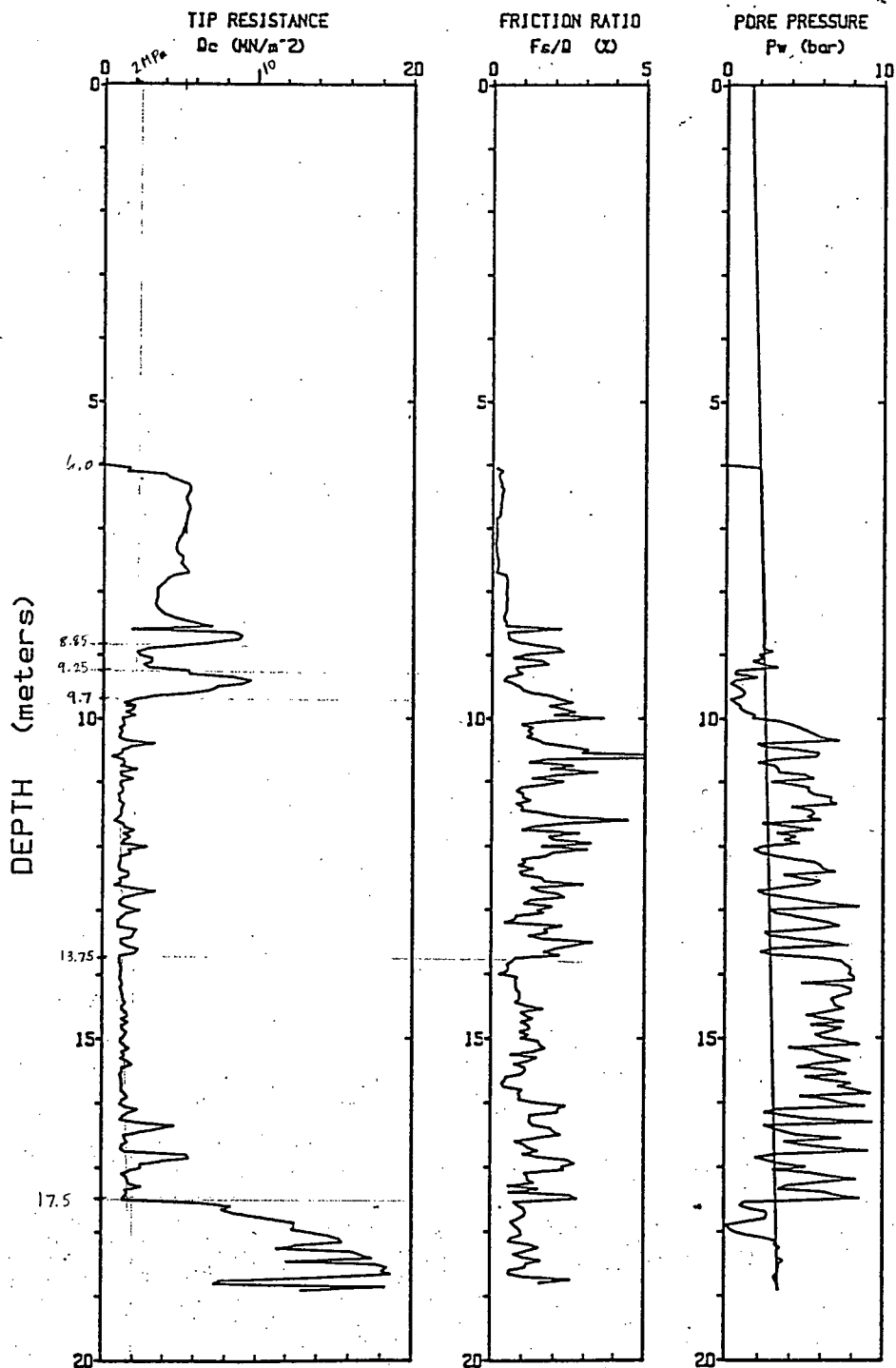
CPT Data : 91/03/14 13:30

Sounding : 16 Pg 1 / 1

Location : MASSEY 91-2

Cone Used : NS100 SEISMIC

Job No. : Z



Depth Increment : .05 m

Max Depth : 18.90 m

STRATIGRAPHY Based on CPT 91-2

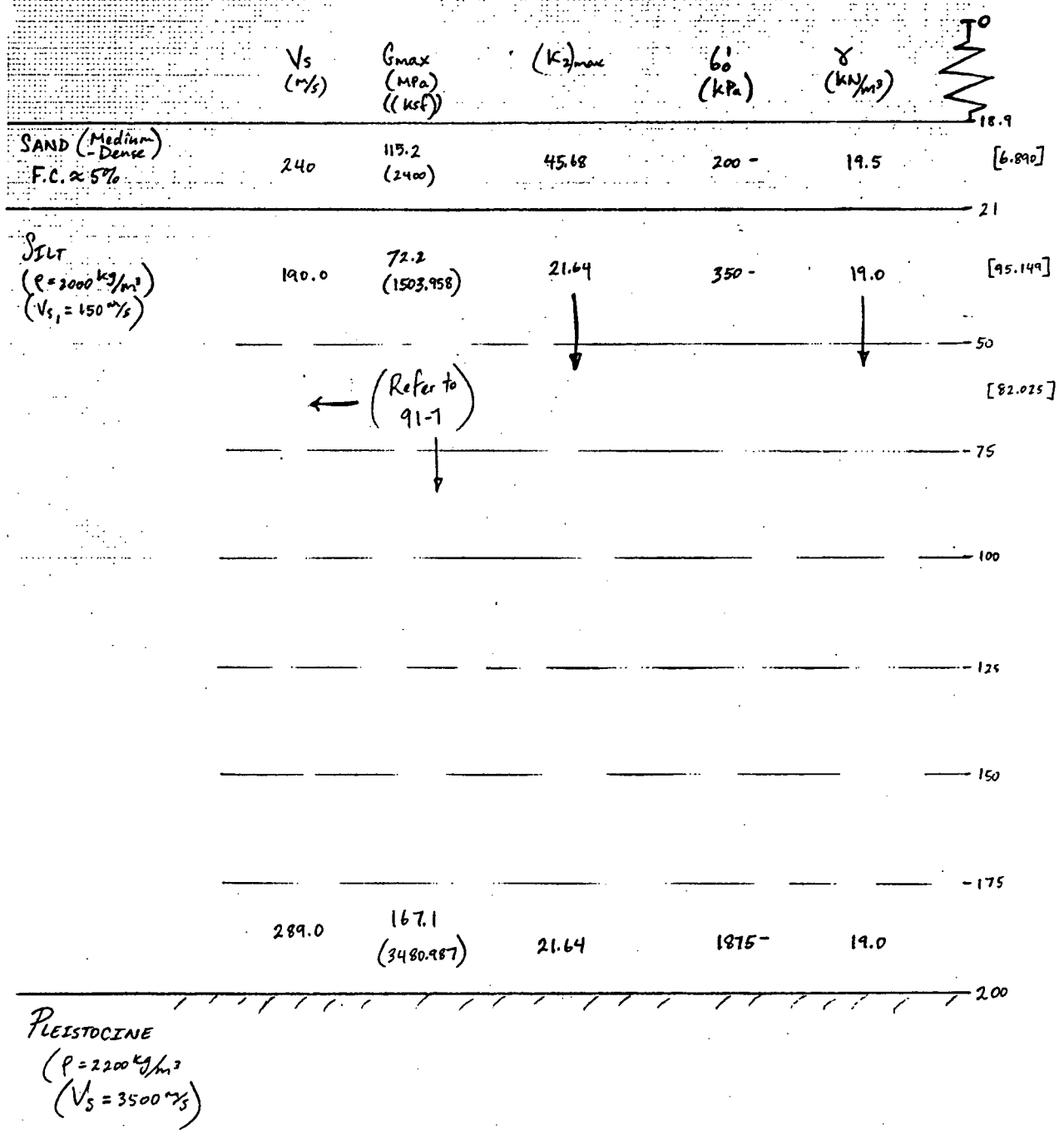
	SHEAR WAVE		R _f	B _g	N _i	6 ₀	D _r	φ	S _u /6 ₀	O.C.R.	C _{max}	γ
	V _s (m/s)	(K _s) _{max} (MPa) (kN/m ²)										
No DATA												
												-1
												-2 m
												-3
SAND* Layer ① L ②	185	63.10 (68.385) (1426.042)										18.5
												-4
	*185	53.25 (1426.042)										18.5
												-5
												-6 m
SAND (Medium) (F.C. ≈ 5%) Layer ① L ②	160	35.34 (51.169) (1066.667)	8	8	13	66	45	39°	N.A.	N.A.	500	18.5
												-7
		31.90 (1066.667)				81						16.5
												-8
												-10 m
Sandy Silt	160	30.45 (1066.667)	7	7	17	89	~	~	1.0	*	500	18.5
Silty Sand (F.C. ≈ 5%)	160	29.77 (1066.667)	8	8	18	93	N.A.	N.A.	N.A.	N.A.	550	19.5
												-9
												-10 m
Clayey Silt (N.C. Clay) (Sub-layers) - Non-Plastic (B.H. #7 & #8)	175	61.192 (1276.042) 33.52	5-6	N.A.	5	97	N.A.	N.A.	1.1	5.5	1100	19.0
						105						-11
						115						-12
												-13
												-14 m
Clayey Silt (High Clay Content) (could be silty clay) - Plastic; Non-liquefiable (based on CHINESE criteria (See B.H. #7))	185	68.985 (1426.042) 31.88	6	N.A.	5	133	N.A.	N.A.	0.25	4.1	1000	19.0
												-15
	195					164						-16
												-17
												-18 m
Sand (Medium-Dense) (F.C. ≈ 5%)	240	115.094 (42.15) (2400)	9	9	17	180	65	39	N.A.	N.A.	1000	19.5
						185						-19
												-19 (End)

Continued on Next Page...

* Judgement

... cont.

CPT 91-2



Massey Tunnel

Operator : GILLESPIE

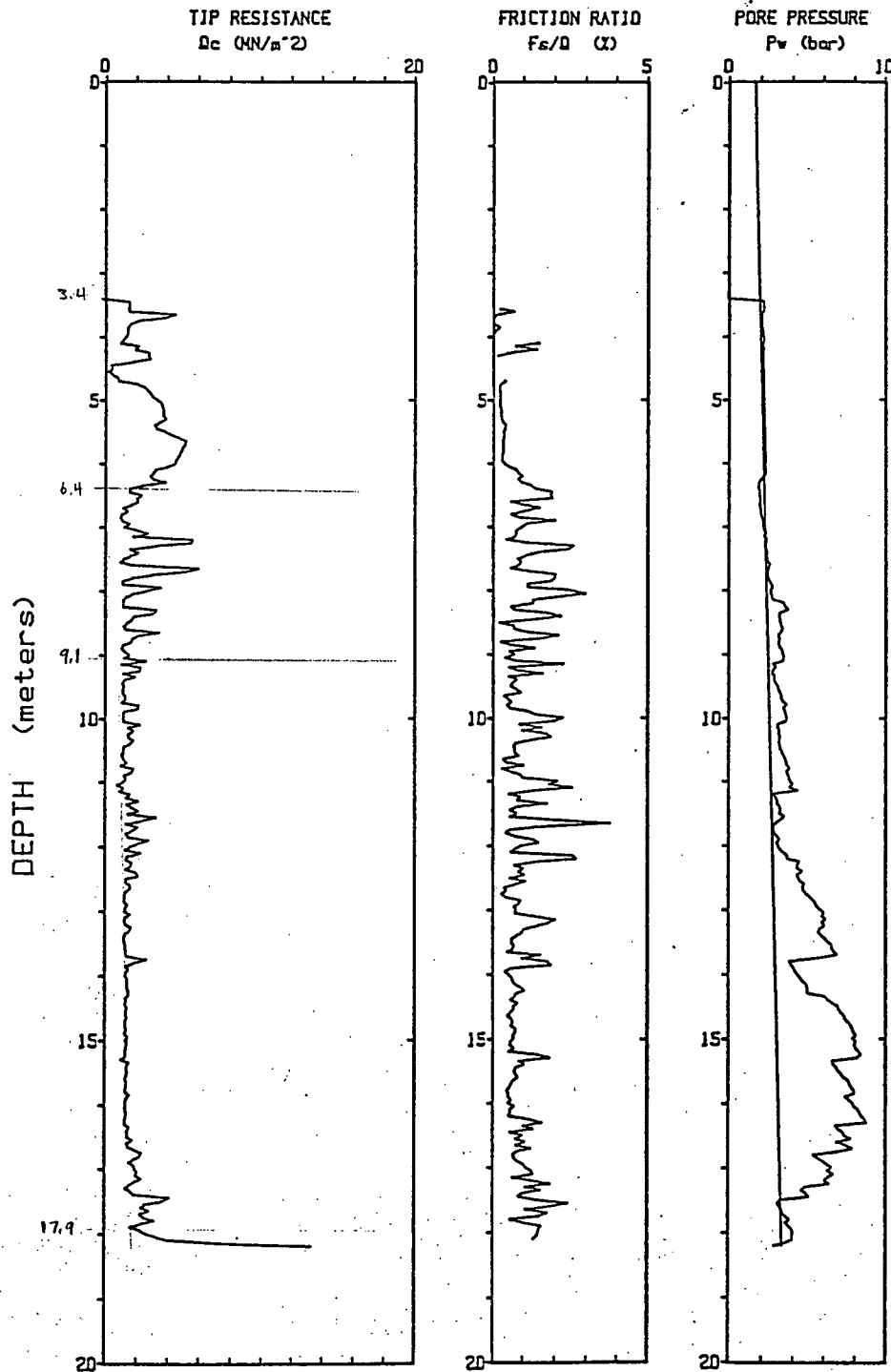
CPT Date : 91/03/15 14:00

Sounding : 16 Pg 1 / 1

Location : MASSEY 91-3

Cone Used : NS100 SEISMIC

Job No. : Z



Depth Increment : .05 m

Max Depth : 18.20 m

Idealized STRATIGRAPHY Based on CPT 91-3

SHEAR WAVE (SEPT)													METER
V_s (m/s) (*Normalized)	G_{max} (MPa) (kip/ft ²)	R_f zone (#)	E_v zone (#)	N_1 (blows/ft) (#)	G_s (kPa) (#)	D_r (%) (Estimate) (from N_1)	ϕ (degrees)	$S_u/60$	O.C.R.	G_{max} (MPa)	γ (%)		
No DATA													0m
													-1
													-1.9
													-3 (4.921)
													-3.4
Silty Sand (loose) (F.C. $\approx 15\%$)													-4 (5.25')
142	39.2 (816.7) $K_2=35.66$	7-8	7-8	11	42	30	37	N.A.	N.A.	30	18.5 (F.C.)	-5	
Sand (loose) (F.C. $\approx 5\%$)													-6 (4.593')
HYDRAULIC FULL ENDS													-6.4
													-7
Sandy Silt Sub ①													-8 (8.858')
143	39.2 (816.7) $K_2=26.09$	6-7	6	8	77	N.A.	N.A.	1.8	11	110	19.0	-9	
- Non-Plastic Sub ②													-9.1
													-10 (9.514')
Clayey Silt Sub ①													-11
155	48.05 = P_{u2} (1001.0) $K_2=27.64$				95			1.3	7.5	110	19.0 (low N_1)	-10	
- (may be) Plastic; Non-liquefiable (see B.H. # 5 Summary)													-11
Sub ②													-12
													-13
Sub ①													-14 (19.357')
													-15
Clayey Silt Sub ②													-16
150	45.0 (937.5) $K_2=21.64$				136			0.75	4.0	105	19.0	-14	
- Non-liquefiable (same as preceeding unit)													-15
Sub ③													-16
													-17
													-18
													-19
													-20
													-21m

(See Next Page for
Extrapolated Layer Inputs)



CPT 91-3

	V_s (m/s) ($V_{s1} = 150$ m/s in SALT)	σ_{max} (MPa) (kip/ft ²)	$(K_p)_{max}$	N_1 (Blow/ft)	σ'_v (kPa)	D_r (%)	S_u (kPa)	σ_{CR} (MPa)	γ (kN/m ³)	z (m)
SAND (Medium-Dense) (F.C. \approx 5%)	240	115.2 (2400)	45.18	17	200	65		1000	19.5	(13.45)
	189.31	67.94 (1415.41)	21.64	310				19.0	(59.25)	22
SILT ($\rho = 2000$ kg/m ³)	207.71	86.28 (1797.57)	21.64	500				19.0	(65.61)	40
	225.93	102.09 (2126.91)	21.64	700				19.0		60
	240.58	115.76 (2411.69)	21.64	900				19.0		80
	261.18	136.43 (2842.21)	21.64	1250				19.0	(82.02)	100
	269.87	145.66 (3034.65)	21.64	1425				19.0	(114.22)	125
SILT ↳ M3-S.dat	[581.07]	[742.81] [15475.12]	[110.34]					19.0	[21.5]	160
[PLEISTOCENE] ↳ M3-P.dat	286.10	163.71 (3410.65)	21.64	1800				19.0	(131.23)	200
	[616.01]	[834.84] [17392.53]	[110.34]					19.0	[21.5]	
PLEISTOCENE ($\rho = 2200$ kg/m ³) * $V_s = 3500$ ft/s	668.74	983.87 (20497.29)	110.34	2500				21.5	(328.08)	300
	[310.59]	[192.94] [4019.49]	[21.64]							
[SILT]	727.43	1164.13 (24252.72)	110.34	3500				21.5		400
	774.60	1320.00 (27500.)	110.34	4500				21.5		500
	814.45	1459.32 (30402.39)	110.34	5500				21.5		600
	849.18	1586.44 (33050.89)	110.34	6500				21.5		700m
BEDROCK								$V_s = 8000$ ft/s $\gamma = 23$ kN/m ³		

These Inputs (for the Pleistocene) were applied for Experimental SHAKE analyses ONLY.
Bedrock Depth Estimate $\approx 700\text{m}$

Massey Tunnel

Operator : GILLESPIE

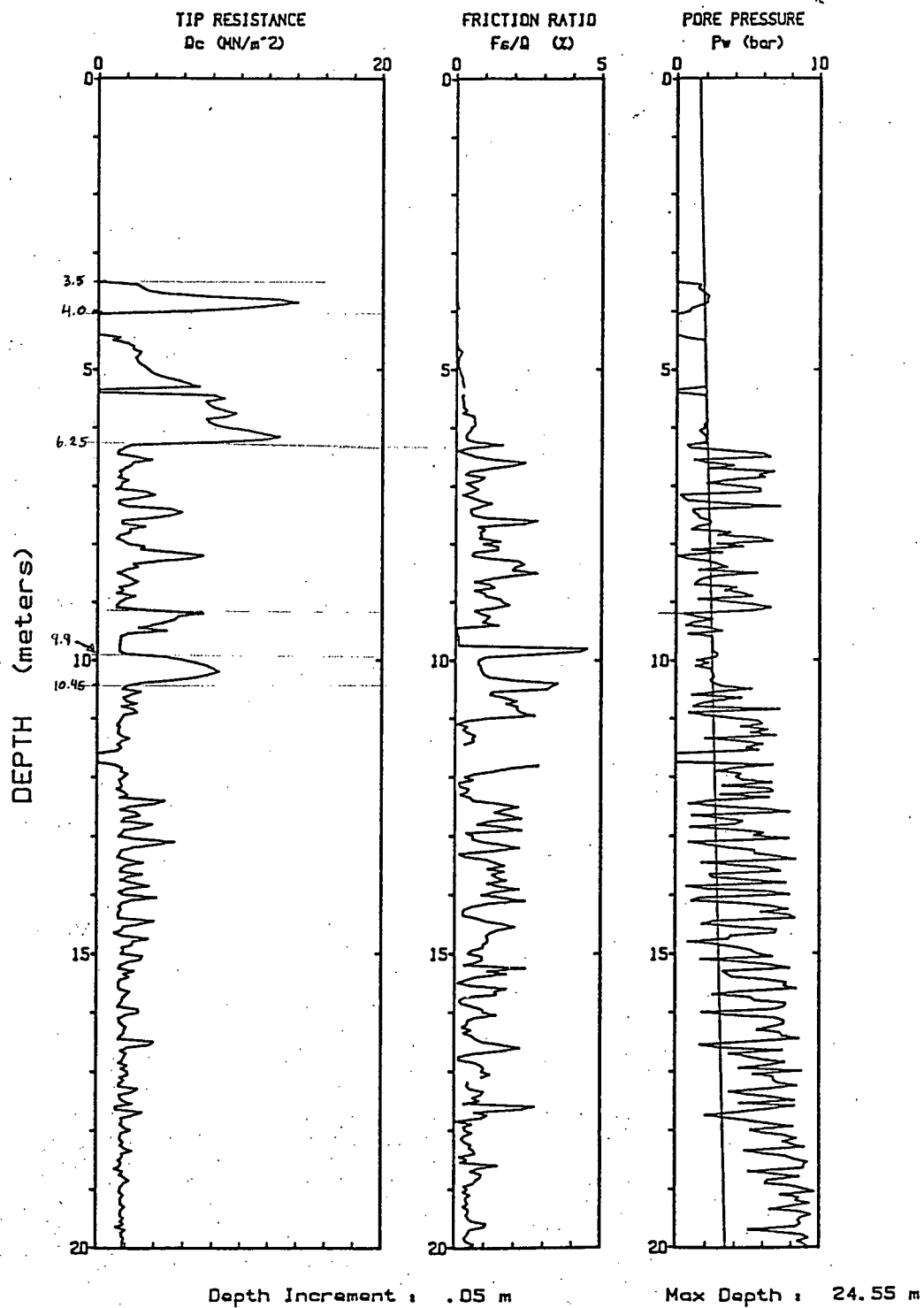
CPT Date : 91/03/16 12:30

Sounding : 19 Pg. 1 / 2

Location : Massey 91-4

Cone Used : NS100 SEISMIC

Job No. : Z



Massey Tunnel

Operator : GILLESPIE

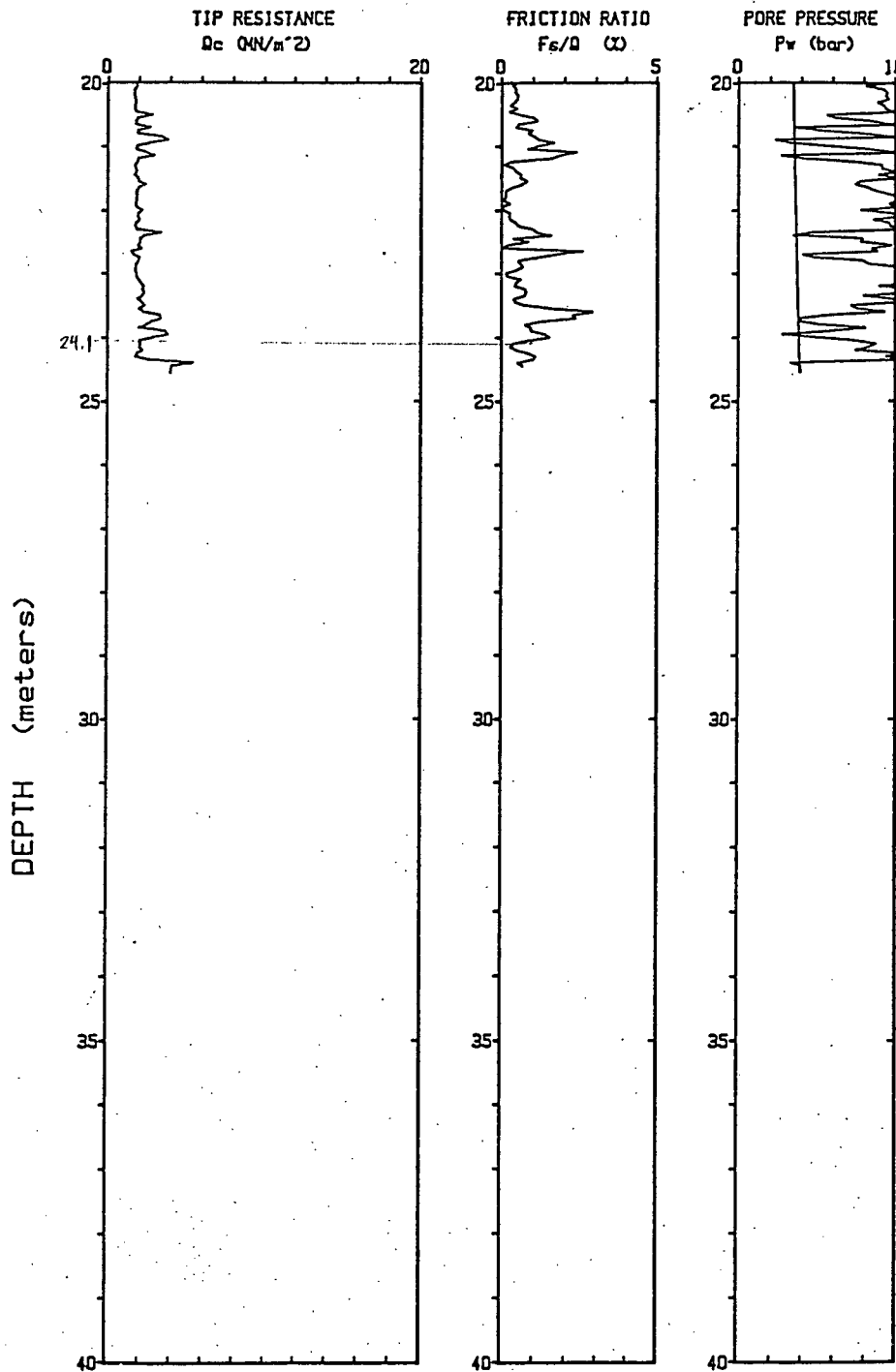
CPT Date : 91/03/16 12:30

Sounding : 19 Pg 2 / 2

Location : Massey 91-4

Cone Used : NS100 SEISMIC

Job No. : Z



Depth Increment : .05 m

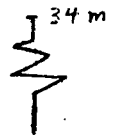
Max Depth : 24.55 m

IDEALIZED STRATIGRAPHY based on CPT 91-4

SHEAR WAVE													
V_s (m/s)	G_{max} (MPa) (ksf)	R_f Zone (#)	B_q Zone (#)	N_i (blows)	b'_0 (kPa)	D_r (%)	ϕ	S_u/b'_0	O.C.R.	G_{max} (bars)	γ (kN/m ³)		
$f(K_2)_{max}$												0	
												-2 m	
SAND (Dense)	184	$K_2 = 62.42$ (57.7 MPa) (1410.6 ksf)	9	9	23	37	80	41	N.A.	N.A.	19.5	3.5	(1.640')
Sand (Medium) (F.C. ~ 5%)	160*	$K_2 = 35.15$ (42 MPa) (876.0 ksf)	8	8	22	40	55	40	N.A.	N.A.	19.0	4	(7.382')
Sandy Silt (Loose) (F.C. ~ 85%)	150*	$K_2 = 27.21$ (937.5 MPa) (208.5 ksf)	6-7	7-8	12	66	N.A.	N.A.	2.5	15	1500	8	(5.988')
Silty Sand (Medium) (F.C. ~ 15%)	160*	$K_2 = 26.17$ (937.5 MPa) (208.5 ksf)	8	8	20	93	50	39	N.A.	N.A.	18.6	10.45	(1.805')
Sandy Silt (Sub-layers)	182	$K_2 = 34.26$ (1365.0 kPa) (306.5 ksf)	6	6	5	130	1.4	8	1650	18.5	12	11.648	
Sandy Silt (Non-liquefiable)	181	$K_2 = 20.54$ (950.0 kPa) (212.5 ksf)	6	6	5	145	N.A.	N.A.	1.1	6.5	1500	12.5	(9.843')
Sandy Silt (Sub-layers)	151	$K_2 = 33.20$ (1700.167 kPa) (375.5 ksf)	4	4	4	175	0.85	4.5	1350	18.5	19.5	16.405	
Sandy Silt (Non-liquefiable)	166	$K_2 = 14.99$ (816.47 kPa) (183.5 ksf)	6-7	6-7	5	215	N.A.	N.A.	3.5	350	18.5	24	(6.890')
Sandy Silt (Non-liquefiable)	140					230						24.1	

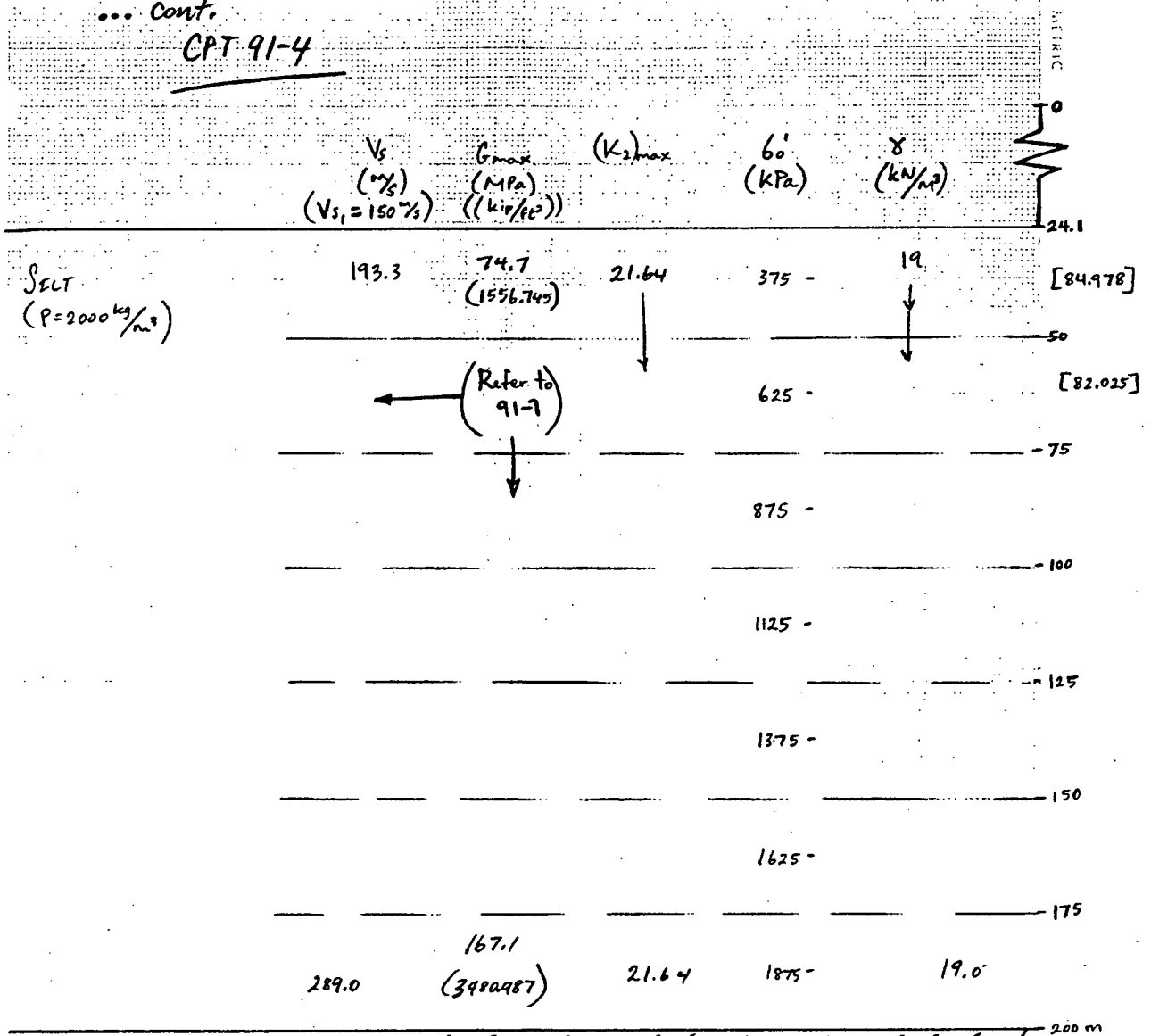
* denotes estimates based on magnitudes within other profiles.

Continued
(Next Page)



... cont.

CPT 91-4



PELLESTOCINE

$V_s = 3500 \text{ m/s}$

Massey Tunnel

Operator : GILLESPIE

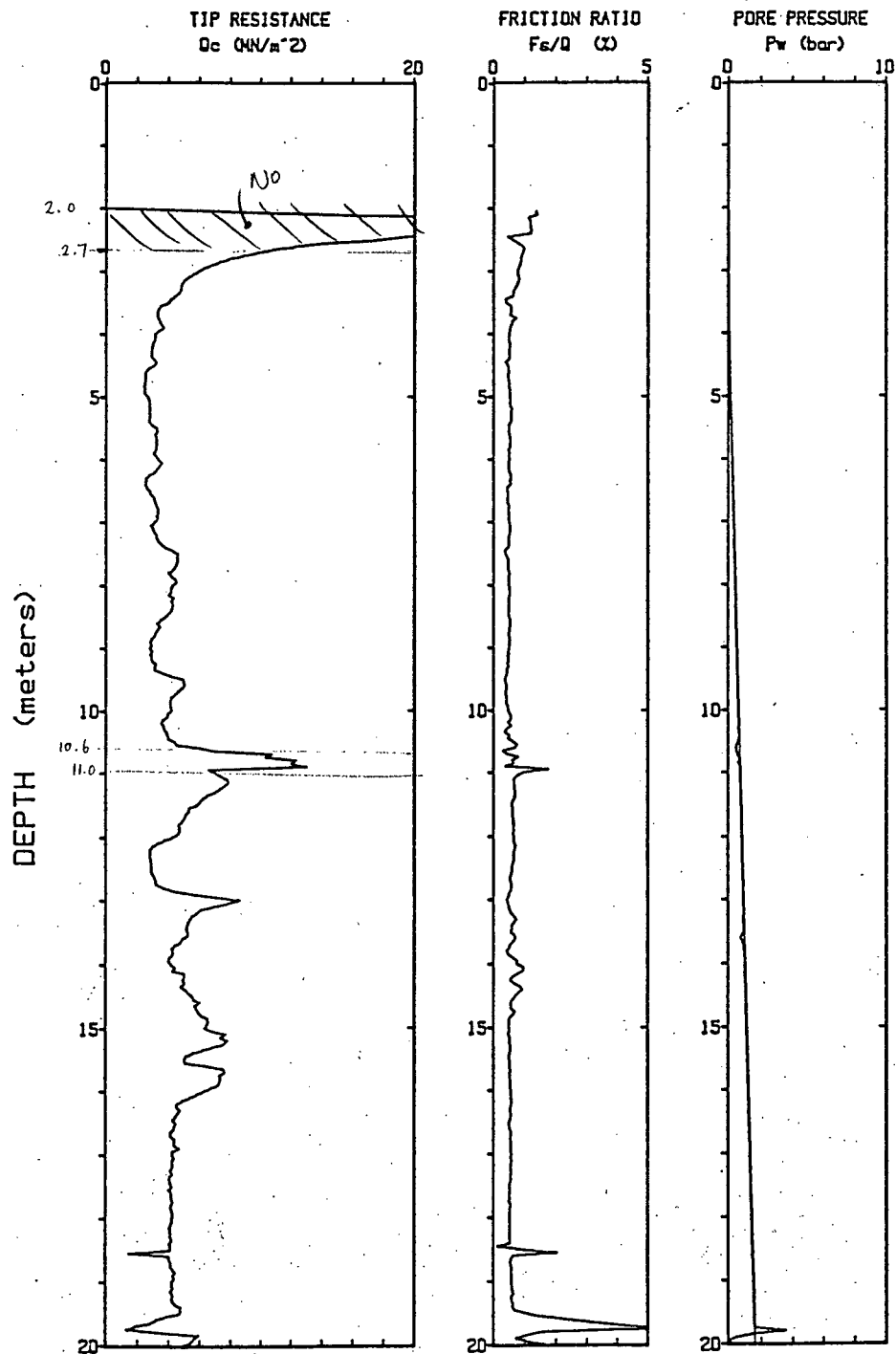
CPT Data : 91/04/10 10:45

Sounding : 41 Pg 1 / 2

Location : MASSEY 91-07

Cone Used : NS100 SEISMIC

Job No. : Z



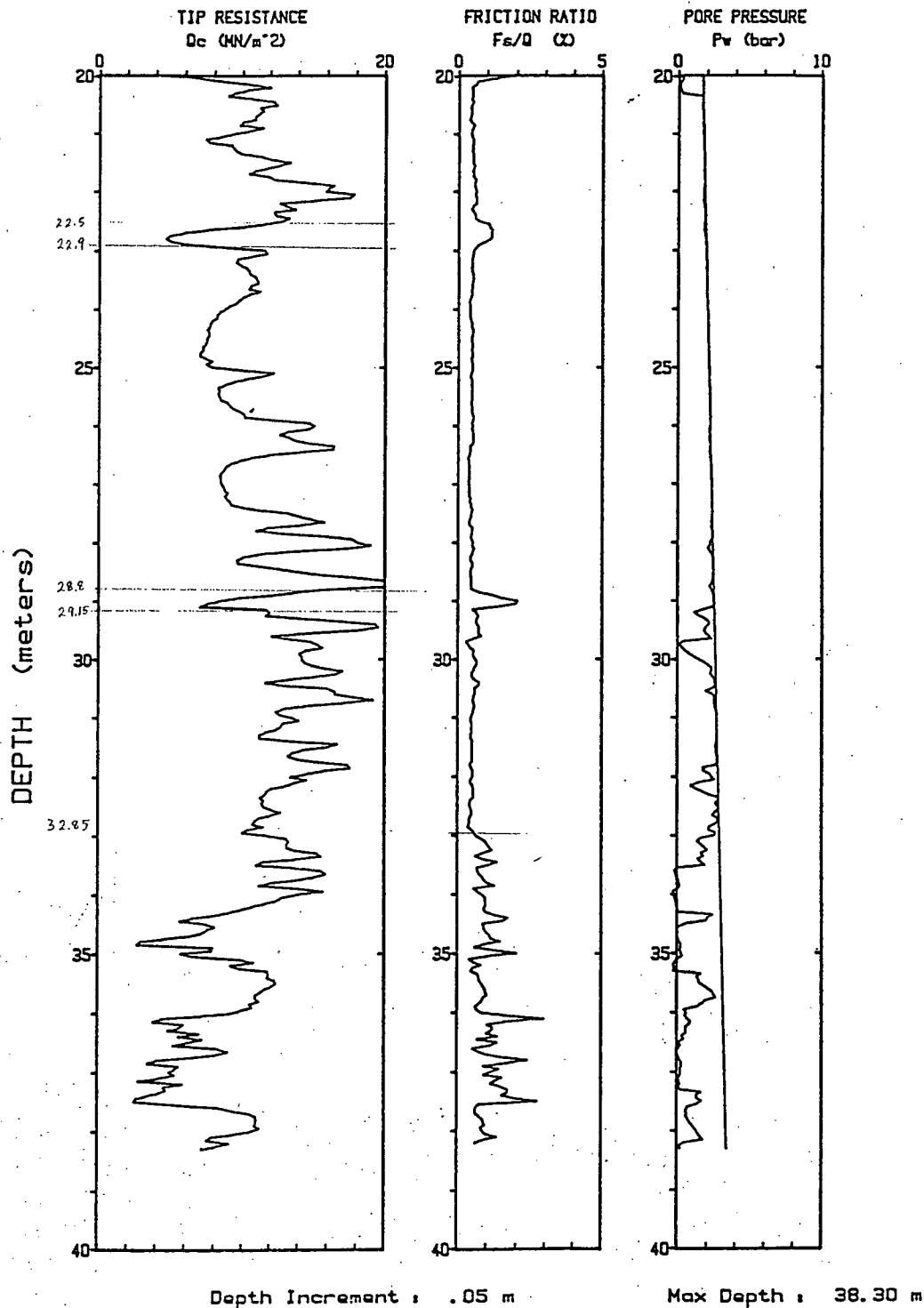
Depth Increment : .05 m

Max Depth : 38.30 m

Massey Tunnel

Operator : GILLESPIE
Sounding : 41 Pg 2 / 2
Cone Used : NS100 SEISMIC

CPT Date : 91/04/10 10:45
Location : MASSEY 91-07
Job No. : Z



STRATIGRAPHY BASED ON CPT 91-7 (W.T. @ 3.3 m)

		SHEAR WAVE (SPT)		R _f		B _f		N _i		G _i		D _r		K _r		G _{max}		γ	
		V _s	G _{max}	Zone	Zone	(#)	(#)	(#)	(#)	(%)	(%)	(%)	(%)	(%)	(%)	(bars)	(kN/m ²)	(%)	(%)
		(# Normalized)	(MPa)	(#)	(#)	(#)	(#)	(#)	(#)	(%)	(%)	(%)	(%)	(%)	(%)	(bars)	(kN/m ²)	(%)	(%)
		f(K _s) _{max}																	
		0																	
		2m																	
Silty Sand (FC=15%)		-110	(504.167) - 24.2MPa K _s =17.82					58											
			(504.167)					66											
			K ₂ =16.70					80											
Silty Sand (Loose) (FC=15%)		-110	(504.167) - 7-8	7-8	12			88	25	35						360	18.5	6m	
			K ₂ =14.47																
			(504.167)					111											
			K ₂ =12.88	7-8	7-8	9			25	35						450	18.0	8m	
			(504.167)					128											
			K ₂ =11.99																
GRAVEL		-160						138	87	89						500	27.0	10.6m	
			(1066.667) - 51.15MPa					145											
			K ₂ =23.84					150											
Sand (Loose) (FC=5%)		-170	(1066.667)	8	8	9		170	30	33						550	18.0	14m	
			(1066.667)																
			K ₂ =21.40					180											
			(816.667) - 39.18MPa																
Silty Sand (FC=15%)		-140	K ₂ =15.54	7	N.A.	7		200	20	31						500	18.5	18m	
			(2016.667) - 96.71MPa																
			K ₂ =34.47					248	50	37						925	18.5	22m	
			(1504.167) - 72.14MPa																
			K ₂ =24.07	9	9			283	40	35						850	18.0	26m	
			(1204.167) - 105.70MPa																
			K ₂ =33.70					310	55	37						1100	18.0	30m	
			(1204.167)					320											
			(1204.167)																
			K ₂ =17.08	7-8	7-8	10		360	30	31						N.A.	N.A.	650	18.0
			(1204.167)																
			(1204.167)																
			K ₂ =17.08																
			(1204.167)																
			(1204.167)																
			(1204.167)																
			(1204.167)																
			(1204.167)																
			(1204.167)																
			(1204.167)																
			(1204.167)																
			(1204.167)																
			(1204.167)																
			(1204.167)																
			(1204.167)																
			(1204.167)																
			(1204.167)																
			(1204.167)																
			(1204.167)																
			(1204.167)																
			(1204.167)																
			(1204.167)																
			(1204.167)																
			(1204.167)																
			(1204.167)																
			(1204.167)																
			(1204.167)																
			(1204.167)																
			(1204.167)																
			(1204.167)																
			(1204.167)																
			(1204.167)																
			(1204.167)																
			(1204.167)																
			(1204.167)																
			(1204.167)																
			(1204.167)																
		</																	

... Cont.
CPT 91-7

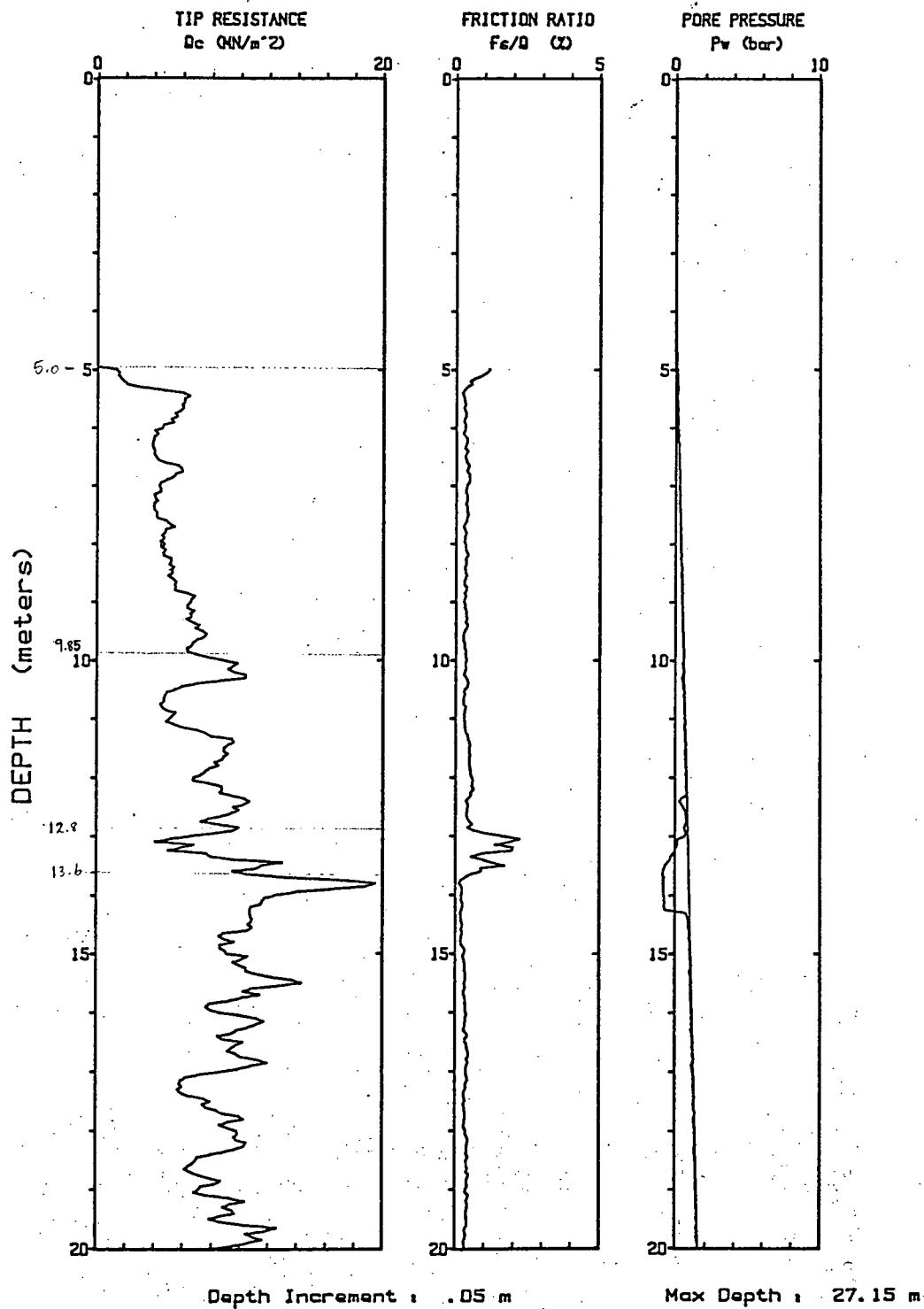
	V_s (m/s) ($V_{s1} = 150 m/s$)	G_{max} (MPa) (Kip/ft^2)	$(K_2)_{max}$	G_o' (KPa)	γ (KN/m^3)
					39.3
SILT ($\rho = 2000 \frac{kg}{m^3}$)	201.2	80.9 (1686.279)	21.64	440 -	19.0 [38.388]
			↓		50
	219.6	96.5 (2009.749)		625 -	[82.625]
					75
	238.9	114.1 (2377.967)		875 -	
					100
	254.4	129.4 (2696.361)		1125 -	
					125
	267.5	143.1 (2980.940)		1375 -	
					150
	278.9	155.6 (3240.623)		1625 -	
					175
	289.0	167.1 (3480.987)	21.64	1875 -	19.0
					200

PLEISTOCENE
($\rho = 2200 \frac{kg}{m^3}$)
 $V_s = 3500 m/s$

Massey Tunnel

Operator : GILLESPIE
Sounding : 13 Pg 1 / 2
Cone Used : NS100 SEISMIC

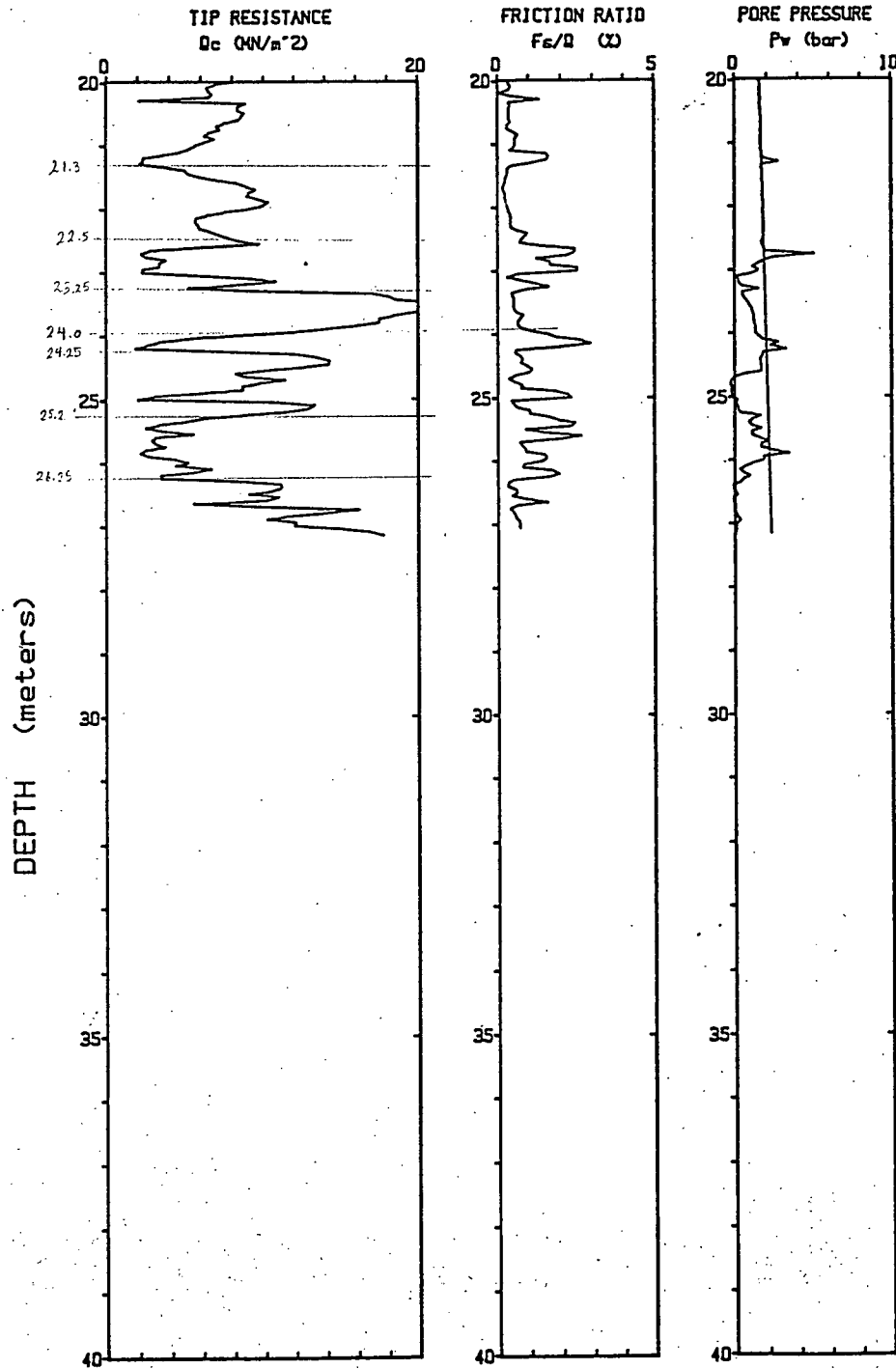
CPT Date : 91/05/15 11:45
Location : MASSEY 91-8
Job No. : Z



Massey Tunnel

Operator : GILLESPIE
Sounding : 13 Pg 2 / 2
Cone Used : NS100 SEISMIC

CPT Date : 91/05/15 11:45
Location : MASSEY 91-8
Job No. : Z



Depth Increment : .05 m

Max Depth : 27.15 m

STRATIGRAPHY BASED ON CPT 91-8 (W.T. @ 4.2 m)

SHEAR WAVE (SCPT)													
(* Normalized)	V _s (m/s)	G _{max} (MPa) (Ksf)	K _s max	R _p Zone (#)	B _q Zone (#)	N _i (blows/ft)	G _o (kPa)	D _r (%)	φ	S _w %	O.C.R.	G _{max} (bars)	γ (KN/m ³)
													0
													-2 m
													-4.2
													50
Sand (Loose - Medium) (F.C. ≈ 5%)	Layer ①	-170	(1204.167) - 57.75 MPa K _s = 32.41				100	-				18.5	-6 (6.398)
	L ②	-150	(937.5) - 44.96 MPa K _s = 23.04	8	8-9	12	120	40	37	N.A.	N.A.	550	" -2 (")
	L ③	-170	(1204.167) K _s = 27.39				140	-					" -7.85 (")
	L ④	-170	(1204.167) K _s = 25.79				158	-					" -12 (")
Silty Sand (F.C. ≈ 15%)		170	(1204.167); K _s = 25.59	7	8	16	161	45	37			720	" -12.8 (2.625)
			(1504.167) - 72.44 MPa										-14
Sand (Loose - Medium) (F.C. ≈ 5%)	Layer ①	-190	K _s = 29.69				186	-					" (7.874)
	L ②	-190	(1504.167) K _s = 28.14	9	9	11	207	50	37	HYDRAULIC FILL		900	" -16 (6.562)
		-190	(1066.667) - 51.15 MPa										-18
Sand (Medium - Loose) (Sub-Layers)		-160	K _s = 18.85	8-9	8-9	9	230	35	35			750	" -20 (14.764)
		-170					234	-					-21.3
													-22
Silty Sand (F.C. ≈ 35%)		170	(1204.167); K _s = 20.50	7	N.A.	8	250	20	30	N.A.	N.A.	520	" -22.5 (2.461)
			(1204.167)										-23.25
Sand (F.C. ≈ 5%)		170	K _s = 19.37	8	9	11	280	40	35			850	" -24 (6.398)
Silty Sand (F.C. ≈ 15%)		170	(1204.167) K _s = 19.38	7-8	8	7	274	30	33			700	" -25.2 (3.281)
Sand (Medium - Loose)		170	(1204.167) K _s = 18.59	9	9	12	304	50	37	N.A.	N.A.	1000	" -26.2 (3.117)
							310	-					-27.15 (END)
													-28
													-30
													-32
													34 m

Continued

... cont.
CPT-91-8

	V_s (m/s) [$V_{s1}=150 \text{ m/s}$]	G_{max} (MPa) (kgf/cm^2)	σ'_v (kPa)	$(K_2)_{max}$	γ (kg/m^3)	
						27.15
SILT ($P=2000 \text{ kg/m}^2$) ($V_s=150 \text{ m/s}$ @ $\sigma'_v=135 \text{ kPa}$)	194.57	75.7 (1577.365)	385 -	21.64 ↓	19.0 ↓	(74.971)
	219.6	96.5 (2009.749)	625 -			50 (82.025)
						- 75
	238.9	114.1 (2377.967)	875 -			- 100
						- 125
	254.4	129.4 (2696.361)	1125 -			- 150
						- 175
	267.5	143.1 (2980.940)	1375 -			- 200 m
	278.9	155.6 (3240.683)	1625 -			
	289.0	167.1 (3480.987)	1875 -	21.64	19.0	

PLEISTOCENE

OFFICE REPORT ON SOIL EXPLORATION

CONTRACT 1277 TUNNEL BORING 2 16-00 40' DATUM GEODETIC CASING 4" PIPE
 BORING DATE MARCH 16-22, 1956 REPORT DATE APRIL 15, 1956 COMPILED BY H.N. CHECKED BY G.T.H.
 SAMPLER HAMMER WT. 140 LBS. DROP 30 INCHES (PENETRATION RESISTANCES CONVERTED TO BLOWS OF 4200 IN - LBS. ENERGY)

SAMPLE CONDITION

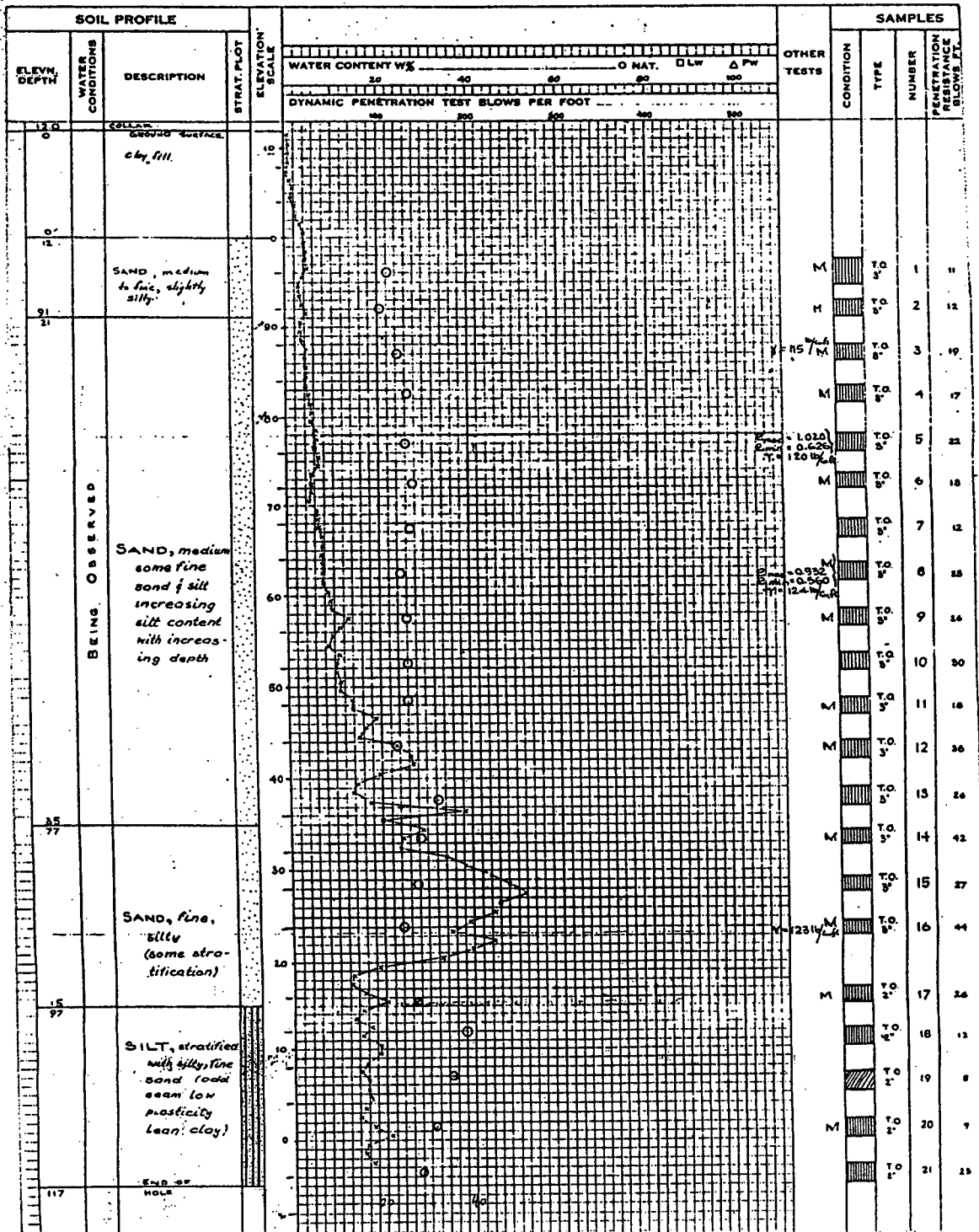
☐ DISTURBED
☐ FAIR
☐ GOOD
☐ LOST

SAMPLE TYPES

A.S. - AUGER SAMPLE
 S.T. - SLOTTED TUBE
 W.S. - WASHED SAMPLE
 D.O. - DRIVE-OPEN
 D.F. - DRIVE-FOOT VALVE
 C.S. - CHURN SAMPLE
 F.S. - FOIL SAMPLE
 S.O. - SLEEVE-OPEN
 S.F. - SLEEVE-FOOT VALVE
 T.O. - THIN WALLED OPEN
 R.C. - ROCK CORE

ABBREVIATIONS

V - IN-SITU VANE TEST
 M - MECHANICAL ANALYSIS
 U - UNCONFINED COMPRESSION
 OC - TRIAXIAL CONSOLIDATED QUICK
 Q - TRIAXIAL QUICK
 S - TRIAXIAL SLOW
 W - WET UNIT WEIGHT
 K - PERMEABILITY
 C - CONSOLIDATION
 WL - WATER LEVEL IN CAS
 WT - WATER TABLE IN SOIL



OFFICE REPORT ON SOIL EXPLORATION

SAMPLE CONDITION

**DISTURBED
FAIR
GOOD
LOST**

A.S. - AUGER SAMPLE
S.T. - SLOTTED TUBE
W.S. - WASHED SAMPLE
D.O. - DRIVE-OPEN
D.F. - DRIVE-FOOT VALVE
C.S. - CHUNK SAMPLE

SAMPLE TYPES

TYPES
F.S. - FOIL SAMPLE
S.O. - SLEEVE OPEN
S.F. - SLEEVE-FOOT VALVE
T.O. - THIN WALLED OPEN
R.C. - ROCK CORE

ABBREVIATIONS

V - IN-SITU VANE TEST
M - MECHANICAL ANALYSIS
U - UNCONFINED COMPRESSION
QC - TRIAXIAL CONSOLIDATED QUICK
Q - TRIAXIAL QUICK
S - TRIAXIAL SLOW

1. WET UNIT WEIGHT
K. PERMEABILITY
C. CONSOLIDATION

WL - WATER LEVEL
WT - WATER TABLE

282

OFFICE REPORT ON SOIL EXPLORATION

SAMPLE CONDITION

SAMPLE TYPES

ABBREVIATIONS

**DISTURBED
FAIR
GOOD
LOST**

A.S. - AUGER SAMPLE
S.T. - SLOTTED TUBE
W.S. - WASHED SAMPLE
D.O. - DRIVE-OPEN
D.F. - DRIVE-FOOT VALVE
C.S. - CHUNK SAMPLE

F.S. - FOIL SAMPLE
S.O. - SLEEVE OPEN
S.F. - SLEEVE-FOOT VALVE
T.O. - THIN WALLED OPEN
R.C. - ROCK CORE

V - IN-SITU VANE TEST
M - MECHANICAL ANALYSIS
U - UNCONFINED COMPRESSION
QC - TRIAXIAL CONSOLIDATED QUICK
Q - TRIAXIAL QUICK
S - TRIAXIAL SLOW

1. WET UNIT WEIGHT
 K. PERMEABILITY
 C. CONSOLIDATION
 WL. WATER LEVEL IN CASING
 WT. WATER TABLE IN SOIL



OFFICE REPORT ON SOIL EXPLORATION

CONTRACT 1277 TUNNEL BORING # 4 DATUM GEOLOGIC CASING 6" 1.4"
 BORING DATE 9-6 APR 1956 REPORT DATE APR 20 1956 COMPILED BY S.A.S. CHECKED BY G.T.H.
 SAMPLER HAMMER WT. 140 LBS. DROP 30 INCHES (PENETRATION RESISTANCES CONVERTED TO BLOWS OF 4200 IN - LBS. ENERGY)

SAMPLE CONDITION

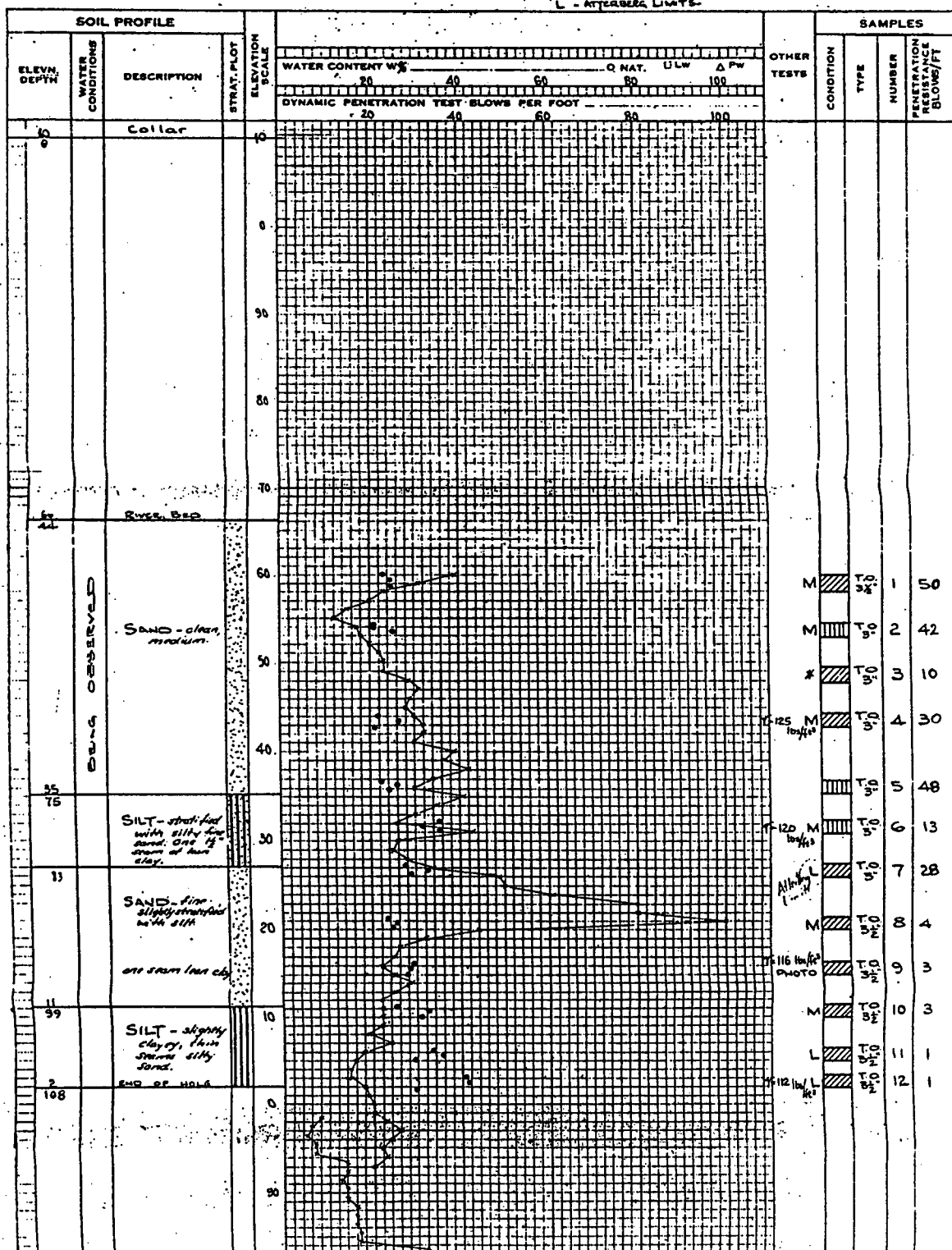
☒ DISTURBED
☐ FAIR
☐ GOOD
☐ LOST

SAMPLE TYPES

A.S. - AUGER SAMPLE
 S.T. - SLOTTED TUBE
 W.S. - WASHED SAMPLE
 D.O. - DRIVE-OPEN
 D.F. - DRIVE-FOOT VALVE
 C.S. - CHUNK SAMPLE
 F.S. - FOIL SAMPLE
 S.O. - SLEEVE-OPEN
 S.F. - SLEEVE-FOOT VALVE
 T.O. - THIN WALLED OPEN
 R.C. - ROCK CORE

ABBREVIATIONS

V - IN-SITU VANE TEST
 M - MECHANICAL ANALYSIS
 U - UNCONFINED COMPRESSION
 QC - TRIAXIAL CONSOLIDATED QUICK
 Q - TRIAXIAL QUICK
 S - TRIAXIAL SLOW
 L - ATTERBERG LIMITS
 W - WET UNIT WEIGHT
 K - PERMEABILITY
 C - CONSOLIDATION
 E - RETAINED IN TUBE
 WL - WATER LEVEL IN CASING
 WT - WATER TABLE IN SOIL



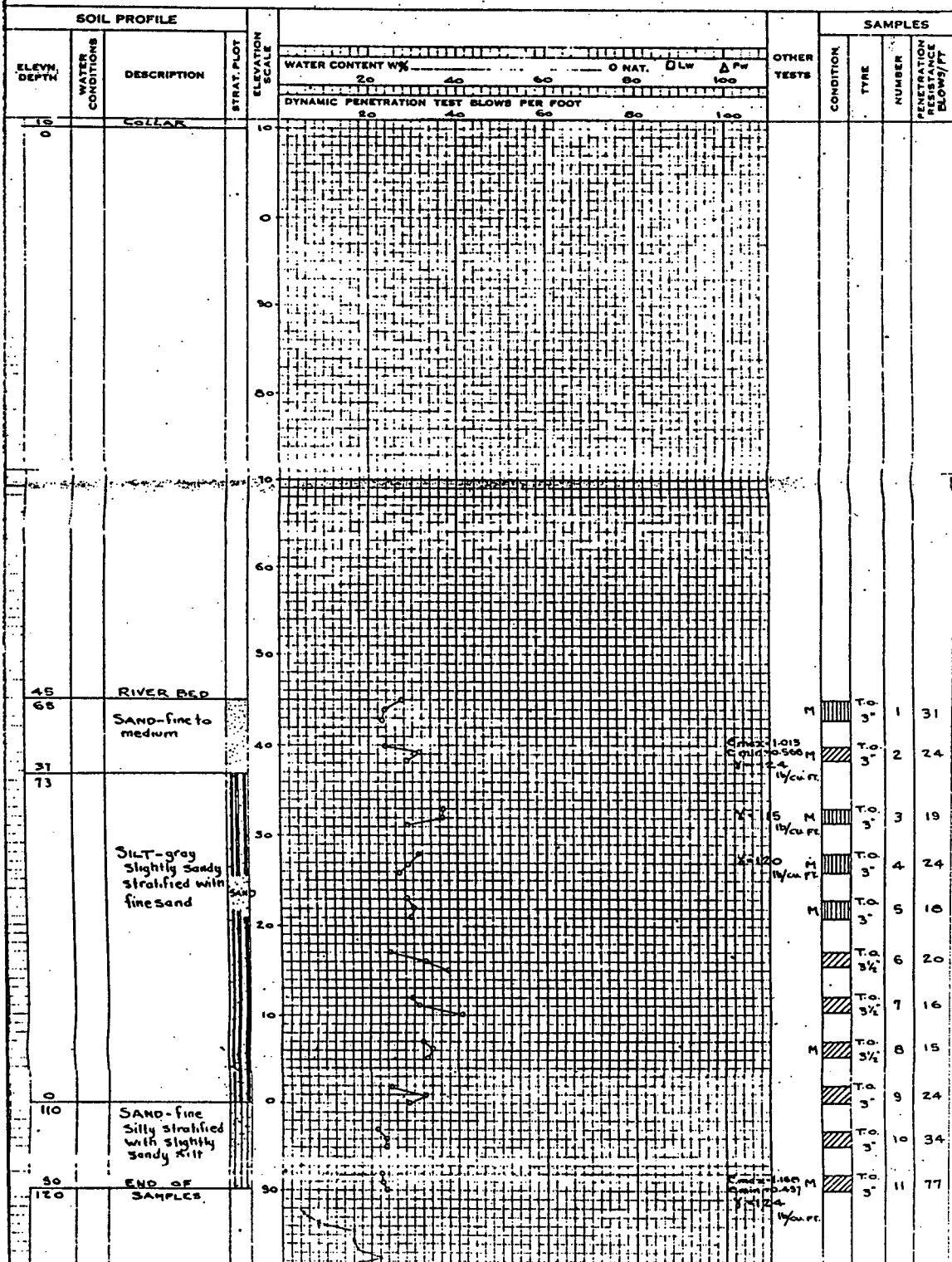
OFFICE REPORT ON SOIL EXPLORATION

CONTRACT 1277-TUNNEL BORING # 6 DATUM GEODETIC CASING 6" & 4" PIPE
 BORING DATE APRIL 23 1966 REPORT DATE APRIL 30 1966 COMPILED BY MN CHECKED BY GTH
 SAMPLER HAMMER WT. 140 LBS. DROP 30 INCHES (PENETRATION RESISTANCES CONVERTED TO BLOWS OF 4200 IN. LBS. ENERGY)

SAMPLE CONDITION
 DISTURBED
 FAIR
 GOOD
 LOST

SAMPLE TYPES
 A.S. - AUGER SAMPLE
 S.T. - SLOTTED TUBE
 W.S. - WASHED SAMPLE
 D.O. - DRIVE-OPEN
 D.F. - DRIVE-FOOT VALVE
 C.S. - CHUNK SAMPLE
 F.S. - FOIL SAMPLE
 S.O. - SLEEVE-OPEN
 S.F. - SLEEVE-FOOT VALVE
 T.O. - THIN WALLED OPEN
 R.C. - ROCK CORE

ABBREVIATIONS
 V - IN-SITU VANE TEST
 M - MECHANICAL ANALYSIS
 U - UNCONFINED COMPRESSION
 CC - TRIAXIAL CONSOLIDATED QUICK
 Q - TRIAXIAL QUICK
 S - TRIAXIAL SLOW
 γ - WET UNIT WEIGHT
 K - PERMEABILITY
 C - CONSOLIDATION
 WL - WATER LEVEL IN CASING
 WT - WATER TABLE IN SOIL

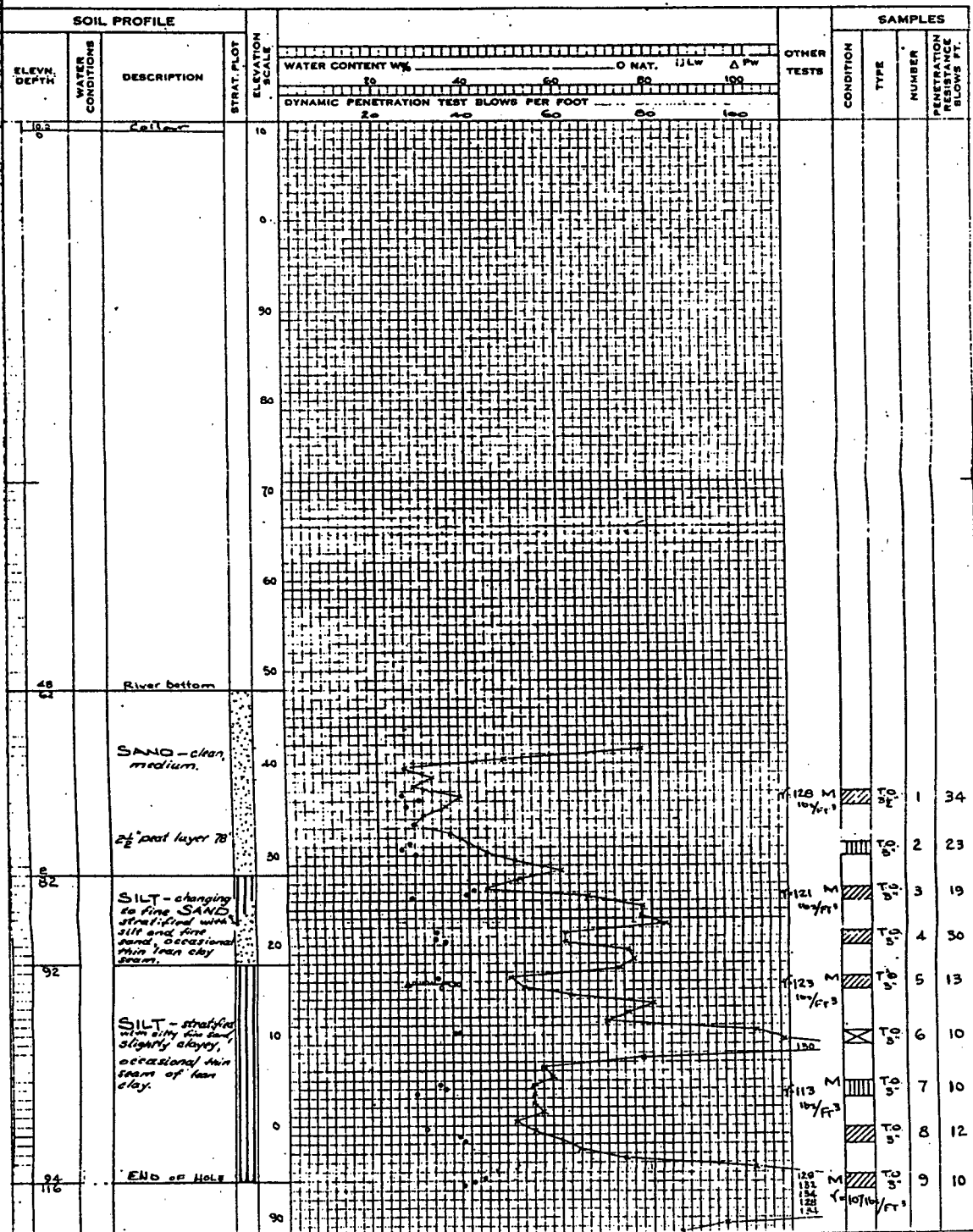


GEOCON

OFFICE REPORT ON SOIL EXPLORATION

CONTRACT 1277 TUNNEL 7 BORING # 7 DATUM GEOPLOTIC CASING 4"
 BORING DATE 7-6 APRIL 1952 REPORT DATE APRIL 30 1952 COMPILED BY RJE CHECKED BY GTH
 SAMPLER HAMMER WT. 140 LBS. DROP 30 INCHES (PENETRATION RESISTANCES CONVERTED TO BLOWS OF 4200 IN - LBS. ENERGY)

SAMPLE CONDITION		SAMPLE TYPES		ABBREVIATIONS	
<input type="checkbox"/> DISTURBED	A.S. - AUGER SAMPLE	F.S. - FOIL SAMPLE	V - IN-SITU VANE TEST	W - WET UNIT WEIGHT	
<input type="checkbox"/> FAIR	S.T. - SLOTTED TUBE	S.O. - SLEEVE-OPEN	M - MECHANICAL ANALYSIS	N - PERMEABILITY	
<input type="checkbox"/> GOOD	W.S. - WASHED SAMPLE	S.F. - SLEEVE-FOOT VALVE	U - UNCONFINED COMPRESSION	C - CONSOLIDATION	
<input type="checkbox"/> LOST	D.O. - DRIVE-OPEN	T.O. - THIN WALLED OPEN	OC - TRIAXIAL CONSOLIDATED QUICK	WL - WATER LEVEL IN CASING	
	D.F. - DRIVE-FOOT VALVE	R.C. - ROCK CORE	Q - TRIAXIAL QUICK	WT - WATER TABLE IN SOIL	
	C.S. - CHUNK SAMPLE		S - TRIAXIAL SLOW		



OFFICE REPORT ON SOIL EXPLORATION

CONTRACT 1277 TUNNEL BORING # B (28.00 404) DATUM GEODETIC CASING 4" PIPE
 BORING DATE MARCH 22-27, 1956 REPORT DATE APRIL 13, 1956 COMPILED BY W.N. CHECKED BY G.T.H.
 SAMPLER HAMMER WT. 140 LBS. DROP 30 INCHES (PENETRATION RESISTANCES CONVERTED TO BLOWS OF 4200 IN. LBS. ENERGY)

SAMPLE CONDITION

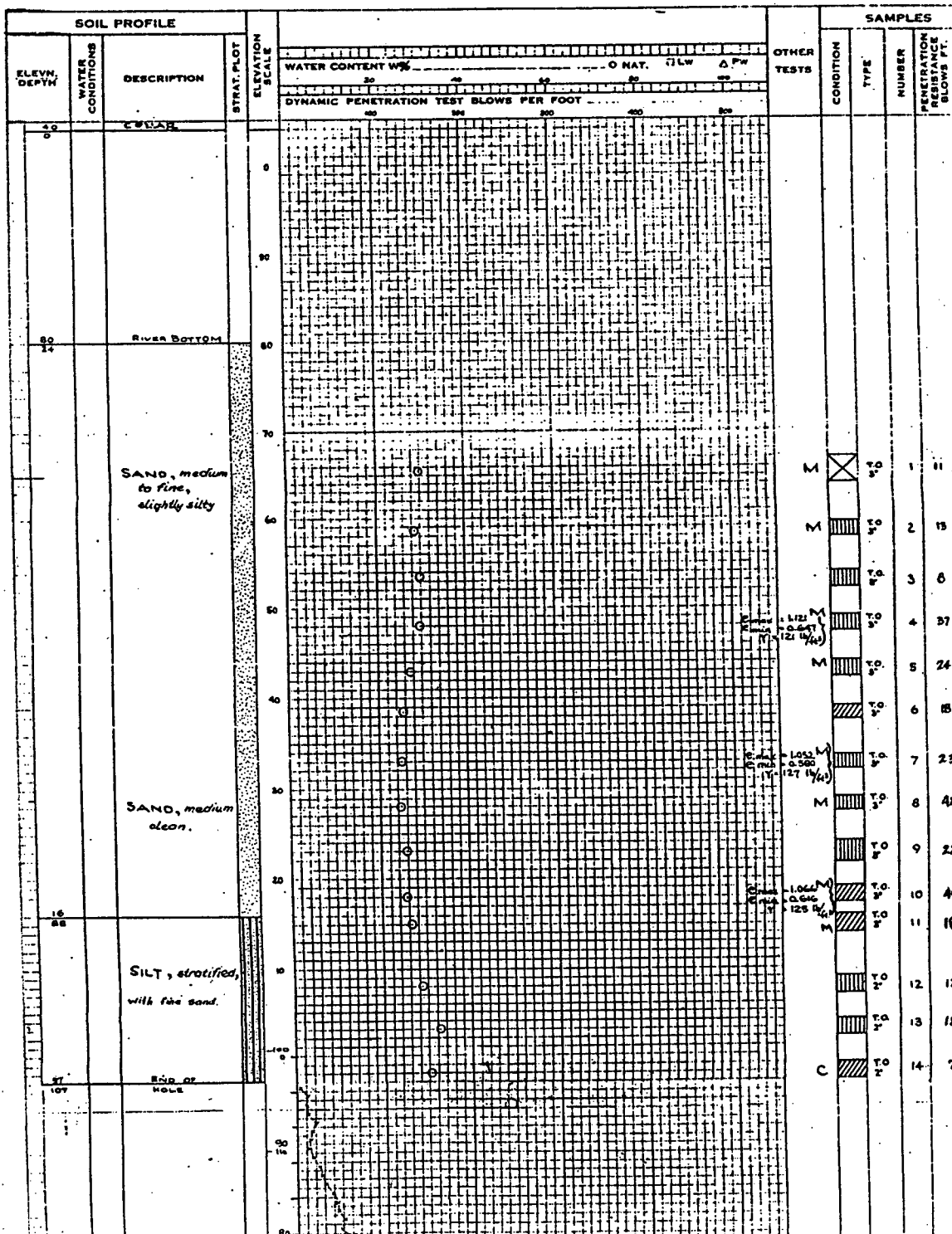
☐ DISTURBED
☐ FAIR
☐ GOOD
☐ LOST

SAMPLE TYPES

A.S. - AUGER SAMPLE
 S.T. - SLOTTED TUBE
 W.S. - WASHED SAMPLE
 D.O. - DRIVE-OPEN
 D.F. - DRIVE-FOOT VALVE
 C.S. - CHUNK SAMPLE
 F.S. - FOIL SAMPLE
 S.O. - SLEEVE-OPEN
 S.F. - SLEEVE-FOOT VALVE
 T.O. - THIN WALLED OPEN
 R.C. - ROCK CORE

ABBREVIATIONS

V - IN-SITU VANE TEST
 M - MECHANICAL ANALYSIS
 U - UNCONFINED COMPRESSION
 QC - TRIAXIAL CONSOLIDATED QUICK
 Q - TRIAXIAL QUICK
 S - TRIAXIAL SLOW
 1 - WET UNIT WEIGHT
 K - PERMEABILITY
 C - CONSOLIDATION
 WL - WATER LEVEL IN CASING
 WT - WATER TABLE IN SOIL



OFFICE REPORT ON SOIL EXPLORATION

CONTRACT 1277 TUNNEL BORING # 9 DATUM GEODETIC CASING 6"
BORING DATE APR 24 TO 30 REPORT DATE MAY 18, 1956 COMPILED BY MN CHECKED BY G7H
SAMPLER HAMMER WT. 140 LBS. DROP 30 INCHES (PENETRATION RESISTANCES CONVERTED TO BLOWS OF 4200 IN - LBS. ENERGY)

[illegible]

CONTRACT 1277 TUNNEL BORING # 10 DATUM GEODETIC CASING 4" PIPE
 BORING DATE APRIL 16-17, 1956 REPORT DATE MAY 17, 1956 COMPILED BY H.N. CHECKED BY GTH
 SAMPLER HAMMER WT. 140 LBS. DROP 30 INCHES (PENETRATION RESISTANCES CONVERTED TO BLOWS OF 4200 IN. LBS ENERGY)

SAMPLE CONDITION

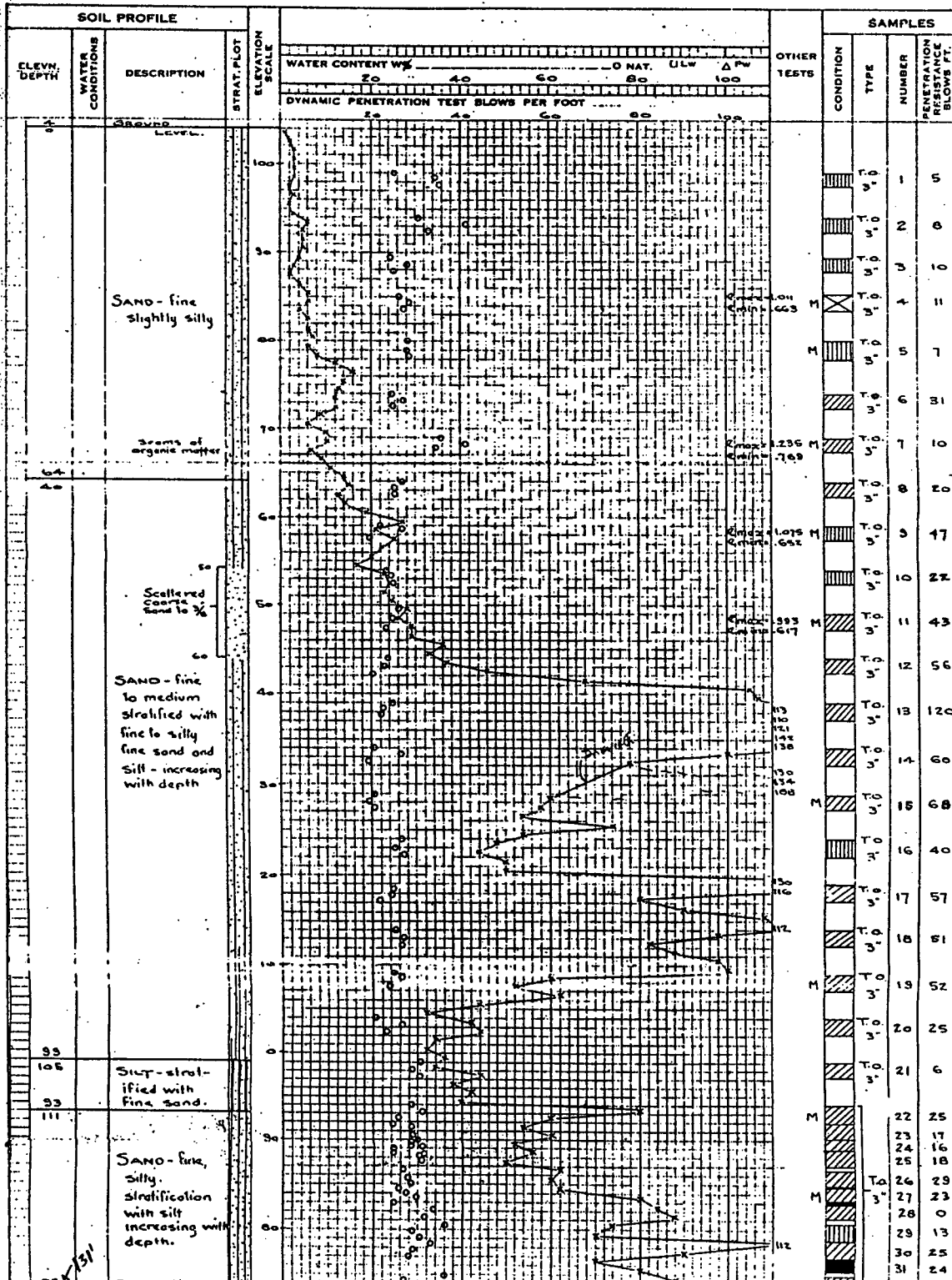
☐ DISTURBED
☐ FAIR
☐ GOOD
☐ LOST

SAMPLE TYPES

A.S. - AUGER SAMPLE
 S.T. - SLOTTED TUBE
 W.S. - WASHED SAMPLE
 D.O. - DRIVE-OPEN
 D.F. - DRIVE-FOOT VALVE
 C.S. - CHUNK SAMPLE
 F.S. - FOIL SAMPLE
 S.O. - SLEEVE-OPEN
 S.F. - SLEEVE-FOOT VALVE
 T.O. - THIN WALLED OPEN
 R.C. - ROCK CORE

ABBREVIATIONS

V - IN-SITU VANE TEST
 M - MECHANICAL ANALYSIS
 U - UNCONFINED COMPRESSION
 QC - TRIAXIAL CONSOLIDATED QUICK
 Q - TRIAXIAL QUICK
 S - TRIAXIAL SLOW
 1 - WET UNIT WEIGHT
 N - PERMEABILITY
 C - CONSOLIDATION
 WL - WATER LEVEL IN CASE
 WT - WATER TABLE IN SOIL



APPENDIX G.2

Fine-Grained Soils Data -- **-- BC Hydro Transmission Tower Study (1991)**

Table 6.2.1
Test Information and Summary of Test Results

Test No.	Water Content %		σ'_{vo} or σ'_{3c} kPa	Cyclic Test Data			Post Cyclic Monotonic		Remarks
				$\sigma_{dcy}/2\sigma'_{3c}$ or τ_{cy}/σ'_{vo}	N	ϵ_1 or γ_{max} %	S_u/σ'_{3c} or S_u/σ'_{vo}	ϵ_{1peak} or γ_{peak} %	
	w_i	w_c							
HSS1	41.5	34.2	80	0.185	20	6.5	0.37	27.1	Cyclic <u>Simple Shear</u>
HSS2	43.6	37.0	80	0.210	12	5.0	0.335	20.5	Cyclic Simple Shear
HCT1	-	37.6	80	0.213	20	4.0	0.456	16.0	Cyclic <u>Triaxial</u>

L.Limit = 30% P.Limit = 27% P.I. = 3%

w_i = initial water content

w_c = water content at end of consolidation

σ'_{vo} = vertical effective consolidation stress in simple shear test

σ'_{3c} = hydrostatic consolidation stress in triaxial test

τ_{cy} = cyclic shear stress in simple shear

$\sigma_{dcy}/2\sigma'_{3c}$ = cyclic shear stress in triaxial

N = no. of cycles to failure (very large strain) or cycles prior to post cyclic monotonic loading

γ_{max} = maximum amplitude of shear strain during cyclic loading in simple shear

ϵ_1 = maximum amplitude of axial strain during cyclic loading in triaxial

γ_{peak} = peak shear strain during monotonic loading in simple shear

ϵ_{1peak} = peak axial strain during monotonic loading in triaxial

S_u = peak undrained shear stress (undrained strength)

= τ_{max} in simple shear

= $1/2 \sigma_{dmax}$ in triaxial

B.C. HYDRO TRANSMISSION TOWER STUDY
SIMPLE SHEAR POST CYCLIC/MONOTONIC LOADING RESULTS - TEST # HSS1

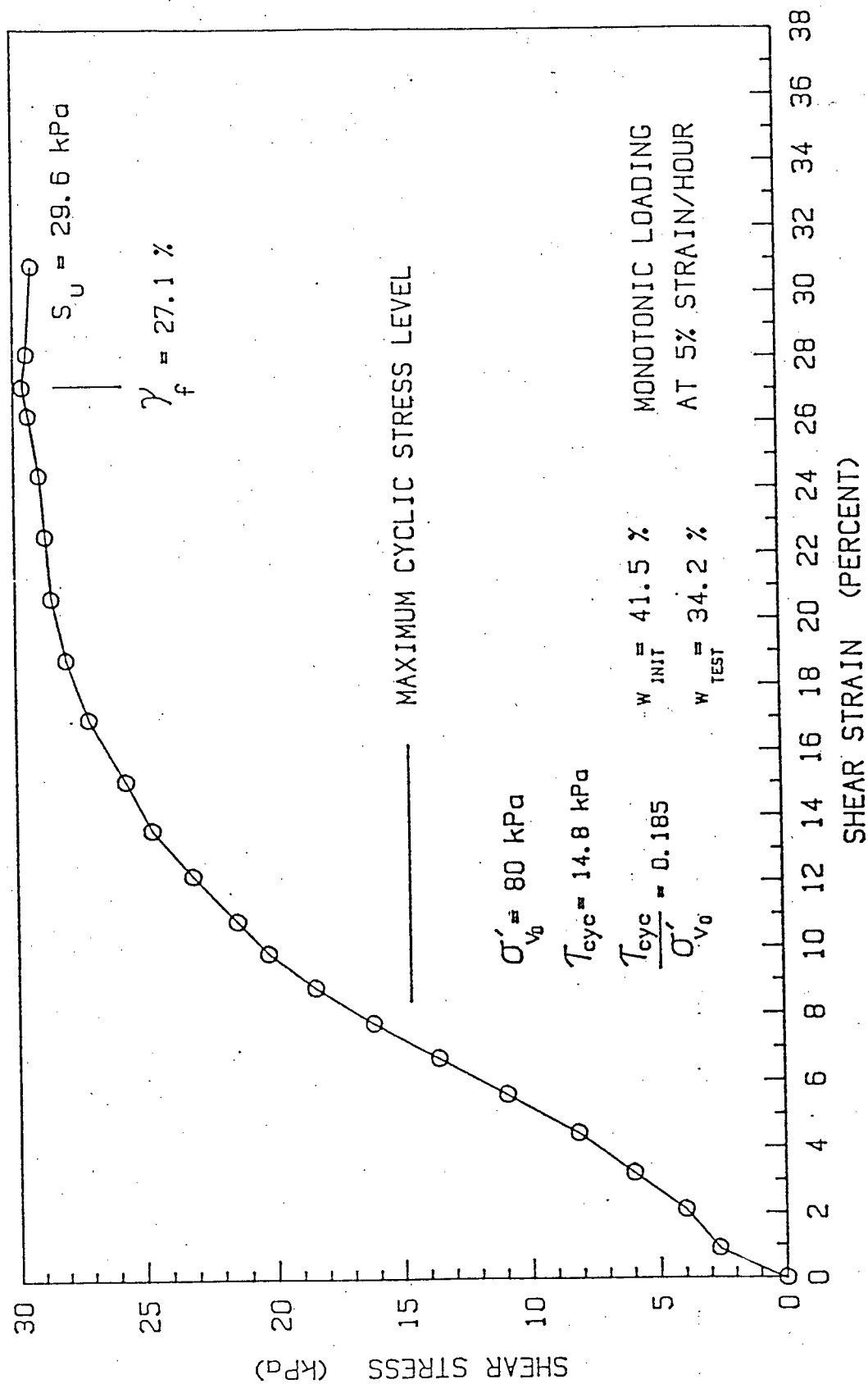


Figure G.2.1 - Post-Cyclic Loading -- Test #HSS1 (BC Hydro, 1991)

B.C. HYDRO TRANSMISSION TOWER STUDY
SIMPLE SHEAR POST CYCLIC/MONOTONIC LOADING RESULTS -- TEST # HSS2

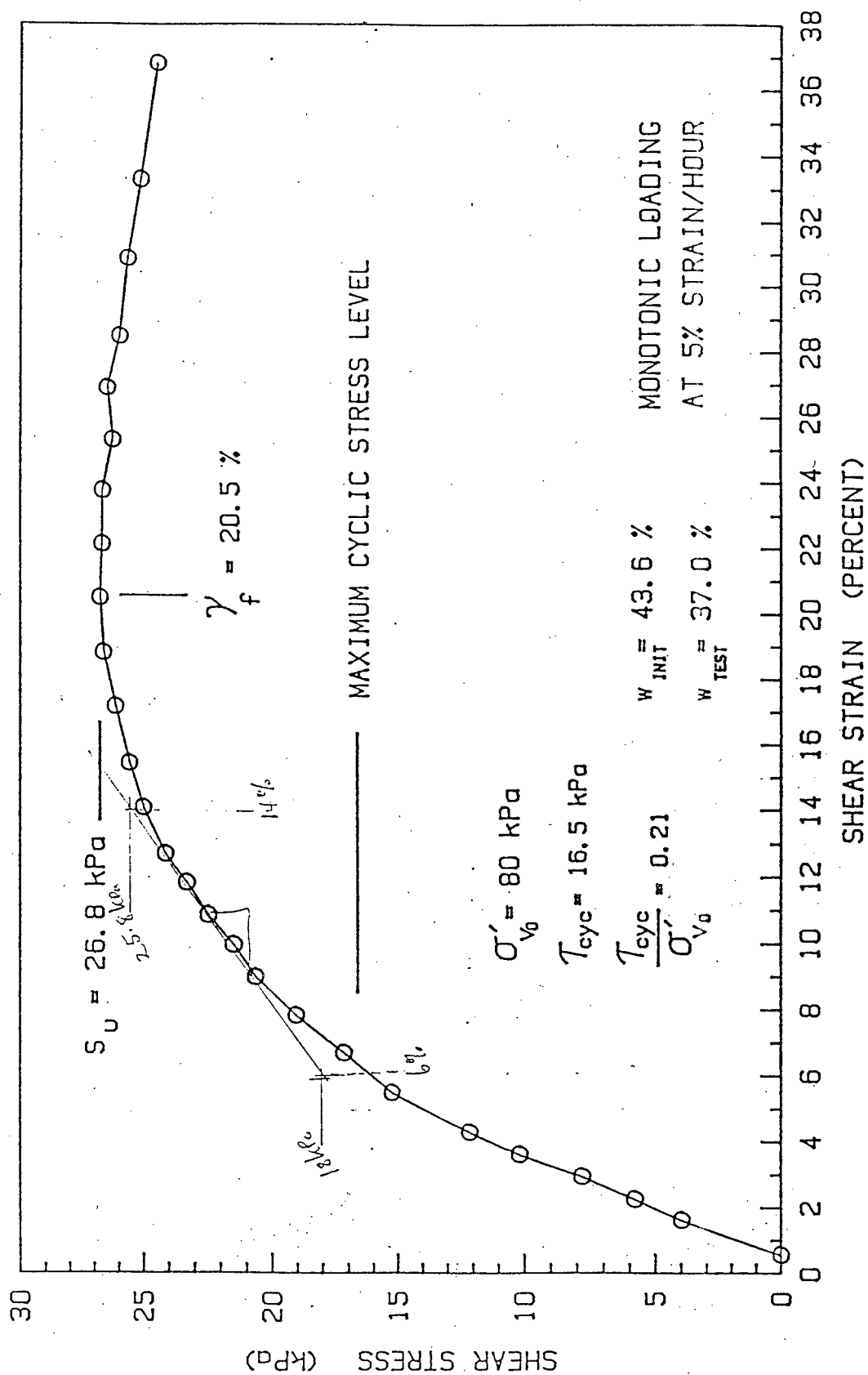


Figure G.2.2 - Post-Cyclic Loading of Silt -- Test #HSS2 (BC Hydro, 1991)